THE DEFORMATION OF BODIES IN CONTACT (WITH SPECIAL REFERENCE TO THOSE USED IN WORK-HOLDING FIXTURES)

A Thesis presented for the Degree of Doctor of Philosophy in Mechanical Engineering in the University of Canterbury, Christchurch, New Zealand

by

N. TRUONG, B.E.(Honours)

University of Canterbury
December 1977

ABSTRACT

This thesis presents the analytical studies of the behaviour of the bodies in contact, particularly with reference to those used in work-holding fixture systems under the action of a static loading. The analyses lead to the development of formulae to predict the deformation of three different systems which commonly occur in practice. For the case of a spherical locator in contact with a flat work-piece, the limit of elasticity is reached so early that the work-piece always deform plastically. Hardness and Meyer constant play important roles in determining the diameter of the indentation and hence the total deformation of the system at the contact zone. The theoretical predictions are in agreement with the experimental values. Shawski's empirical formulae do not follow the experimental results very well, particularly for hard work-pieces, his formula gives negative deformations.

For the case of a flat locator in contact with rough surface work-pieces of varying hardness, the asperities deform plastically while the material supporting them deforms elastically. The peak heights of the asperities are assumed to be isotropic and represented by the normal probability distribution. The deformation of the asperities can be evaluated accurately by the theory of Williamson up to $q/M = .1$ where q and M are the applied pressure and the Meyer hardness of the work-piece respectively. Our theoretical predictions for the deformations of the rough work-pieces indented by a flat locator show better agreement with the empirical formulae of Shawki than the theoretical curves proposed in his article.

The compression of a long cylinder by two narrow bands of pressure of distribution $q = q_o \left(1 - \frac{y^2}{\ell^2}\right)^{\beta}$ (β is a real number) is found. The

displacement of a semi-infinite solid under the same band of pressure is similarly derived. These results are combined with the deformation of the asperities to produce the approach of two hard planes compressing a rough turned cylinder of the same material. The asperities deform plastically while the material of the cylinder supporting the asperities and the planes deform elastically. The analysis ceases to apply when the cylinder and the planes start deforming plastically. This study may be used as an approximation for the evaluation of the approach of two Vee locators compressing a rough cylinder investigated by Shawki.

ACKNOWLEDGEMENTS

I wish to express my sincere thanks to Professor H. McCallion, my supervisor, for his valuable suggestions and assistance throughout this work.

I am also indebted to many members of the staff of the Department of Mechanical Engineering: Mr J. S. Smaill for his assistance in operating the Mini-computer, Mr D. Somerville for his assistance in the use of facilities in the Materials Laboratory, Mr H. J. Bright for his advice and the setting up of the valuable apparatus in the Metrology Laboratory, Mr E. D. Retallick and Mr A. E. Taylor for their construction of my design apparatus, Mrs J. Ritchie for her care in the preparation of many photographs, Mr H. J. Anink for the use of the valuable Phillips bridges and pick ups.

I am also grateful to Mr M. E. Webb for his help and patience in supplying the materials used in the tests and to Mrs P. Dowell for her care and enthusiasm in the typing of the thesis.

An inestimable debt is owed to several colleagues, especially T. G. Truong for sharing his experience in the computer programming.

The continual encouragement and assistance given by my wife, Helene, has enabled me to complete this difficult study.

TABLE OF CONTENTS

APPENDICES PAGE

NOTATION

Unless otherwise specified in the text, the following are the symbols used in the thesis:

Symbol		Equation of Origin
a	Deformation of the asperities from the highest peak	3.21
A	Real area of contact	3.5
A_n	Nominal area of contact	3.5
d	Diameter of indentation	2.1
D	Ball diameter	2.17
D_o	Ball diameter used in Brinell hardness test	2.45
E_1, E_2	Young modulii	2.1
g	Density of the asperities	6.58a
H, H_B	Brinell hardness	
ℓ	Half width of the contact area	4.6
log	natural logarithm	4.29
$\log_{10}$	logarithm of base 10	
L	Half length of the cylinder	5.1
L_o	Bearing length of the base of the surface profile	3.2
ΔL	Bearing length of the bearing curve at the level of contact	3.2
M	Meyer hardness	2.47
n	Meyer constant	2.44
p	load per unit length	
q_m	mean pressure	
q_m^*	mean yield pressure when full plasticity is reached	2.18
q	pressure	3.21
q_o	maximum pressure	4.8
r	radius of curvature of the asperity tips	3.26

Symbol		Equation of Origin
R_a	Centre line average (CLA)	
R_h	Peak-valley height (according to Shawki)	3.44
R_p	Depth of flattening of the profile	3.20
R_m	Peak-valley height	6.9
s	Net separation	3.10
s^*	Dimensionless separation	3.13
t	Dimensionless peak height = u/σ	3.13
u	Asperity peak height	3.1
v	Rise of material	3.15
v^*	Dimensionless rise in material	3.16
W	Load	
W_E	Load at the onset of plasticity	2.14
W_o	Standard load used for Brinell hardness test	2.45
Y	Yield stress	
Y_o	Yield stress of fully work-hardened material	
Y_r	Representative yield stress	
Z	Specific loading = W_o/D_o^2	2.45
$c\sigma_o$	Flow pressure of the asperity	3.24
η	Degree of contact = $\Delta L/L_o$	3.19
ρ	Dimensionless compliance = a/R_m	3.19
ε	Strain (in Chapter 2 only)	
ε_o	Initial strain due to cold work	2.17
δ	Deformation	2.2
δ_e	Elastic deformation component	2.20
δ_p	Plastic deformation component	2.28
δ_t	Total deformation = $\delta_e + \delta_p$	2.31
τ_m	Maximum shear stress	6.59

Symbol		Equation of Origin
μ	Poisson ratio	2.1
ν	Bearing parameter of the no-load bearing curve	3.19
ϕ	Bearing parameter of the deformed bearing curve	
Δ	Total approach of the two planes	6.13
Γ	Gamma function	3.22
ψ	Psi function	4.52
u, v, w	Displacements in the x, y, z directions respectively	4.40
$w_b =$	$2w_R$, the compression of the cylinder at line y = b in the yz plane	4.49
$w_{(c,b)}$	Displacement of the point (c, b, o) in the z direction	5.6
w^W, w^L	Whole body and local components of the displacement	5.7

CHAPTER 1

1.1 BACKGROUND OF WORK

Jigs and fixtures are devices for holding a work-piece during machine operations. They are always fastened to a machine or a bench in a fixed position. Recent developments in production engineering have revealed their significant role in increasing production rates, enhancing dimensional accuracy and interchangeability of mass produced articles. It is obvious in the production line that an average of ten fixtures are used for each component and the expenditure on fixtures amounts to some 15 - 20 per cent of the expenditure on production tooling. Designers of fixtures are constrained by a number of requirements such as: rigidity of clamping devices, locating positions, economy, etc ..... in their goal of producing accurate work for large quantities of high precision products. Factors affecting the dimensional accuracy of the work-pieces are:

- Cutting force : dynamic with its points of application varying during the machine operation.
- Clamping force : static, fixed in both magnitude and direction and is applied at a certain location.
- Machine tool rigidity.
- Work-piece material properties and dimensions, e.g., Young modulus, Poisson ratio , Hardness etc.....
- Work-piece topographic properties - CLA (centre-line-average) surface profile.
- Method of support for the work-piece.
- Deformation of fixture and work-piece system at the contact surface.

In machines with complex operating movements along a number of slideways, the contact deformation in the beds, tables and columns of

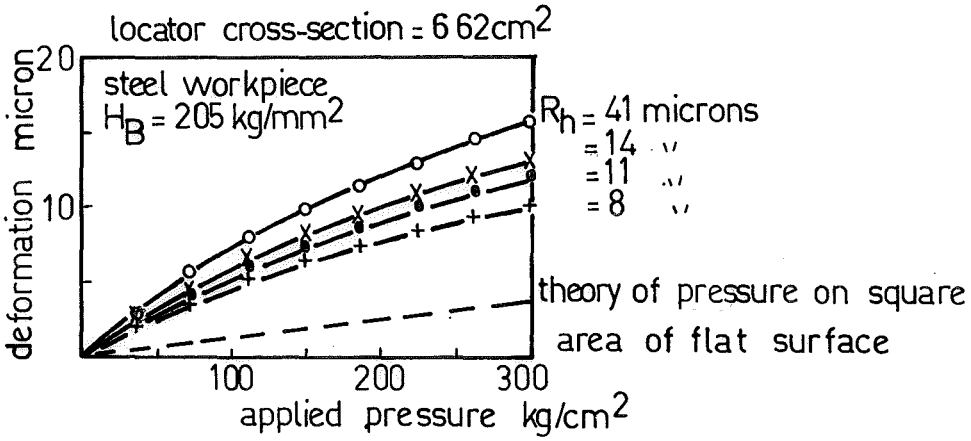

Fig. 1.1 The relation between the pressure and the deformation for steel workpieces indented by a hard flat locator. (Shawki[90])

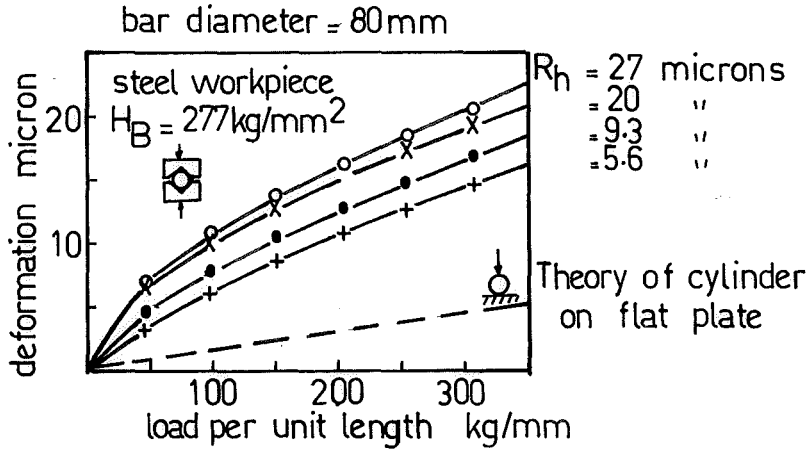

Fig. 1.2 The relation between the load per unit length and the deformation for steel bar compressed by two Vee locators. (Shawki[90]) R_h = average peak-valley height of the rough surface.

machine tools accounts for as much as 85 to 90% of the overall deformation of a given part[57]. Recent studies[46, 57, 70, 101, 108, 113] on the deformation of the asperities on a machine surface proved that it plays an important part in the contact stiffness of bodies in contact. The experimental results for the contact between a work-piece and various types of locating element used in fixtures was probably first published by Shawki *et al*[90]. For the three types of locators employed, they simply assumed that there exists a non-linear relationship $\delta = cP^n$ where δ is the deformation, P is the load for spherical locator cases, the pressure for flat locator cases, or the load per unit length for Vee locator cases; n is a constant depending on the material of the work-piece and c is a constant depending on the dimension and mechanical properties of the work-piece and the locator. In deriving their theoretical values they did not correctly account for all the possible elastic deformations occurring in the system under investigation. Hence their comparison between theoretical and experimental results is difficult to interpret and still more difficult to accept.

Considering the cases of the flat and Vee locators drawn by Shawki[90] (Figs.1.1 and 1.2), the differences between the experimental curves and those he prediced by the theory of elasticity were, in some cases, bigger than the peak to valley heights of the asperities of the work-pieces. However, experiments performed by Williamson[113], Uppal[107], Child[11], and Demkin[22] showed that the asperities still persist at very high load, up to six times of their yield stress, and they can only be deformed up to half of their peak to valley height. In the case of spherical locators, the empirical formula of Shawki may be questioned for predicting negative deformations in hard work-pieces (Fig.2.5).

1.2 SCOPE OF THE STUDY

With these doubts in relation to Shawki's empirical formulae, we

decided to study the deformation of the above types of bodies in contact and to carry out the experiments if thought necessary. The whole thesis is divided into five different chapters:

(i) Chapter 2: A study is made of the approach of a hard steel ball indented into a flat work-piece. It is then applied to the case of a spherical locator in contact with a flat surface. The investigation involved the work of Tabor on the elastic recovery of an elastic surface after the removal of the spherical indenter, the Meyer law of indentation in the fully plastic zone, and the theory of elastic contact due to Hertz.

(ii) Chapter 3: A study is made of the contact between rough surfaces. This case is applied to the approach of a hard smooth flat locator indented into a flat surface of varying roughness and hardness. The investigation involved the theory of elasticity for bodies under direct bearing and the theories of Hisakado, Williamson and Demkin for the deformation of the asperities of a flat surface in contact with another smooth flat surface.

(iii) Chapter 4: A study is made of a cylinder being compressed between two narrow bands of elliptic- paraboloidal pressure distribution. The works of Föppl and Lundberg are also considered.

(iv) Chapter 5: A study is made of the displacement of a semi-infinite solid under a finite uniform band of elliptic-paraboloidal pressure distribution. The results of the studies of Prescott, Puttock and Lundberg were also referred.

(v) Chapter 6: A study is made of the approach of two hard flat planes compressing a rough cylinder of varying hardness and roughness. It is used as an approximation for the case of two Vee locators

compressing a rough cylinder of the same modulus of elasticity. The work involved solving the three homogeneous equations obtained from the results of Chapters 3, 4 and 5.

Our theoretical and experimental results have been compared with with the values given by the empirical formulae of Shawki.

CHAPTER 2

2.1 REVIEWS OF PAST INVESTIGATIONS OF THE INDENTATION ON A FLAT SURFACE BY SPHERICAL BALLS

The classical theory of contact between elastic bodies was derived by Hertz (1881) with the following assumptions:

1) Reactions must be normal to the contact surfaces which are frictionless.

2) No tangential forces must be induced between the bodies in contact.

3) Contact is limited to small portions of the surface.

4) The bodies must be elastic and isotropic.

5) The bodies must be at rest in relation to each other.

6) Strain must be within the elastic limit.

When two spheres with smooth surfaces are placed together (Fig.2.1) they instantaneously make contact at a mathematical point which has an infinitely small area, so that even under a small load, the intensity of pressure instantaneously becomes infinitely great. Yield inevitably takes place and an equal amount of material at each contact point is forced into the mass of each body if the material in both is identical in structure and physical characteristics. This process goes on until the resistance of the material to further deformation balances the applied load W, a certain amount of time elapsing before the process is completed and the projected outline of the contact area is a circle of diameter d. Hertz proved that

$$d = 2 \left(\frac{3\pi}{4} \quad \frac{W(k_1 + k_2)\, R_1 R_2}{R_1 + R_2} \right)^{1/3} \qquad 2.1$$

where k_1, k_2 are equal to $\frac{1 - \mu_1^2}{\pi E_1}$, $\frac{1 - \mu_2^2}{\pi E_2}$ respectively

E_1, E_2 are Young modulii of elasticity of the balls 1 and 2 respectively.

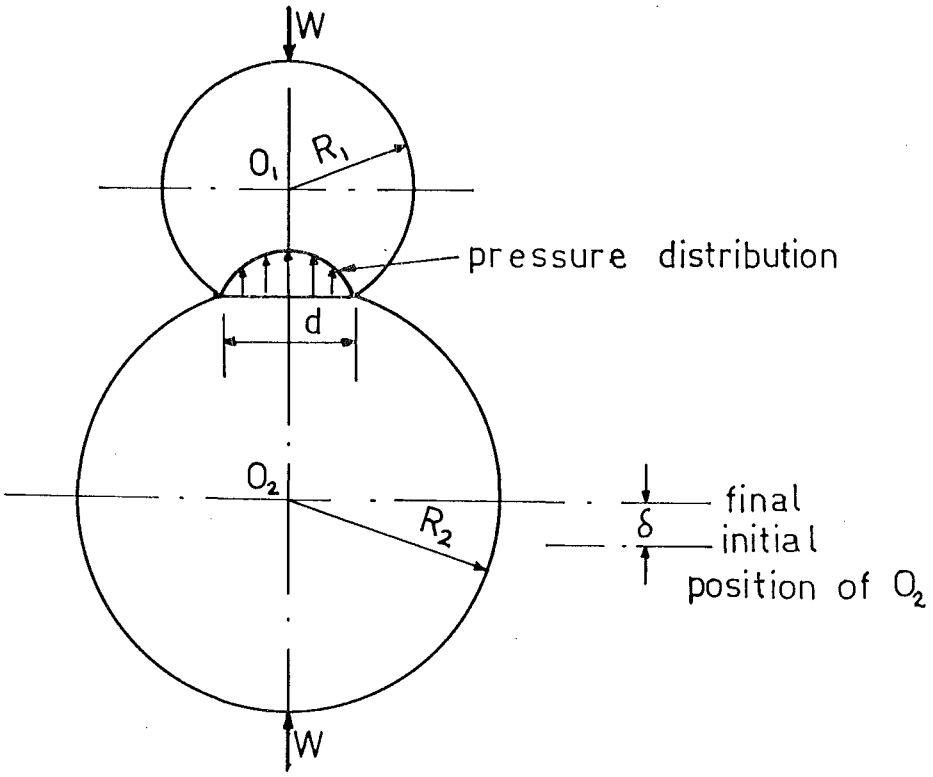

Fig. 2.1 The compression of two spheres

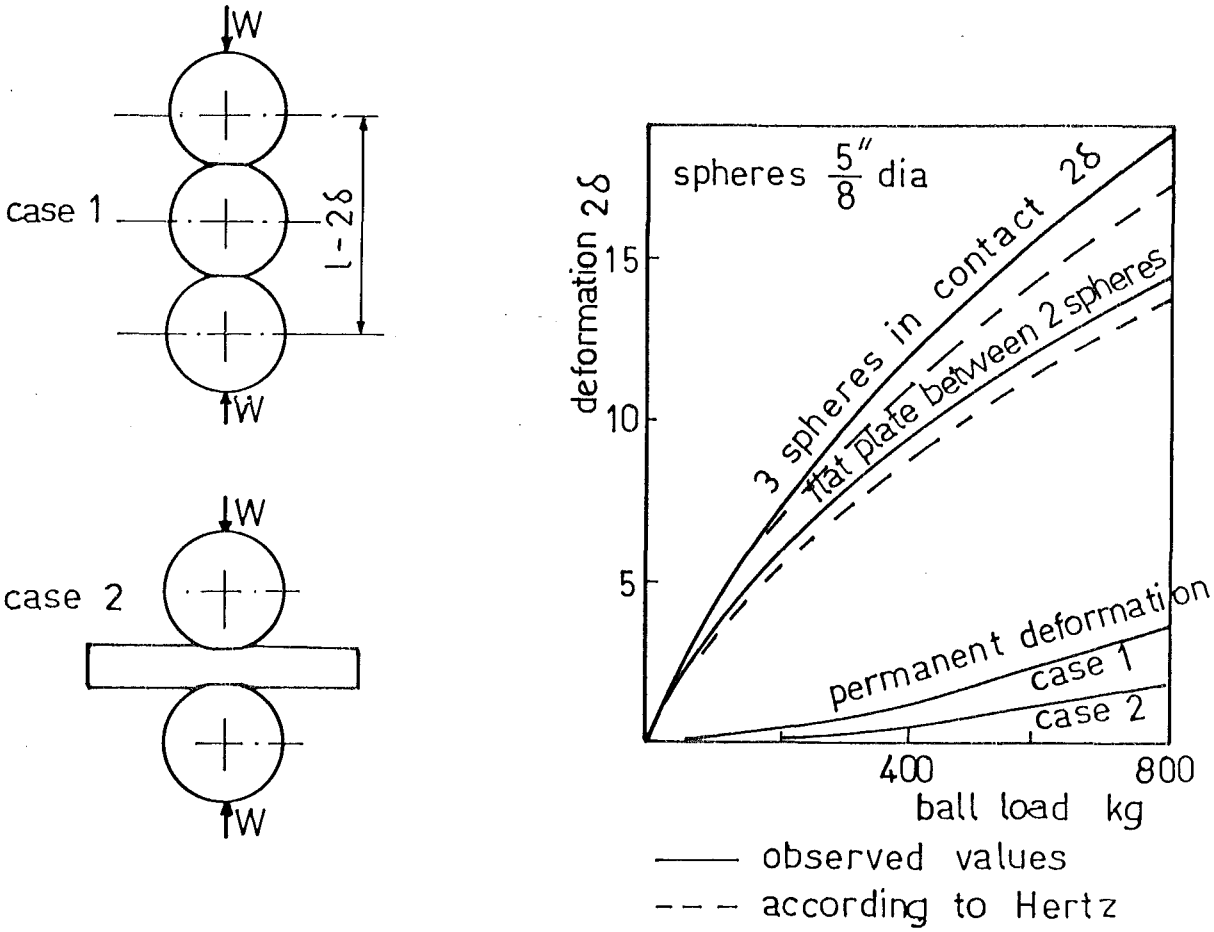

Fig. 2.2 The experimental results of Stribeck(95)

The distance the two centres (of the spheres) come together due to the deformation under load W is

$$\delta = \left(\frac{9\pi^2}{16} \quad \frac{W^2 \ (k_1 + k_2)^2 \quad (R_1 + R_2)}{R_1 \ R_2} \right)^{1/3} \qquad 2.2$$

These two equations apply for the case of loading shown in Fig.2.1.

The distribution of pressure q over the contact surface is represented by the ordinate of a hemisphere radius $d/2$ constructed on the surface of contact.

If $R_2 \to \infty$ i.e., the case of ball radius R_1 indented into a semi-infinite solid then the above equations become

$$d = 2 \left(\frac{3\pi}{4} \quad W(k_1 + k_2) \ R_1 \right) 1/3 \qquad 2.3$$

$$\delta = \left(\frac{9\pi^2}{16} \quad \frac{W^2}{R_1} (k_1 + k_2)^2 \right) 1/3 \qquad 2.4$$

Thus the projected area of the indentation is proportional to $W^{2/3}$ and the mean pressure q_m over the region of contact is proportional to $W^{1/3}$, the pressure q at any distance x from the centre of the indentation has the value

$$q = q_o \left(1 - \frac{4x^2}{d^2} \right)^{\frac{1}{2}} \qquad 2.5$$

where q_o is the pressure at the centre of the circle of contact. See Fig.2.1. It follows that

$$q_o = 1.5 \ q_m \quad \text{where } q_m = 4W/\pi d^2$$

For most materials, Poisson ratio is about 0.3, then

$$d = 1.761 \left(WR_1 \quad (\frac{1}{E_1} - \frac{1}{E_2}) \right) 1/3 \qquad 2.6$$

$$\delta = 0.775 \left(\frac{W^2}{R_1} \left(\frac{1}{E_1} + \frac{1}{E_2} \right)^2 \right)^{1/3} \qquad 2.7$$

The experiments by Professor Stribeck[32] (1900) on steel balls and ball bearings proved that Hertz theory is very good at low loads (Fig.2.2). The permanent deformation for the case of three spheres in contact is higher than for the case of a flat plate between two spheres. Obviously permanent deformation cannot be calculated by the Hertz theory since it applies only within the elastic range. Investigations by Palmgren[79] (1945) gave a relatively simple formula to indicate the magnitude as well as the variation of the permanent deformation within a limited range, in the neighbourhood of the elastic limit, which is of interest for practical steel ball-bearing engineering. According to Palmgren

$$\delta_p = 1.25 \times 10^{-2} \frac{W^2}{D_W} (\rho_1 I + \rho_1 II) (\rho_2 I + \rho_2 II) \text{ micron} \qquad 2.8$$

where δ_p = total permanent deformation at contact area

W = load in kg

D_w = diameter of the rolling element in mm

$\rho_1 I$, $\rho_2 I$ and $\rho_1 II$, $\rho_2 II$ are the reciprocals of the principal radii of curvature at the point of contact between bodies I and II. If body II is a plane, $\rho_1 II = \rho_2 II = 0$ and body I is a sphere of diameter D, then

$$\rho_1 I = \rho_2 I = 2/D$$

and Equation 2.8 becomes

$\delta_p = .05W^2/D^2$ microns (2.9). This expression applies for flat steel with a hardness of 63.5 - 65.5 Rockwell C. The effect of differences in hardness and in materials was not fully investigated by Palmgren.

In Equation 2.7, the radius of curvature is positive for a convex surface and negative for a concave surface.

In 1965, in an investigation into fixture design, in particular into the contact rigidity with spherical locating elements, Professor Shawki[90] set up an experiment to record the total deformation in indenting spherical locators of various radii of curvature into steel and cast iron flat work pieces with varying degrees of hardness. Unfortunately, the results were far from those given by the Hertz theory (Figs. 2.3 and 2.4). Without attempting to account for this difference, he then proposed two empirical formulae for the deformation of the system he investigated. They were

for steel work-pieces $$\delta = (.67 - .0031H_B + 6.23/\rho)\ W^{.8} \text{ micron} \qquad 2.10$$

and for cast iron work-pieces

$$\delta = (2.7 - .008\ H_B + 9.23/\rho)\ W^{.6} \text{ micron} \qquad 2.11$$

where H_B = Brinell hardness of the work-piece in kg/mm^2

ρ = radius of curvature of the spherical locator in mm

W = load in kg.

These spherical locators were made of extra high grade carbon steel. They were heat treated to a hardness of 55 - 60 Rockwell C and the surfaces of contact were finely finished. It is also interesting to observe that from the above empirical formulae, curves of zero deformation were drawn in Fig.2.5 for both steel and cast iron work-pieces, e.g., these curves indicate that a steel work-piece of 280 kg/mm^2 hardness will not deform under any load if the ball, or spherical locator, has the radius of curvature above 30 mm. This is a 'fact' that can hardly be accepted.

This doubt is reinforced by the results of an experiment performed by Professor Goodman[32] in 1923 to measure the approach of two hard flat dies under load, when separated by a ball of the same hardness. Though the hardness of both dies and the ball was not given, it can be assumed that its minimum value would be 45 Rockwell C, i.e., approximately 400 Brinell hardness. With a ball of diamter 8" (203.2 mm) significant deformations were recorded, as shown in Fig.2.6. This implies that Shawki's formula is

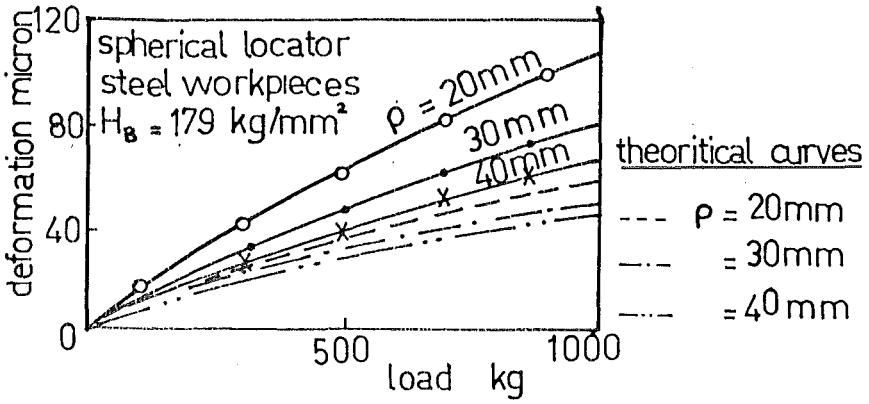

Fig. 2.3 Load-deformation characteristics for steel workpieces indented by a spherical locator.(Shawki[90])

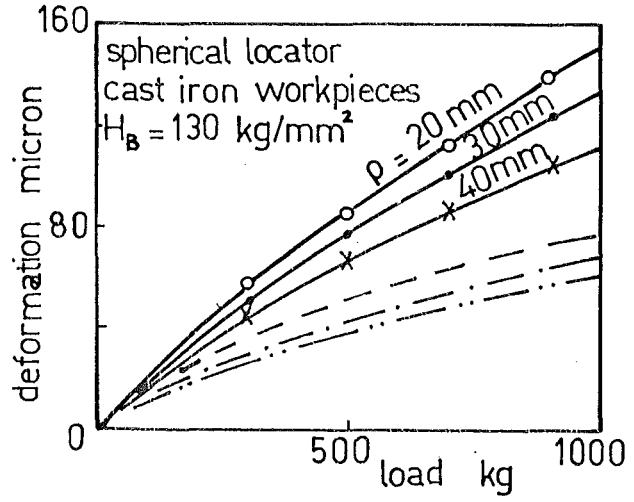

Fig. 2.4 Load-deformation characteristics for cast-iron workpieces indented by a spherical locator.(Shawki[97])

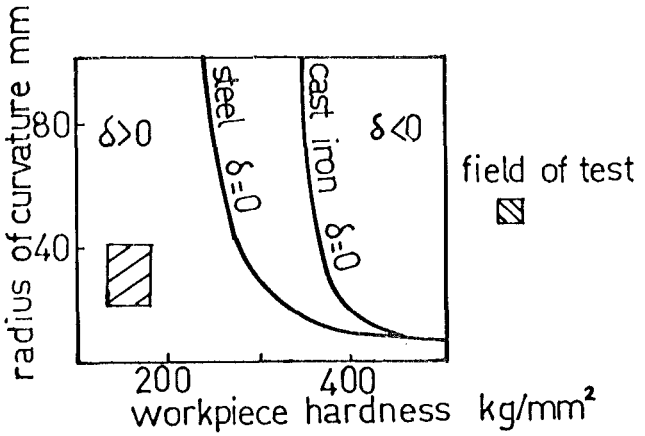

Fig. 2.5 The curves of zero deformation of steel and cast-iron workpieces indented by a spherical locator.(Shawki[97])

in error for hard steel surfaces.

The deformation of a hard steel ball on a hard steel surface has long since been investigated in the ball bearing field. Experiments have shown that the actual value is slightly higher than the predicted Hertz value, due to plastic deformation and empirical formulae having been established for practical purposes.

According to Palmgren[79] (1945)

$$\delta = e_{\delta}\ \varepsilon_E^2\ (W^2\ \Sigma\rho)^{1/3} \quad \text{mm} \qquad 2.12$$

where e_{δ}, ε_E are coefficients given in Tables 2.1 and 2.2 of Reference 79

W = load in kg

$\Sigma\rho$ = sum of the reciprocals of all the principal radii of curvature of the bodies in contact. For a sphere of diameter D in contact with a flat surface $\Sigma\rho = 4/D$, where D is measured in mm.

This Equation applies for steel of hardness 63.5 - 65.5 Rockwell C, bronze and cast iron. Unfortunately the hardnesses of the bronze and the cast iron were not stated, but since they are intended for use in bearings, I assume that they would be heat-treated to the hardest possible state.

According to Goodman[32] (1923)

$$\delta = \frac{W^{0.673}}{64000D^{1/3}} \quad \text{inch} \qquad 2.13$$

where W = load in lbs

D = ball diameter in inch.

The work of Shawki seems to be the only investigation reporting on the deformation of steel and cast iron flat work-pieces of varying degrees of

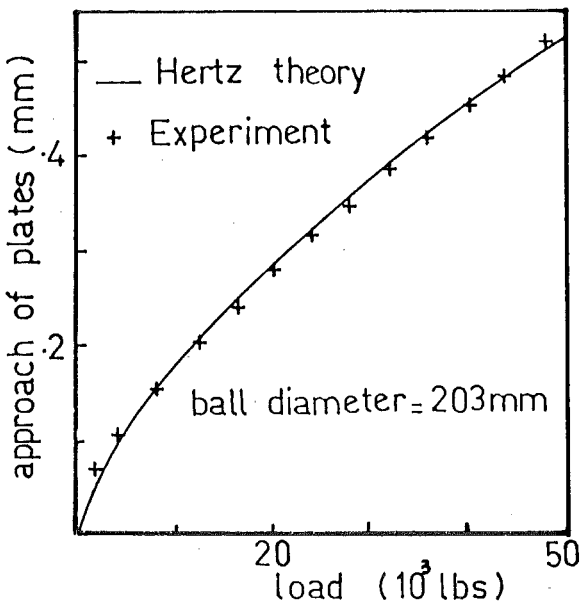

Fig. 2.6 The approach of two hard flat steel dies compressing a hard steel ball.(Goodman[32])

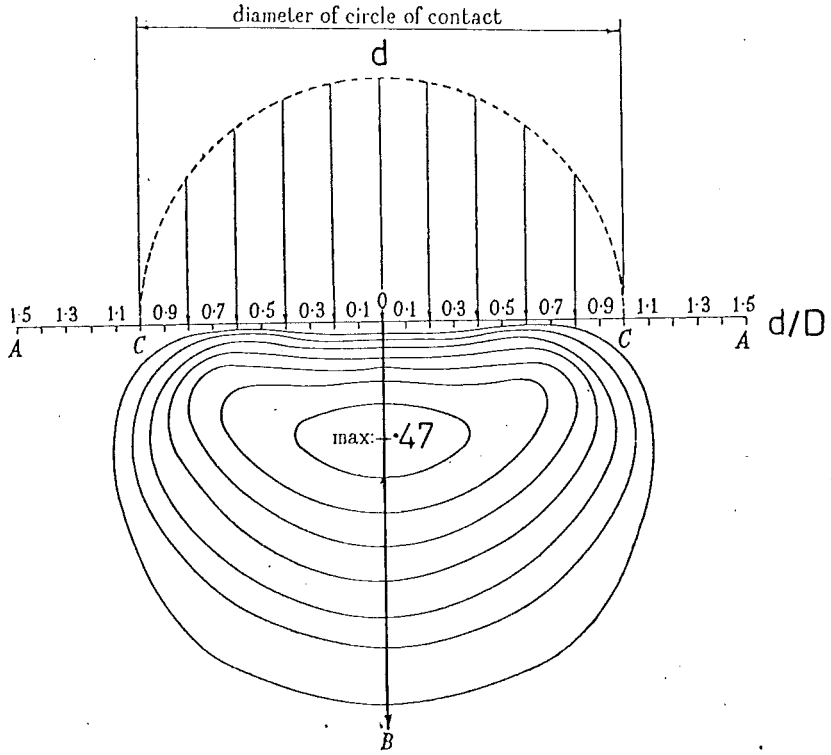

Fig. 2.7 Elastic deformation of a flat surface by a sphere, showing the maximum shear stress below the deformed surface.(Davies (16))

hardness indented by a hard steel spherical surface.(*) However, he has raised an uncertainty on the Hertz theory which past investigators have shown to be relatively satisfactory. The simplest approach to an explanation for the difference between the experimental and theoretical curves drawn in Figs 2.3 and 2.4 would be to consider the limit of the elasticity law used by Hertz, i.e., to determine the load at which the Hertz theory ceases to be valid. Tabor[97] (1951) called this load the onset of plasticity load W_E.

Davies[16] (1949) found that the condition of plastic flow is first reached at a point z, Fig.2.7, below the actual surface of contact, since at this point the calculated maximum radial shear stresses are equal and have a value of $.47q_m$ (assuming Poisson ratio is 0.3 for all common metals), by applying the Tresca or the Huber-Mises criterion, plastic flow can be expected to occur when the shear stress equal $Y/2$, i.e., when $q_m \simeq 1.1\ Y$. This means that as the load increases and reaches the value of 1.1 Y some plastic deformation occurs at z, the rest of the material deforms elastically. As the load is further increased, the amount of plastic deformation around the indentation increases, and on removing the load a permanent deformation is left on the work-piece surface.

Onset-of-Plasticity Load

Let W_E be the load at which the onset of plasticity is reached, i.e., mean pressure at load W_E

then $q_{mE} = 1.1\ Y$

where $q_{mE} = 4W_E/\pi d_E^2$

---

* I was not aware of the finite element analysis of a work-hardened flat plate indented by a tungsten carbide ball[56] until after the manuscript of this thesis was completed in November 1977.

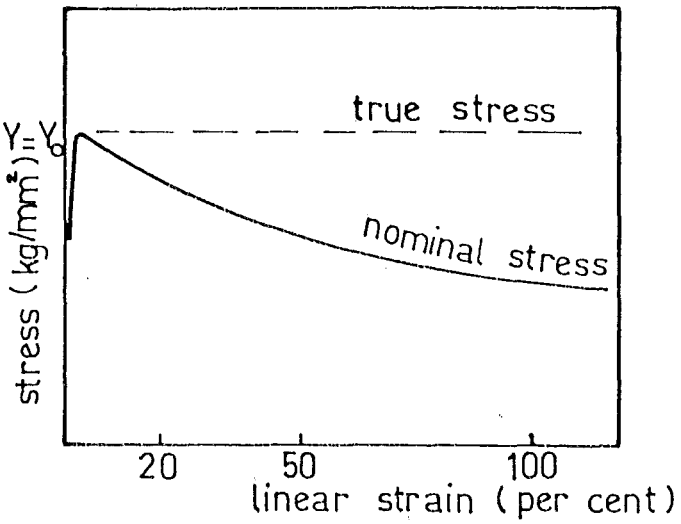

Fig. 2.8 The stress-strain curve under tension for an ideal plastic material.(Tabor[97])

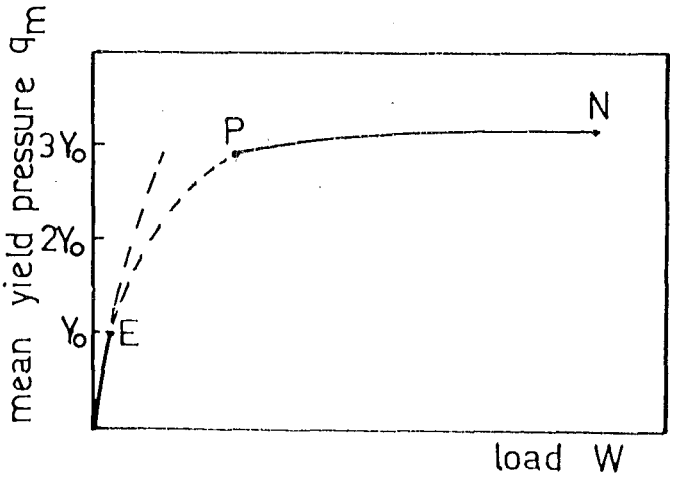

Fig. 2.9 Theoretical pressure-load relationship of an ideal plastic metal deformed by a spherical indenter.(Tabor[97])

i.e., $W_E = \pi d_E^2 q_{mE}/4$

Raising both sides to the power 3 and substituting d_E from Equation 2.6, gives

$$W_E^3 = \frac{1}{64}\pi^3 q_{mE}^3 (1.761)^6 W_E^2 R_1^2 \left(\frac{1}{E_1} + \frac{1}{E_2}\right)^2$$

or

$$W_E = 14.461\, q_{mE}^3 R_1^2 \left(\frac{1}{E_1} + \frac{1}{E_2}\right)^2 \qquad 2.14$$

It should be noted that with the same approach, Tabor[97] got the slightly smaller value (probably due to the accumulation of truncation error) given below:

$$W_E = 13.1\, q_{mE}^3 R_1^2 \left(\frac{1}{E_1} + \frac{1}{E_2}\right)^2 \qquad 2.15$$

If the yield stress Y of each work-piece is given (for some metals, the 0.2% Proof Stress is used) we can substitute $q_{mE} = 1.1\ Y$ into Equation 2.14 to obtain its own onset of plasticity load. The only given property of the test pieces used in Shawki's experiments is Brinell hardness, hence we must find a relationship between Brinell hardness and yield stress of each work-piece in order to obtain a rough idea of what the onset of plasticity load is.

(a) <u>When the Work-Piece is fully Work-Hardened</u>

Tabor[97] showed experimentally that in the fully work-hardened state it has constant yield stress Y_o and behaves similarly to an ideal plastic material; Fig.2.8 shows the stress-strain curve under tension for an ideal plastic metal. In the Meyer formula $W = kd^n$ where W is load applied, d is the diameter of the indentation, k and n are two constants for the material, for fully work-hardened material n is very close to 2. Fig.2.9 shows the theoretical mean pressure-load characteristic for an ideal plastic metal deformed by a spherical indenter. It shows that the mean pressure q_m does not increase at high

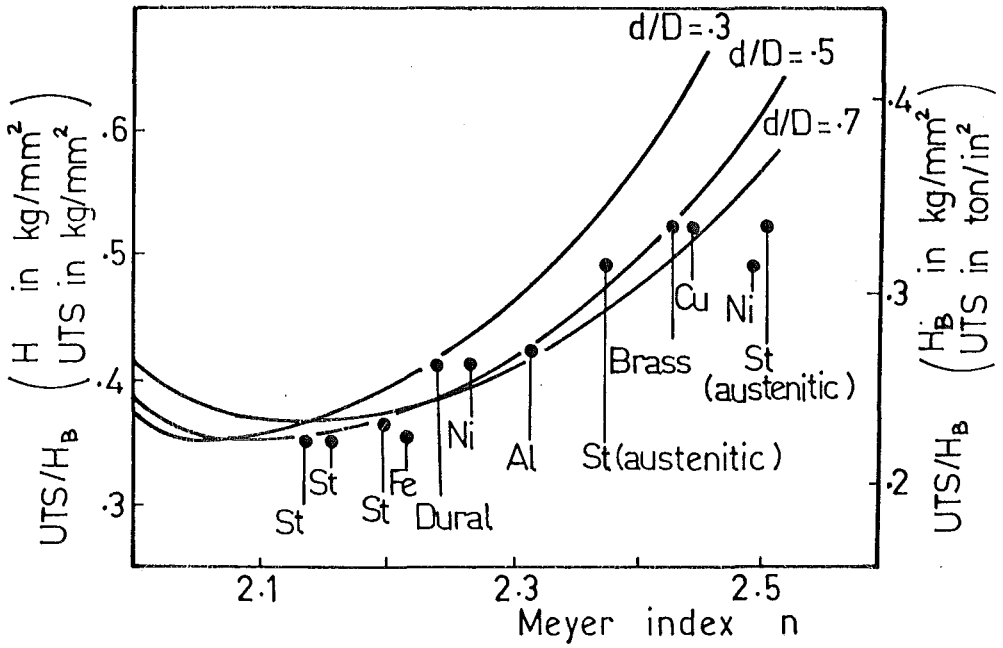

Fig. 2.10 Ratio of Brinell hardness to ultimate tensile strength as a function of the Meyer constant n. Experimental data by O'neill, drawn by Tabor[97].

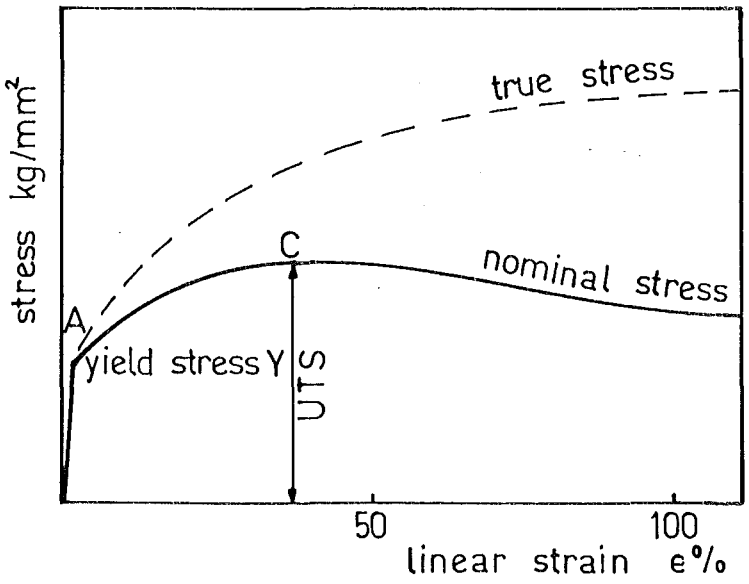

Fig. 2.11 The stress-strain curve under tension for a material which work-hardens. (Tabor[97])

load and it happens to be equal to the Meyer hardness.

That is

$$\text{Meyer hardness} = 4W/\pi d^2 = q_m \text{ at high load}$$

where $q_m \simeq 3\ Y_o$ at high load.

Since the Brinell hardness is very close to the Meyer hardness, we may assume that Brinell hardness is approximately equal to three times the yield stress Y_o with small error.

(b) <u>When the Work-Piece is in an Annealed or in a Partially Work-Hardened State or it has been Heat Treated in any way</u>

Published results (Appendices 2.1 and 2.2) show that n is now greater than 2 and less than 2.6. Theoretically the ratio of UTS over Brinell hardness was found to depend on the Meyer index n and on the ratio of the indentation diameter over ball diameter, Fig.2.10. Experimental results also show that the minimum ratio of $\frac{UTS}{HB}$ is about 0.36. Fig.2.11 shows the stress-strain curve under tension for a material which work-hardened: the yield stress Y is always smaller than the UTS value. Therefore, the maximum yield stress for this type of metal can be assumed to be about 1/3 of the Brinell hardness.

From the above, for the purpose of estimating a value for the onset of plasticity load of Shawki's work-pieces, we assumed that the yield stress of each individual work-piece was about 1/3 of its own Brinell hardness value.

If we substitute $q_{mE} = 1.1\ Y = 1.1\ H_B/3$ into Equation 2.14, we have

$$W_E = .7128\ H_B^3\ R_1^2 \left(\frac{1}{E_1} + \frac{1}{E_2} \right)^2 \qquad 2.16$$

Taking $E_{\text{Steel}} = 21500\ kg/mm^2$ from Shawki's article

and $E_{\text{Grey cast iron}} = 17 \times 10^6\ lb/in^2$ (Ref. 84, page 416)

$$\simeq 12000\ kg/mm^2$$

gives the maximum value of W_E for the six different cases in Table 2.1 as 56.5 kg. This means that the classical law of elasticity ceases to be valid at a load below 100 kg, and the difference in deformation increases greatly as the load becomes much higher than W_E. Another way of determining whether the flat surface deforms elastically or plastically was introduced by Johnson[49]. As the quantity $\frac{E}{Y}\tan\beta$ is less than 2, the deformation is entirely elastic, as it reaches 50 the deformation is entirely plastic. E, Y are Young modulus and Yield stress of the body respectively, and β is the angle of inclination of the sphere to the surface at the edge of the indentation. Due to doubts about Shawki's empirical formulae, we felt that there was a need to repeat his experiment and to establish a method to predict the total deformation of the experimental system for a range of metals.

TABLE 2.1

The estimation of the onset of plasticity load W_E for some of Shawki's work-pieces.

R_1 (mm)	W_E (kg)	
	Steel H_B = 179 kg/mm^2	Cast Iron H_B = 130 kg/mm^2
20	14.1	10.6
30	31.8	23.8
40	56.5	42.2

R_1: the radius of curvature of the spherical locator.

2.2 INDENTING PHENOMENON AND ANALYSIS

The surface deformation resulting from indenting a ball into a flat surface of different material may vary considerably in form. In some cases the material is raised and "piled up" around the impression, while in others

It may be "sunk in" so that the circumference of the impression is considerably below the original surface. It has been found that for highly worked metals, the flow of metal around the indenter produces "piling up". This is the behaviour of "ideal plastic material" i.e., when the metal is displaced by penetration of the indenter it flows out between AC and BD (Fig.2.12b), so that the material in this region is raised above the general level. As the indenter descends there is also a marked lateral movement near A and B because of the increase in diameter of the indentation so that most marked piling up occurs around the edge of the indentation.

If the material is in annealed state, however, the behaviour is different, the early displacement of metal in the plastic region produces appreciable work-hardening and it becomes easier to displace the adjacent metal which lies deeper below the indentation. Consequently, the displaced metal flows out at the region outside C and D (Fig.2.12c). Once this material has yielded it also work-hardens and further displacement of metal occurs at a still greater depth. As a result, the material around the indentation itself is left at lower level than the material further away from the indenter.

A theoretical treatment of this problem involves mathematical difficulties. Even for the easiest case of ideal plastic material, some assumptions have to be made. Ishlinsky[48] (1944) has proposed a slip-line pattern for a spherical indenter deforming an ideal plastic metal, using a finite difference method. The analysis is based on the Haar-Karman criterion of plasticity which does not deal with the displacement of the deformed material (Fig.2.13). This assumption is not strictly valid, but the type of error involved does not appear to be serious and the result may be considered to be a good approximation, the pressure distribution at the contact area is shown in Fig.2.14, and the mean pressure $q_m \simeq 3Y$. However, the solution of Ishlingsky was incomplete and when the corresponding velocities are determined, the plastic work inequality is violated[83]. The finite difference method

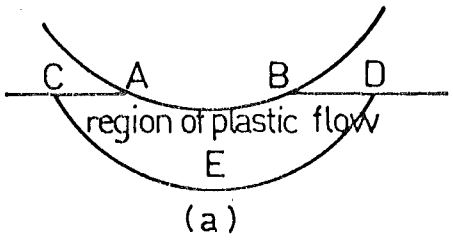

(a)

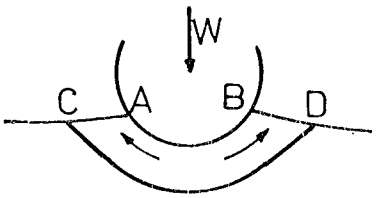

(b)

piling up

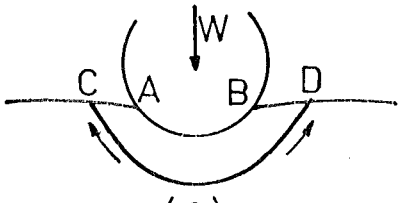

(c)

sinking down

Fig. 2.12 Two common behaviours of a flat surface under a spherical indenter.

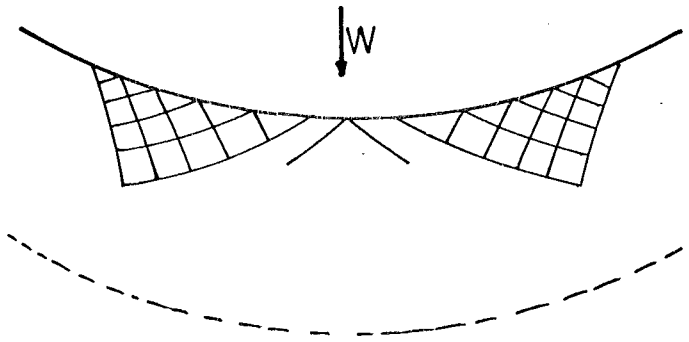

Fig. 2.13 The slip-line pattern obtained by Ishlinsky for a spherical indenter deforming an ideally plastic metal.

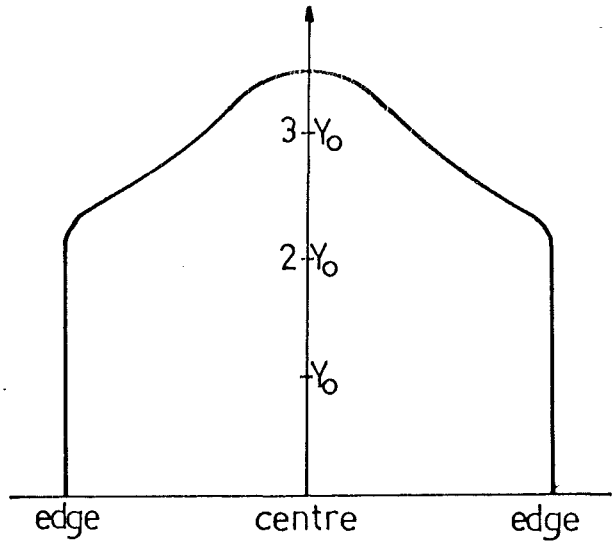

Fig. 2.14 The pressure distribution over the indentation of an ideally plastic material

proposed by Richmond[23] (1974) for the indentation of a rigid sphere into a rigid-perfectly plastic material can be used to evaluate the ball penetration, the diameter of the indentation and remarkably, the piling up height around the tip of the indentation. Tabor[97] (1951) plotted the theoretical pressure load characteristic of a spherical indenter penetrating an ideal plastic body in Fig.2.9. The portion OE represents the initial elastic deformation where the mean pressure q_m is proportional to $W^{1/3}$ (the Hertz law). The point E corresponds to the onset of plasticity which occurs when $q_m = 1.1\ Y_o$. The dotted portion EP represents a transitional region as the amount of plastic flow increases while PN represents the condition of full plasticity where $q_m \simeq 3Y_o$. Tabor called this value of mean pressure the "yield pressure q_m^*" of metal. In highly worked metal, yield pressure q_m^* at fully plastic condition is approximately equal to $3\ Y_o$ at large Brinell indentation since the specimen is incapable of appreciable further work-hardening and may be considered to possess a constant yield stress Y_o. Alternatively, we may say that at full plasticity condition q_m^* varies very little with further increase in indentation size, since $q_m^* = 4W/\pi d^2 \simeq$ constant A then the Meyer law becomes $W = kd^2$, where $k = \pi A/4$, and the Meyer constant $n = 2$. Experiments by Tabor showed that full plasticity is reached or the validity of Meyer law starts from $\frac{d}{D} > 0.1$.

In general, for a material which is in an annealed state or in a partially work-hardened state, the Meyer constant is no longer equal to 2, but higher in value; experiments also show that even at full plasticity, the mean yield pressure q_m^* increases with increase of load or increase of size of indentation. The theoretical analysis becomes so difficult that it cannot be solved even for the 2 dimensional case. We therefore have to study the problem by an empirical approach.

Since the deformation or strain varies from point to point, the elastic stress Y will not be constant at every point. However, we expect that when

full plasticity is reached there will exist an average or "representative" value of elastic stress, say Y_r, which is related to the mean yield pressure q_m^* by a relation of the type $q_m^* = cY_r$ where c is a constant Tabor found experimentally to be close to 3.

Note: q_m = mean pressure in general

q_m^* = mean pressure in the fully plastic zone only

Suppose the indentation has a chordal diameter d and a radius of curvature r_2, since it is a portion of a sphere its shape is completely defined by the dimensionless ratio d/r_2. Then, for all indentations for which d/r_2 is the same, the amount of deformation or strain at the representative region will be the same. This is true since strain itself is a dimensionless parameter which depends only on the fractional change of dimensions and not on the absolute change. We may therefore say that the strain ε_1 produced at the representative region will be simply a function of d/r_2. In practice $r_2 \simeq D/2$ so that

$$\varepsilon_1 = \text{fn}(d/r_2) = \text{fn}(d/D)$$

If the metal is fully annealed, ε_1 is the total strain produced at the representative region by the indentation process. If, however, the metal has been previously cold worked, we may consider it as annealed material that has undergone an initial strain ε_0 and the total strain produced at the representative region is found to be

$$\varepsilon = \varepsilon_0 + \text{fn}(d/D)$$

Since elastic stress Y is a single value function of the strain

$$Y = \phi\ (\varepsilon)$$

so that the representative value of the elastic stress becomes

$$Y_r = \phi\ (\varepsilon_0 + \text{fn}(d/D)\ ) \qquad 2.17$$

when full plasticity is reached. Tabor proved that there exists a relation-

ship between yield pressure q_m^* and Y_r

$$q_m^* = c\phi\ (\varepsilon_0 + fn(d/D)) \qquad 2.18$$

where c is a constant having a value of about 3.

His empirical tests suggest that the elastic stress at the edge of the indentation may be used as the representative value for the whole of the deformed material around the impression. Tabor[97] found that

$$\varepsilon_1 \simeq 20\ d/D$$

i.e., a ball of diameter 10 mm, gives an impression of 5 mm in a specimen, the ratio of d/D is ½; this means that the representative deformation is equivalent to a strain of 10% and the mean pressure involved in producing this indentation is about 2.8 Y. Again, Tabor defined full plasticity as being reached when $q_m \simeq c\ Y_r$ and for mild steel it happens when $d/D > 0.1$ and slightly smaller for copper.

The most interesting extension of Tabor's analysis is that the experiments showed that the representative deformation is approximately additive to the initial deformation

$$\varepsilon = \varepsilon_0 + fn(d/D)$$

also

$$q_m^* = cY \qquad (c = 2.8)$$

and

$$Y = b\varepsilon^x \qquad \text{(Nadai, 1931)}$$

where b and x are constants for the metal.

He obtained a series of q_m^*-d/D curves that have been displaced along the strain-axis by the amount equal to the initial deformation of the specimen. An idealized curve is shown in Fig.2.15 for a specimen that has been deformed by 0, 30, 70 per cent. Experiments with annealed copper and

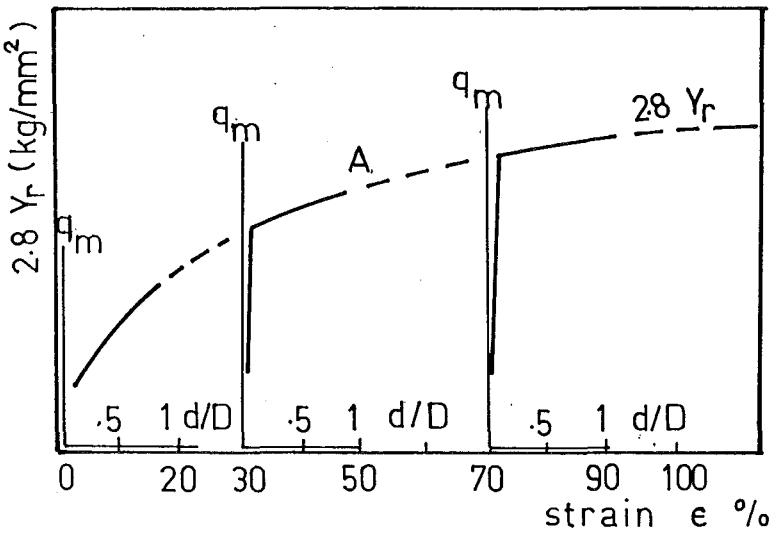

Fig. 2.15 Idealized curve showing the 2.8Y - strain and the mean pressure - d/D curves for specimen deformed by 0, 30 and 70%. (Tabor[97])

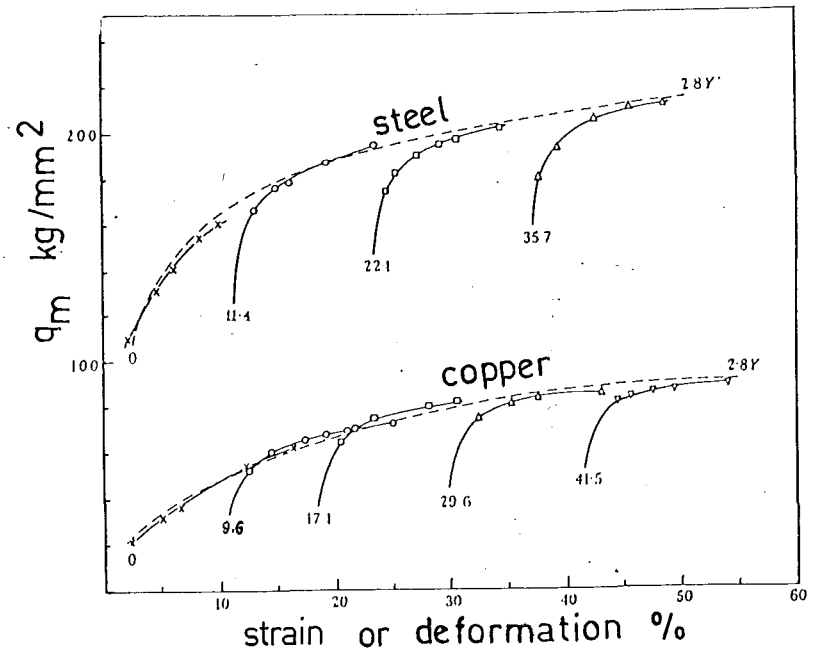

Fig. 2.16 Experimental results of mild steel and annealed copper specimens which have been deformed by various amounts. (Tabor[96])

bright mild steel specimens that have been deformed in compression by various amounts follow very well with the idealized curve except at low small indentations (Fig.2.16). This is to be expected for practical situations where q_m cannot change abruptly as suggested in the ideal curve. He also noted that for partially work-hardened material full plasticity is only reached for relatively large indentations so that c can be considered constant.

As the amount of initial cold work increases, the q_m-d/D curve is shifted to the right and eventually q_m will not increase at large indentation; this is the stage of fully work-hardened metal or ideal plastic behaviour.

Though the stress-strain curves for an annealed metal (Fig.2.11) and for the same metal which is fully work-hardened (Fig.2.8) are completely different in shape, they have, in fact, a relationship that is explainable (Fig.2.16). Let Y be the yield stress of a metal at any state (the more cold work, the higher Y). As the loading increases:

- Within the elastic zone q_m rises till 1.1 Y and is proportional to $W^{1/3}$ (according to Hertz)
- In the transitional zone q_m rises with a slower rate than $W^{1/3}$ that we have yet to determine
- When full plasticity is reached, i.e. d/D = .1 for steel and slightly smaller for copper, the mean pressure q_m is called the yield pressure q_m^*. If, as in Fig.2.15, we draw a curve (A) of 2.8 Y_r vs ε from origin 0, and with moving coordinates q_m-d/D (with d/D = $\varepsilon_1/20$) shift the origin to 0' along the ε axis, then 00' represents the initial amount of cold work and q_m^* will follow closely the curve (A).

In the next section we will consider a theory based on the elastic recovery of the metal in any state (annealed, partially or fully work-hardened) which enables us to determine the total approach of a hard sphere indented on

a flat surface.

2.3 THEORY

The process of loading a hard sphere of radius R_1 on to a flat work piece can be described in the following order. Let E_1, E_2 be Young's modulus of elasticity of the sphere and work-piece respectively. For most materials Poisson's ratio is about 0.3, hence assume $\mu_1 = \mu_2 = 0.3$

(a) The Work-Piece in a Wholly Elastic State

Past published results have shown that the Hertz law is valid below the load W_E which is called by Tabor the onset-of-plasticity load. On the removal of this applied load, no permanent deformation is left in the work-piece. Under these conditions the diameter of the contact circle is

$$d = 1.761 \left[WR_1 \left(\frac{1}{E_1} + \frac{1}{E_2} \right) \right]^{1/3} \qquad 2.19$$

and the total deformation of the system is:

$$\delta_e = 0.775 \left[\frac{W^2}{R_1} \left(\frac{1}{E_1} + \frac{1}{E_2} \right)^2 \right]^{1/3} \qquad 2.20$$

Davies[16] (1949) found that the maximum radial shear stresses at a point z (Fig.2.7) occur at about 0.25 d below the centre of the circle of contact, are equal and have a value of 0.47 q_m. From the Tresca criterion, plastic flow will occur when these shear stresses equal Y /2, i.e., $q_m \simeq 1.1\ Y$. The onset of plasticity load W was found to be

$$W_E = 14.461\ q_{mE}^{\ 3}\ R_1^{\ 2} \left(\frac{1}{E_1} + \frac{1}{E_2} \right)^2 \qquad 2.21$$

with $q_{mE} = 1.1\ Y$, Y is the yield stress or, where the yield stress does not exist, the 0.2% proof stress of that material.

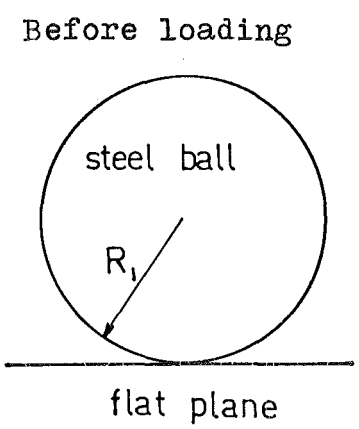

Fig. 2.17

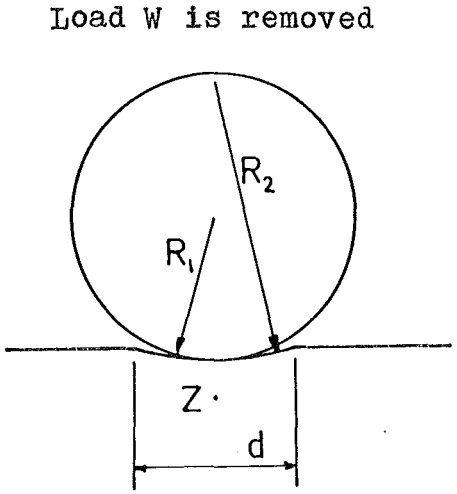

Fig. 2.18 Shape of the indentation.

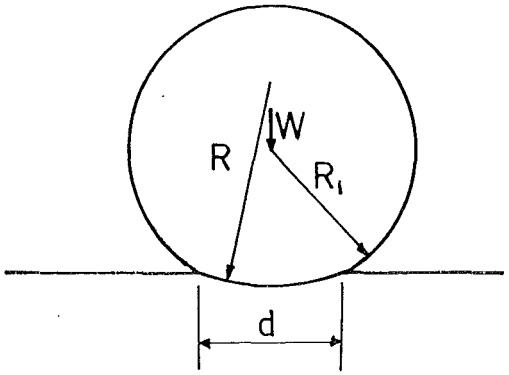

Fig. 2.19 The shape of the system under loading.

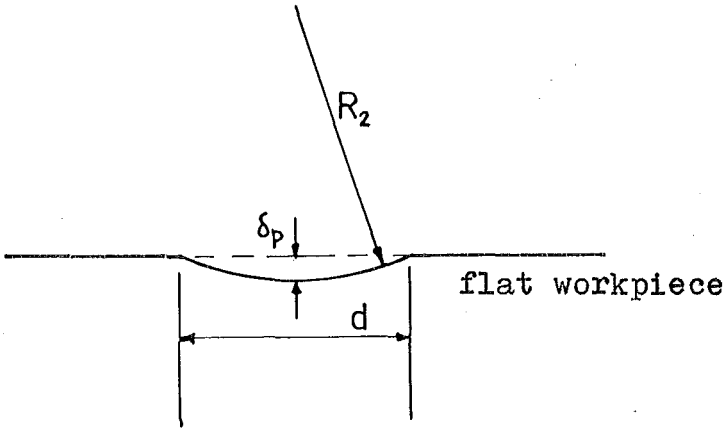

Fig. 2.20 The plastic component of the deformation.

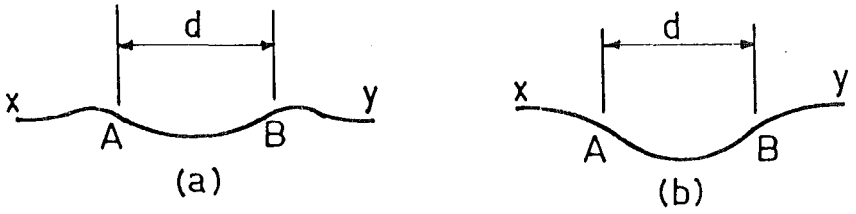

Fig. 2.21 Two typical shapes of the indentation.

(b) The Work-Piece partly in an Elastic and partly in a Plastic State

As the load increases above W_E, the amount of plastic deformation around the indentation increases and on removing the load, a permanent deformation is left in the work-piece surface. Careful measurement by Foss and Brumfield[28] (1922) has shown that the indentation is of spherical form but its radius of curvature may, for hard metals, be as much as three times that of the indenter. In a study on various metals Tabor[96] (1948) found that the diameter of this indentation increases only a few per cent if the same load is applied and removed a number of times. He described this as the release of elastic stresses in the work-piece, making the recovery of the indentation when the load is removed "reversible". To relate this elastic recovery with Hertz's law, let us consider the indentation by a very hard sphere of radius R_1 on a spherical surface of the work-piece of radius R_2 under a load W, both surfaces deforming elastically to a common radius of curvature R where $R_1 < R < R_2$ Figs. 2.18 and 2.19. It is interesting to find that the diameter of the contact surface calculated from Hertz's theory is approximately equal to the diameter of the indentation left in the work-piece after the removal of load W. Experiments by Tabor[96] (1948), Batson[96] (1918) and Foss and Brumfield[28] (1922) on different metals for ranges of loadings and ball diameters (Table 2.2) showed the agreement with the Hertz values to within a few per cent for most cases.

From these results we propose to consider the total deformation of the indentation of a ball into any metal as composed of two components as follows:

(i) Plastic Deformation δ_p is calculated by the permanent indentation diameter d and radius of curvature R_2 left on the surface of the work-piece after the removal of load W, Fig.2.20

TABLE 2.2

Material	E_2 $10^3 kg/mm^2$	Load (kg)	Observed values (cm)			Calculated d (cm)
			R_1	R_2	d	
(A)						
Brass	10	250	0.5	0.64	0.160	0.17
	10	500	0.952	1.21	0.27	0.26
Al.alloy	7	250	0.5	0.66	0.178	0.18
	7	500	0.952	1.15	0.26	0.30
Mild steel	20	500	0.5	0.605	0.183	0.20
Hardened steel	20	1000	0.5	0.677	0.202	0.22
	20	3000	0.952	1.39	0.330	0.36
	20	3000	1.59	2.80	0.370	0.38
(B)						
Ni-Cr Steel	20	3000	0.5	.627	.324	.34
Manganese steel	20	3000	0.5	.569	.407	.41
Rail steel	20	3000	0.5	.537	.445	.49
(C)						
Soft brass 1	9	3000	0.5	.518	.555	.7
2	9	500	0.5	.521	.330	.38
Hard bronze 3	7.2	3000	0.5	.527	.497	.66
Soft bronze 4	7.2	500	0.5	.557	.276	.28
Hard bronze 5	7.2	3000	0.5	.531	.499	.60
Soft bronze 6	7.2	500	0.5	.566	.302	.28
Steel .5C-A	20	3000	0.5	.56	.440	.43
Steel .5C-W	20	3000	0.5	1.03	.26	.25
Steel .9C-T	20	3000	0.5	.814	.31	.28
Steel .9C-W	20	3000	0.5	1.372	.24	.23
Steel MKD 455	20	3000	0.5	.568	.349	.36

A = By Tabor[96]

B = By Batson quoted in Ref. 96.

C = By Foss and Brumfreld[28]

$$\delta_p \ (2R_2 - \delta_p) = d^2/4$$

$$\therefore \quad \delta_p = d^2/4 \ (2R_2 - \delta_p) \simeq d^2/8R_2 \qquad 2.21$$

since $\delta_p << 2R_2$ > Ball dia.

(ii) Elastic Deformation δ_e

Applying Hertz's theory to the case of loading two spherical surfaces of radius R_1 and R_2 by a load W (Fig.2.18), where R_2 is a concave radius of curvature, Equation 2.2 becomes

$$\delta_e = \left[\frac{9\pi^2}{16} \ \frac{W^2 (k_1 + k_2)^2 \ (R_2 - R_1)}{R_1 \ R_2} \right]^{1/3} \qquad 2.22$$

$$\text{i.e., } \delta_e = .775 \left[\frac{W^2 \ (R_2 - R_1)}{R_1 \ R_2} \ \left(\frac{1}{E_1} + \frac{1}{E_2} \right)^2 \right]^{1/3} \qquad 2.23$$

when $\mu_1 = \mu_2 = 0.3$, the value of Poisson's ratio for most metal.

The total deformation of the system is

$$\delta_t = \delta_p + \delta_e \qquad 2.24$$

The diameter d of the contact area can be found from the Hertz equation for any given load W, ball radius R_1 and the measured value of the radius of curvature R_2 of the permanent deformation on the work piece surface. From Equation 2.1, for a concave radius R_2

$$d = 2 \left[\frac{3\pi}{4} \ \frac{WR_1 \ R_2}{R_2 - R_1} \ \frac{1}{\pi} \left[\frac{1 - \mu_1^2}{E_1} + \frac{1 - \mu_2^2}{E_2} \right) \right]^{1/3} \qquad 2.25$$

In a discussion of the derivation of this equation, Prescott[80] has indicated that even if the surface XABY is not a plane, the same equation will result. If, for example, the surface piles up at the region A & B as in Fig.2la or falls as in Figure 2.21b, the above equation is still valid

provided the projections or depressions at A and B are not too marked.

With $\mu_1 = \mu_2 = 0.3$

$$d = 1.761 \left[\frac{WR_1 R_2}{R_2 - R_1} \left(\frac{1}{E_1} + \frac{1}{E_2} \right) \right]^{1/3} \qquad 2.26$$

However, since the diameter of the impression is easier to be measured than the radius of curvature R_2, it is wiser to find R_2 from W, R_1 and d. Taking both sides of Equation 2.26 to the power of 3 and rearrange to get

$$R_2 - R_1 = 1.761^3 \frac{WR_1 R_2}{d^3} \left(\frac{1}{E_1} + \frac{1}{E_2} \right)$$

Divide both sides by $R_1 R_2$ and rearrange to get

$$\frac{1}{R_2} = \frac{1}{R_1} - 5.46 \frac{W}{d^3} \left(\frac{1}{E_1} + \frac{1}{E_2} \right) \qquad 2.27$$

If we substitute this result into Equations 2.21 and 2.23

$$\delta_p = \frac{d^2}{8} \left[\frac{2}{D} - 5.46 \frac{W}{d^3} \left(\frac{1}{E_1} + \frac{1}{E_2} \right) \right] \qquad \text{where } D = 2R_1$$

$$\delta_p = \frac{d^2}{4D} - .682 \frac{W}{d} \left(\frac{1}{E_1} + \frac{1}{E_2} \right) \qquad 2.28$$

while
$$\delta_e = .775 \left[\frac{W^2}{R_1} \left(\frac{1}{E_1} + \frac{1}{E_2} \right)^2 - \frac{W^2}{R_1} \left(\frac{1}{E_1} + \frac{1}{E_2} \right)^2 + \right.$$

$$\left. + 5.46 \frac{W^3}{d^3} \left(\frac{1}{E_1} + \frac{1}{E_2} \right)^3 \right]^{1/3}$$

i.e.
$$\delta_e = 1.364 \frac{W}{d} \left(\frac{1}{E_1} + \frac{1}{E_2} \right) \qquad 2.29$$

then
$$\delta_t = \delta_p + \delta_e = \frac{d^2}{4D} + .682 \frac{W}{d} \left(\frac{1}{E_1} + \frac{1}{E_2} \right) \qquad 2.30$$

or $$\delta_t = \frac{d^2}{4D} + \frac{\delta_e}{2} \qquad 2.31$$

Equation 2.31 is very interesting since for any given load W, the total deformation δ_t can be calculated easily provided the corresponding diameter of indentation d is also known. This implies that it is not necessary to calculate the plastic deformation δ_p and the elastic deformation can be calculated easily.

Assuming that at a given load W we overstimate the value of the indentation diameter, then the first term in the RHS of Equation 2.30 is larger than its actual value, while the second term is smaller than its actual value and vice versa. In effect, this behaviour minimises the error in δ_t for an estimated value of indentation diameter at a certain load slightly higher or lower than the actual value.

In the next part we intend to report our study in two sections:

1. The first reports the outcome of the following proposed courses of action, carry out experimentally a series of indentation from a very low load by a ball of diameter D on a flat work-piece, measure the diameter of indentation, obtain W-d curve, predict the total deformation using Equation 2.30, then compare this with the actual deformation recorded experimentally with our apparatus, which is described in Section 2.5.

   Repeat the whole process with the same metal at different conditions of heat treatment. Repeat for other metals as well.

2. In the second, we set out to find some way to establish the relationship W-d without carrying out the whole series of indentation, by using the least possible properties of that metal.

2.4 SECTION 1: OBTAIN W-d EXPERIMENTALLY - COMPARE OUR PROPOSED VALUE OF THE TOTAL DEFORMATION WITH THE ACTUAL VALUE

Before carrying out the experiment, it would be a good idea to give a rough picture of the relationship W-d in different zones.

(a) Within the Elastic State, i.e. when $W < W_E$,the Hertz law gives

$$d = 1.761 \left[W R_1 \left(\frac{1}{E_1} + \frac{1}{E_2} \right) \right]^{1/3}$$

i.e., $W \alpha d^3$ or $W = kd^3$ where k is a constant, i.e., the slope of the straight line logW - logd is 3 and ends at load W_E where

$$W_E = 14.461 \, q_{mE}^{\ 3} \, R_1^{\ 2} \left(\frac{1}{E_1} + \frac{1}{E_2} \right) \qquad 2.32$$

Substitute $q_{mE} = 1.1 Y$ and assume that the maximum possible value for Y is $\frac{1}{3} H_B$. Since q_{mE} has the highest power in Equation 2.24, it dominates the value of Young's modulus E_2. We may say that the harder the material the higher W_E. Calculation for various materials show that the ratio d_E/D is very much smaller than 0.10. e.g., for Steel $H_B = 354$ kg/mm^2, $d_E/D \simeq 0.03$. The value of W_E/D^2 is also of interest, for steel $W_E/D^2 \simeq 0.08$. More details are shown in Table 2.9 for our work pieces when D = 31.75 mm.

(b) In Fully Plastic State

The first well known relationship between load and size of the indentation by a ball of diameter D is the Meyer law (1908)

$$W = kd^n$$

where k and n are constants for the material. Experiments showed that n is independent of ball size and generally greater than or equal to 2. It was found that for fully work-hardened material n is close to 2 and for some fully annealed metals, n might reach 2.6 (Fig.2.22). A detailed collection of values of n is shown in Appendices 2.1 and

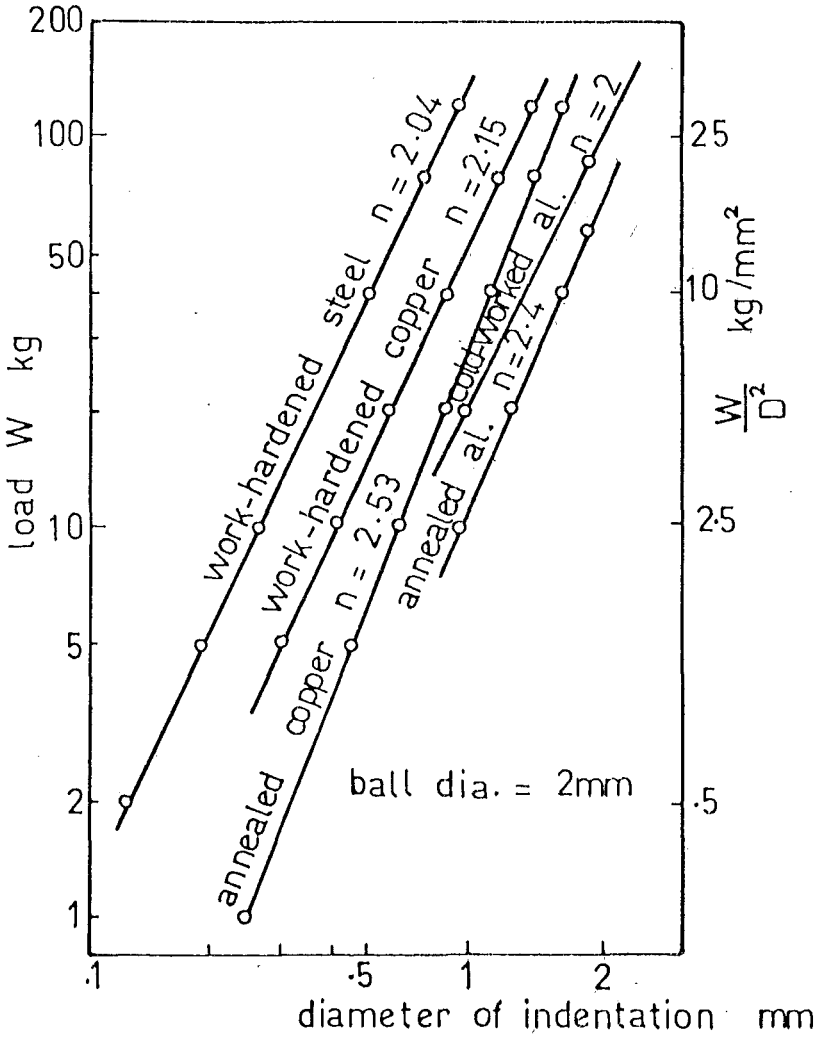

Fig. 2.22 The relation between W and d. (Tabor[97])

2.2. It is observed that these values of n are obtained experimentally for a range of the loading ratio W/D^2 from 5 to 50 for steels, and from 1.25 to 30 for softer metals like copper and aluminium alloys. A careful study by Tabor[97] (1951) concluded that full plasticity will be reached for mild steel when $\frac{d}{D}$ is greater than about 0.1, and at a slightly smaller value for copper. Meyer's theory is, in fact, only valid in the fully plastic state, i.e., where the constant n does not change as the load or the size of indentation increases. It is also of interest to observe that the standard ratio of loading $\frac{W}{D^2}$ recommended in BS 240, Part 1 (1962) Table 2.3, to obtain Brinell hardness is lying in the middle of the fully plastic zone.

Following Tabor we will assume that the fully plastic zone of the graph lowW-logd to start from $\frac{d}{D} = 0.1$ for steel and possibly from 0.08 for softer metals such as Copper, Aluminium alloys, Brass, Nickel etc.

(c) In the Transition Zone between the Elastic and fully Plastic Zones.

It is logical to say that the transition zone can be represented by one or more straight lines connecting W_E and W_P and having slopes decreasing steadily from 3 to the Meyer constant n (Fig.2.23). Indentations by O'Neill[75] (1923) at low loads, plotted by Tabor (Fig.2.24) for different steels, and an experiment by Tabor with fully work-hardened steel (Fig.2.25) also show the same trend. At this stage we do not know exactly how to assess the change in the slope of the straight lines within the transition zone, but a need has arisen to test the fitness of the proposed theory for the deformation in the transition zone and in fully plastic zone as well.

2.5 APPARATUS AND SPECIMENS

Due to the availability of various sizes of ball bearings, an apparatus (Fig.2.26) was made to attach the ball into the 30000 lbs W & T Avery

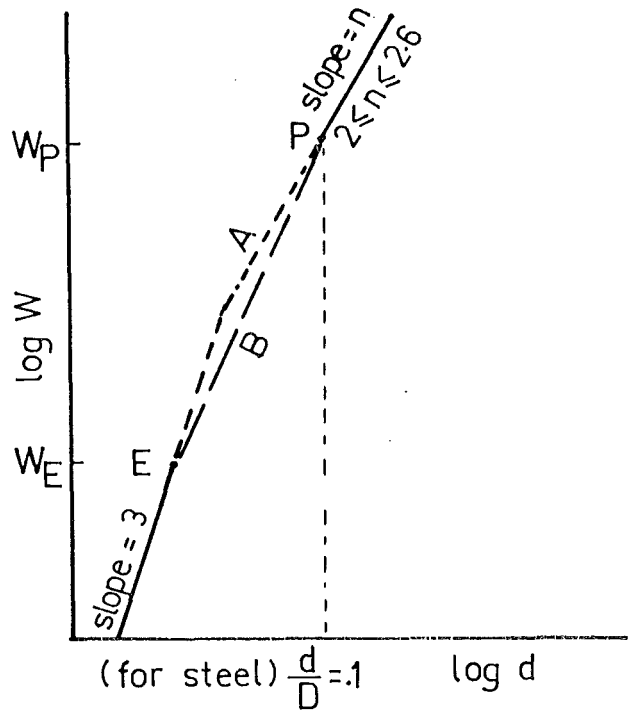

Fig. 2.23 The relation between logW and logd.

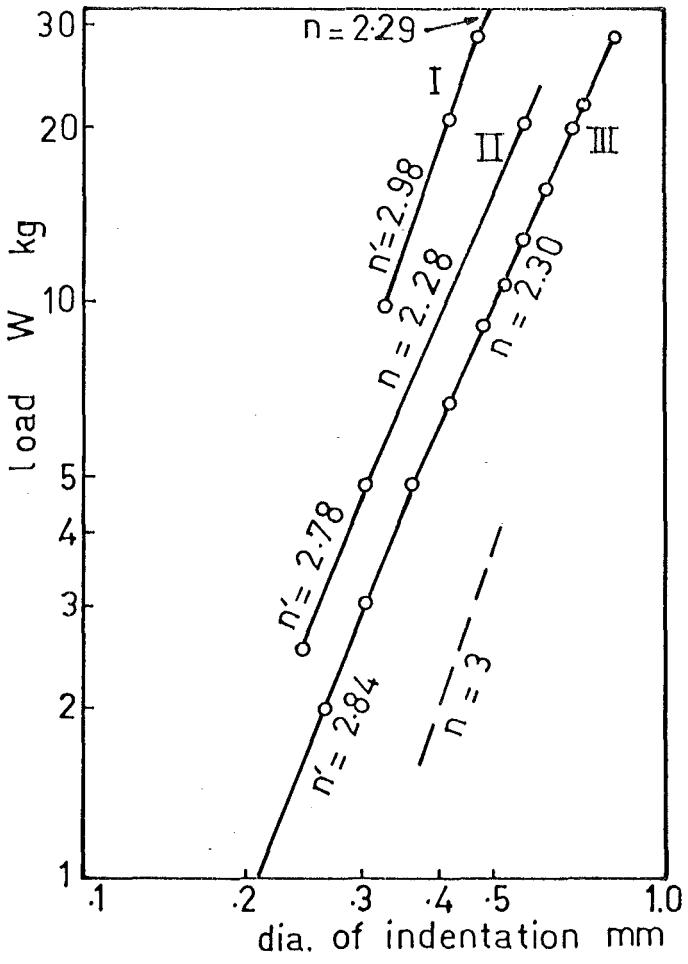

Fig. 2.24 For smaller indentations n increases towards 3. Curves I,II,III are for steels W,A and soft iron respectively.(Tabor (97))

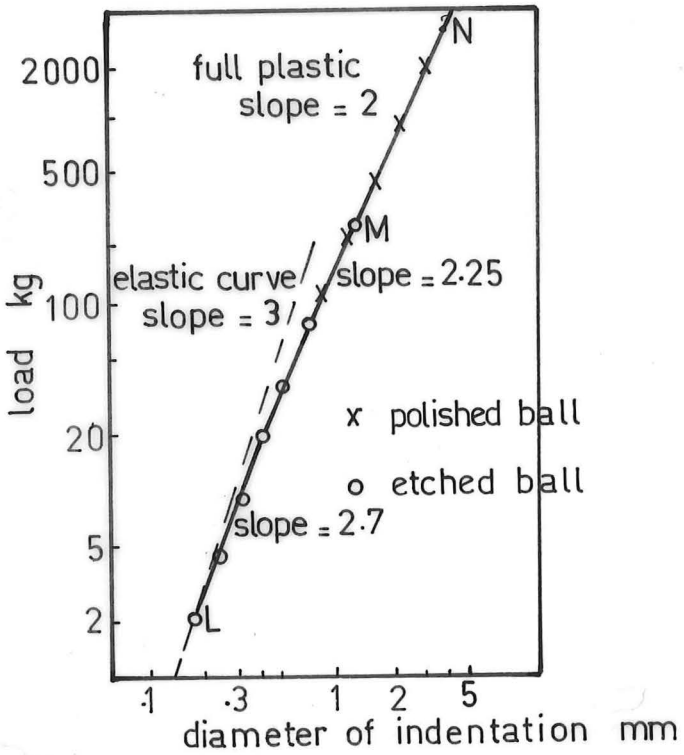

Fig. 2.25 Indentation of work-hardened mild steel $Y_o = 77\ kg/mm^2$ Experimental data plotted by Tabor[97]. Ball diameter 10mm.

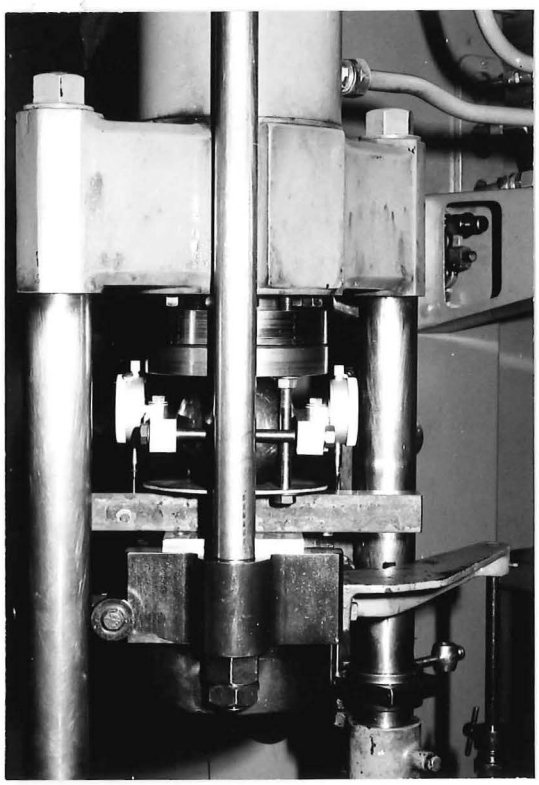

Fig. 2.26 Ball used is 100 mm diameter.

hydraulic press in our Department. The general arrangement of the machine and the apparatus is shown in Fig.2.27a. Detailed pictures can be seen in Figs.2.27b and 2.27c. An electric motor was used to supply oil from the reservoir to the cylinder, to lift the ram as well as the lower compression platen at a strain rate controlled by the straining rods. The ball was attached to the upper compression platen locator by two tie bolts. The two dial gauges, reading up to 1 micron, were symmetrically bolted to the two tie bars, the latter were also bolted rigidly to the ball at its horizontal diameter.

The materials of the test pieces were steel, water quenched then tempered to different temperatures, Aluminium alloy, Copper and Brass. A detailed summary of their properties is shown in Table 2.4.

The Brinell hardness of each individual work-piece was measured by the Avery No. 6403 Brinell hardness tester, with indenters made of hard steel balls of 5 and 10 mm diameter. The specific loading $Z = \frac{W}{D^2}$ (W = load in kg, D = ball diameter in mm) is specified in BS 240, Part 1, 1962, i.e., 30 for steel and 10 for other work-pieces. (Table 2.3).

The diameter of the indentation was recorded by the Nikkon shadowgraphs, magnification 20X with a resolution of about ±.02 mm. The error increases for the shallow indentation.

The Meyer constant n was obtained by carrying out a series of indentation in the fully plastic zone (i.e., the ratio of $\frac{d}{D} > 0.1$). The load-indentation diameter data were fed into the 'least square power curve $W = Ad^B$' program of the Hewlett Packard 9100 Calculator in our Department, see Table 2.5.

At below 100 lbs the actual deformation was small and readings on the dial gauges were unreliable owing to the uneven loading on the two symmetrical straining rods of the machine. Therefore, deformations

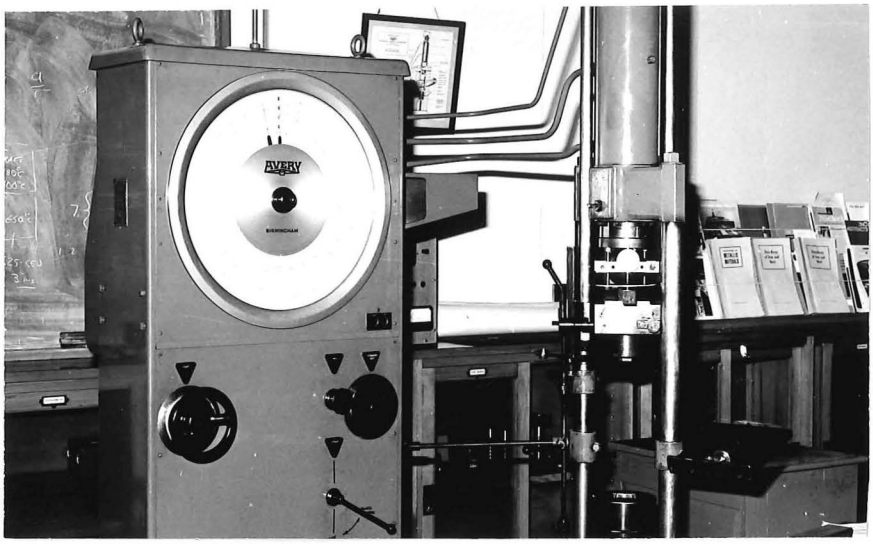

(a)

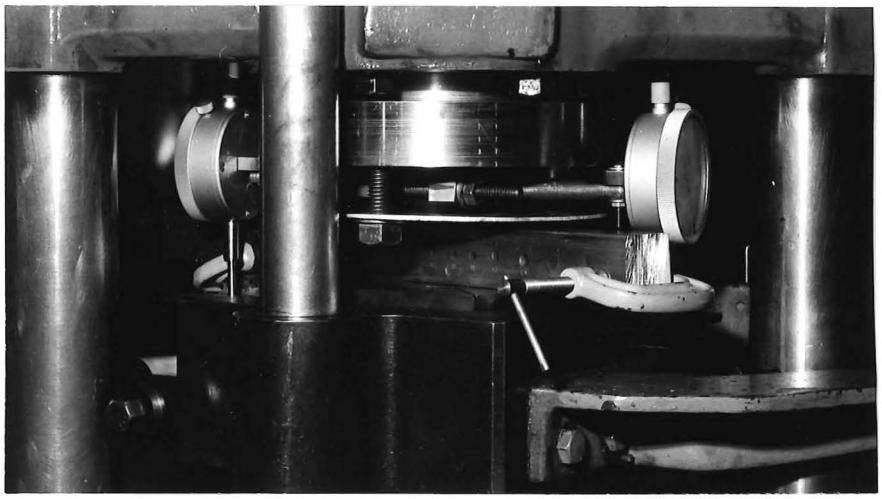

(b)

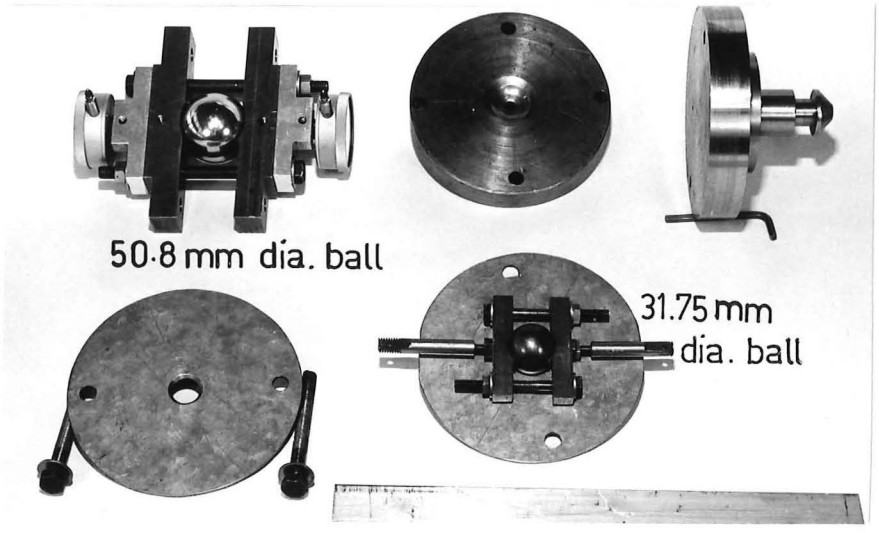

(c)

Fig. 2.27 (a) General arrangement of the machine & apparatus.

(b) Ball used is 31.75 mm diameter.

(c) Designed apparatus to attach the ball into the upper platen of the machine.

Table 2.4 Specifications of the workpieces

Symbol	Material	H_B (kg/mm²)	Meyer n	W_{min}/D^2 (kg/mm²)	W_{max}/D^2 (kg/mm²)
AL1	Al.alloy BS1476 HE30 W.P. $1\frac{1}{4}$" square bar, annealed at 300°C	31.3	2·25	2.5	15
AL2	Al.alloy BS 1476 HE 30 W.P. 1" square bar	97	2·10	2·5	30
CO1	Copper 1" square bar	75	2.15	2.5	30
CO2	CO1 then annealed at 800°C cooled in oven	44.6	2·467	2·5	17.5
BR	Brass BS 2874 CZ 121 1" square bar	112	2·30	2·5	30
S1	Steel $1\frac{1}{4}$" square bar, as rolled	188	2·36	10	50
S2	S1 then water quenched at 850°C, tempered at 600°C	249	2.15	10	50
S3	〃 〃 450°C	306	2·16	〃	〃
S4	〃 〃 300°C	354	2·09	〃	〃
S5	Bright cold drawn steel 1" square bar	156	2·10	〃	〃
S6	Mild steel BS 4360-43A 1" square bar, as rolled	137	2.20	〃	〃

Table 2.3 BS 240 Part 1 (1962)

Specimen suggested range of H_B (kg/mm²)	over 100	30 – 200	15 – 100	3 – 20
Loading ratio W/D^2 (kg/mm²)	30	10	5	1

Table 2.5 Indentation in the fully plastic zone of flat workpieces (to obtain Meyer constant n)

†	STEEL						AL. ALLOY		COPPER		BRASS
Brinell Hardness	137	cold drawn 156	188	249	306	354	31.3	97	75	44.6	112
W (kg)	Indentation diameter (mm)										
250	1,54	1.46	1·40	1.12	1·05	·94	3·21	1·84	2.10	2·295	1·80
500	2.12	2.01	1.87	1.54	1.45	1·35	4.34	2.56	2·93	3.88	2.47
750	2.55	2.43	2·19	1.92	1.74	1·62	5·23	3.11	3·53	4·61	2·93
1000	2·89	2.81	2·53	2.12	2.02	1·82	6.04	3.54	4·03	5·15	3.32
1250	3.20	3.12	2.77	2.35	2.20	2.05	6.53	3.95		5.66	
1500		3·43					7.19	4·34	4·90		3·94
1750								4.66		6·48	
2000								4.98	5.60		4.48
2250								5.31			
2500								5.48			
3000								6.03	6.85		5.34
Meyer constants k	96·11	114·34	114·35	194·83	224·86	227.34	18.89	70.01	52.19	17,42	63.87
Meyer constants n	2·203	2·10	2·355	2·152	2·156	2·086	2.222	2.091	2.112	2.467	2.296

$W = kd^n$ (kg) (mm)

† For steel : ball used is 5mm diamter ; for others : ball used is 10 mm diameter

were recorded relative to the deformation at 100 lbs, i.e., it was assumed that the deformation at 100 lbs was zero. Later on, depending on each particular case, we will estimate a value for the deformation of the system at 100 lbs and add this amount to the previously recorded deformation to get an estimated actual deformation at any particular load.

The ball bearings were supplied by SKF, their hardnesses were within the range of 60 - 66 Rockwell C[87]. The equivalent Brinell hardness is

(765 - 960 Vickers Hardness)
(627 - 712 HBN) . To avoid the plastic deformation of the ball itself, it requires that the hardness of the work-pieces must be at most 1/2.5 of the ball hardness[97]. For soft metals Brinell and Vicker hardnesses are approximately the same, for hard metals, the Vickers hardness is a better measurement and is preferred. Our hardest work-piece, with H_B = 354 kg/mm^2, is possibly the maximum allowable without the risk of plastic deformation of the ball.

2.6 EXPERIMENT AND COMPARISON

A series of indentation tests was carried out with a ball of 31.75 mm diameter from the lowest load possible at which the impression was sufficiently distinct for its diameter to be measured without much error on the Nikkon shadowgraph. Attempts were made to lower the load to the onset of plasticity load W_E of each work-piece. Unfortunately, the impression was so shallow and light that the error in recording its diameter increased significantly. Therefore, we had to limit our minimum load according to the hardness of the individual metal.

- For steel, the minimum load was about 500 lbs and the maximum at least 10,000 lbs.
- For other metals, minimum and maximum loads are shown in Table 2.6.

Due to the limitation of our minimum load, we can only obtain the

Table 2.6

MATERIAL	BALL DIA. = 31.75 mm				50.8 mm			100 mm		
	$d_1 = A_1 W^{B_1}$		Range of validity		$d_2 = A_2 W^{B_1}$	Range of validity		$d_3 = A_3 W^{B_1}$	Range of validity	
	A_1	B_1	W_{min} lbs	W_{max} lbs	A_2	W_{min} lbs	W_{max} lbs	A_3	W_{min} lbs	W_{max} lbs
S1 : H_B = 188	·1294	·4166	500	10000	·1400	1280	25600	·1567	5000	99200
S2 : = 249	.0839	.4462	〃	〃	.0883	〃		.0949	〃	〃
S3 : = 306	.0785	.4456	〃	12000	.0826	〃	30700	.0889	〃	120000
S4 : = 354	.0753	.4447	1000	17000	.0793	2560	43500	.0855	10000	170000
S5 : = 156	.1148	.4352	500	27000	.1229	1280	69100	.1332	5000	270000
S6 : = 137	·1089	·4520	〃	10000	·1139	〃	25600	.1216	〃	100000
CO1 : = 75	·1286	.4582	350	16000	.1338	900	40900	.1415	3500	160000
CO2 : = 44.6	.3008	.4021	90	5000	.3298	230	12800	.3766	900	50000
AL1 : = 31.3	.1930	.4461	200	5000	.2002	500	〃	.2110	2000	〃
AL2 : = 97	.1192	.4514	80	4000	.1248	200	10000	.1333	800	40000
BR : = 112	·1393	.4315	400	10000	.1486	1000	25600	·1630	4000	100000

Table 2.7 Experimental results of the indentation of steel bars by a 31.75mm dia. steel ball

Material	S6		S5		S1		S2		S3		S4	
	W lbs	d mm	W lbs	d mm	W lbs	d mm	W lbs	d mm	W lbs	d mm	W lbs	d mm
	500	1·82	550	1.74	300	1.37	500	1.40	500	1·23	1000	1.63
	750	2·20	750	2.13	500	1·70	1000	1.78	1000	1·77	2000	2·20
	1000	2.39	1000	2·32	750	2.07	2000	2.40	2000	2.28	4000	3.05
	1500	2.09	4000	4.17	1000	2.36	4000	3·42	3000	2·79	6000	3·55
	2500	3·76	6000	5.03	2000	3.04	6000	4.08	4500	3·29	8000	4·10
	3500	4·39	8000	5·73	3000	3.61	3500	4.70	6500	3.96	11000	4·75
	5000	5.15	12000	6.93	4000	4.09	11000	5·49	10000	4·76	17000	5·60
	6500	5.73	16000	7.95	5000	4.50	16000	6·27	12000	5·16		
	7000	5.95	20000	9.11	6000	4·83	21000	7·17				
	8000	6.34	27000	10.41	8000	5.54	25000	7.76				
	9000	6.66			10000	8·98						
	10000	7.01										
least square power relation	·4520 d = ·1089W		·4352 d = ·1148W		·4166 d = ·1294W		·4462 d = ·0839W		·4456 d = ·0785W		·4447 d = ·0753W	
correlation coeficient	·9997		·9992		·9996		·9984		·9993		·9997	

experimental curve logW - logd for the upper part of the transition zone and the lower part of the fully plastic zone. The data W-d was fed into the program "least square fit power curve $Y = aX^b$" to obtain $d = AW^{1/n}$. This means that we are assuming there exists a straight line relationship logW - logd having a slope 1/n for the range of experimental loadings. This assumption holds very well since the correlation coefficient of fitness of the data was less than 1% error for all cases, see Tables 2.7 and 2.8.

The theoretical deformation was calculated by the following steps:

1. At a given load W, calculate the corresponding diameter of indentation d from the relationship $d = AW^{1/n}$ produced from the above program

2. Calculate elastic deformation δ_e by Equation 2.29.

3. Calculate the total deformation δ_t by Equation 2.31 with D = 31.75 mm.

Compare this theoretical δ_t call it δ_{tt}, with the actual deformation δ_{ta} obtained experimentally by our apparatus. Due to experimental difficulties, the following points must be noted in the comparison:

(1) δ_{tt} is valid only in the range of loading (e.g., 500 - 10,000 lbs for steel) in which we assume a straight line logW - logd relationship of slope 1/n. Since the onset of plasticity load W_E for most cases is below 500 lbs, to get δ_{tt} between W_E and 500 lbs using the same power equation, we must realise that the relative error may be high but the absolute error is small, i.e., in the order of a few microns, see Table 2.9.

(2) At below 100 lbs the actual deformation δ_{ta} is small. Since W_E is not far from 100 lbs we may assume that δ_{ta} at 100 lbs is completely elastic, and may be calculated by Equation 2.7 - i.e, the plastic component may be assumed negligible. This assumption is reasonable since the amount δ_{ta} at 100 lbs is very small compared with the

Table 2.8 Experimental results of the indentation of non-ferrous bars by a 31.75mm dia. steel ball

Material	AL1		AL2		CO2		CO1		BR	
	W lbs	d mm	W lbs	d mm	W lbs	d mm	W lbs	d mm	W lbs	d mm
	200	2.21	80	.87	350	1.89	90	1.90	400	1.87
	400	3.07	150	1.15	700	2.58	160	2.32	800	2.48
	750	4.11	300	1.57	2000	4.20	320	2.91	1500	3.24
	2000	6.38	500	1.94	4000	5.70	600	3.91	3000	4.39
	4000	8.78	750	2.34	7500	7.68	1400	5.52	5000	5.45
	5000	9.84	1000	2.69			3000	7.70	7500	6.50
			1500	3.22			5000	9.24	10000	7.55
			2100	3.80						
			2800	4.26						
			4000	5.01						
least square power relationship	$d = .1930 W^{.4461}$		$d = .1192 W^{.4514}$		$d = .1286 W^{.4582}$		$d = 3008 W^{.4021}$		$d = .1393 W^{.4315}$	
correlation coefficient	1.0000		.9999		1.0000		.9990		.9990	

Table 2.9 Comparision between experimental and theoretical deformations

	MATERIAL																	
	S1		S2		S3		S4		S5		AL1		AL2		BR		CO1	
(lbs) load	deformation (micron)																	
	δ_{ta}	δ_{tt}	δ_{ta}	δ_{tt}	δ_{ta}	δ_{tt}	δ_{ta}	δ_{tt}	δ_{ta}	δ_{tt}	δ_{ta}	δ_{tt}	δ_{ta}	δ_{tt}	δ_{ta}	δ_{tt}	δ_{ta}	δ_{tt}
100	7		7		7		7		7		24	24	13	13	12	12	13	13
200	16		15		14		12		18		48	44	23	22	24	21	23	22
500	28	32	25	25	25	24	21	23	32	32	110	99	46	45	45	43	44	48
1000	47	54	43	42	40	40	35	39	56	55	200	184	81	79	78	75	83	86
2000	83	93	73	72	68	67	61	65	100	96	368	343	148	139	136	131	154	157
3000	116	128	100	99	93	92	82	88	137	133	530	495	208	193	190	183	215	224
5000	187	191	151	149	139	137	125	130	209	203	830	786	323	297	285	278	340	351
7000	256	250	200	196	181	179	164	170	280	268					375	366	464	472
8000	291	278	225	218	200	199	183	188	313	299					420	408	520	532
W_E (lbs)	25.6		59		110		171		14.6		.5		14.4		12.4		3	
d_E / D	.014		.019		.023		.027		.012		.005		.015		.013		.008	
W_P (lbs)	3830		5160		5990		6830		2850		330		1080		1200		820	

† Assume $Y = 1.1 \times 1.04 H_B / 3$

deformation δ_{ta} at high load where close agreement between δ_{tt} and δ_{ta} was found.

Table 2.9 shows that the maximum relative error between δ_{tt} and δ_{ta} is about ± 6% for all cases. This result is quite satisfactory for the few assumptions we have made both in the theory and the experiment. Results of Table 2.9 are plotted in Fig. 2.28.

To get an idea of how small the onset of plasticity load W_E is, we assume that the yield stress is about 1/3 of the Brinell hardness and since the average ratio of the Meyer hardness over the Brinell hardness for our work-pieces is about 1.04, we have $Y \simeq (1.04/3\ H_B)$. The values of W_E can be calculated from Equation 2.32 with $q_m = (1.04 \times 1.1)/3\ H_B$ and are shown in Table 2.9. The ratio of d_E/D(d_E is the diameter of the indentation at load W_E) is also interesting since they are much less than .1 where full plasticity is reached (for steel) and 0.08 for Copper and Aluminium alloys.

The same experiment was repeated for non-ferrous metals and the comparison is shown in Table 2.9 or in Fig. 2.29. This time, the fully plastic load is calculated at $\frac{d}{D} = 0.08$ instead of .1. The assumption (2) above does not hold very well since the plastic deformation may be as much as twice the elastic deformation at 100 lbs for soft metals. In this case, it is much better to assume $\delta_{ta} = \delta_{tt}$ at 100 lbs.

The same experiment is now carried out with different balls of diameter 50.8 and 100 mm. Instead of repeating the whole series of indentation again with those balls in order to get the new logW - logd relationship, we can make use of the old relationship (i.e., of the equation obtained for the ball diameter 31.75 mm) found in the previous part with a few correction factors that we are going to discuss below:

- In the elastic zone, mean pressure

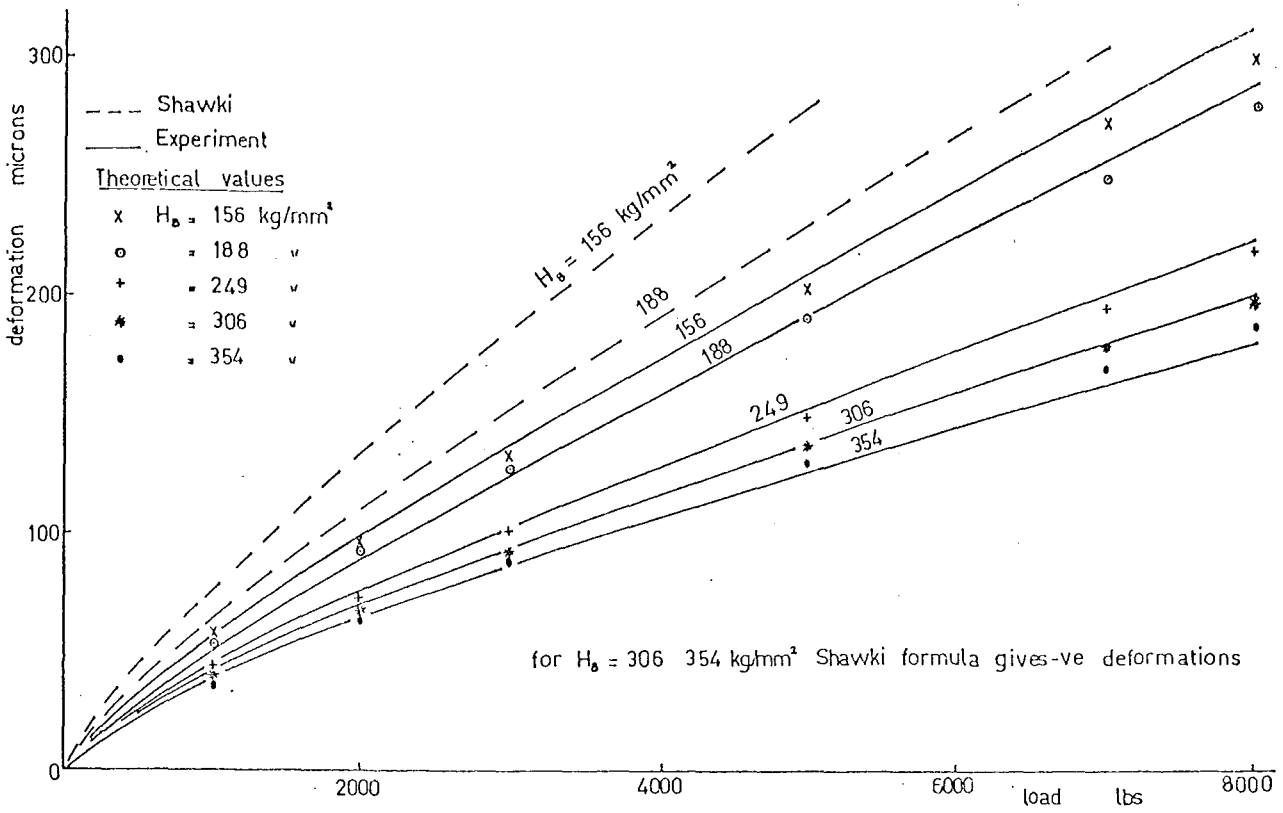

Fig. 2.28 The deformation of steel flat workpieces under a hard steel ball of diameter 31.75mm.

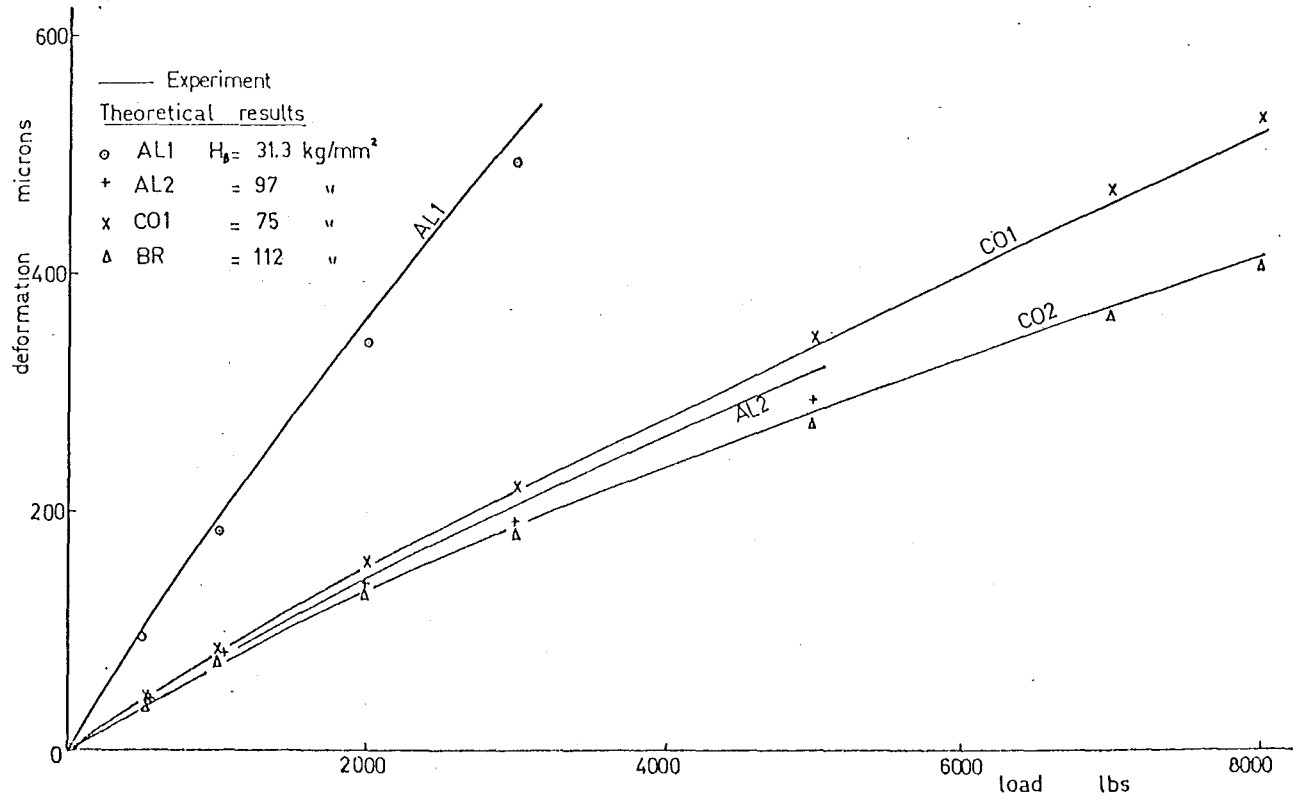

Fig. 2.29 The deformation of non-ferrous flat workpieces under a hard steel ball of diameter 31.75mm.

$$q_m = 4W/\pi D^2$$

Substitute for W by d in Equation 2.19 to get

$$q_m = \frac{4d}{\pi (1.761)^3 \frac{D}{2} \left(\frac{1}{E_1} + \frac{1}{E_2}\right)}$$

i.e.

$$q_m = .466 \left(\frac{E_1 E_2}{E_1 + E_2}\right) \left(\frac{d}{D}\right) \qquad 2.33$$

In general, we expect the mean pressure q_m to be a function of d/D. Experiments made by Krupkowski (Fig.2.30) on annealed copper with various ball diameters ranging from 1 to 30 mm showed that all the points q_m - d/D lie about a smooth curve. Our experiment on bright drawn steel also shows the same trend, see Fig. 2.31.

If we indent two balls of diameter D_1 and D_2 into the same metal, with loads W_1, W_2 respectively so that the same mean pressure occurs at the contact area, we always have

$$d_1/D_1 = d_2/D_2 \Rightarrow d_1 = (D_1/D_2)\, d_2 \qquad 2.34$$

Within the range of loading of the ball diameter D_1, assuming there exists

$$d_1 = A_1 W_1^{B_1}$$

i.e.

$$W_1 = (d_1/A_1)^{1/B_1} \qquad 2.35$$

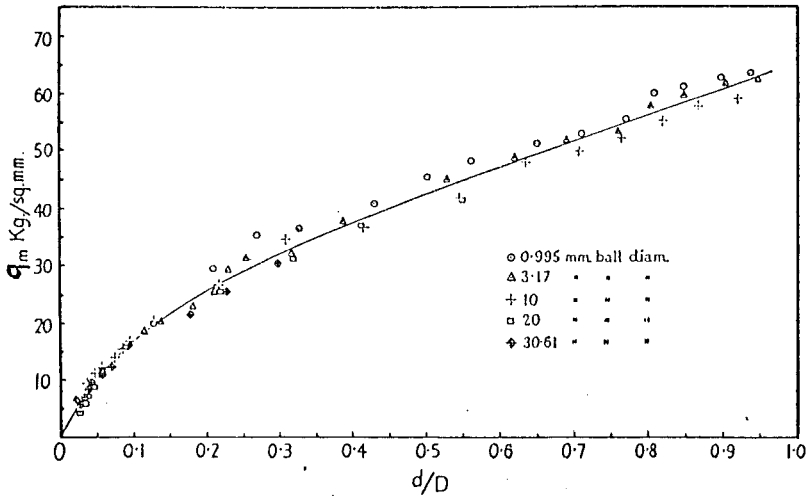

Fig. 2.30 The indentation of annealed copper for various loads and balls of various diameters. Data from Krupkowski (1931) drawn by Tabor[97].

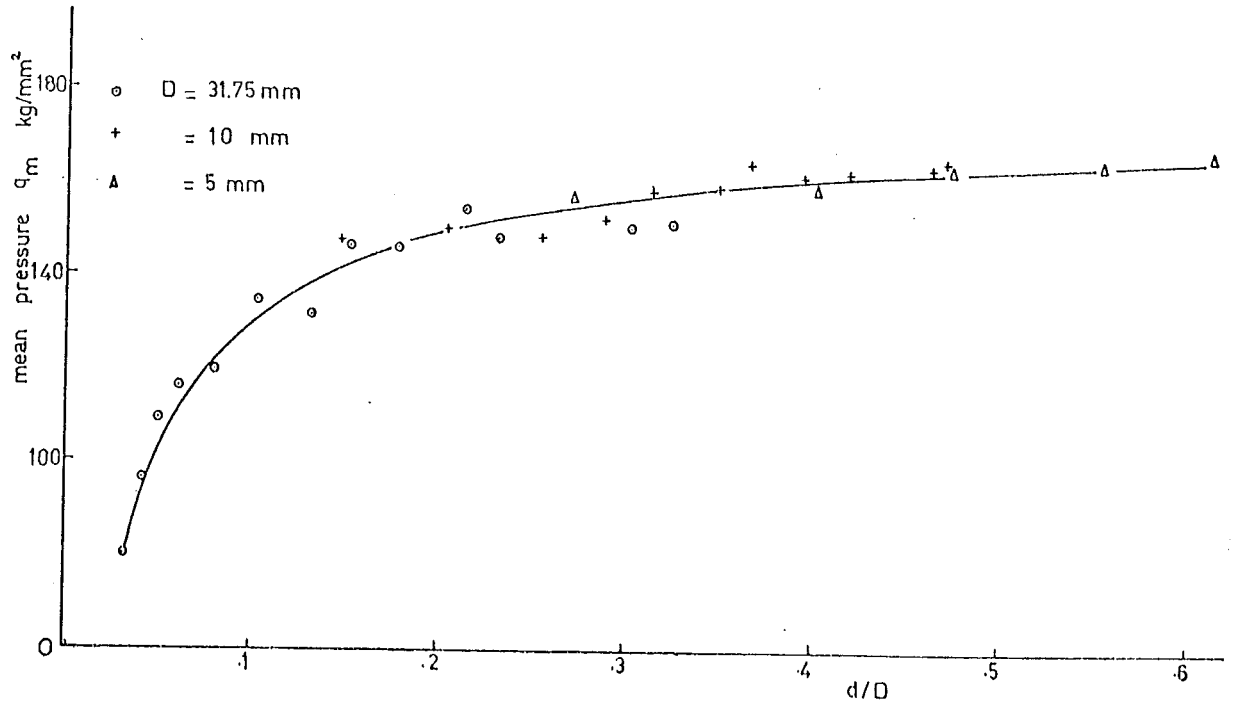

Fig. 2.31 The relation between mean pressure q_m and d/D for balls of various diameters indented on workpiece S5.

Mean pressure $q_m = 4W_1/\pi d_1^2 = 4W_2/\pi d_2^2$, i.e. $d_2^2 = (W_2/W_1)\, d_1^2$ 2.36

Substituting W_1 from Equation 2.35 into Equation 2.36

$$d_2^2 = (W_2/(d_1/A_1)^{1/B_1})\, d_1^2 = W_2\, A_1^{1/B_1}\, d_1^{2-(1/B_1)}$$

Substitute d_1 from Equation 2.34 into this Equation

$$d_2^2 = W_2 A_1^{1/B_1}\, (D_1/D_2)^{2-(1/B_1)}\, d_2^{2-(1/B_1)}$$

i.e. $$d_2 = A_1 (D_1/D_2)^{2B_1 - 1}\, W_2^{B_1} \qquad 2.37$$

Hence we have obtained a new relationship between d_2 and W_2 for the ball diameter of D_2 from the given relationship for the ball of diameter D_1. We can write

$$d_2 = A_2 W_2^{B_2}$$

where $$A_2 = A_1 (D_1/D_2)^{2B_1 - 1} \qquad 2.38$$

and $$B_2 = B_1 \qquad 2.39$$

Table 2.6 shows the new relationship between d - W for steels and other metals for ball diameters 50.8 and 100 mm derived from the relationship obtained experimentally for the ball of diameter 31.75 mm. Since the mean pressure $q_m = 4W/\pi d^2$ and for geometrical similarity d/D is constant, it follows that for similarity W/D^2 is a constant. If $d_1 = A_1 W_1^{B_1}$ holds only in the range W_1 min - W_1 max, the relationship $d_2 = A_2 W_2^{B_2}$ will hold for the range W_2 min - W_2 max where

$$W_1 \text{min}/D_1^2 = W_2 \text{min}/D_2^2$$

and

$$W_1 \text{max}/D_1^2 = W_2 \text{max}/D_2^2$$

i.e. $$W_2 min = (D_2^2/D_1^2)\ W_1 min$$

and $$W_2 max = (D_2^2/D_1^2)\ W_1 max \qquad 2.40$$

The d-W relationships were established experimentally for indentations with ball diameters of 50.8 and 100 mm and the above steps repeated to calculate the theoretical deformation δ_{tt} for each case. Again, the theoretical values have been compared with the actual deformation δ_{ta} in Figs. 2.32, 2.33 and 2.34. It is best to compare them in the range from minimum to maximum loads only. However, it may be of interest to note that the difference between δ_{tt} and δ_{ta} values below W_{min} was within ± 15%.

From these experiments, we found that the relationship between W and d is of primary importance for the determination of the total deformation of the indentation by a hard ball into a flat surface. In the next section we are going to discuss a method for deriving this relationship from a few mechanical properties of the work-piece.

In Figures 2.32 and 2.33, Shawki's predictions for the deformation of some of the work-pieces are also plotted to show the difference between his empirical formula and our experimental values.

2.7 SECTION 2: THE RELATIONSHIP BETWEEN LOAD AND THE DIAMETER OF THE INDENTATION

As we have pointed out in the last section, the total deformation of a hard steel ball on a flat surface can be calculated provided the relationship W-d is known. It is therefore necessary to study this relationship more carefully. The two well-known theories that can be used to establish d-W in two different zones of loading are as follows:

(1) When the applied load is so low that the flat surface still deforms elastically, Hertz proved that

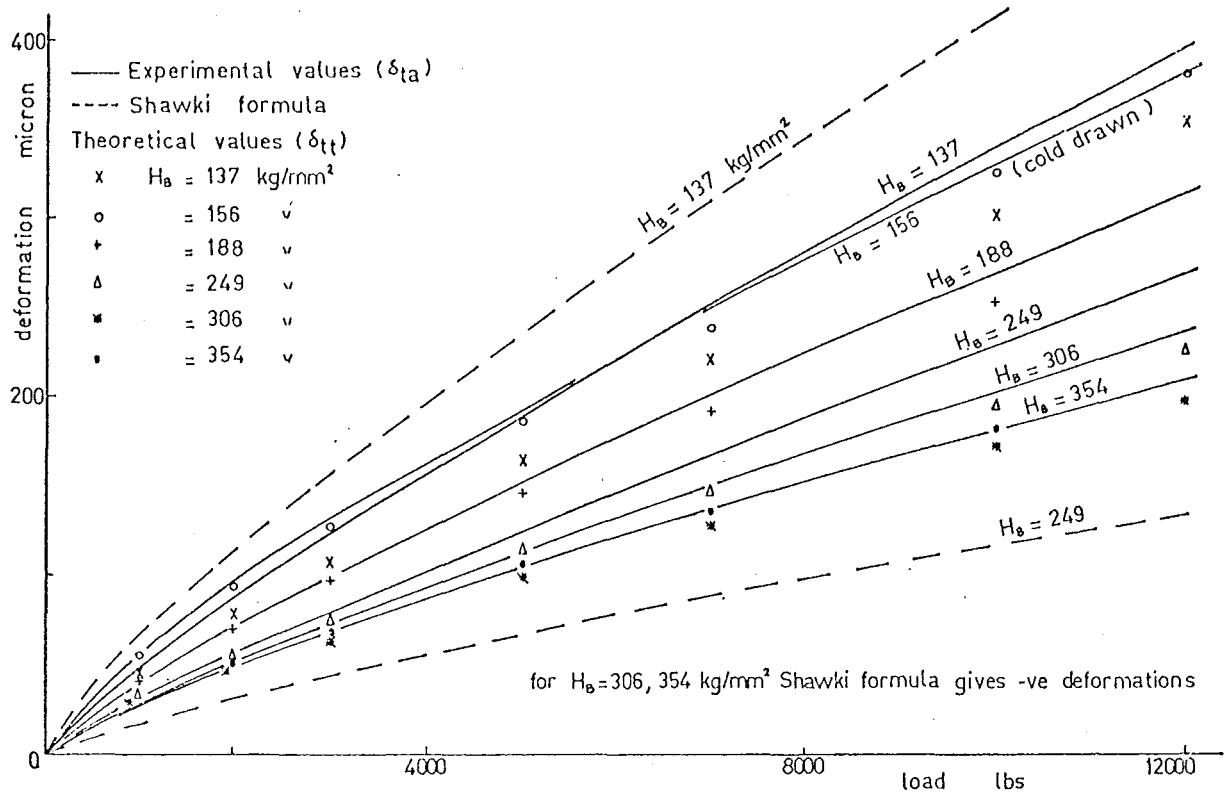

Fig. 2.32 The deformation of flat steel workpieces under a hard steel ball of diameter 50.8mm.

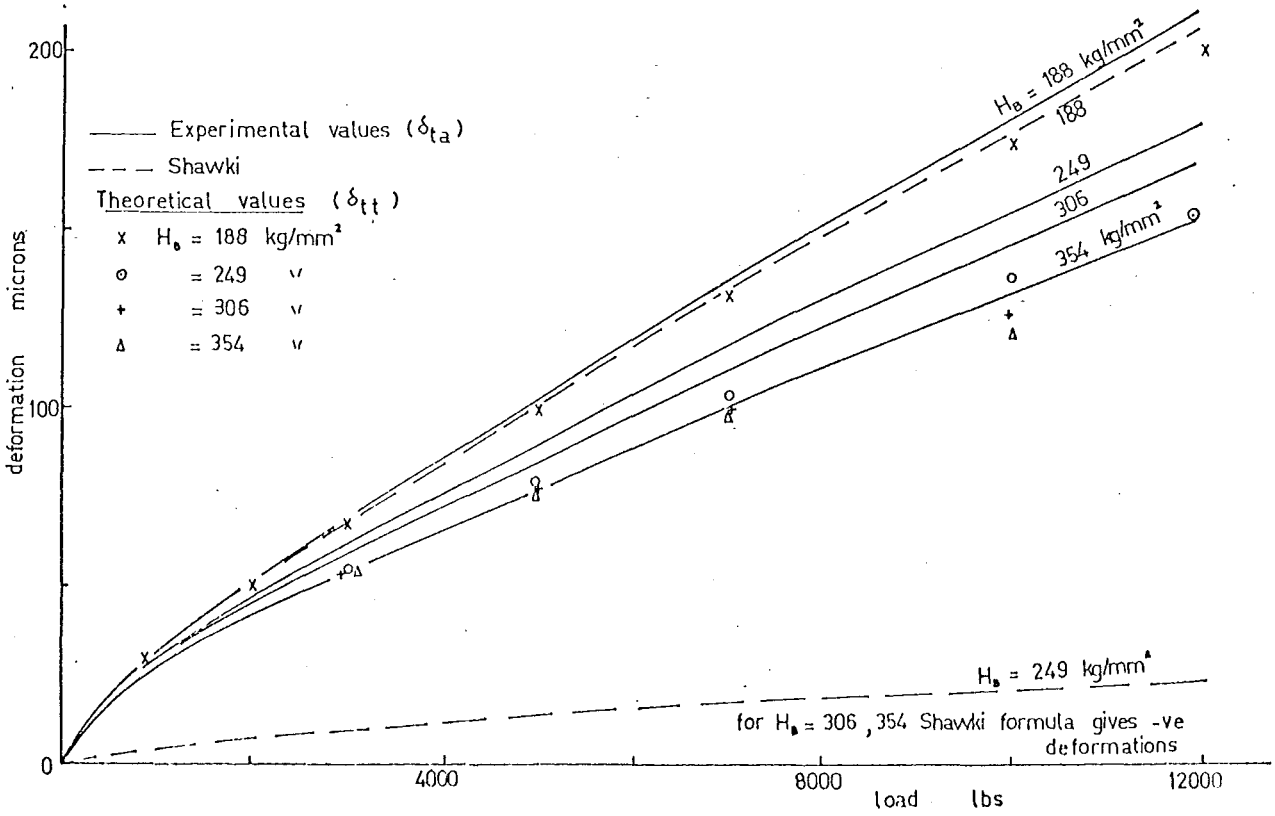

Fig. 2.33 The deformation of flat steel workpieces under a ball of diameter 100mm.

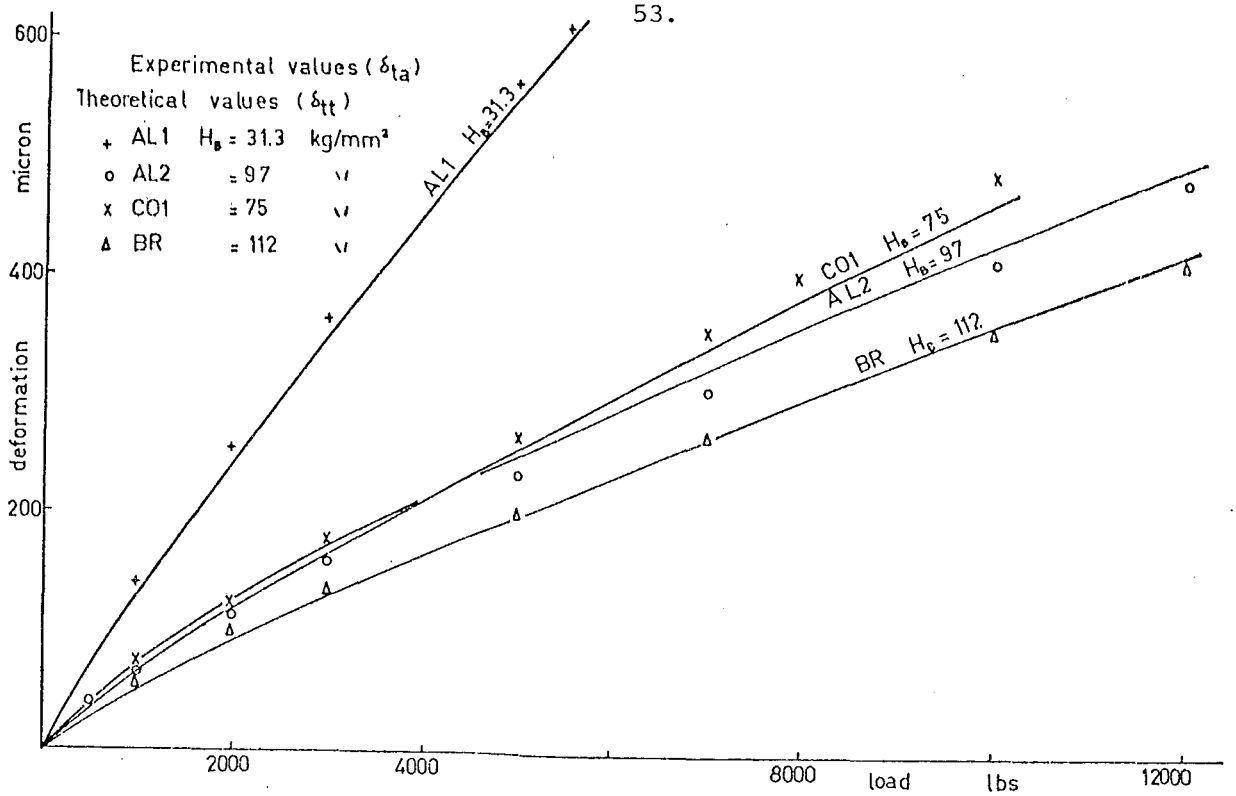

Fig. 2.34 The deformation of flat(copper,aluminium and brass) workpieces under a ball of diameter 50.8mm.

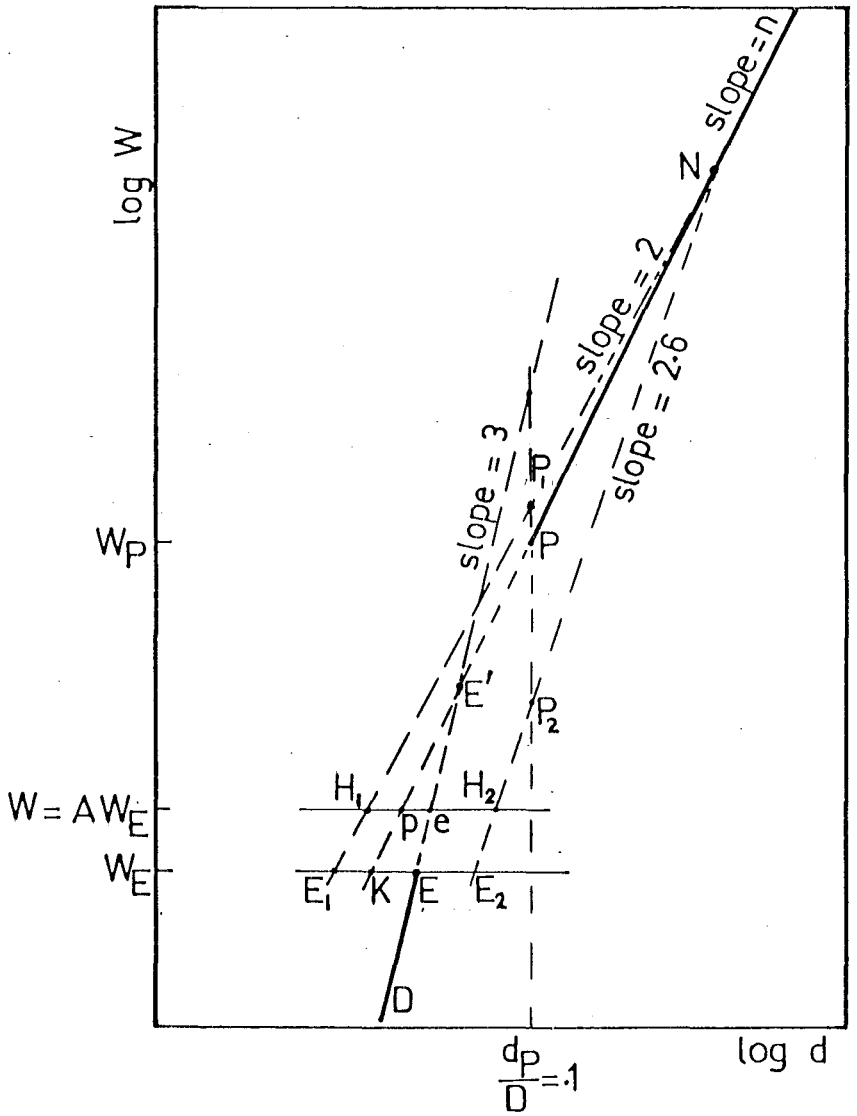

Fig. 2.35 The relation between logW and logd in the elastic and fully plastic zones.

$$d = 1.398 \left[D \left(\frac{1}{E_1} + \frac{1}{E_2} \right) W \right]^{1/3} \qquad 2.41$$

This theory has long been widely supported by experiments (95, 79, 32) particularly in the field of ball bearing where the flat surface is heat treated to about the same hardness as of the ball. The limit load for the validity of Hertz theory was proposed by Tabor[97] to be

$$W_E = 14.461\, q_m^{\,3}\, R_1^{\,2} \left(\frac{1}{E_1} + \frac{1}{E_2} \right)^2 \qquad 2.42$$

If Y is the yield stress of the flat surface, the $q_m \simeq 1.1\ Y$ and

$$W_E = 4.81\ Y^{\,3}\ D^2 \left(\frac{1}{E_1} + \frac{1}{E_2} \right)^2 \qquad 2.43$$

where D is the diameter of the ball = $2R_1$.

Usually the yield stress Y increases as the hardness increases, hence for hard, flat surfaces, the onset of plasticity increases significantly due to Y^3 and in the ball bearing field, the Hertz theory can be used with tolerable errors.

(2) The Meyer law (1908) shows that at high load, there exists a relationship $W = kd^n$ where k and n are material constants; n is independent of the ball diameter and varies from 2 to 2.6, but k is dependent on the diameter of the indenter. The Meyer formula applies for large indentations. In 1951, Tabor expressed the view that this formula is valid from a minimum value of $\frac{d}{D}$ of approximate 0.1 for mild steel and from a smaller value for Copper (due to lower Young modulus and hardness values). He described this limit as a state when "full plasticity" is reached. This does not imply that the plastic deformation of the work-piece (flat surface) is much higher than its elastic deformation, but that there exists a relationship $q_m \simeq 3Y_r$ where q_m is the mean pressure at the contact area and Y_r is the representative

stress of the flat surface which was found to be at the edge of the indentation. When "full plasticity" is reached the deformations are geometrically similar, i.e., d/D is a constant. This is the why the Brinell hardness is always measured within the full plasticity region.

The Meyer constant n is of great importance. For cold worked metals it is close to 2 and for annealed materials it is closer to 2.6. In 1944 from an investigation of the variation of this constant for steel with variations in carbon content and in form of heat treatment, O'Neill[77] made the following observations:

- Increases slightly in normalised steels with rise of carbon content.
- Increases when a given normalised steel is quenched to become austenitic or martensitic.
- Decreases when pearlite or sorbite is spheroidized.
- Decreases when a steel, by oil-quenching or water quenching and tempering, is given a sorbitic type of microstructure.

A summary is shown in Table 2.10, together with the direction of hardness variations.

TABLE 2.10

Effect of n and hardness due to heat treatment and cold-work on steel.

n	Treatment	Hardness
↗	as % content of carbon	↗
↗	Normalised steel is quenched to become austenitic and martensitic	↗
↘	Pearlite and sorbite becomes spheroidic	Unsure
↘	Oil, water quenched and tempered	↗
↘	As tempered temperature ↘	↗
↘	As the amount of cold-work ↗	↗

Baker and Russell[8] (1920) found that the Meyer constant decreases as the amount of cold work increases. This applies for steel; fortunately it also applies for other metals.

From Table 2.10 we observe that there is no way of devising a general relationship between hardness and the Meyer constant n. In some cases n increases as hardness increases, but in others it decreases. We can only treat individual cases, e.g., for cold worked metals, as the amount of cold work increases, n decreases and hardness increaseses, and there may exist a relationship between hardness and n. However, this becomes so detailed that the analysis may be difficult or tedious to apply in practice, so for the following analysis, we shall assume that n is independent of hardness.

Meyer's formula $W = kd^n$

that is $d = k'W^{1/n}$ k' is a constant 2.44

To find an expression for k', let D_o, W_o be the ball diameter and the load that is used to obtain the Brinell hardness for any metal, then

$$Z = W_o/D_o^2 \qquad 2.45$$

where Z is called the specific loading and satisfies the requirement in BS 240 Part 1, 1962.

Let d_o, M, be the corresponding indentation diameter and Meyer hardness of the flat surface then

$$M = 4W_o/\pi d_o^2 \qquad 2.46$$

i.e. $d_o = (4W_o/\pi M)^{\frac{1}{2}}$

Meyer's law gives $d_o = k'W_o$

hence $$k' = (1/W_o)^{1/n} (4W_o/\pi M)^{\frac{1}{2}} \qquad 2.47$$

Replace W_o in Equation 2.47 by $Z\ D_o^2$, i.e.

$$k' = 2\ (\pi M)^{-\frac{1}{2}}\ (Z\ D_o^2)^{\frac{1}{2}}\ -1/n$$

Since Meyer hardness is independent of the ball used, provided we keep the specific loading Z constant. The constant k' for any ball D is

$$k' = 2(\pi M)^{-\frac{1}{2}}\ (Z\ D^2)^{\frac{1}{2}} - 1/n$$

$$= 1.128\ M^{-\frac{1}{2}}\ (Z\ D^2)^{\frac{1}{2}} - 1/n \qquad 2.48$$

Substitute this result into Equation 2.44 to get

$$d = 1.128\ M^{-\frac{1}{2}}\ (Z\ D^2)^{\frac{1}{2}-1/n}\ W^{1/n} \qquad 2.49$$

Hence it follows that for a flat work-piece of given hardness M, we can draw the curve d-W in the "fully plastic" zone for any ball diameter D, from Equation 2.49.

Consider Fig.2.35, the straight line ED represents the elastic curve satisfying Equation 2.41, i.e., ED has slope of 3 and W_E satisfies Equation 2.43 line P_N represents the fully plastic zone, P is the point at which d/D = .1. W_N is the load at which the Brinell hardness is measured if a ball of diameter D is used and specific loading $Z = W_N/D^2$ satisfies BS 240. Since n varies from 2 to 2.6, let P_1N, P_2N be two straight lines of slope 2 and 2.6 respectively. P_1 and P_2 lie on the vertical line of d/D = 0.1. Of course, PN must lie in the $P_1N\ P_2$ zone, since $2.0 < n < 2.6$. (Actually, this range applies for Copper and its alloys only, for steel, Aluminium, and their alloys n is between 2 and 2.5, see Appendices 2.1 and 2.2.)

The horizontal line $W = AW_E$, where A is a constant, intersects P_1N, PN, ED and P_2N at H_1, p, e, H_2 respectively. Equations 2.41 and 2.43 give

$$d_e = 1.398\ D^{1/3}\ X^{1/3}\ A^{1/3}\ 4.81^{1/3}\ Y\ D^{2/3}\ X^{2/3} \text{ where } X = 1/E_1 + 1/E_2$$

i.e. $d_e/D = 2.358\ Y\ X\ A^{1/3}$

Similarly Equations 2.43 and 2.49 give

$$d_p = 1.128\ M^{-\frac{1}{2}}\ (Z\ D^2)^{\frac{1}{2}\ -1/n}\ 4.81^{1/n}\ Y^{3/n}\ D^{2/n}\ X^{2/n}\ A^{1/n}$$

$$d_p/D = 1.128\ (Z/M)^{\frac{1}{2}}\ (4.81/Z)^{1/n}\ Y^{3/n}\ X^{2/n}\ A^{1/n} \qquad 2.51$$

then $$d_e/d_p = 2.09\ Z^{-\frac{1}{2}}\ M^{\frac{1}{2}}\ Y^{1-3/n}\ (Z/4.81)^{1/n}\ X^{1-2/n}\ A^{1/3\ -\ 1/n} \qquad 2.52$$

if $A = 1$, i.e., $W = W_E$ then

$$R = (d_e/d_p)_{\text{at } W_E} = d_E/d_K = 2.09A^{-\frac{1}{2}}\ M^{\frac{1}{2}}\ Y^{1-3/n}\ (Z/4.81)^{1/n}\ X^{1-2/n} \qquad 2.53$$

Note for $n = 2$, $d_E/d_{E_1} = .953\ (M/Y)^{\frac{1}{2}}$ 2.54

In practice $M \geqslant 3Y$ for all cases $\therefore\ d_E > d_{E_1}$ 2.55

Also note for $n = 2.5$ (for steel, line P_2N has slope 2.5 instead of 2.6)

$$d_E/d_{E_2} = 1.41\ X^{.2}\ M^{.5}/Z^{.1}\ Y^{.2} \qquad 2.56$$

This equation is very complicated due to the variation of Z, Y , X and M with different materials, different types of heat treatment, and different amounts of cold work. Since M is of the highest power, it dominates the other terms and it was found that usually $d_E > d_{E_2}$ but in some cases of soft metals $d_E < d_{E_2}$.

(A)

Consider the case where PN intersects ED at a point E' above E, i.e. $W_E' > W_E$. It is logical to say that the transition zone PE can be made of a series of straight lines with slopes decreasing steadily from 3 to n. In fact, two straight lines of slope $3 - (3-n)/4$ and $n + (3-n)/4$ drawn from E and P respectively is satisfactory representation.

Summarising the process, to obtain this graph given Y , D, E_1, E_2, M, n

(i) Calculate W_E by Equation 2.43, substitute into Equation 2.41, to obtain d_E

$$d_E = 2.358\ D\ Y\ (1/E_1 + 1/E_2) \qquad 2.57$$

(ii) Plot point E (W_E ,d_E) on the logW-logd graph.

(iii) Calculate W_P from Equation 2.49 by putting $d_P = .1D$. Plot the point P (W_P, D/10).

(iv) Draw straight lines of slope 3, n from E and P respectively.

(v) In the transition zone, draw two straight lines of slopes 3 -(3-n)/4 and n +(3-n)/4 from E and P respectively (see Fig.2.36).

A very similar way was done by Tabor[97] to fit his experimental diameters of indentation at varying loadings for the case of a 10 mm diameter hard steel ball indented into a fully work-hardened steel (n = 2) of yield stress $Y_o = 77\ kg/mm^2$ (i.e. $H_B \simeq 231\ kg/mm^2$).

The graph is then complete, and for any load W we can read d directly from the curve. Unfortunately, when the ball diameter is changed, a new curve has to be drawn. This is long and tedious, but a computer program can be written to reduce the tedious.

(B)

The above method works well provided $W_{E'} > W_E$ but what will happen if $W_{E'} < W_E$?, i.e., the straight line PN intersects ED at E' below E (Fig.2.37).

The two straight lines drawn from P and E described in (v) of Part (A) above, will not meet each other inside the space limited by two lines $W = W_E$ and $W = W_P$. The simplest procedure would be to connect PE; this straight line, of course, has a slope smaller than n which would make the graph appear unrealistic. Calculations for most metals have shown that this situation occurs frequently for $n > 2.4$ especially for low hardness metals. However, as W_P is very much higher than W_E, the slope of the line EP becomes

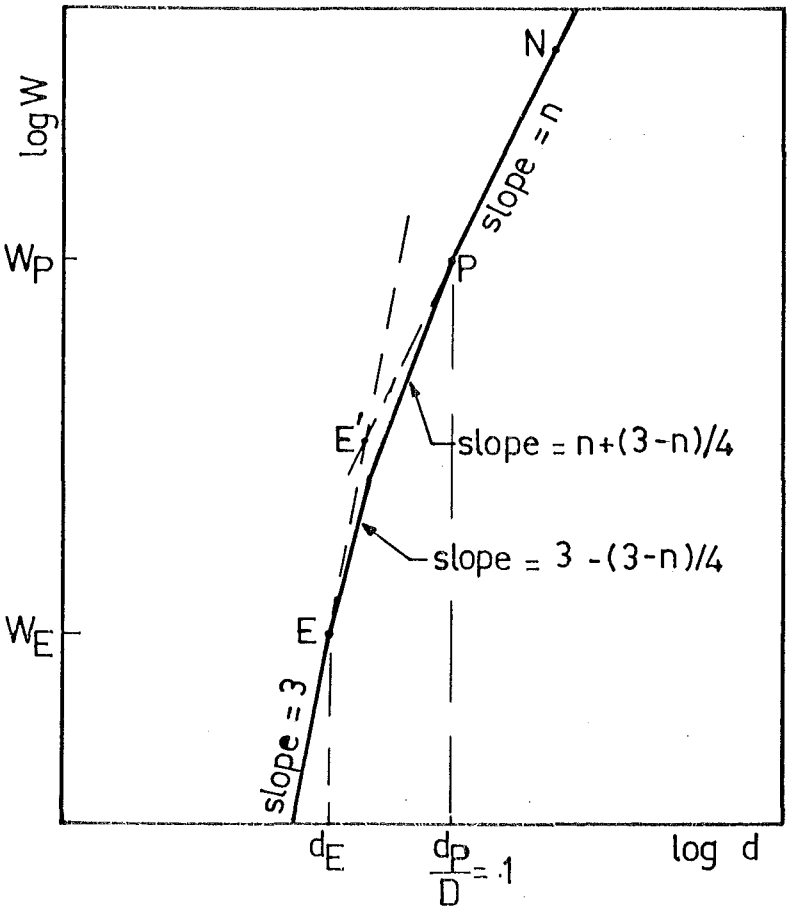

Fig. 2.36 The proposed logW-logd graph for the case $W_{E'} > W_E$.

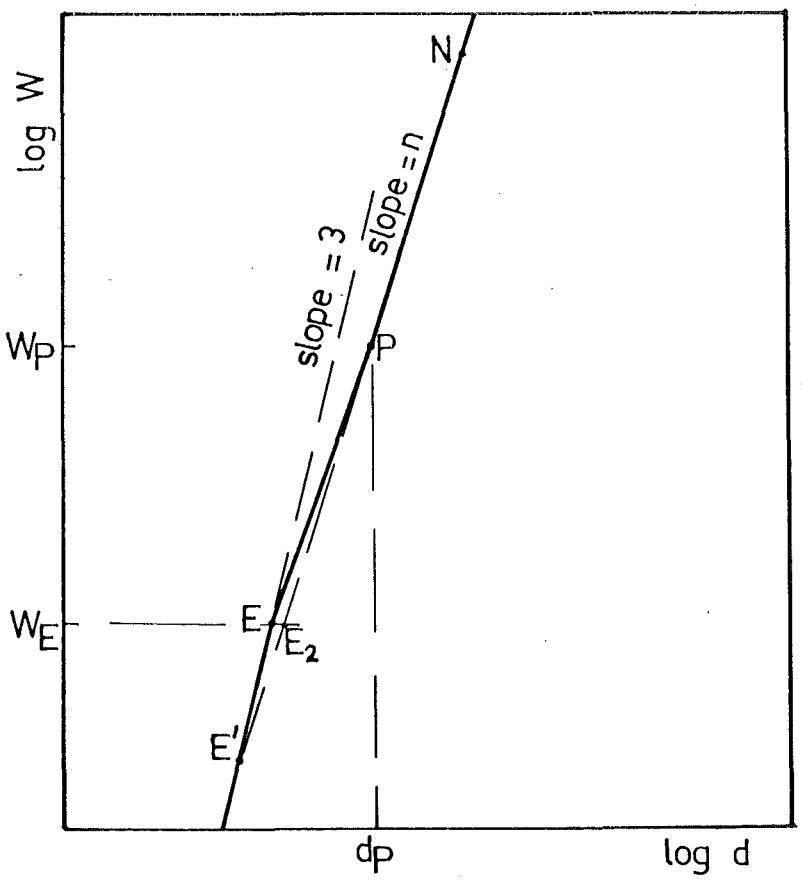

Fig. 2.37 The proposed logW-logd graph for the case $W_{E'} < W_E$

very close to n (see Figs. 2.43c and 2.44c) and the changes in the slopes at E and P are not very marked; we took this straight line connection to be acceptable.

It must be emphasised that the fully plastic Meyer formula applies for steel from d/D = .1 and from a smaller ratio for Copper. Therefore, in applying this method to soft metals like Copper, Brass, Aluminium and its alloys, we have to reduce it to a reasonable value, say d/D = .08.

At this stage we can obtain the curve for d-W with any given combination of M, D, Y , E_1, E_2, n. However, the above graphical method, due to its complexity and the large amount of required information, still leaves a lot to be desired. In the next section we are going to discuss another approximate method which may be easier to use in practice. It eliminates the requirement for much information by assumptions and curve fitting.

The first assumption is Y = M/5 which will be discussed later (see Section 3.10).

Equations 2.43 and 2.52 then become

$$W_E = .0385\ D^2 M^3 X^2 \qquad 2.58$$

and

$$d_e/d_p = 2.09\ Z^{-\frac{1}{2}}\ M^{\frac{1}{2}} (M/5)^{1-3/n} (Z/4.81)^{1/n}\ X^{1-2/n}\ A^{1/3\ -1/n}$$

i.e. $$d_e/d_p = .418\ Z^{-\frac{1}{2}}\ (26Z)^{1/n}\ M^{1.5-3/n}\ X^{1\ -2/n}\ A^{1/3\ -\ 1/n} \qquad 2.59$$

for A = 1 i.e. $W = W_E$ let

$$R = (d_e/d_p)_{at\ W_E} = .418\ Z^{-1/2} (26Z)^{1/n}\ M^{1.5\ -\ 3/n}\ X^{1\ -\ 2/n} \qquad 2.60$$

when A = 1 and n = 2 then $(d_e/d_p)_{at\ W_E} = 2.13$ (from Equation 2.54)

That is it is independent of the properties of the flat surface and of the diameter of the indenter. Variation of R with respect to n and hardness

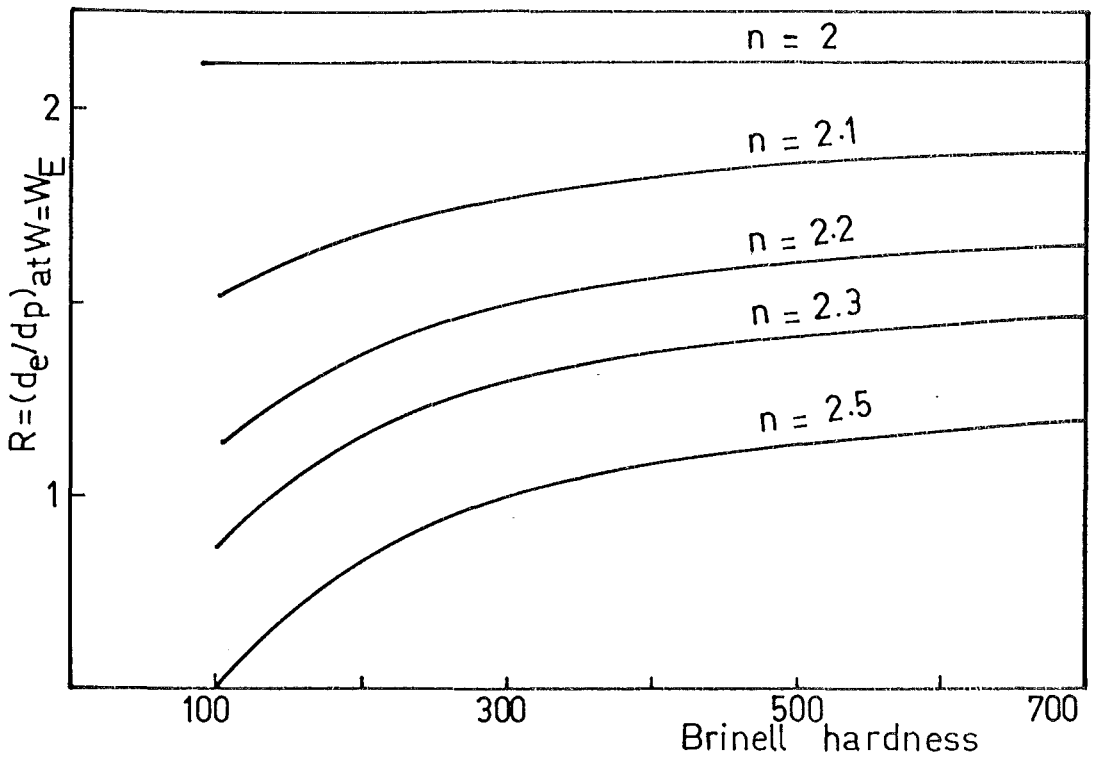

Fig.2.38 The relation between R and Brinell hardness for steel.

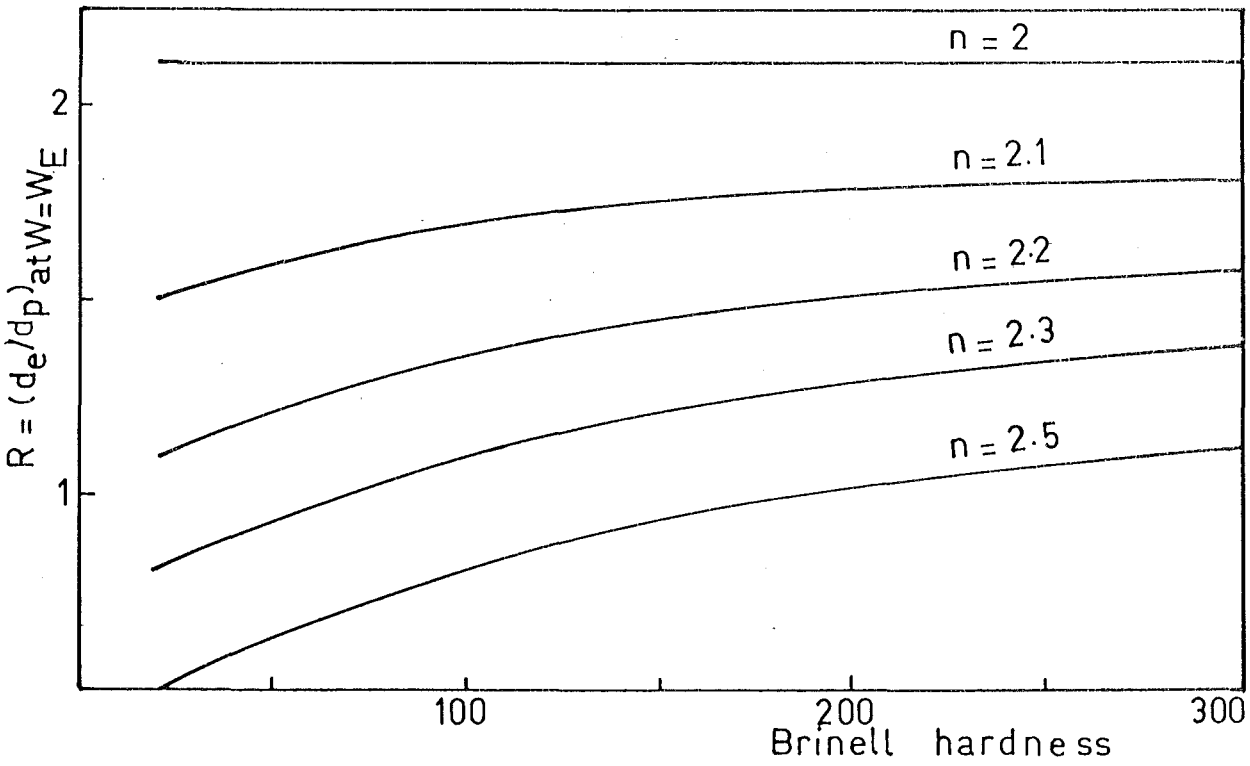

Fig. 2.39 The relation between R and Brinell hardness for copper and aluminium alloys.

can be seen in Figs. 2.38 and 2.39 for the following cases:

For Steel Z = 30, range of hardness = 50 - 700 kg/mm^2

For Copper, Aluminium alloy, Brass Z = 10, range of hardness = 20 - 300 kg/mm^2. It is observed that the values of R lie between 1/2 and 2.13.

Substitute Y = M/5 into Equations 2.50 and 2.51 to get

$$d_e/D = .472\ MXA^{1/3} \qquad 2.61$$

$$d_p/D = 1.128\ (.0385)^{1/n}\ Z^{\frac{1}{2}\ -1/n}\ M^{-\frac{1}{2}}\ +\ 3/n\ X^{2/n}\ A^{1/n} \qquad 2.62$$

Attempts have been made to find two functions f_1 and f_2 such that the diameter of the indentation at any load is

$$d = f_1\ d_e + f_2\ d_p \qquad 2.63$$

where f_1 and f_2 have the following property:

As

Load W	0	W_E	W_P	∞
f_1	about 1	decreasing to 0		about 0
f_2	about 0	increasing to 1		about 1

f_1 and f_2 must be such that the diameter of indentation d in Equation 2.63 has a variation with load as shown in Fig.2.41.

To simplify the problem we use

$$f_1 = 1 - f_2$$

where f_2 has the shape shown in Fig. 2.40a.

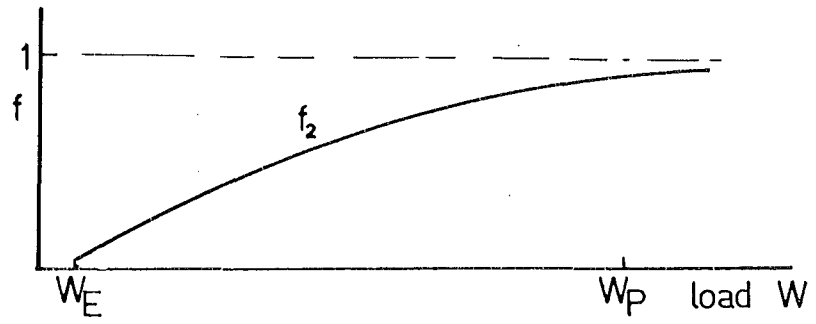

Fig. 2.40a The proposed shape of function f_2.

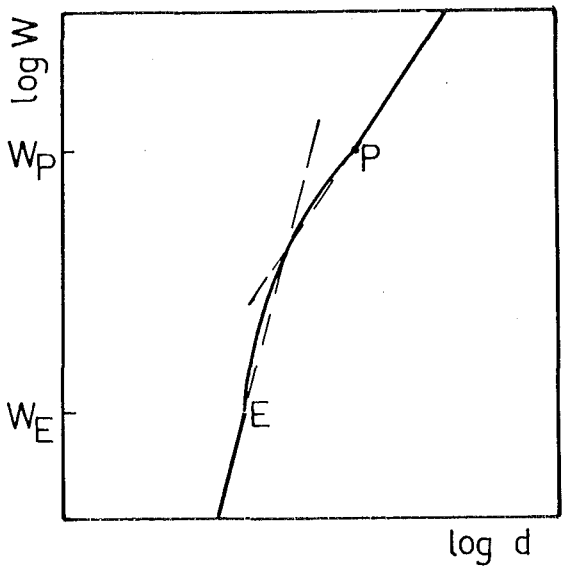

Fig. 2.40b The shape of the logW-logd curve for the case of $d=f_1 d_e+f_2 d_p$.

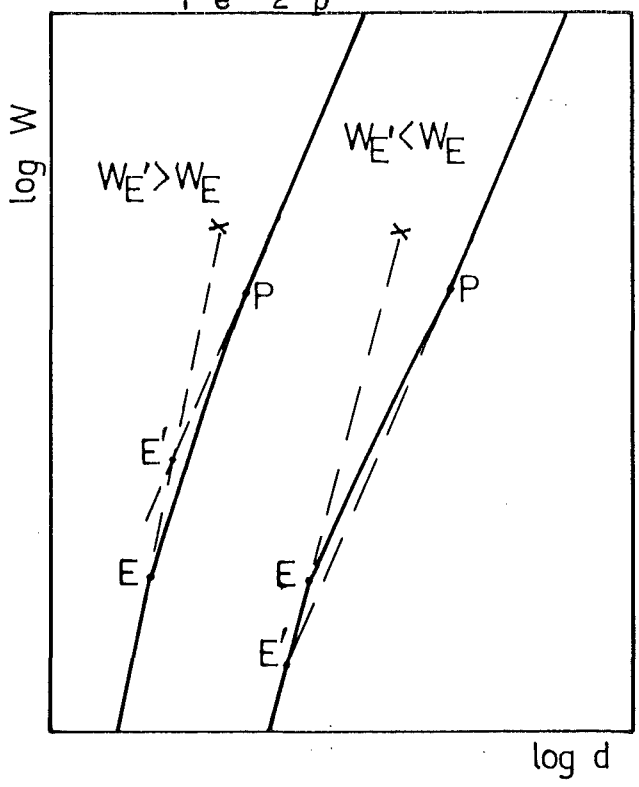

Fig. 2.41 The proposed logW-logd curves for the two possible cases.

There are a few functions which have the characteristic desired for f_2 such as

a) $$f_2 = \left(\frac{2}{\pi} \tan^{-1} W\right)^2$$

b) $$f_2 = \text{erf}W = \frac{2}{\pi} \int_o^W e^{-t^2} \, dt$$

c) $$f_2 = \frac{e^W}{1+e^W} \quad \text{etc.}$$

For each function, constants must be inserted to satisfy the conditions at $W = W_E$ and $W = W_P$.

All of the above f_2 and their corresponding f_1 functions, making up $d = f_1 d_e + f_2 d_p$, produce a similar shape to that shown in Fig. 2.40b, which is not acceptable.

An alternative is to look for a function F such that

$$d = F d_p = F \left[1.128 \, (.0385)^{1/n} \, z^{1/2 - 1/n} \, M^{-1/2 + 3/n} \, X^{2/n} \, A^{1/n}\right] \qquad 2.64$$

Since W_E is usually very small and applied loads above W_E commonly occur in practice, Equation 2.64 is designed so as to obtain the diameter of the impression for $W > W_E$. The property of F with respect to load is

W	W_E		W_P	∞
F	R	approach 1		about 1

where R is the ratio (d_e/d_p) at W_E it was noted that $\frac{1}{2} < R \leq 2.13$ for $Y = M/5$.

The function F was found to have the following form

$$F = \frac{W + CRW_E}{W + CW_E} \qquad 2.65$$

where C is a constant. The larger the value of C the slower F approaches 1. Fig. 2.42 shows the curve of F vs load W for R >1 and R <1. It is easier to investigate Equation 2.64 in a dimensionless form, i.e., to study the relation

$$\frac{d}{D} = \frac{A + CR}{A + C}\, 1.128Z^{\frac{1}{2}} \left(\frac{3.85 \times 10^{-2} X^2}{Z}\right)^{1/n} M^{-\frac{1}{2}+3/n} A^{1/n} \qquad 2.66$$

where $W = AW_E$ and $Y = M/5$.

Graphs of $\frac{d}{D}$ vs A are drawn for two cases.

(i) For Steel: $Z = 30$, $E_1 = E_2 = 21500$ kg/mm^2, $M = 188$ kg/mm^2 in Fig.2.43.

(ii) For Copper: $Z = 10$, $E_1 = 21500$, $E_2 = 12200$ kg/mm^2, $M = 75$ kg/mm^2 in Fig. 2.44.

In each case the effect of the variation of $n = 2, 2.25, 2.5$ and $C = 10, 15, 20$ are clearly displayed.

Note the following:

- When $A = 1$, $W = W_E$, a straight line of slope 3 passes through point E ($A = 1$, $d/D = d_E/D$), which represents the extended part of the elastic curve, i.e., Equation 2.61.

- Straight lines of slopes $n = 2, 2.25, 2.5$ representing the fully plastic zone (Equation 2.62). Each line must pass through P ($d_P/D = .1$ or $.08$ for Steel or Copper respectively), the starting point of the fully plastic zone.

- If we connect the points together, we will obtain $\frac{d}{D}$ versus A. It is very interesting to find that it does not matter whether R is larger or smaller than 1, the resultant d/D vs A curves appear to be what we were looking for.

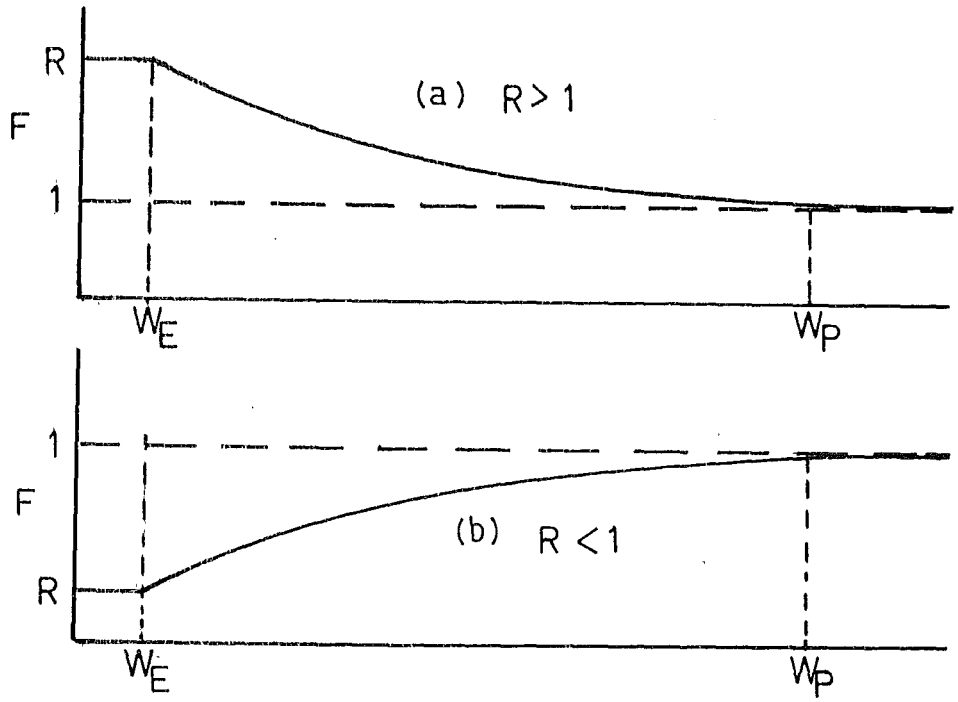

Fig. 2.42 The relation between function F and load for two possible cases of R.

Material	H_B kg/mm^2	d mm	d/D	δ_e micron	δ_p micron	δ_e / δ_p micron
S 6	137	11.67	.37	148	998	.15
S 5	156	10.75	.34	160	829	.19
S 1	188	10.19	.32	169	733	.23
S 2	249	8.60	.27	201	482	.42
S 3	306	7.79	.25	222	367	.60
S 4	354	7.20	.23	239	289	.83
CO1	75	15.08	.47	158	1710	.09
AL1	31.3	23.17	.73	151	4151	.04
AL2	97	13.29	.42	263	1258	.21
BR	112	12.20	.38	214	1064	.20

Table 2.11

The ratio of elastic over plastic deformations at 30000 lbs for various metals.

- The constant C is chosen in such a way that the curve $d = Fd_p$ branches off the straight line E_x at E with a slope slightly less than 3 and reaches the point P of the straight line PN at a slope very close to n. The best values for C have been found to lie between 10 and 20. For simplicity, we chose C = 15 for all cases.

A program (see Appendix 2.3) was written to tabulate the difference in d/D for varying values of A ($=W/W_E$) between the following three cases:

1) Dimensionless fully plastic diameter d_p/D (Equation 2.62).
2) Dimensionless elastic diameter d_e/D (Equation 2.61).
3) Dimensionless diameter $d/D = F(d_p/D)$ from Equation 2.66 for cases of C = 10, 15, 20, and n = 2, 2.25, 2.5

The flow chart is shown in Fig. 2.45. The data used for the calculation were:

(i) Steel H_B = 188 kg/mm^2
(ii) Steel H_B = 354 kg/mm^2
(iii) Copper H_B = 75 kg/mm^2

Cases (i) and (iii) are drawn in Figs. 2.43 and 2.44.

2.8 SUMMARY OF THE STEPS LEADING TO THE CALCULATION OF THE TOTAL DEFORMATION OF A HARD STEEL BALL ON A FLAT SURFACE

Given 1) Ball diameter D, Young Modulus of steel E_1 = 21500 kg/mm^2.

2) Young modulus, Brinell hardness, Meyer constant of work-piece, E_2, $H_B(\simeq M)$, n

3) Specific loading Z, which was used to determine the Brinell hardness of the work-piece, if it is not indicated, a value of Z may be assumed from BS 240, Part 1, 1962.

4) The load W at which we want to know the deformation δ_t.

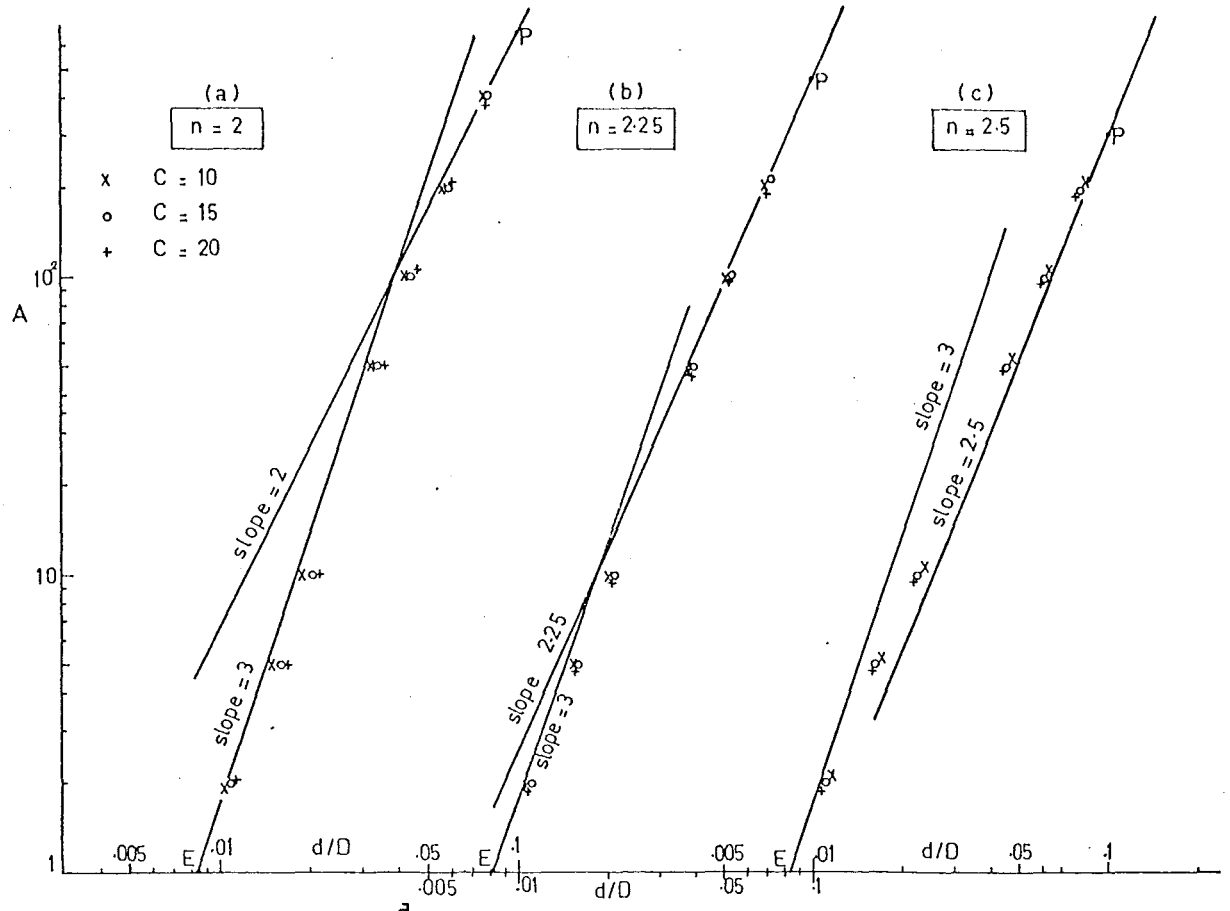

Fig. 2.43 LogW-log$\frac{d}{D}$ for various values of n and C.(Steel workpieces)

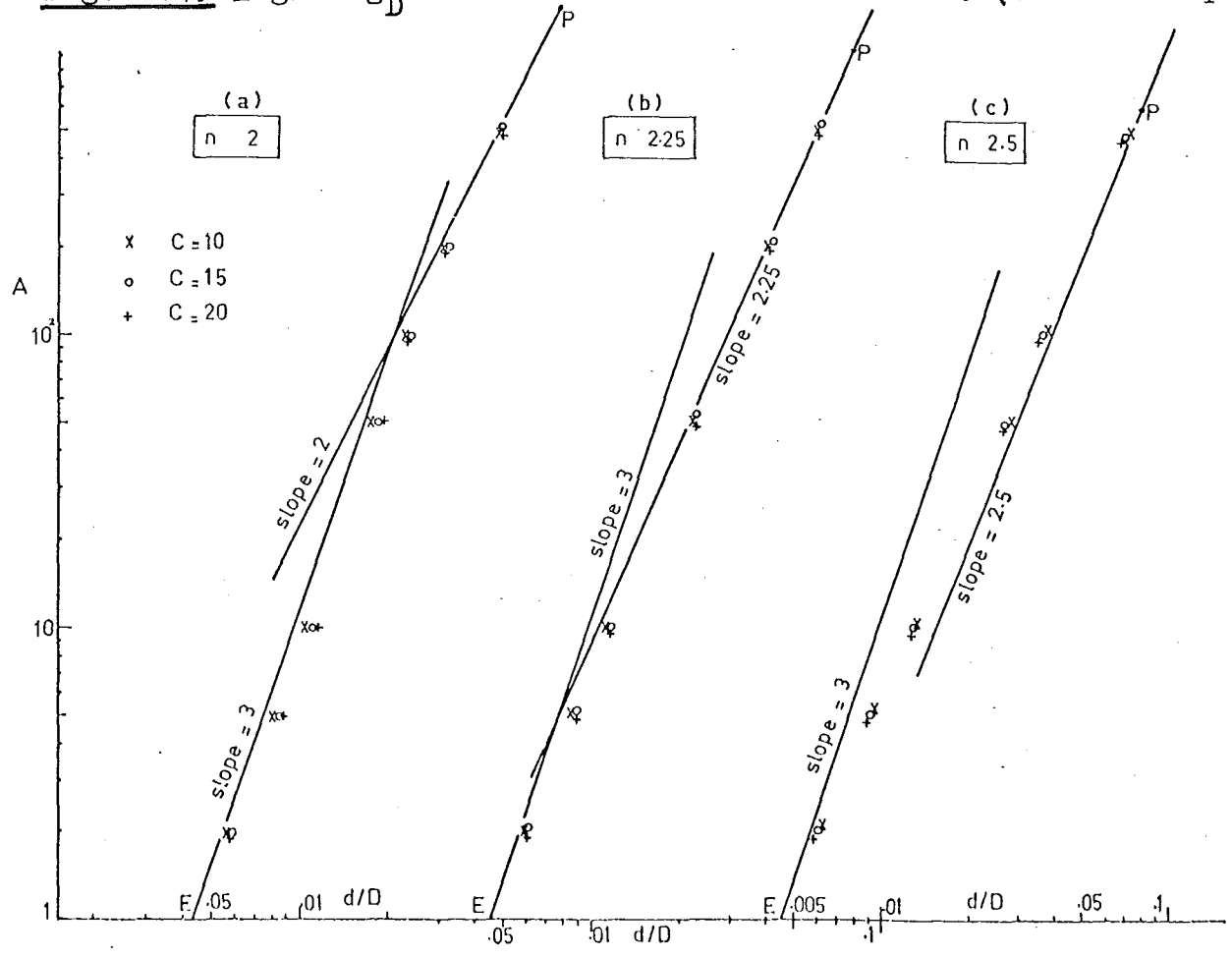

Fig. 2.44 LogW-log$\frac{d}{D}$ for various values of n and C.(Copper workpieces)

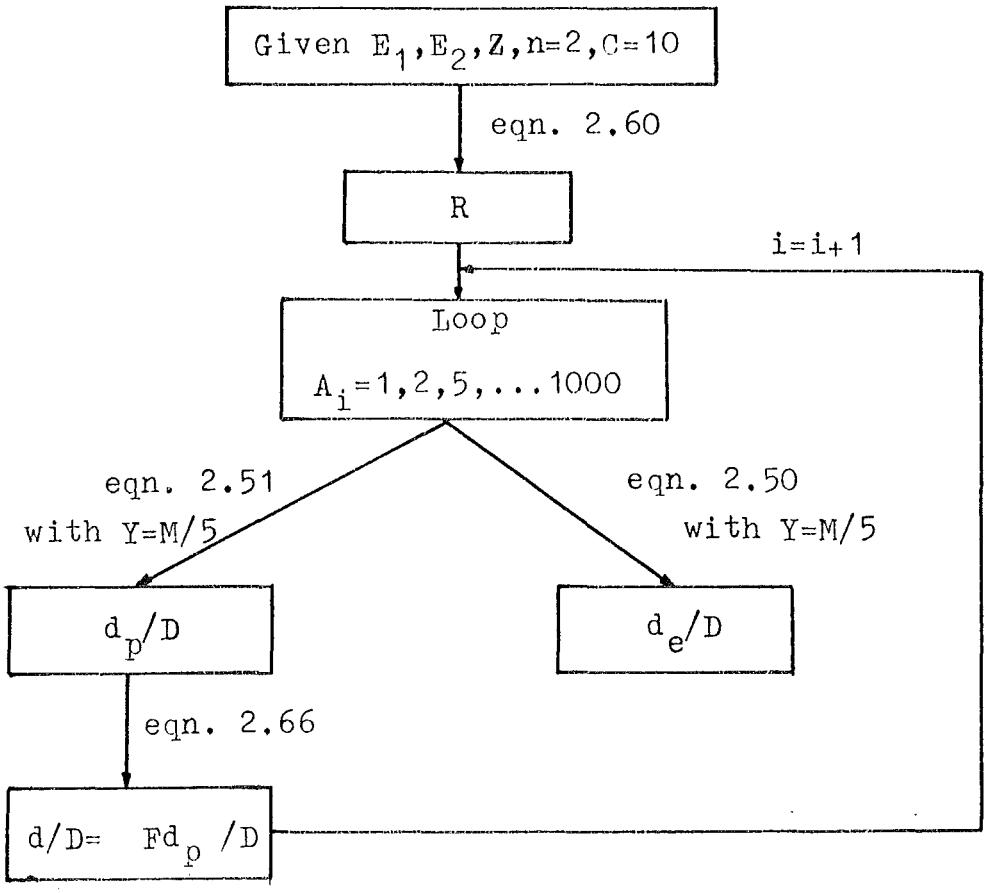

The process is repeated for C=15 and 20

All is then repeated for n=2.25 and 2.5

Fig. 2.45 Flow chart of program PLOT (Appendix 2.3)

SYMBOLS

Results	Inside program	Meanings
FACTOR	A(J)	A
PLAS DIA	DP	Ratio d_p/D
CORR DIA	DD	" d/D
ELAS DIA	DE	" d_e/D
DIA RAT	R	R
MEYER	B(3)	Meyer constant n
Z	B(4)	Specific loading Z
C	B(5)	Constant C

Assumptions 1) Yield stress of work-piece $Y = M/5 \simeq H_B/5$.

2) Constant C in function F equals 15.

3) Indentation is shallow, i.e., plastic deformation of work-piece $<< D$.

Calculation 1) Calculate the onset of plasticity W_E from Equation 2.58

$$W_E = .0385\ D^2 M^3 X^2 \quad \text{where } X = \frac{1}{E_1} + \frac{1}{E_2} \qquad 2.67$$

2) Calculate the ratio (d_e/d_p) from Equation 2.59 with A=1

i.e. $$R = .418\ Z^{\frac{1}{2}} (26Z)^{1/n}\ M^{1.5-3/n}\ X^{1-2/n} \qquad 2.68$$

3) Calculate from Equation 2.66

$$\frac{d}{D} = \frac{A+15R}{A+15}\ 1.128 Z^{\frac{1}{2}} \left(\frac{3.85 \times 10^{-2} X^2}{Z} \right)^{1/n} M^{-1/2+3/n}\ A^{1/n} \qquad 2.69$$

where $A = W/W_E$

4) Calculate total deformation δ_t from Equation 2.30

$$\delta_t = \frac{d^2}{4D} + .682\ \frac{W}{d}\ X \qquad 2.70$$

This calculation is most valuable for evaluating the total approach of a ball indenting a flat surface which deforms partly elastic and partly plastic, i.e., up to loadings that cause the dimensionless diameter of indentation to be less than approximately .1. For large indentations, the method still applies very well; it was found that for $d/D > .45$ the elastic deformation is found to be small compared with the plastic deformation (about 10% - see Table 2.11), in that case

$$\delta_t \simeq d^2/4D \qquad 2.70a$$

2.9 COMPARISON BETWEEN THE ACTUAL DIAMETERS OF INDENTATIONS AND THE THEORETICAL VALUES OBTAINED FROM THE EQUATION $d = Fd_p$

From the summary we can predict the diameter of the indentation at any load W, Equation 2.69 gives

$$d = \frac{A + 15R}{A + 15} \; 1.128Z^{\frac{1}{2}} \left(\frac{3.85 \times 10^{-2} X^2}{Z} \right)^{1/n} M^{-1/2+3/n} \; A^{1/n} \; D \qquad 2.71$$

A computer program (named FINAL) has been written to compute this equation for given values of E_1, E_2, H_B or M, Z, n and ball diameter D (Appendix 2.4). The total deformation δ_t was also computed in this program (for comparison with the experimental deformation if required).

The theoretical d calculated for Steel, Aluminium alloy, Copper and Brass are also tabulated in Appendix 2.4 and the values are plotted in Figs. 2.46 and 2.47, together with the experimental diameter of indentation for comparison. The maximum error may be ±10% at low load, that is close to W_E (assuming Y = M/5) it becomes less than ±5% for $W > 20\ W_E$ and when full plasticity is reached, the difference becomes negligible.

In order to show the effectiveness of our theoretical prediction, we have searched for published experimental results obtained by other investigators. So far we have found only four sources of published data that contain enough information for us to check our theory:

1) Tabor[97] (1951): the experiment was done using a 10 mm diameter hard steel ball on a fully work-hardened steel Y_o = 77 kg/mm^2, according to Tabor the Meyer constant n = 2.0, and hence Brinell hardness was approximately equal to 3 Y_o, i.e. 231 kg/mm^2.

2) O'Neill[75] (1923): the experiments were done on steel A and steel W the hardnesses and Meyer constants are 140, 327 and 2.288, 2.292 respectively. Figs 2.48 and 2.49 show the comparison of their experimental diameters of indentations with our theoretical predictions. The results are in close agreement.

3) Richmond *et al*[83] (1974): the experiments were made for the indentation of a 10 mm diameter tungsten carbide ball (E_1 = 60,000 kg/mm^2) into two copper bars: one was cold worked (n = 2.03) and the other was

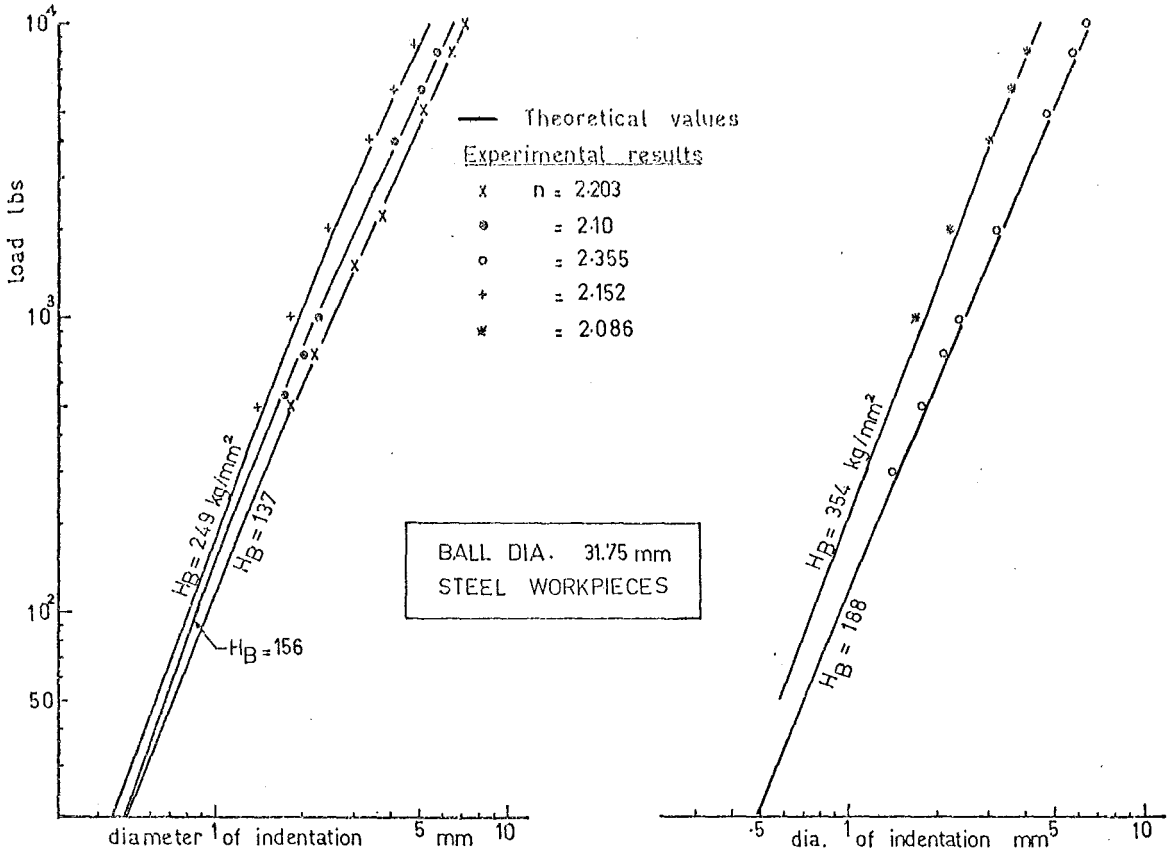

Fig. 2.46 The comparison between the actual and theoretical diameter of indentation $d = Fd_p$ for steel workpieces.

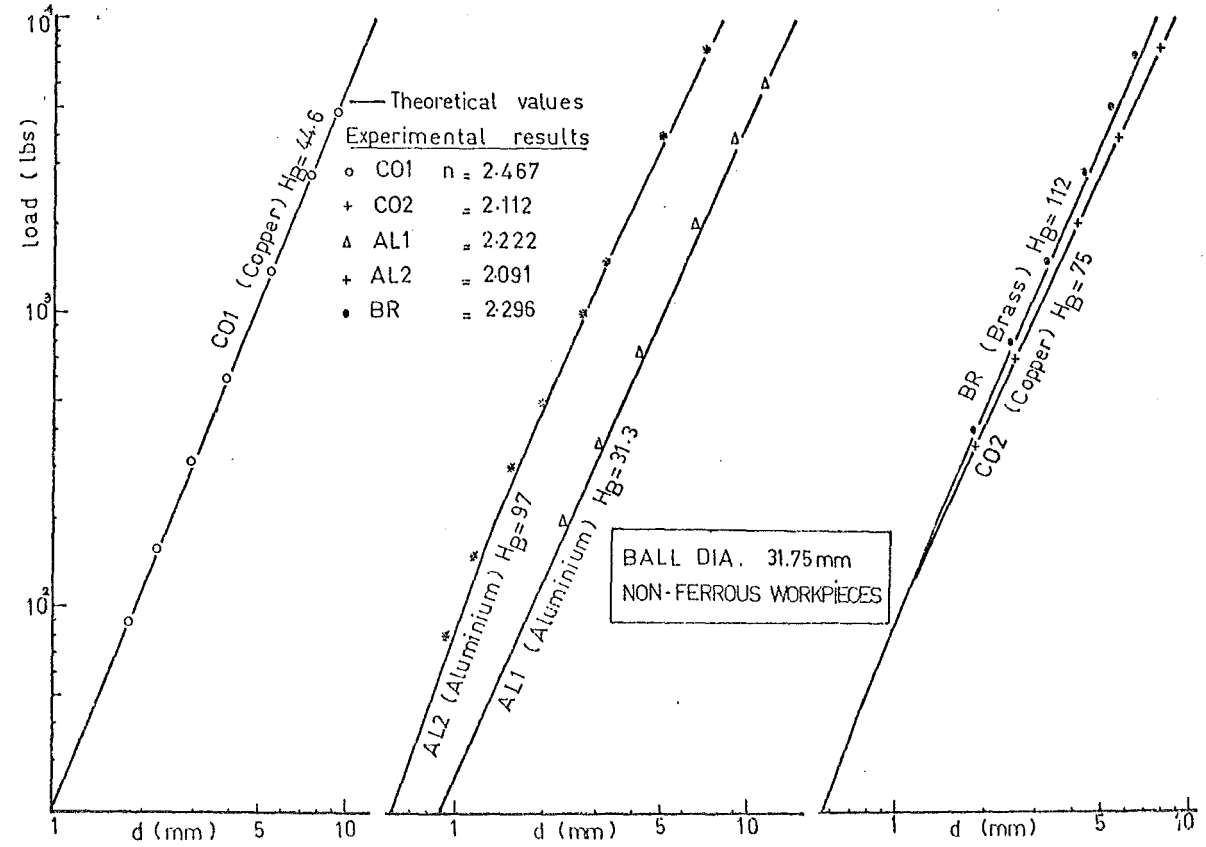

Fig. 2.47 The comparison between the actual and theoretical diameter of indentation $d = Fd_p$ for copper and aluminium alloys.

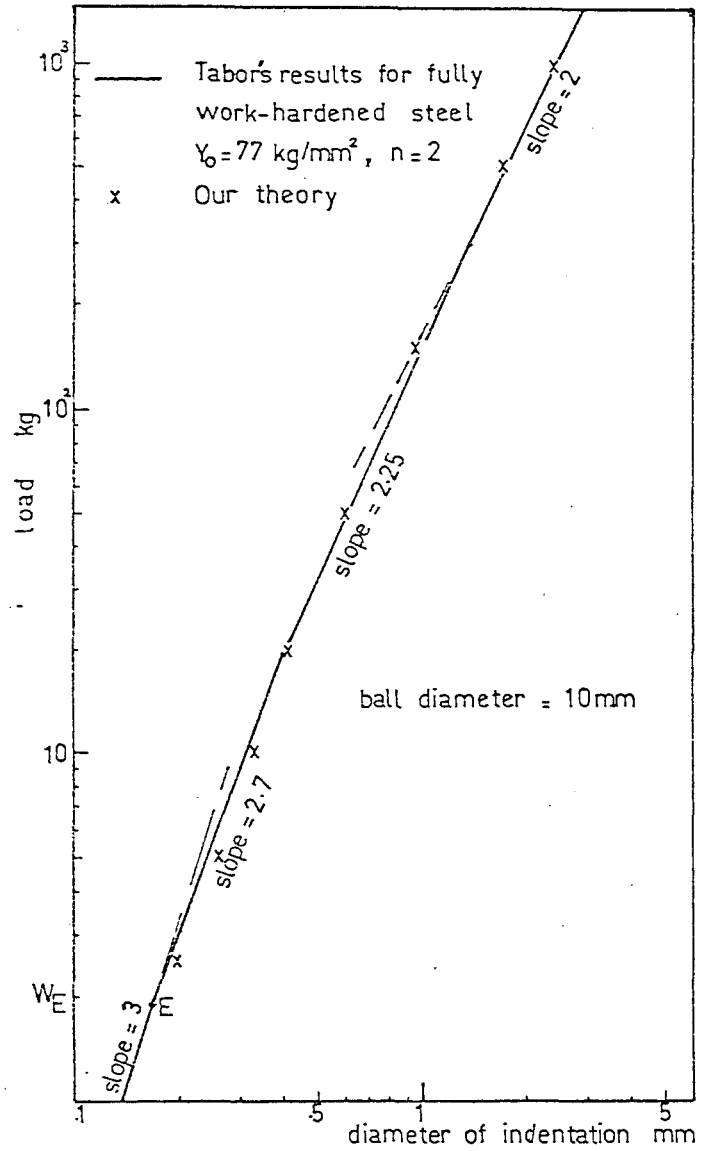

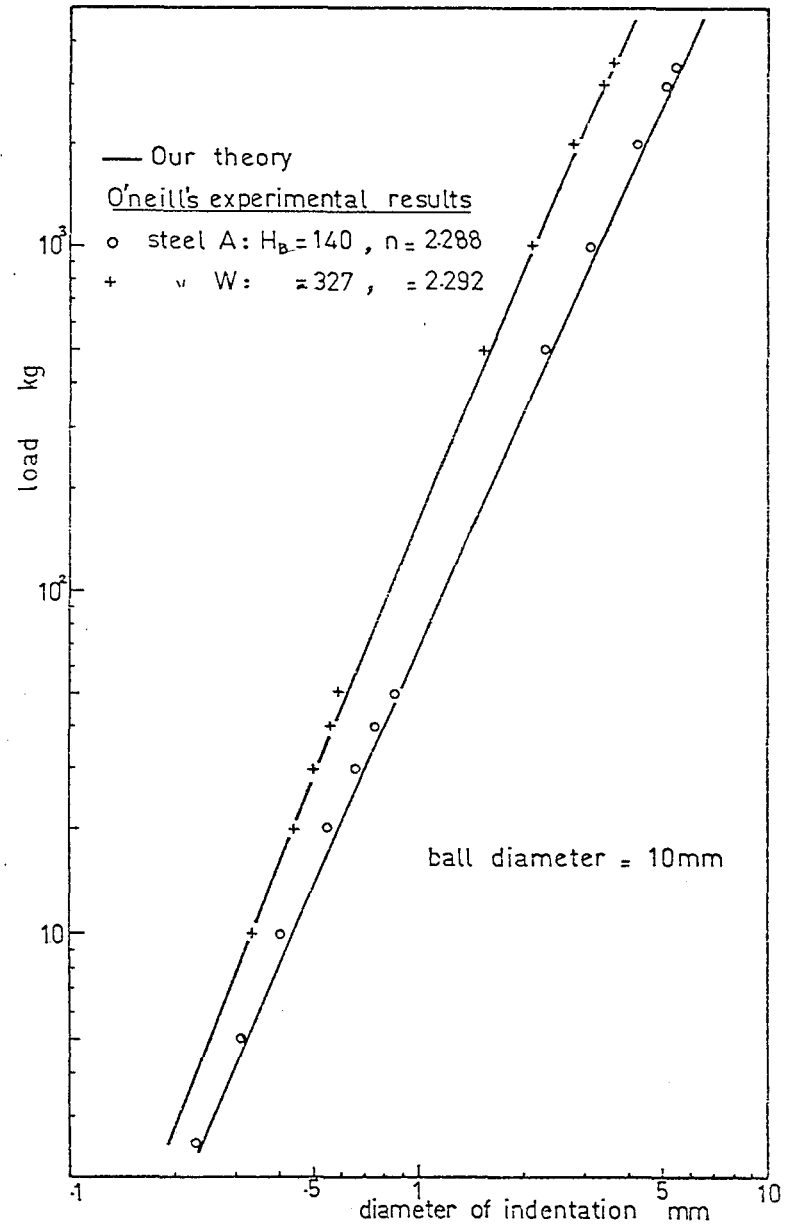

Figs. 2.48 (left) and 2.49 (right) The comparison of the experimental data (Tabor[97] and O'neill[75] respectively) and our theoretical predictions.

annealed (n = 2.48). Our calculation applies for the case of the indentation by a "steel" ball since it involves the specific loading Z which was used in the Brinell hardness test with a steel ball. However, if we assume that by keeping the same Z as before and replace the steel ball by the tungsten carbide ball, the diameter of indentation does not reduce very much and hence it can be used to estimate the Brinell hardness of the work-piece. The only change we have to make in our calculation is the Young modulus of the ball. Their assumed Brinell hardnesses may be calculated at the specific loading Z = 10 as 117 and 48.6 kg/mm^2 respectively. Our predicted diameters of indentation are very close to their experimental results (Fig.2.50). The ball penetration measured in their experiment may also be compared with our theoretical deformation δ_t in Fig.2.51. The error is within ±15%.

4) Lee *et al*[56] (1972): the experiment was made for the indentation of a 10 mm diameter tungsten carbide ball into a bar of steel SAE 4340. The Meyer constant n and the assumed Brinell hardness at the specific loading Z = 30 (for steel) are calculated from their experimental results as 2.12 and 398 kg/mm^2 respectively. Our theoretical prediction for the total deformations δ_t follow their experimental results much better than their theoretical results (Fig.2.52).

All of our theoretical values are tabulated in Appendices 2.5 and 2.6. The theoretical predictions for the deformations (TOTAL DEF., Appendix 2.4) of our work-pieces were found to be within ±15% of the experimental data (δ_{ta}, Table 2.9).

2.10 DISCUSSION OF THE ASSUMPTION M = 5Y

Experimentally it has been shown that for ideal plastic or fully work-hardened metal $M \simeq 3\ Y_o$ (Tabor 1951).

For annealed metals $\frac{H_B}{UTS}$ varies slightly with the Meyer constant n,

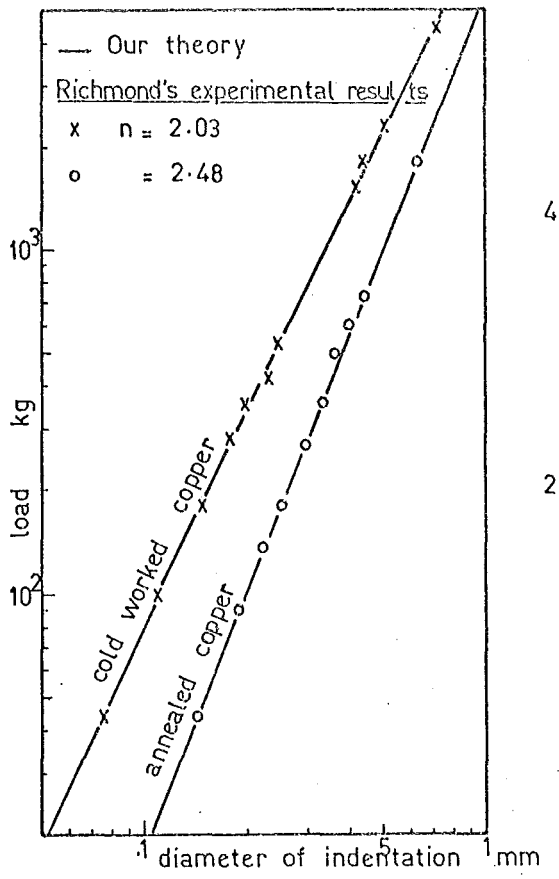

Fig. 2.50

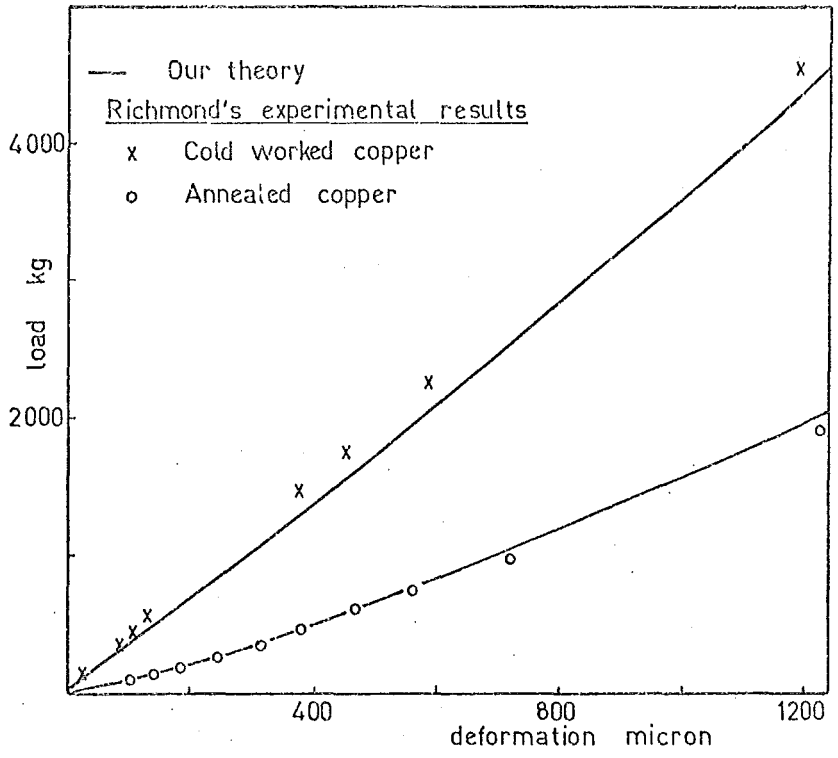

Fig. 2.51

The comparison between the experimental data (Richmond[83]) and our theoretical prediction.

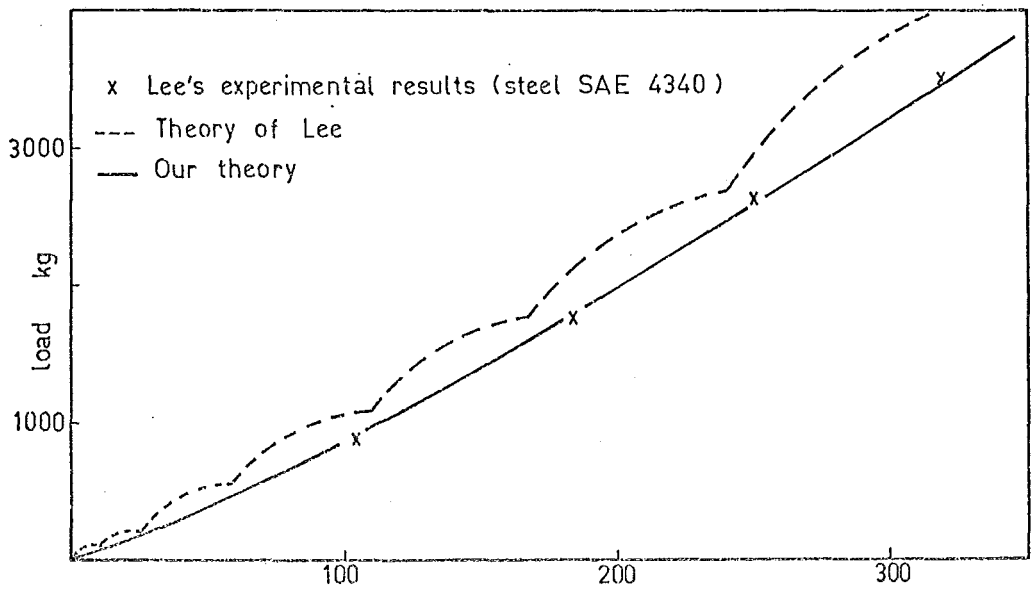

Fig. 2.52 The comparison between the experimental data (Lee[55]) and our theoretical prediction.

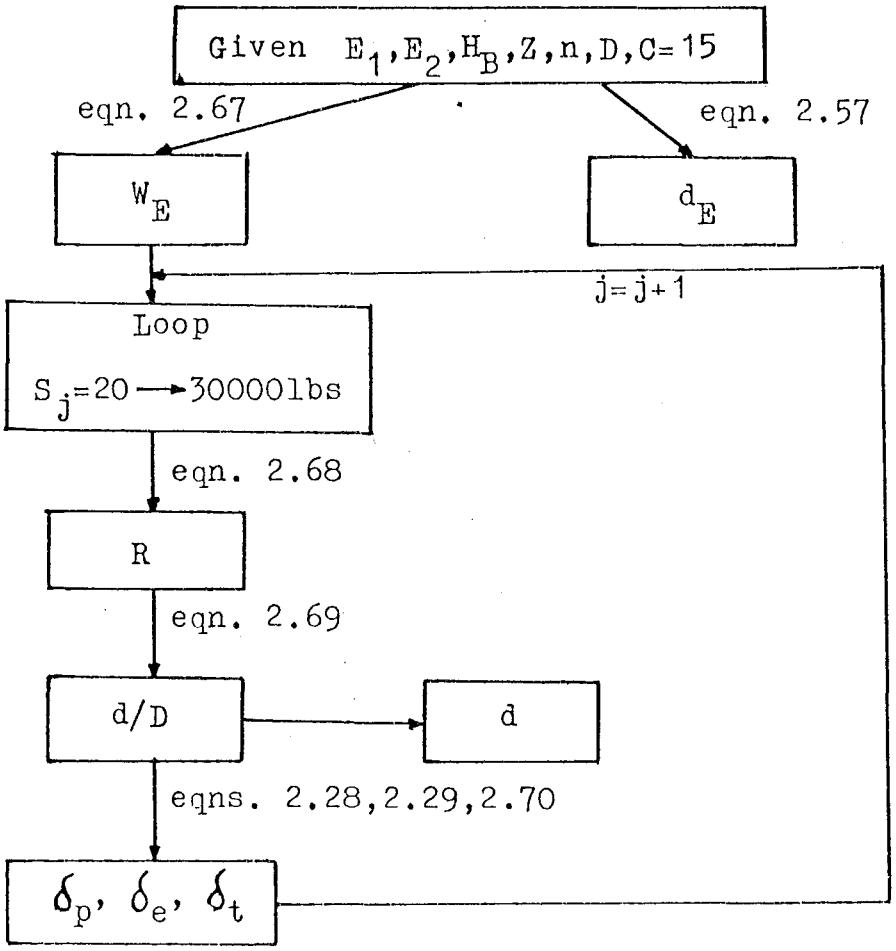

Fig. 2.53 Flow chart of program FINAL (Appendix 2.4)

SYMBOLS

Results	Inside program	Meanings
LOAD	S(I)	Load W (lbs)
INDEN DIA	DIA	Diameter of indentation d
ELAS DEF	DELE	Elastic deformation δ_e
PLAS DEF	DELP	Plastic deformation δ_p
TOTAL DEF	DELT	Total deformation δ_t
D	D	Ball diameter

see Fig. 2.10. Generally, Tabor[97] found that the ratio is about 3 to 3.6. In 1944, to investigate the ratio of $\frac{\text{UTS}}{\text{Yield stress Y}}$ (or $\frac{\text{UTS}}{\text{.2\% PS}}$ for steels which do not yield) which is termed Plasticity ratio, O'Neill plotted a graph to show its variation with respect to the amount of carbon content in steels heat-treated different ways (Fig.2.54). The average value was found to be about 1.6. Since the Meyer hardness is slightly larger than the Brinell hardness, we may assume that on average, the Meyer hardness (or the Brinell hardness) is about five times yield stress.

This assumption also applies for Aluminium alloys- see Reference 110, pages 314-315, and for Copper and its alloys, Reference 82.

For most metals, the actual yield stress commonly varies between $\frac{1}{7}$ to $\frac{1}{3}$ of its Brinell hardness; therefore, it is reasonable to assume that the yield stress is approximate $H_B/5$. It is observed that the onset of plasticity load W_E, which depends on yield stress, is generally small and common loadings usually occur at A (= W/W_E) above 20, where the Meyer constant n already dominates the shape of the curve $d = Fd_p$ and the effect of the difference between the assumed and the actual yield stress is negligible.

In making this assumption, we intend to pay more attention to the calculation of the diameter of the indentation at practical loadings, which occur at the value of 20 W_E and above, than loadings near W_E.

2.11 VARIATION OF MEYER CONSTANT n OF STEELS

Generally annealed metals have n close to 2.6. This is clearly seen in non-ferrous metals - see Appendix 2.2. However, seldom do cases of heat treated steel have $n \simeq 2.5$ - see Appendix 2.1. A graph plotted by O'Neill[77] for the variation of the Meyer constant n with respect to the carbon content in steels altered by various kinds of heat treatment, clearly shows that, commonly $2.15 < n < 2.35$, Fig. 2.55. From the above

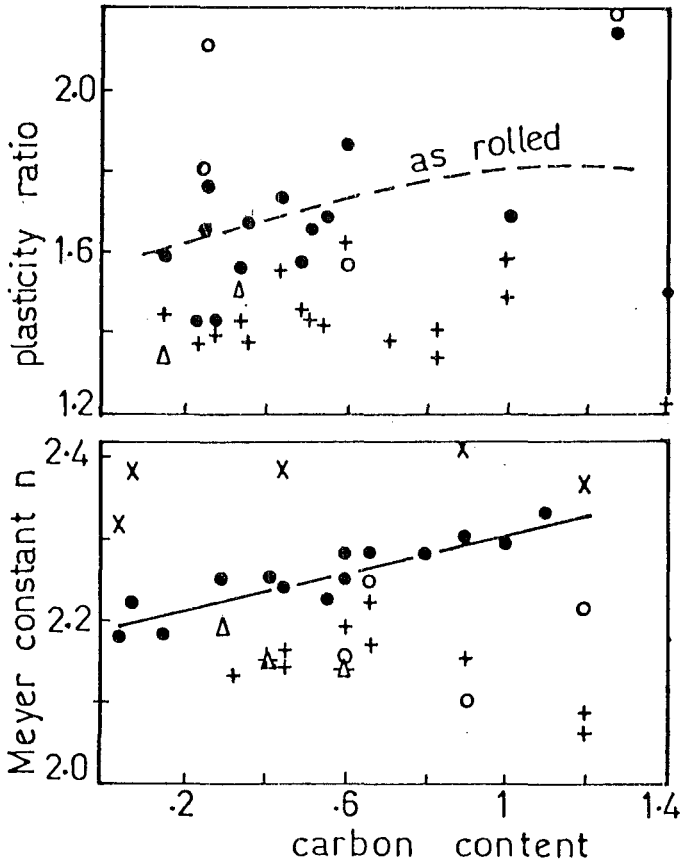

Fig. 2.54(top)-Fig. 2.55(center) The experimental data obtained by O'neill(79).

- • As rolled.
- o Spheroidized.
- + Quenched & tempered.
- X Quenched.
- Δ Oil-quenched.

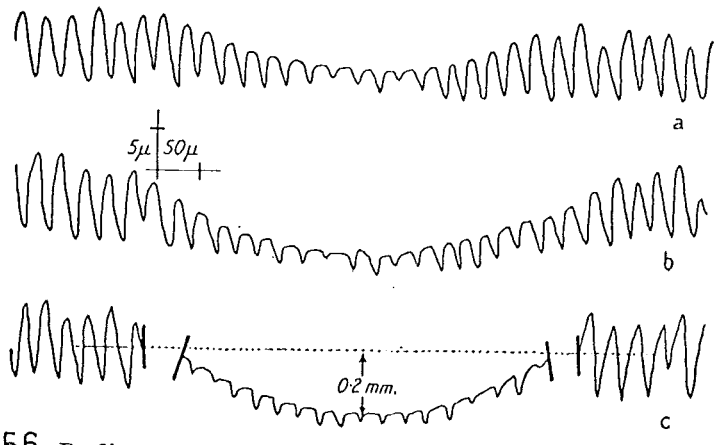

Fig. 2.56 Profilometer records of a grooved surface deformed by a hard cylinder placed with its axis parallel to the grooves: (*a*) light load, (*b*) heavier load, (*c*) very heavy load. For light loads the plastic deformation is restricted to the tips of the asperities. Only at heavier loads is the underlying metal deformed plastically, but even here the irregularities retain their identity. (Moore(66))

observation we may assume that n is approximately 2.25 for heat treated steels (i.e., we do not include the cold worked steel in this group).

For steel work-pieces: Z = 30 and X = 9.302×10^{-5}, substitute these into Equations 2.68 and 2.69 to get

$$R = (d_e/d_p)_{\text{at } W_E} = (.418/\sqrt{30})\ (26 \times 30)^{1/2.25}\ M^{1.5-3/2.25} \times$$

$$\times (9.302 \times 10^{-5})^{1-2/2.25} = .123M^{.167} \qquad 2.72$$

and

$$\frac{d}{D} = \frac{A + 15R}{A + 15}\ 1.128\ (30)^{\frac{1}{2}} \left\{\frac{.0385 \times 9.302^2 \times 10^{-10}}{30}\right\}^{1/2.25} \times$$

$$\times M^{-1/2 + 3/2.25}\ A^{1/2.25} = \frac{A + 15R}{A + 15}\ 8.36 \times 10^{-5}\ M^{.833}\ A^{.444} \qquad 2.73$$

Substitute back into Equation 2.70 we can evaluate the total deformation δ_t with slightly less work.

The assumption that n = 2.25 is made in cases where we do not have the facility to obtain the value of the Meyer constant n and where we wish to estimate the deformation within a tolerable error, say ±20%.

In practice, steel work-pieces which are undergoing such operations as drilling, milling etc., are soft steels (as rolled state), Fig. 2.55 shows that for them, n is approximately 2.25.

2.12 EFFECT OF THE SURFACE ROUGHNESS ON THE TOTAL DEFORMATION δ_t

For simplicity we assume that the asperities have tips of spherical shape and the steel indenter is perfectly smooth and of large radius of curvature compared with the asperities. Thus the deformation at each asperity may be considered as occurring between a hard flat surface and a spherical softer surface. The behaviour is essentially the same as that occurring between a hard spherical indenter pressing on to the plane of a

softer metal. The load which is required to initiate plastic deformation in asperities of specified radius of curvature will be the same. An example illustrating the order of magnitude of this load:

For fully work-hardened steel Y_o = 133 kg/mm^2 equation 2.32 gives

Radius of curvature of asperities (cm)	Onset of plastic load W_E 10^{-3}kg
10^{-4}	3.9×10^{-4}
10^{-2}	3.9

It follows that when the indenter presses on a rough surface, the indenter will, in fact, be supported by asperities that have flowed plastically until their area is sufficient to support the applied load. However, the bulk material below the asperities will initially deform elastically, until its own onset of plasticity load is reached, then it will flow plastically.

Experiments were conducted[66] by Moore: a smooth cylindrical indenter was pressed into a flat surface of work-hardened Copper in which a series of fine parallel grooves had been cut. The cylinder was arranged with its axis parallel to the grooves and indentations made at various loads. Fig. 2.56 shows that under the heavy plastic deformations of bulk material underneath the indenter, the asperities still remain visible even at the bottom of the indentation.

In practice, the plastic deformation of the asperities for the case of a spherical indenter on a rough surface is small compared with the total deformation at high load, say $W > 20\ W_E$. When the applied load is small, the deformation of the asperities is significant, as in the cases of electric resistance, friction, wear etc. investigations into the elastic and

plastic deformation of the asperities on a flat plate indented by a sphere conducted by Greenwood[38] in 1967 and Demkin[23] in 1976.

2.13 CONCLUSION

Shawki's empirical formula does not show good agreement with our experimental results for the very soft and very hard steels. The disadvantage of Shawki's empirical formula is that for each new material, the whole experiment has to be repeated, and to ensure that the formula holds well, a large field of test had to be carried out. We have presented a more powerful method for predicting the total deformation of a hard steel ball indented into a flat surface.

There are a few points to note in using our method.

- It is general, applied for any elastic material and the results can be obtained at once.

- The remarkable fact is that the total deformation δ_t can be established by a formula which is as simple as the elastic deformation formula derived by Hertz years ago.

- The elastic and plastic deformation components of δ_t are inversely proportional to the diameter of the indentation; this minimizes the error in δ_t as an error in the estimated value of the diameter of the indentation at a certain load occurs.

- The difference between the experimental and predicted theoretical diameter of indentation calculated from the equation $d = Fd_p$ is small and tolerable.

- It applies for a practical range of loading which varies from very small load to the load at which the ratio of the indentation diameter over ball diameter is less than .45.

The finite element method of Lee *et al*[55] in 1972 is undoubtedly more costly and time-consuming than ours. Our theoretical results do follow their experimental results better than their theoretical results.

CHAPTER 3

REVIEW OF THE CONTACT BETWEEN ROUGH SURFACES

3.1 INTRODUCTION

Microscopic and sometimes macroscopic irregularities or asperities exist all over a workpiece surface. The distribution of asperities, generally called roughness, is dependent on the machine process used to prepare the surface. Even on very smooth surfaces produced by lapping or honing, very fine asperities still exist. Abbott and Firestone[1] showed that it was possible to predict the area of the surface, or the land, above any given datum from a single surface profile. Thus, what became known as Abbott's bearing area curve, was first used for analysing the contact between surfaces. When two nominally flat surfaces are brought together, the contact first occurs where the asperities meet. The asperities resist deformation and cause the real area of contact to be less than the nominal area. This concept of surfaces touching over discrete small areas is fundamental to modern theories of surface contact. An increase in load brings more asperities to load sharing rather than enlarge the asperity contact radius[5]. Moore[66], on the basis of his experiments on the compression of a hard steel roller against work-hardened as well as annealed grooved copper plates, concluded that even at light loads the asperities deform plastically while the bulk material deforms elastically. Greenwood and Rowe[35] (1965) compressed a rough end face of an aluminium cylinder against a flat rigid mild steel plate. They found that when the length of the cylinder was approximately equal to its diameter, little deformation of the asperities occurred at as high a compression of the cylinder as 10% of its length. However, for the case of penny-shaped (i.e. short) cylinders, considerable flattening of asperities is inevitable. Asperities essentially retain their original shape when the plastic deformation of the bulk material does not extend to the interface, as in the case of the end compression of long cylinders. For the penny-shaped cylinder, the

asperities deform considerably since the plastically deformed region does extend to the interface. Thus the deformation of asperities on a rough surface is dependent on the thickness of the underlying bulk material. This dependence means that the study of rough surfaces in compression cannot be made on the assumption that the individual asperities deform as ideal Hertzian bodies. Early attempts to develop a mathematical treatment applied this law of deformation of ideal macroscopic bodies to individual asperities; for example, the classical elastic theory of Hertz (1881) was applied to the contact between a spherical asperity and a flat surface to obtain the relation $A \alpha W^{2/3}$ where A and W are the area of contact and the applied load respectively. Meyer's law for the plastic contact between a sphere and a plane (1908) was also used to support the assumption that the contact area is proportional to the load. Archard[5] (1957) extended the spherical asperity model and showed that for rough surfaces usually touching at so many points, the area tends to become proportional to the load even when the contact is elastic. For most asperities the radius of curvature of the tips is of the order of 1 micron and the load at which plastic flow occurs varies from .04g for soft metal like tin, to 6g for very hard steel[97]. Although the plastic flow of asperities occurs so readily, this does not mean that the underlying metal is also deformed plastically. Based on this fact Ling[58] (1958) in an effort to obtain the compliance between two rough surfaces, assumed the asperities to be symmetrical cones of angle $\frac{\pi}{2}$ and the heights of which can be represented by different types of probability distributions such as uniform, linear, normal and Poisson. Later Greenwood and Williamson (1966) assumed that the heights of the asperities were represented by a well-defined continuous distribution: the normal (also called Gaussian) distribution. This has been widely accepted. Figure 3.1 shows the cumulative height distribution of bead-blasted aluminium. Both the distribution of all heights and peak heights are Gaussian, at least in the range ±2 standard deviations.

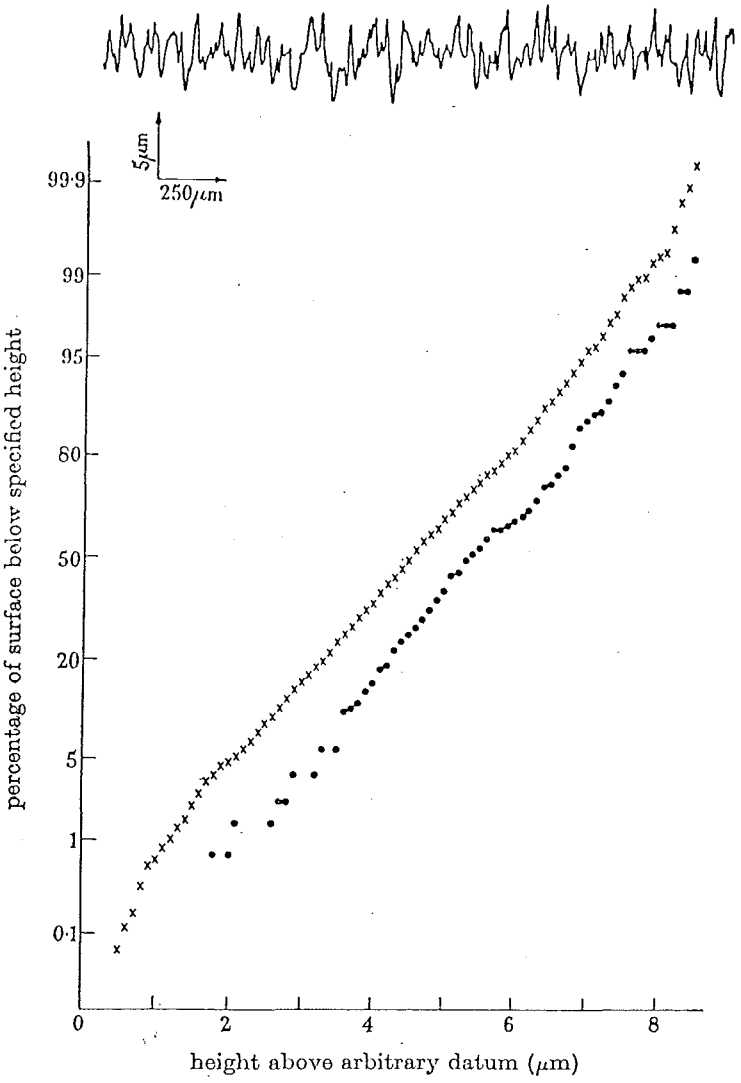

FIG. 3.1 Cumulative height distribution of bead-blasted aluminium. Both the distributions of all heights (×) and of peak heights (●) are Gaussian, at least in the range ± 2 standard deviations. The profile of the same surface is shown in the upper diagram: the vertical magnification is 50 times the horizontal magnification.

(Greenwood(36))

Originally it was thought by Greenwood and Williamson that the deformation of the asperities is elastic at light loads, becoming plastic when the load increases beyond some critical value. They defined the limit of the elastic state as when the ratio of the plastic area of contact over the total area of contact $\frac{A_p}{A}$ has a value of .02, i.e. this value is taken as the criterion for the onset of a significant degree of plasticity. On the assumption that all asperity summits have the same radius of curvature r and that their heights vary randomly according to the Gaussian distribution, applying the classical law of elasticity of contact between a sphere and a plane, they found that the dimensionless deformation δ^* of the surface asperities is equal to $\frac{\delta}{\sigma} = \frac{r}{\sigma}\left(\frac{H}{E'}\right)^2$

where

σ = standard deviation of the surface heights

r = radius of curvature of the asperity

H = Hardness of the rough material

E' = the equivalent hardness where $\frac{1}{E'} = \frac{1}{E_1} + \frac{1}{E_2}$, E_1 and E_2 are Young's modulii for the two surfaces.

Since δ^* increases when the standard deviation of roughness increases, they introduced the plasticity index

$\psi = (\delta^*)^{-\frac{1}{2}} = \frac{E'}{H}\left(\frac{\sigma}{r}\right)^{\frac{1}{2}}$ which combines the material and topographic properties of the solids in contact. In principle the plasticity index merely determines the critical load at which the deformation changes from elastic to plastic. In practice the topography exerts such an overriding influence that for most surfaces the critical load is either impractically high or negligibly low, i.e. the deformation is either always elastic or plastic by considering the numerical value of the plasticity index ψ of the surface. When $\psi > 1$ plastic deformation occurs, and when $\psi < 0.7$

elastic deformation usually occurs in very smooth surfaces. It is noted that ψ is independent of load and dependent totally on the topography of the surfaces. Most common surfaces used in normal engineering practice have plasticity index well above 1[36].

O'Callaghan and Probert[72] (1973) observed that, as the load increases, the standard deviation decreases while the radius of curvature of the asperity increases, resulting in the gradual decrease of the plasticity index ψ. This implies that the deformation of the asperities in plastic at first but later elastic, when the surfaces have been modified to produce a value of $\psi < .7$. However, this possibility remains untested. Some investigators still argue that the deformation must be both elastic and plastic and the ratio of elastic to plastic deformation will vary with the surface geometry, surface properties and sometimes the applied load (Rohsenow and Yovanovich in the discussion of reference 39). Recently in a careful experiment to measure the normal approach between rough and flat surfaces in contact, Nuri and Halling[70] (1975) also assumed that the deformation of the asperities is always composed of two components: elastic and plastic. For smooth surfaces, the deformation is almost elastic even at high load, the plastic component is small at low load and increases with the load. With increasing roughness the rate of increase in the plastic component increases significantly compared with the rate of increase in the elastic component.

Hisakado and Tsukizoe[43] (1965) assumed the material displaced by the truncation of the asperity tips, as a result of the approach of the flat surface, is negligible. Their theory proved to be valid at very low pressure (Uppal and Probert[107]). Experiments of the indentation on aluminium and indium by a hard steel punch, Williamson *et al*[113] (1972) observed the rise of the valley floor at even the slightest load; this leads to Williamson's theory in which the volume of the metal truncated is

conserved. The fact that the asperities still persist at pressure up to six times the yield stress of the asperity was seen in Williamson's experiments. This theory showed a better result than the former. In 1975, from the study of the spherical indentations in various metals at low loads, Halling[41] found that the work-hardening effect of the asperities increases the stiffness of the surface texture significantly.

By a different approach Kragelsky and Demkin[18] (1960) tried to establish the initial part of the bearing area curve to be of the form $b\rho^{\nu}$ where b is a constant depending on the topographic properties of the surface, ρ is the dimensionless compliance $(=\frac{a}{R_m}$ where a is the deformation and R_m the peak-valley height of the asperity, see Figure 3.9), ν is the bearing area curve parameter. Theory developed by Demkin[19] (1970) for low pressure and later (1975) for high pressure are also very interesting. For the deformation of rough curved bodies we found that the Demkin theory[23] is easier to use than that of Williamson (Greenwood and Tripp[38] (1967) and Lo[60] (1969)).

The elastic contact between rough and flat surfaces remains an interesting topic for scientists and engineers. A paraboloidal model with the same curvature representing the asperities was considered by Bush and Gibson[9] (1975). A distribution of the surface slopes of the asperities, conical models with different apex angles, variation of the flow pressure of each contact due to the work-hardening of the asperities were studied by Tsukizoe and Hisakado[43-47] (1974-1976).

Until a well-proven unified theory is widely accepted, the best that can be done is to present a number of possible theories with their regions of validity proved by experimental results. They are later used for practical application such as evaluation of the deformation of a system of a flat locator indented into flat workpieces of different hardness and varying degrees of roughness.

3.2 THEORY OF HISAKADO AND TSUKIZOE[43]

Assumptions

1) The distribution curve of the surface heights is normal, that is

$$f(u) = \frac{1}{\sigma\sqrt{2\pi}} \exp\left[-\frac{1}{2}\left(\frac{u}{\sigma}\right)^2\right] \qquad 3.1$$

2) Plastic deformation of the metal occurs at the contact.

3) The flow pressure $q_m = \frac{W}{A}$ is constant (i.e. it is independent of load W which implies no work-hardening of the asperities, A being the real area of contact). The flow pressure is also assumed to be equivalent to the indentation hardness M (Meyer's hardness).

4) Interaction between asperities is negligible.

5) The ratio of real over apparent area of contact is equivalent to the bearing fraction of the surface profile at a particular level, i.e. $\frac{A}{A_n} = \frac{\Delta L}{L_o}$ (Figure 3.2) since the surface is assumed to be isotropic, a traverse in any direction gives the same profile.

6) The material displaced by the truncation of the asperity tips as a result of the approach of the flat surface is negligible.

7) The standard deviation and the mean slope of the asperities are considered invariant during the deformation.

8) The interaction between neighbouring asperities is not considered.

Hisakado and Tsukizoe proved that

$$\frac{\Delta L}{L_o} = \frac{\int_u^{\varepsilon\sigma} f(u)\,du}{\int_{-\varepsilon\sigma}^{\varepsilon\sigma} f(u)\,du} \qquad 3.2$$

where $u = t\sigma$ is the separation between two mean planes.

Substituting $u = t\sigma$ into Equation 3.1 to obtain the standard normal distribution

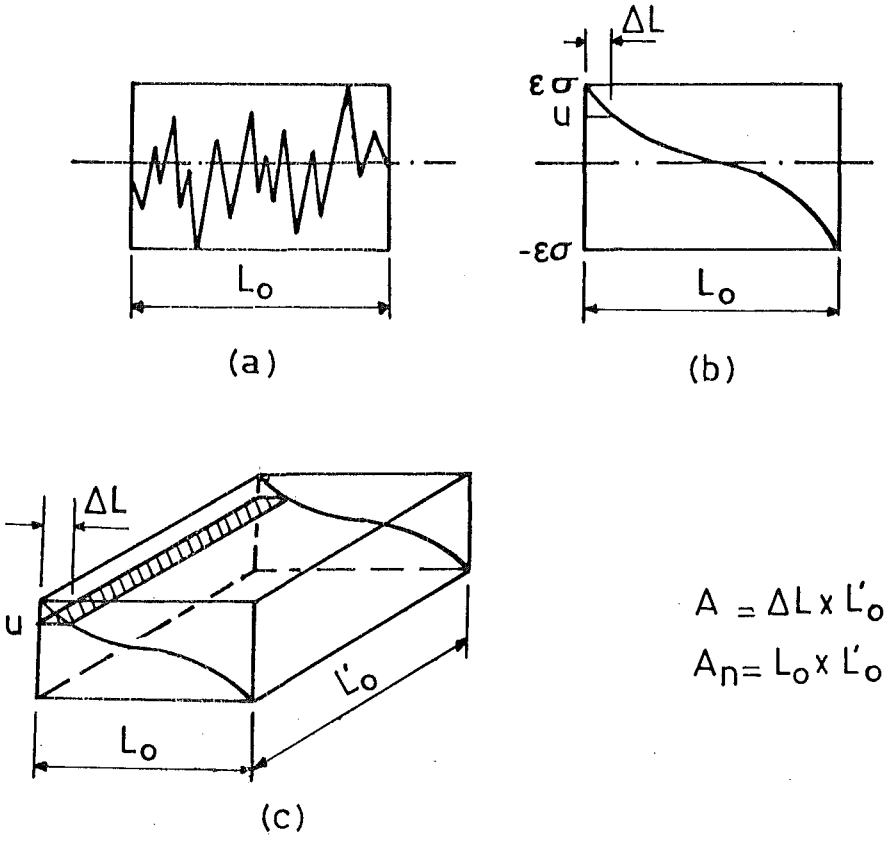

Fig. 3.2 The surface profile and Abbott bearing area curve.

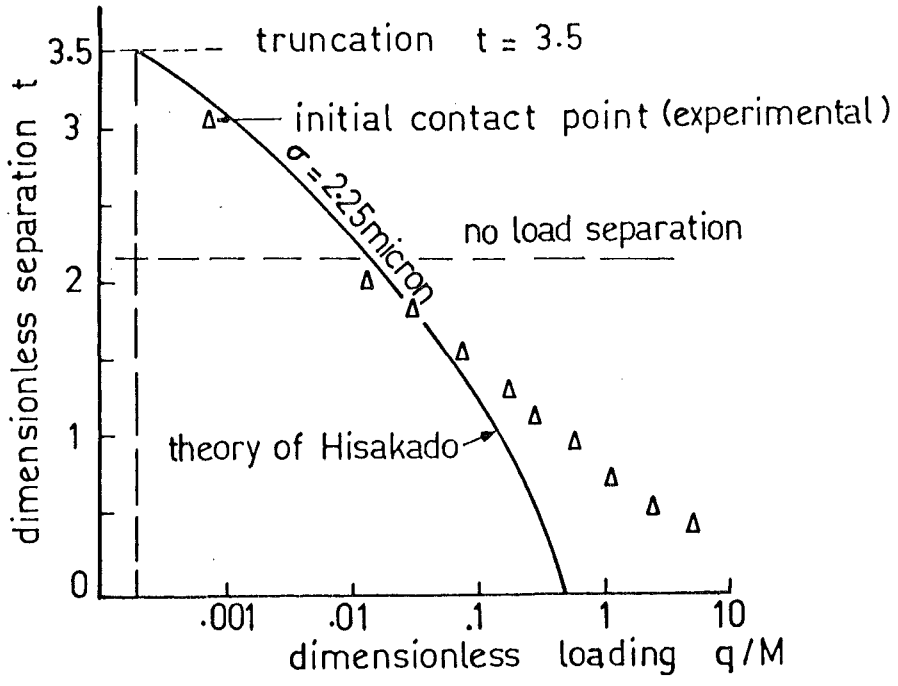

Fig. 3.3 The theory of Hisakado is compared with the experimental data of Uppal[107] on an aluminium model.

$$f(t) = \frac{1}{\sqrt{2\pi}} \exp\left(-\frac{t^2}{2}\right) \qquad 3.3$$

Also noted that $\int_{-\varepsilon\sigma}^{\varepsilon\sigma} f(u)\,du = \int_{-\varepsilon}^{\varepsilon} f(t)\,dt$

As $\varepsilon \to \infty$ this integral tends to a value of unity. For $\varepsilon \geqslant 3$ it can be concluded from tabulated values of the integral that the departure from unity is less than 1%. Therefore Equation 3.2 becomes

$$\frac{\Delta L}{L_o} = \int_{u}^{\varepsilon\sigma} f(u)\,du = \int_{t}^{\varepsilon} f(t)\,dt$$

$$= \int_{0}^{\varepsilon} f(t)\,dt - \int_{0}^{t} f(t)\,dt$$

The function $\phi(\varepsilon) = \int_{0}^{\varepsilon} f(t)\,dt$ may be seen from tables[26] that

$$\phi(\varepsilon) \simeq \frac{1}{2} \text{ for } \varepsilon \geqslant 3$$

thus

$$\frac{\Delta L}{L_o} = .5 - \phi(t) \qquad 3.4$$

Since the deformation is assumed to be entirely plastic

$$\frac{q}{M} = \frac{A}{A_n} \text{ where } q = \frac{W}{A_n}, \text{ load per unit apparent area}$$

Also it has been shown that $\frac{\Delta L}{L_o} = \frac{A}{A_n}$

Thus

$$\frac{q}{M} = \frac{A}{A_n} = \frac{\Delta L}{L_o} = .5 - \phi(t) \qquad 3.5$$

The separation $u = t\sigma$ between two surfaces can be found if the standard deviation σ of the rough surface is known. The function $\phi(t)$ is tabulated in most mathematical and statistical textbooks. Experiments by Uppal and Probert[107] on aluminium, tin and silver, showed that the initial contact

occurs nearer t = 3.5 than t = 3.0. They also plotted the comparison between their experimental results and Hisakado's predictions (Fig.3.3). The divergence ensues in the regions of $\frac{q}{M} \simeq .1$, .05 and .025 for tin, aluminium and silver surfaces respectively. At higher pressure the plastic deformation of the aseprities requires the invoking of a hypothesis for asperity interaction. According to Hisakado, the separation between two surfaces becomes zero as $\frac{q}{M}$ tends to .5, but this was not found true in experiments by Uppal and Probert[107] or by Williamson *et al*[113]. In reality separation will not become zero even at very high load[11].

3.3 THE THEORY OF WILLIAMSON[113] (1972)

Investigating the failure of the theory of contact of Hisakado at high loads, Williamson found that the asperities still persist at pressures up to two times the hardness of the metal. Williamson proposed a theory which takes into account the amount of the metal displaced from the crushed asperities and claimed to predict accurately the variation of both the true area of contact and the separation with pressure up to several times the yield pressure of the asperities. When asperities are crushed, the material displaced from the truncated tips has been ignored in Hisakado's theory. Williamson assumed that the volume is conserved and the material displaced from the contacting regions reappears by raising all parts of the non-contacting surface. The constant volume assumption implies that the mean plane of the surface remains fixed.

Williamson observed that the valley floor begins to rise immediately as the lightest load is applied to the contacting asperities, material from which is displaced downwards. All of the surface not in contact rises. It is assumed that the plastic rise of non contacting surface can be treated as uniform (Fig.3.4). All assumptions except the No.6, made by Hisakado are also used in Williamson's theory.

nominal pressure $q = W/A_n$

mean pressure $q_m = W/A$

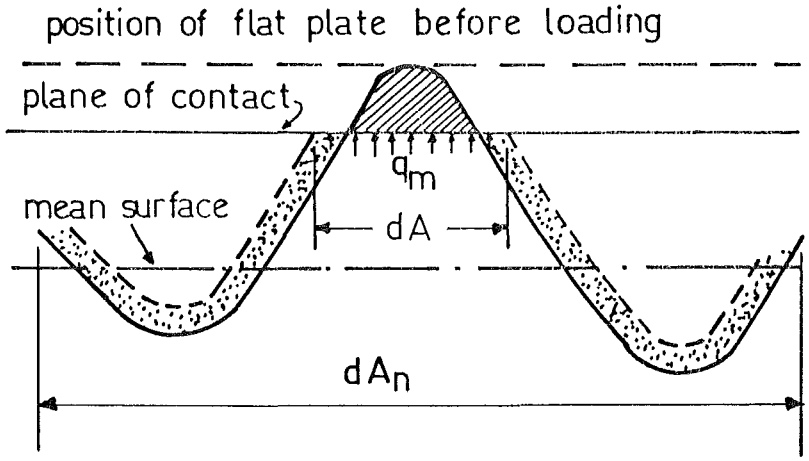

Fig. 3.4 The uniform redistribution of the truncated tip.

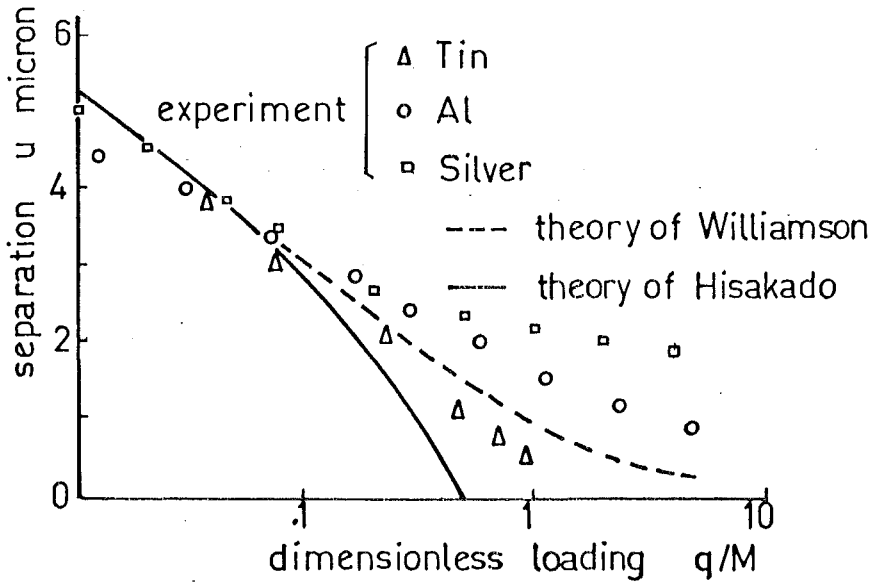

Fig. 3.5 The theories of Hisakado and Williamson are compared with the experimental data obtained by Uppal[107].

Consider an asperity crushed by a moving hard flat plate downwards a distance ds under an applied load W. According to the uniform rise assumption the displaced material reappears as a rise v in the non-contacting surface. The relative movement of the flat plate is ds + v. Summing over the array of the asperities gives the total work done as $q_m A(ds + v)$.

This equals the work done by the applied force, i.e.

$$Wds = q_m A(ds + v) \qquad 3.6$$

Since the volume of the affected material is conserved

$$Ads = v(A_n - A)$$

$$\text{or} \quad v = \frac{Ads}{A_n - A}$$

Substituting for v into Equation 3.6 to get

$$q_m \frac{W}{A_n} = \frac{A}{A_n - A}$$

$$\text{or} \quad W^* = \frac{\eta}{1-\eta} \qquad 3.7$$

where $\eta = \frac{A}{A_n}$, the dimensionless area of contact or the degree of contact

and $W^* = \frac{q}{M} = \frac{W}{q_m A_n}$, the dimensionless load.

Equation 3.7 is independent of the geometry of the individual asperities. The derivation, however, does not take into account the interaction between neighbouring asperities, therefore Equation 3.7 provides a lower limit estimate for W*.

Let f(z) be the distribution function of the peak heights of the rough surface, i.e.

$$f(z) = \frac{1}{\sigma\sqrt{2\pi}} \exp\left[-\frac{1}{2}\left(\frac{z}{\sigma}\right)^2\right]$$

the degree of contact η of the crushed surface, corresponding to a separation u may be written as

$$\eta = \int_u^\infty f(z)\, dz \qquad 3.8$$

Adopting the "uniform rise" of the material hypothesis, Williamson suggested that the true separation is not u but $u + v$ since the displaced volume is conserved.

$$v = \int_u^\infty (z - u)\, f(z)\, dz \qquad 3.9$$

The net separation s is therefore given by $s = u + v$ or

$$s = u + \int_u^\infty (z - u)\, f(z)\, dz \qquad 3.10$$

In the dimensionless form put

$$x = z/\sigma \quad , \quad t = u/\sigma \quad \text{and} \quad s^* = s/\sigma$$

then

$$\eta = \int_u^\infty f(z)\, dz = \int_t^\infty f(x)\, dx = F(t) \qquad 3.11$$

and

$$s^* = t + \int_t^\infty (x - t)\, f(x)\, dx$$

where

$$f(x) = \frac{1}{\sqrt{2\pi}} \exp\left(-\frac{x^2}{2}\right) \qquad 3.12$$

i.e.

$$s^* = \frac{s}{\sigma} = t - tF(t) + f(t) \qquad 3.13$$

From Equations 3.7 and 3.11 it may be deduced that

$$\eta = F(t) = \frac{W^*}{1+W^*} \qquad 3.14$$

Equations 3.13 and 3.14, together with the appropriate data from the statistical tables, permit the load and the corresponding separation s to be evaluated.

The rise of the material v may also be obtained

$$v = \int_u^\infty (z - u)f(z)\,dz = \int_u^\infty zf(z)\,dz - \int_u^\infty uf(z)\,dz \qquad 3.15$$

or in the dimensionless form

$$v^* = \frac{v}{\sigma} = \int_t^\infty xf(x)\,dx - \int_t^\infty tf(x)\,dx$$

i.e.

$$v^* = f(t) - tF(t) \qquad 3.16$$

Equation 3.14 gives the value of the function F(t) at any load and hence the dimensionless rise of the material can be found.

Values of the dimensionless separation t, actual dimensionless separation s* and dimensionless loading $W^* = \frac{q}{M}$ are tabulated in Appendix 3.1.

Discussion

In reality the rise of the non-contacting parts of the surface is not uniform. Experiments by Uppal and Probert[107] showed that for an aluminium surface, under the loads at which $\frac{q}{M} \sim 1.0$, there was a tendency for the bottoms of all valleys to rise. However, deep valleys only exhibited a small effect whereas for shallow valleys, rises of as much as nine times were observed.

Experiments by Williamson and Pullen[113] showed a close agreement with the theoretical values (Fig.3.6). However, Uppal and Probert observed a divergence between the theoretical values and their experimental results

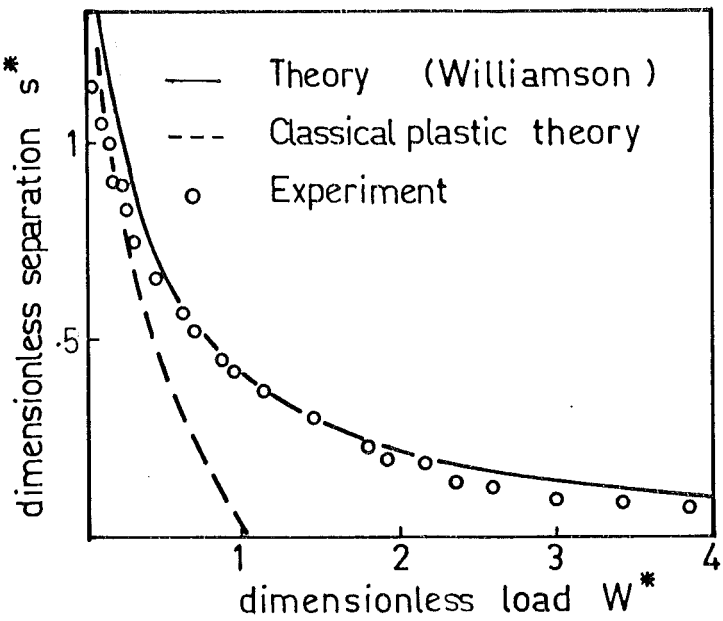

Fig. 3.6 The theoretical relation between load and separation is compared with the experimental data of Williamson[113]

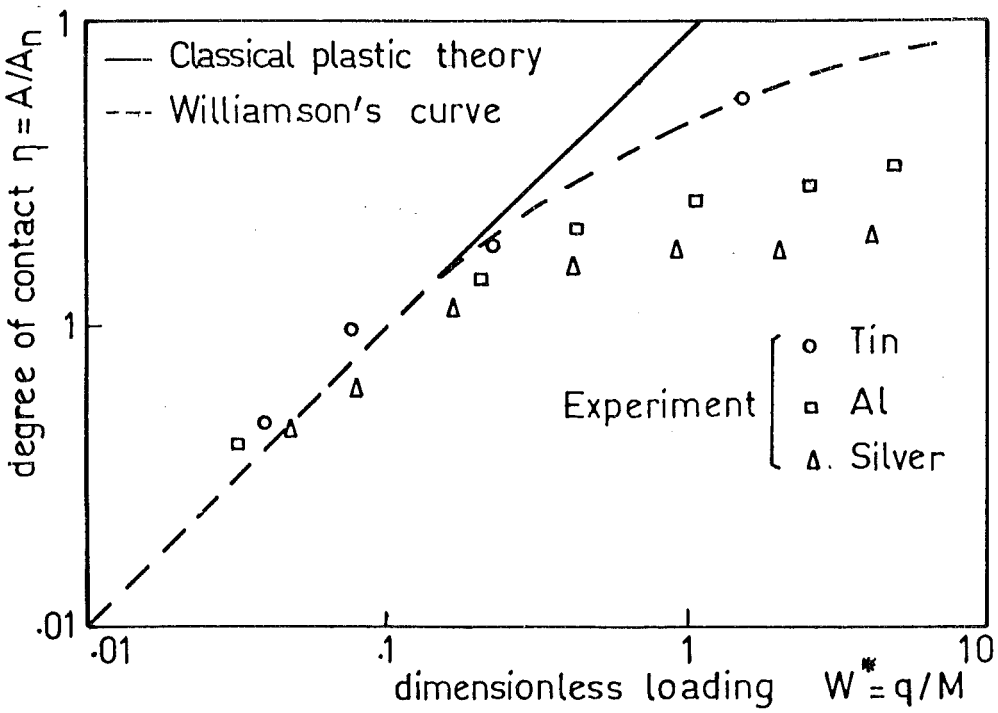

Fig. 3.7 The comparison between the theoretical and experimental data obtained by Uppal[107].

(Fig.3.5). It appears to apply very well to tin, but for silver and aluminium, the degree of contact is overestimated for loading higher than $\frac{q}{M} \sim .1$.

Williamson's approach does not take into account the interaction between neighbouring asperities. This interaction, together with the persistence of asperities even at very high loads, results in the lower value for the degree of contact.

Williamson's theory is in general a better estimation than Hisakado's theory at higher loads (Fig.3.5).

As the dimensionless load W* tends to unity, the theoretical degree of contact η tends to .5 while the classical plastic theory (asperities deform plastically, flow pressure is equal to the asperity hardness, i.e. real dimensionless area of contact $\eta = \frac{A}{A_n}$ is equal to $W^* = \frac{q}{M}$) shows unity (Fig.3.7) also as the dimensionless load W* tends to infinity, the degree of contact η tends to infinity.

Empirical formulae for the relationship between the degree of contact η and the dimensionless load were proposed for aluminium by Uppal and Probert [107] to fit the experimental curve.

A careful study of O'Callaghan and Probert [72] (1973) on the compression of a rough aluminium surface by a harder flat surface found that the effective surface hardness and topographical parameters of the rough surface are load dependent and consequently the experiments suggested the degree of contact as

$$\eta = \frac{q}{M^*} = 6.95 \times 10^{-4} \left(\frac{q}{M}\right)^{.35} \qquad 3.17$$

where M* is the effective contact hardness

$$\frac{M^*}{M} = 1440 \left(\frac{q}{M}\right)^{.65} \qquad 3.18$$

They concluded that the application of any formula involving surface topographical parameters requires that the histories of the surfaces be considered.

3.4 THE THEORY OF DEMKIN (1970 - 1975)

The theory of contact between rough surfaces under low normal pressure was initiated by Kragelsky and Demkin[18] (1960). It was later modified and published by Demkin[19] (1970) in the form of a book written in Russian (which we have not been able to obtain in New Zealand). However, almost all of the important results have been published in some of his articles which were written in English[20-23]. In 1975 Demkin and Izmailov[22] proposed a theory for the deformation of wedge model asperities under high normal pressure. This theory was based on the slip-line theory of plasticity.

The surface of a body is not only rough but also wavy. The existence of roughness and waviness is responsible for the fact that two unlubricated surfaces are always in contact at some spots and owing to the waviness, the spots are found in definite regions. The number of spots and regions of contact are dependent on the load, mechanical characteristics of the surface, and its geometrical shape.

Depending on the particular conditions, the types of contact may be described by the following:

a) Apparent area of contact A_n - confined by the dimension of the contact zone of the bodies. It is the envelope of all possible real areas of contact.

b) Contour area of contact A_c - the area formed by the bulk compression of the waves.

c) Real area of contact A - the sum of all the small actual areas of contact. This depends on the load.

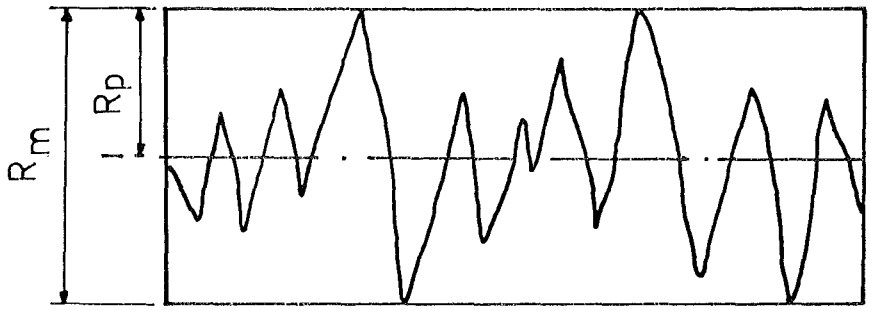

Fig. 3.8 The surface profile within a contour area.

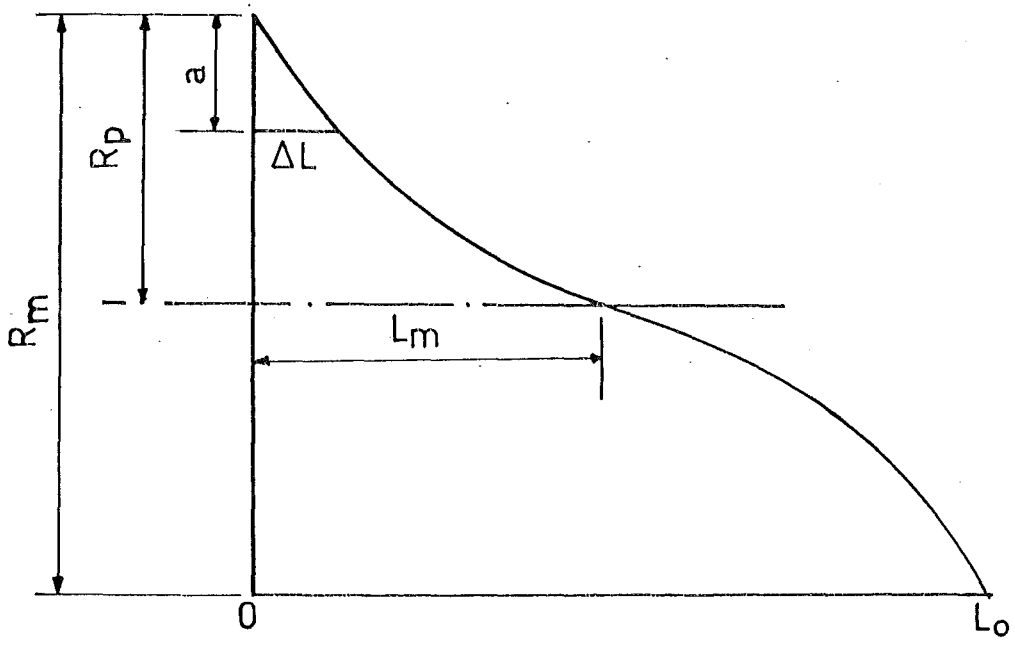

Fig. 3.9 The Abbott bearing area curve.

Expressing in more convenient dimensionless value

- the relative area of contact with roughness but without waviness

$$\eta_1 = \frac{A}{A_c}$$

- the relative area of contact with waviness but without roughness

$$\eta_2 = \frac{A_c}{A_n}$$

- the relative area of contact with both roughness and waviness

$$\eta_3 = \frac{A}{A_n} = \eta_1 \eta_2$$

Figures 3.8 and 3.9 show a surface profile inside a contour area and its reference curve. Defining the following terms

R_m = peak-valley height of the profile

R_p = depth of flattening of the profile

a = the depth from the highest peak

$\rho = \frac{a}{R_m}$ the dimensionless compliance (deformation of the asperities)

If we assume the surface has no waviness and the asperities are random and isotropic so that any profile curve is the same, then the degree of contact $\eta = \eta_3 = \frac{A}{A_n}$ is the same as the relative bearing length $\frac{\Delta L}{L_o}$ at any reference level.

3.4.1 Low Normal Pressure

Having studied a great number of differently machined surfaces, Kragelsky and Demkin[18] found that all kinds of treatment are represented by an exponential relationship between η and ρ . The expression is complicated. However, for practical application it is necessary to take into account that under low normal pressure the real area of contact is never more than $\frac{1}{10}$ to $\frac{1}{5}$ of the apparent area. Thus, it is of practical interest to investigate the initial part of the bearing area curve which

can be expressed with a sufficient degree of precision by a parabolic function

$$\eta = b\rho^{\nu} \qquad 3.19$$

where ν is called the bearing curve parameter.

Demkin[21] also found that the degree of contact η can also be written in the form

$$\eta = \frac{A}{A_n} = \frac{\Delta L}{L_o} = b\rho^{\nu} = L_m\left(\frac{a}{R_m}\right)^{\nu} \qquad 3.20$$

Let q be the pressure acting on the apparent area A_n, then the deformation, a, from the highest peak of the asperities is[23]

$$a = Dq^{\frac{1}{\nu+\gamma}} \qquad 3.21$$

the coefficient D depends on the geometrical and mechanical properties and on the mode of contact (elastic or plastic).

γ depends on the mode of contact only.

In general the coefficient D is given by

$$D = R_p\,(\alpha_o k \eta_o B)^{-\frac{1}{\nu+\gamma}} \qquad 3.22$$

where

$$k = \frac{\Gamma(\nu+1)\Gamma(\gamma+1)}{\Gamma(\nu+\gamma+1)}$$

Γ is the gamma function

$\eta_o = \frac{L_m}{L_o}$ is the ratio of bearing length on the mean line depth to the profile length - approximately $\frac{1}{2}$ for most cases

α_o, B depend on the shape of a single asperity and the mode of deformation

The bearing curve parameter ν can be obtained from the profile characteristics derived from the profilometry

$$\nu = 2\eta_o \frac{R_p}{R_a} - 1 \qquad 3.23$$

where R_a is CLA (centre line average)

In particular

1) For plastic deformation $\gamma = 0$

$$a = R_p \left(\frac{q}{\eta_o c\sigma_o}\right)^{1/\nu} \qquad 3.24$$

where $c\sigma_o$ is the asperity flow pressure.

2) For elastic deformation of asperity $\gamma = \frac{1}{2}$

$$a = R_p^{2\nu/2\nu+1} \left(\frac{q}{.5\eta_o VB}\right)^{1/2\nu+1} \qquad 3.25$$

where $V = 3\sqrt{\pi}\frac{\Gamma(\nu+1)}{4\Gamma(\nu+1.5)}$ $\qquad B = .43\frac{E}{(1-\mu^2)r^{.5}}$ $\qquad 3.26$

r is the radius of curvature of the asperity, E, μ are Young modulus and Poisson ratio respectively.

Units: a, r, R_p, R_a are in mm

E, q are in kg/mm^2

3.4.2 High Normal Pressure

Under low pressure an individual asperity is only slightly deformed, hence it can be considered to be independent of the neighbouring asperities. However, under high pressure this is no longer valid as the real contact area exceeds a critical value. Two models of a single asperity are studied

1) Conical type corresponding to the ground and polished surfaces.

2) Wedge type corresponding to planed, turned and milled surfaces

Assumptions used for the models are

a) The material is considered to be rigid-plastic.

b) The rough surface has no waviness.

c) The volume of metal is conserved.

d) The surface is anisotropic with directional asperities of wedge type

and isotropic of conical type.

During compression, the material of the truncated tip is redistributed on the shoulder (Fig.3.10). For volume conservation the area of the triangle ABC is equal to the trapezium ABED. Calculation by Demkin *et al*[22] shows that

$$\tan\theta = \tan\theta' \left[\frac{\sin\theta' (2 + \sin\theta') + 1}{\sin\theta' (2 + \sin\theta')} \right] \qquad 3.27$$

For most usual values of θ ($>60^{o}$) the difference between θ and θ' is less than 10^{o}.

Similarly for the cone

$$\tan\theta = \tan\theta' \frac{(2\sin\theta' + 1)^3}{(2\sin\theta' + 1)^3 - 1} \qquad 3.28$$

Let $\alpha = \frac{DE}{EF}$ be the ratio of the final and initial bearing length then for wedge model

$$\alpha (2 - \alpha) = \frac{\tan\theta'}{\tan\theta} \qquad 3.29$$

For apex angles $120^{o} < 2\theta < 170^{o}$ and $1.56 < \alpha < 1.50$ (Fig.3.12)

From Fig.3.10 it is seen that the deformation of the asperity is independent until the plastically deformed zone AB is equal to the wedge base L_o. The degree of contact for the wedge is $\eta = \frac{\Delta L}{L_o}$ and for the cone $\eta = (\frac{\Delta L}{L_o})^2$. Hence the critical values of the dimensionless real contact area η_{cr} which corresponds to the beginning of the asperity interaction will be

a) For maximum friction on the asperity face (slip line field is shown in Fig.3.10).

The critical value of η_{cr} for usual values of tip angles $\theta > 60^{o}$ is

wedge model $\qquad .34 < \eta_{cr} = \frac{1}{2 + \sin\theta'} < .37 \qquad 3.30$

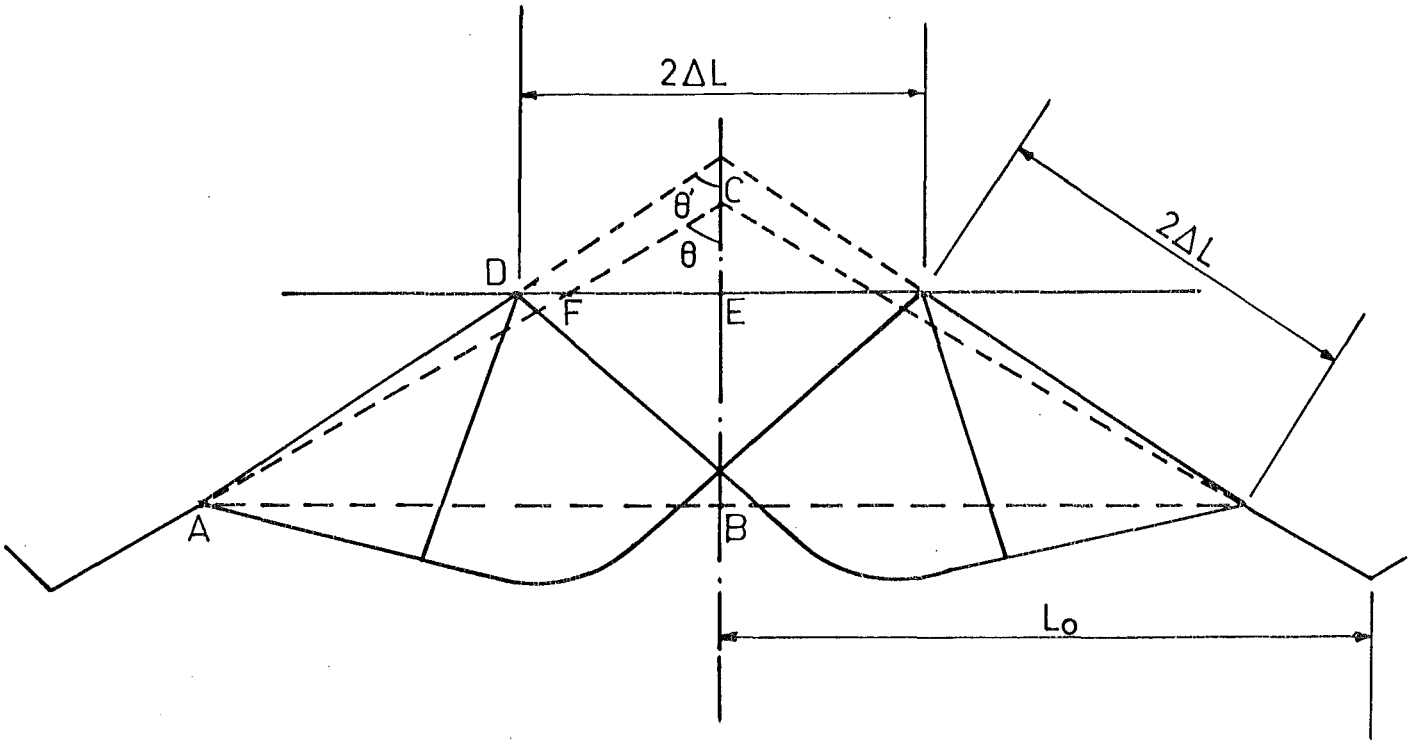

Fig. 3.10 The slip-line field for the compression of a plastic wedge by a hard punch with maximum interfacial friction (Demkin[22]).

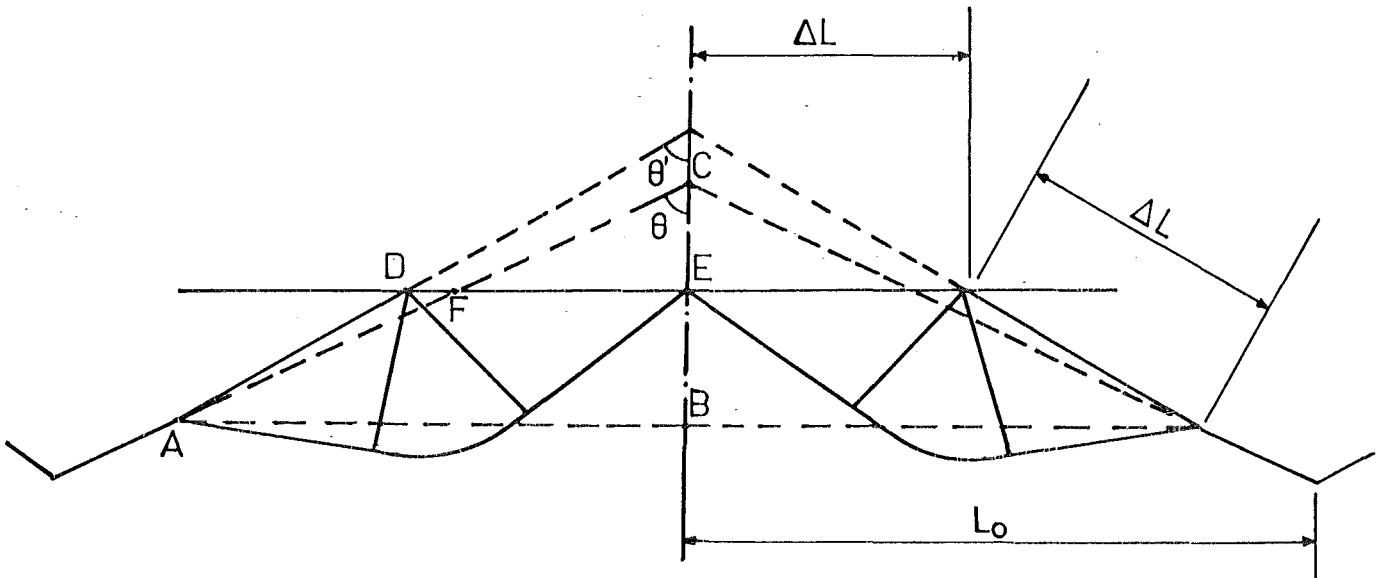

Fig. 3.11 The slip-line field for the compression of a plastic wedge by a hard punch without interfacial friction (Demkin[22]).

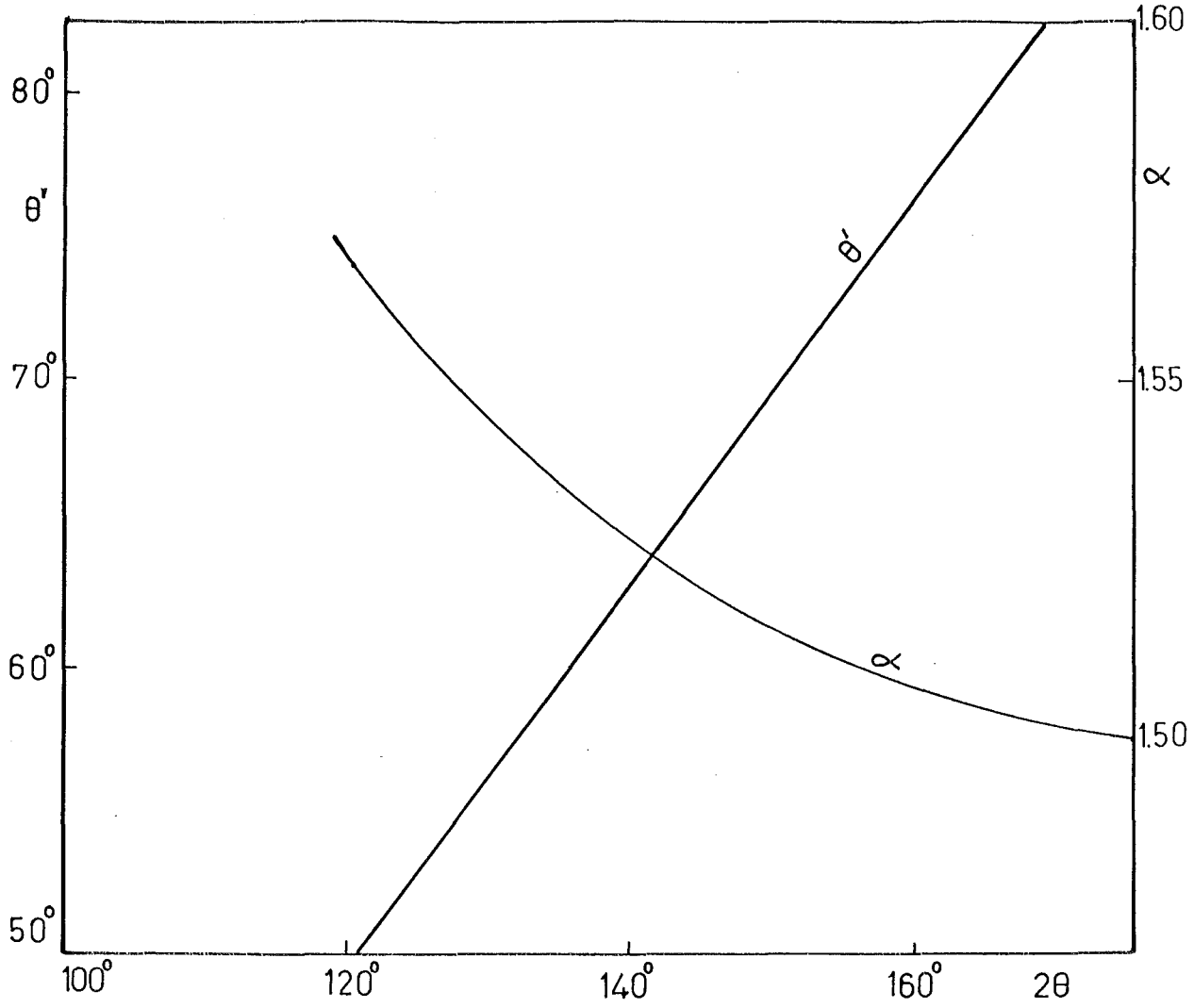

Fig. 3.12 Wedge model asperity.

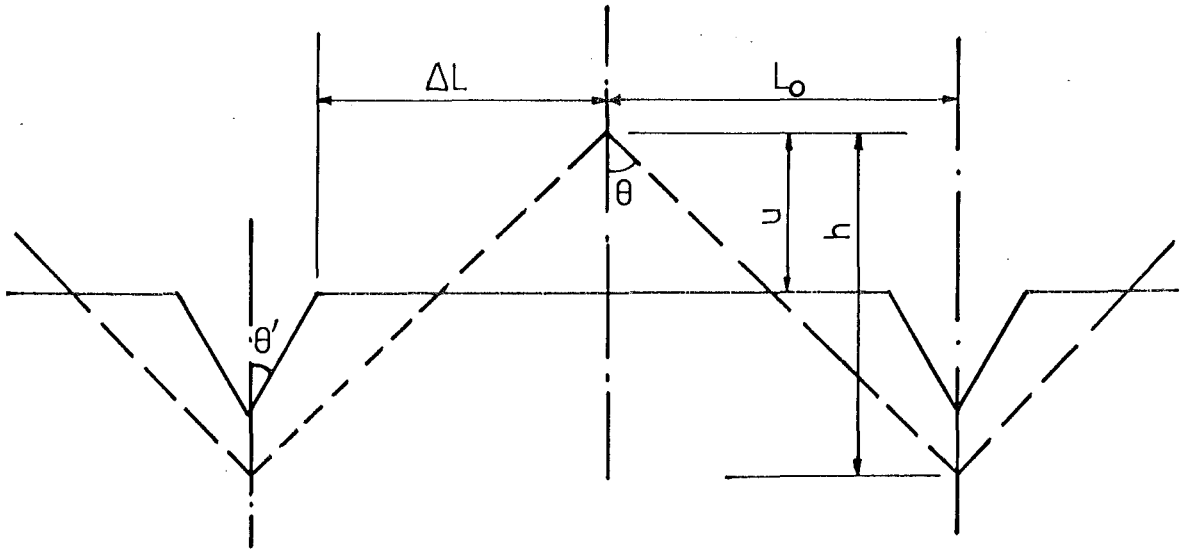

Fig. 3.13 Deformation of a plastic wedge under high normal pressure ie. for $\eta > \eta_{cr}$ (Demkin[22])

cone model $\quad .11 < \eta_{cr} = \dfrac{1}{(2 + \sin \theta')^2} < .13 \qquad 3.31$

b) For no friction on the asperity face (Fig.3.11)

The critical value of η_{cr} for common values of tip angles $\theta > 60^{o}$ is

wedge model $\quad .5 < \eta_{cr} = \dfrac{\sin \theta'}{1 + \sin \theta'} < .53 \qquad 3.32$

cone model $\quad .25 < \eta_{cr} = \dfrac{1}{\sin \theta' + 1} < .3 \qquad 3.33$

The above results were established by Demkin[22]. They are valid for rough surfaces with asperities of equal height. For asperities of various heights the critical values of the dimensionless real contact area (degree of contact) may differ slightly from the obtained values[22].

WEDGE MODEL ASPERITY

Consider a no-load bearing curve for a rough surface with equal height. The degree of contact η is given as

$$\eta = \rho \qquad 3.34$$

During the first stage of deformation the redistribution of the asperity flattening will change the bearing area curve to

$$\eta = \alpha\rho \qquad 3.35$$

where α is the ratio defined by Equation 3.29.

As the deformation exceeds the critical value η_{cr}, the rise of the bottom of the valley begins due to the asperity interaction and the volume conservation. Fig. 3.13 gives

$$u^2 \tan \theta = (L_o - u \tan \theta)(h - u) \frac{(L_o - \Delta L)^2}{\tan \theta'}$$

Substitute $\rho = \dfrac{u}{h}$ and $\eta = \dfrac{\Delta L}{L_o}$ to get

$$\rho = .5 - .5 (1 - \eta^2) \frac{\tan \theta}{\tan \theta'} \qquad 3.37$$

Hence the degree of contact of the second stage $\eta > \eta_{cr}$ of the deformation of the asperities is

$$\eta = 1 - [\alpha(2 - \alpha)(1 - 2\rho)]^{\frac{1}{2}} \qquad 3.38$$

i.e., the degree of contact tends to 1 as the dimensionless compliance ρ tends to .5 and not to unity as it follows from the no-load bearing curve.

The two curves representing Equations 3.35 and 3.38 intersect each other at point C (Fig.3.14) corresponding to the critical value of the degree of contact

$$\eta_{cr} = \alpha - 1 \qquad 3.39$$

The value of α varies with the tip angle θ of the asperity (Equation 3.29) and so does η_{cr}. For most common values of θ ($>60^{o}$) α is approximately 1.5, hence $\eta_{cr} \sim .5$ which is in good agreement with Equation 3.32.

Fig.3.14 shows the no-load and deformed bearing curves for the surface having wedge asperities of equal height.

By using the kinematic slip line theory and plotting the velocity hodograph for the indentation of a hard wedge asperity into a soft flat surface, Demkin obtained the relationship between the applied pressure q yield stress Y of the soft surface, and the degree of contact η

$$\frac{q}{Y} = (\eta+1)\ (\eta/1-\eta)^{\frac{1}{2}} \qquad 3.40$$

The same relation is obtained for the compression of a plastic wedge asperity by a hard flat punch[22]. This Equation shows that as q tends to infinity, the degree of contact tends to unity, this implies that the asperity still persists for very high pressure up to 6Y (experiments by Uppal and Probert[107] and Child[11] (1973), Demkin (1975). The relationship between η and $\frac{q}{Y}$ in Equation 3.40 is drawn in Fig.3.15. Combination of two Equations 3.38 and 3.40, with α= 1.5 gives the relationship between the dimensionless compliance ρ and $\frac{q}{Y}$. Fig.3.15 also shows the agreement of

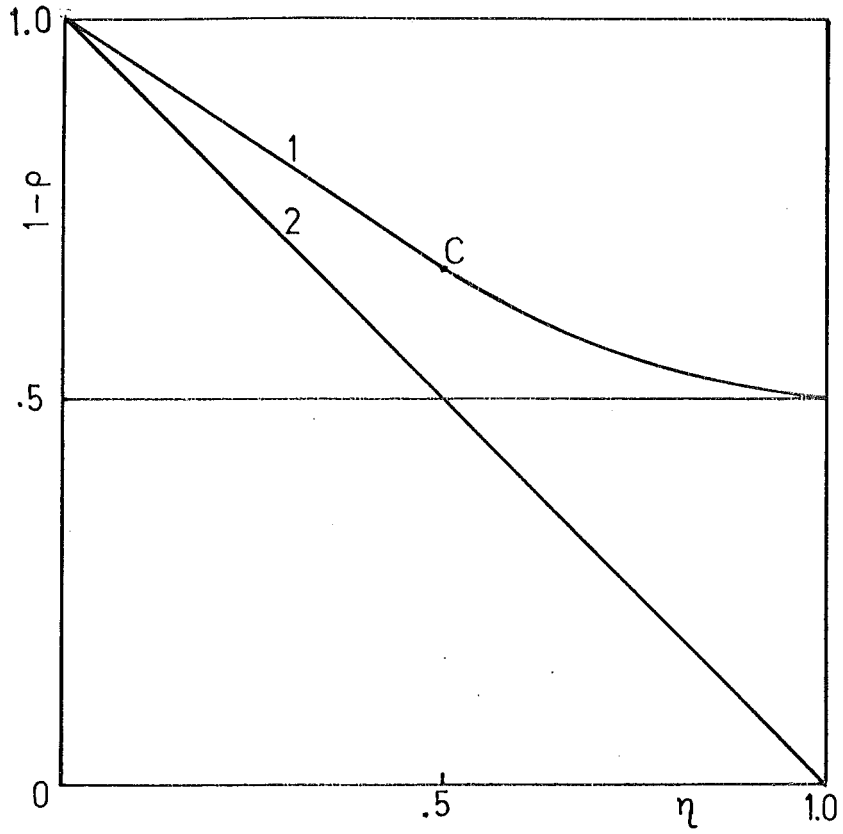

Fig. 3.14 Bearing area curves for the wedge model asperity of equal height. 1: Deformed , 2: No-load.

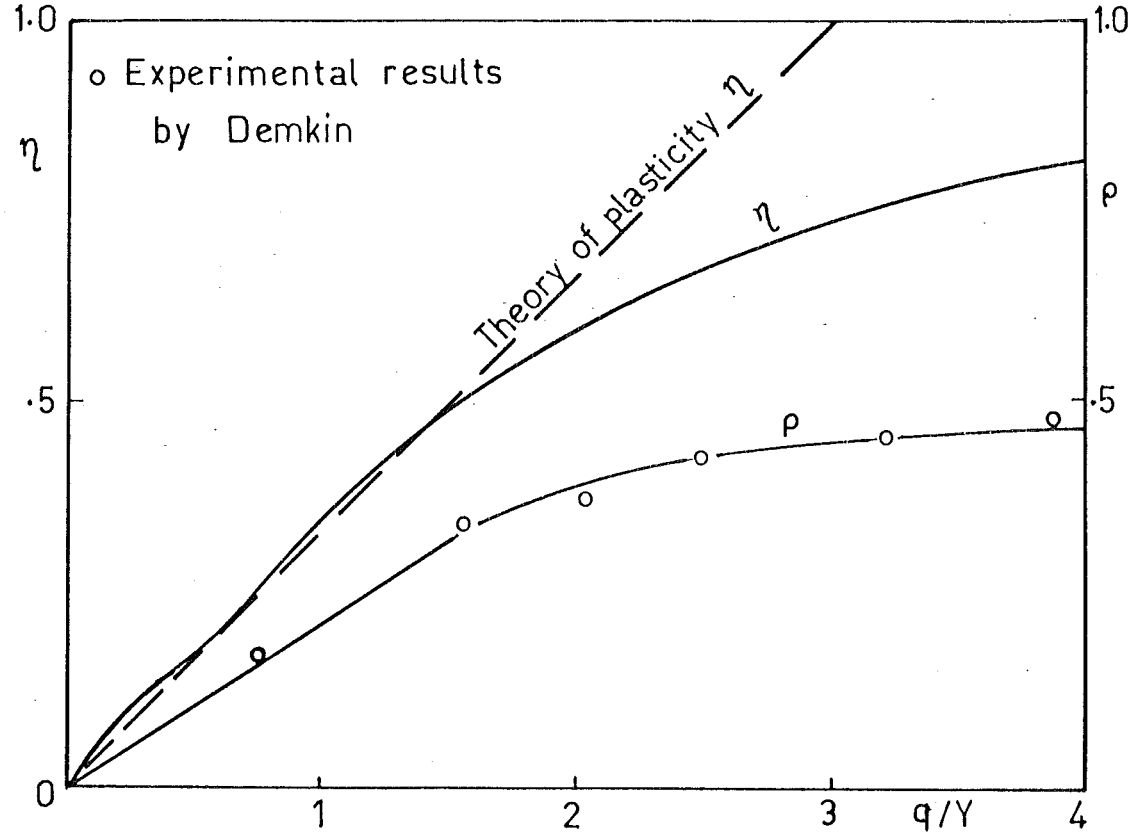

Fig. 3.15 The relation of the degree of contact η and dimensionless compliance ρ with the dimensionless pressure. (Demkin [22])

this curve with the experimental values of the compression of a rough aluminium surface by a smooth hard steel punch made by Demkin and Izmailov[22].

Classical theory of plasticity indicated that the degree of contact η tends to unity as the pressure approaches the hardness M of the asperity

$$\eta = \frac{q}{M}$$

This relationship is also drawn in Fig.3.15 with the assumption that $M \simeq 3Y$[98].

3.5 DISCUSSION

Although the mode of deformation of the asperities has not been agreed among investigators, a few theories developed in the past may be employed within their valid zones. The theories of Hisakado and Williamson assumed plastic deformation of the asperities, a normal distribution of the peak heights and negligible interaction between the asperities. Williamson additionally assumed the conservation of material of the truncated tips which resulted in a better estimation of the deformation of the asperities. Both theories are acceptable for low loadings the theory of Williamson being accurate up to $\frac{q}{M} = .1$. The different approach studied by Demkin considered the elastic or plastic deformation of the asperities at low loadings such that the real area of contact is smaller than $\frac{1}{5}$ of the nominal area. His theory was based heavily on the bearing area curve of the surface profile. This is of practical interest since different machining operations yield different surface profiles and hence different bearing area curves. Therefore, we may expect different asperity deformations for different bearing area curves at the same loading. For higher loadings, the asperities were assumed to behave as rigid plastic bodies: a wedge model asperity surface of uniform height was studied allowing for the volume conservation and interaction of the asperities. Modification

and application of Demkin's theory to our rough turned cylindrical workpieces will later be introduced (Section 6.1) to suit the purpose of our investigation. In the following, the application of Williamson's theory is employed to predict the indentation of a hard flat locator on a rough flat workpiece.

3.6 APPLICATION OF THE THEORY OF CONTACT BETWEEN A ROUGH AND A FLAT SURFACE INTO SHAWKI'S EXPERIMENTS

The experiment made by Shawki and Abdel-Aal[90] to record the deformation of rough steel and cast iron workpieces indented by a hard flat surface (locator) may be illustrated by Fig.3.16.

Assuming that the deformation of the asperities can be calculated by Williamson's theory, we can readily calculate the total deformation of the whole system recorded by the dial gauges. Under load W, the indicators will record the sum of two different sources of deformation.

1) δ_1: of the flat locator due to the compression of length ℓ = 35 mm.

2) δ_2: of the workpiece at the contact surface.

(i) Calculation of δ_1

Let us take the case of the nominal cross-sectional area A_n of the locator to be 6.62 cm^2. The compression of the block of steel of length 35 mm due to pressure $q = \frac{W}{A_n}$ is found by Hooke's law.

$$\delta_1 = \frac{q\ell}{E} \qquad 3.41$$

For steel locator E = 21500 kg/mm^2 (Shawki's value)

the compression of the locator is shown in Table 3.1.

TABLE 3.1

$q(kg/cm^2)$	100	200	300
δ_1(micron)	1.62	3.25	4.88

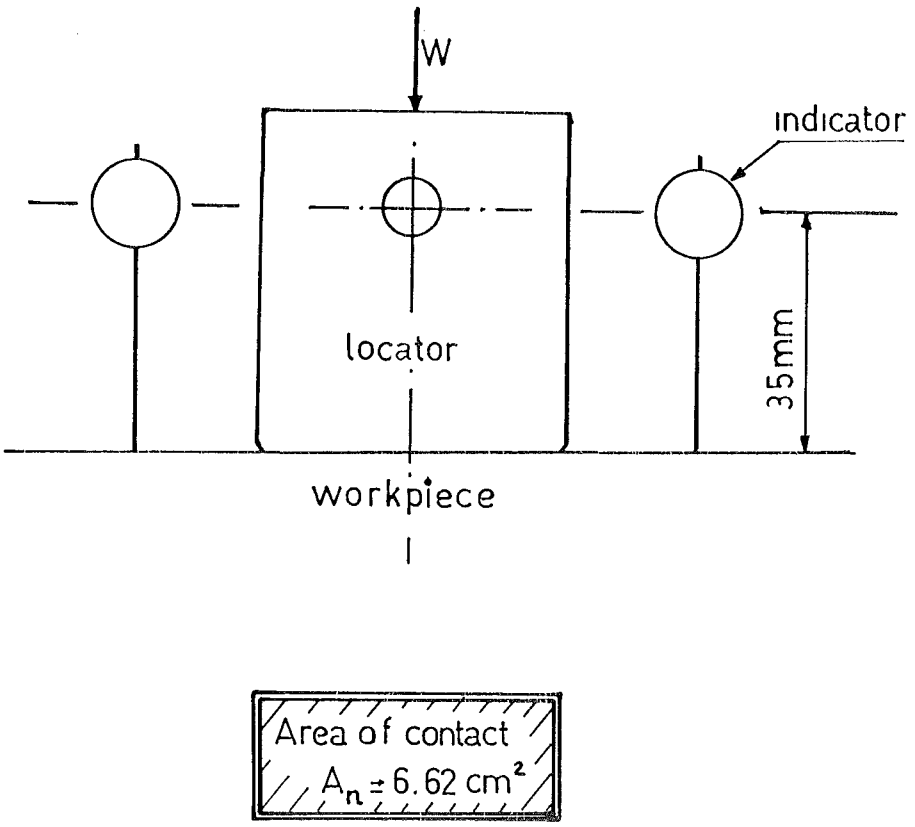

Fig. 3.16 A simplified diagram of the experiment of Shawki[90] on the indentation of a flat locator on flat workpieces of varying degrees of roughness.

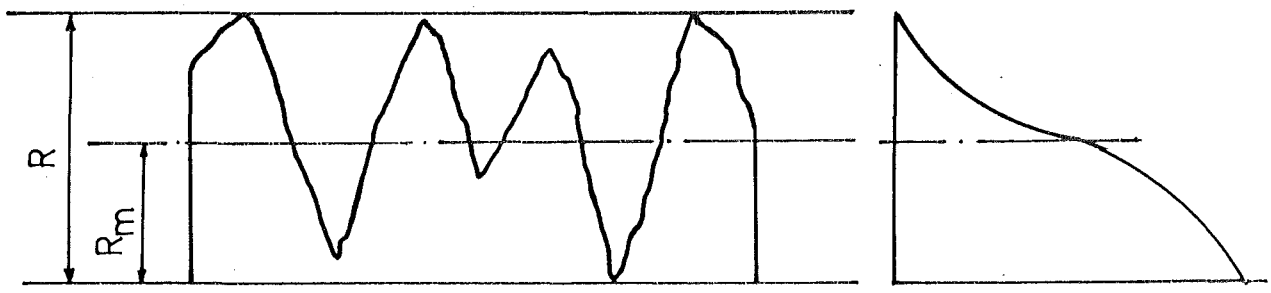

Fig. 3.17 The profile and Abbott bearing area curve drawn by Olsen[74].

(ii) Calculation of δ_2

The deformation of the workpiece at the contact area is composed of two components

(a) the deformation of the asperities δ_2'';

(b) the deformation of the bulk material supporting the asperities δ_2'.

It is elastic if the maximum pressure is smaller than the yield stress of the workpiece. Assuming the yield stress of the workpiece has the maximum value of one-third of the Brinell hardness H_B then for steel workpieces in which

$$140 < H_B < 280 \quad kg/mm^2$$

this gives

$$4670 < Y \simeq \frac{H_B}{3} < 9330 \quad kg/cm^2$$

and for cast iron workpieces in which

$$120 < H_B < 170 \quad kg/mm^2$$

this gives

$$4000 < Y \simeq \frac{H_B}{3} < 5670 \quad kg/cm^2$$

The maximum pressure applied by Shawki in his experiments was probably 300 kg/cm^2 (extracted from Fig.9[90]) which is very much below the probable range for the Yield stress of the steel and the cast iron workpieces: hence the deformation may be taken as completely elastic.

The deformation based upon the theory of elasticity of a square area A_n under uniform pressure q is given by Roark[66]. The maximum deformation occurring at the centre of the square is

$$\delta_2 = 102 \quad \frac{qA_n^{.5}}{E} \quad \text{micron}$$

with q in kg/cm^2, E in kg/mm^2, and A_n in cm^2

for STEEL and for CAST IRON

$E = 21500 \text{ kg/mm}^2$ $E = 10^4 \text{ kg/mm}^2$

giving $\delta_2' = 4.74 \ qA_n^{.5} \times 10^{-3}$ and $\delta_2' = 10.2 \ qA_n^{.5} \times 10^{-3}$ micron

Table 3.2 gives the values of δ_2' at different pressures.

TABLE 3.2

q (kg/km^2	100	150	200	250	300
Steel δ_2' (micron)	1.22	1.83	2.44	3.04	3.66
Cast Iron δ_2' (micron)	2.62	3.94	5.25	6.56	7.87

(iii) Calculation of δ_2''

Assuming the Brinell hardness H_B of the work-piece to be approximately the same as the Meyer hardness M, (acutally for $120 < H_B < 280$ kg/mm^2 $\frac{M}{H_B}$ is between 1.03 and 1.07), the maximum dimensionless loading for all of the work pieces will lie in the following ranges

for Steel workpieces $$\frac{300}{14000} < \frac{q}{M} < \frac{300}{28000}$$

i.e. $$.021 < \frac{q}{M} < .011$$

and for Cast iron workpieces

$$\frac{300}{12000} < \frac{q}{M} < \frac{300}{17000}$$

i.e. $$.025 < \frac{q}{M} < .018$$

which is well below .1, the maximum value for which Williamson's theory can be applied with small error. Williamson's theory requires the standard derivation σ of the work-pieces to be known. However, the only given measure of the roughness of the work-pieces is the "average peak-valley height", according to Olsen[74], who made a survey (1951) of the standards of the surface roughness measurements of various leading industrialised

countries, the "average peak-valley height" of the surface is R_m (Fig.3.17). Unfortunately, no country uses it as a standard property to represent a particular surface. Most of them adopt the centre line average (CLA) and the "peak-valley height" R (Fig.3.17). In giving the surface roughness of the locators, Shawki showed that the "average peak-valley height" is about five times its own CLA. Profiles of the work pieces used in our experiments (Chapter 6) also show that the "peak-valley height" is about 5-6 times the CLA. Hence we may conclude that R_h, the "average peak-valley height" employed in Shawki's article is, in fact, the "peak-valley height" R denoted in Olsen's publication.

Experiments by Uppal and Probert[86] showed that the initial contact usually occurred at 3.5 times the standard deviation σ hence we may assume that

$$R_h \simeq 7\,\sigma$$

Table 3.3 shows the approximate values for the standard deviation σ of the work pieces used in Shawki's experiments.

TABLE 3.3

R_h (micron)	8	11	14	41
σ (micron)	1.145	1.57	2	5.86

Let t be the dimensionless separation between two surfaces then the dimensionless deformation t' of the asperities is

$$t' = 3.5 - t$$

Once the dimensionless loading is known, the dimensionless separation t can be found from Fig.3.18 (the graphs of the dimensionless separation t versus dimensionless loading $\frac{q}{M}$ for Williamson's and Hisakado's theories).

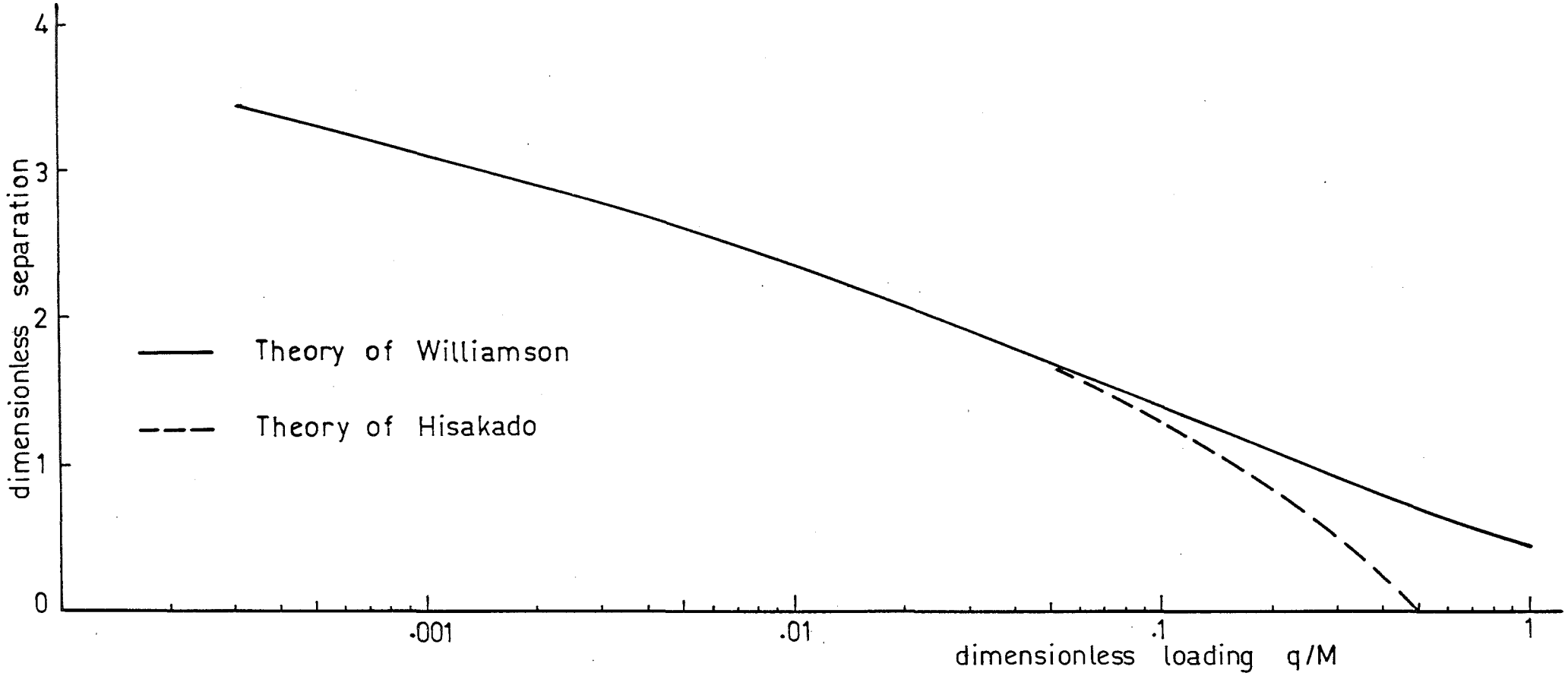

Fig. 3.18 The relation of the dimensionless separation of a hard flat plane and a rough surface with the dimensionless loading.

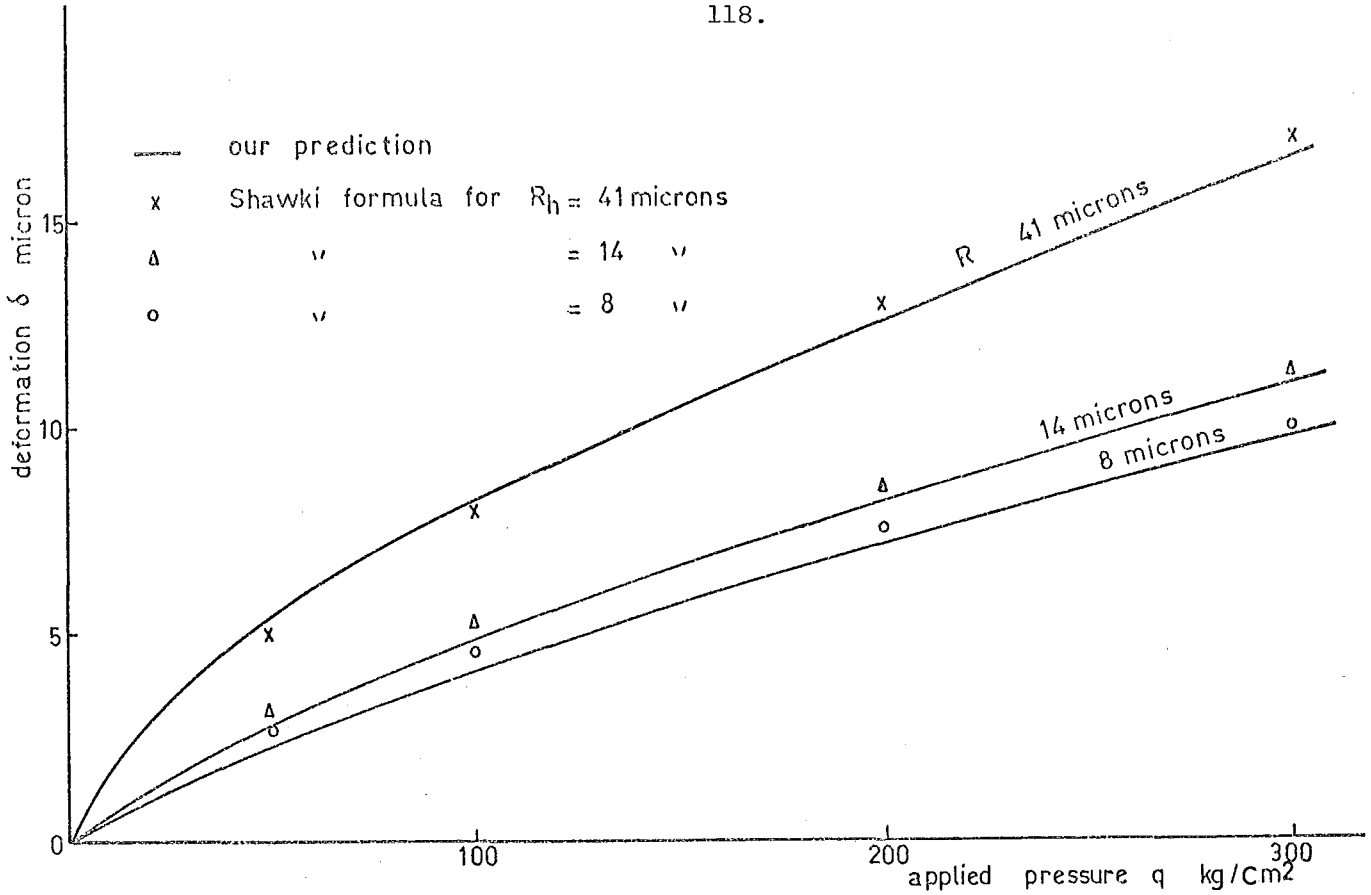

Fig.3.19 The indentation of steel workpieces of hardness 205 kg/mm^2 by a hard flat locator of cross-section 6.62 cm^2

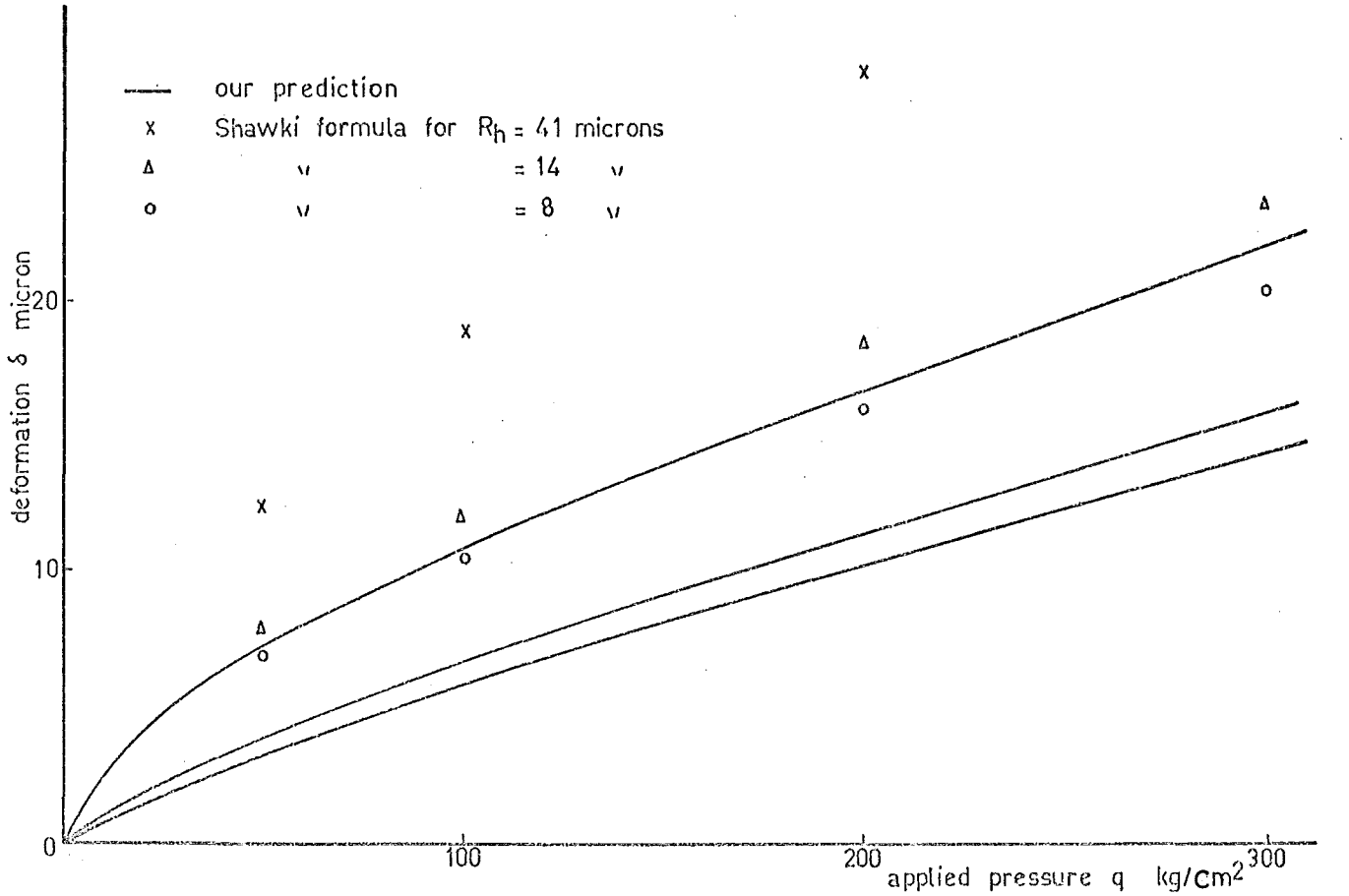

Fig. 3.20 The indentation of cast-iron workpieces of hardness 130 kg/mm^2 by a hard flat locator of X-section 6.62cm^2

Table 3.4 shows the deformation δ_2'' at different loadings for steel and cast iron work pieces. The hardness of the steel work pieces 205 kg/mm^2 is taken since it is the case drawn in Shawki's article.

Experiments by Shawki for the indentation of flat locators of different cross sections on steel and cast-iron work pieces of different hardness and surface roughness resulting in the following empirical formulae:

- for steel work pieces

$$\delta(\text{micron}) = (.4 - .0016\ H + .012\ A_n + .004\ R_h)\ q^{.7} \qquad 3.44$$

and for cast-iron work pieces

$$\delta(\text{micron}) = (.776 - .0045\ H + .053\ A_n + .016\ R_h)\ q^{.6} \qquad 3.45$$

where H, A_n, R_h, q, are in kg/mm^2, cm^2, micron and kg/cm^2 respectively.

Comparison between Shawki's formulae and our calculation for δ is drawn in Figures 3.19 and 3.20. It is lucky that with the given conditions on the cross section of the flat locator and the hardness of the steel work pieces, that the comparison shows such good agreement. A similarly good fit was found again for A_n = 20 cm^2 and H = 280 kg/mm^2; however, for other cases the difference may be as large as 50%. For the cast-iron work pieces, the difference is always large and may be as much as 100%. For most cases the difference shows clearly at low dimensionless loading $\frac{q}{M} < .007$ then increases only slighly as the loading increases.

(iv) Discussion

The result from the comparison for the steel work pieces implies that our prediction is in the order expected by Shawki's experiments.

The deformation is non-linear which is in agreement with this observation.

From the experience of the experiments for the deformation of a rough cylinder between two flat surfaces (Chapter 6), we realised that to perform an experiment similar to that conducted by Shawki would involve the following difficulties:

a) The work pieces must have no waviness which could never be achieved in practice. The amount of waviness may be measured by a similar method used by Thornley *et al*[101].

b) The waviness makes it difficult to fix the initial contact between the flat locator and the work piece.

c) Ensuring the two mean surfaces remain parallel during loading.

Our calculations assume that these ideal conditions are met and hence they result in the under-estimation of the deformation of the system. It is thought that if the above conditions could be met, better agreement between the theoretical and experimental values would result. We had thought of performing this experiment to check the calculation, but were deterred by the experimental difficulties. It will be noted that the calculations of the components of the deformation were based on well-supported premises, i.e. Hooke's law, theory of elasticity of bodies under direct bearing, Williamson's theory of contact under low loadings.

CHAPTER 4

THE ELASTIC DEFORMATION OF A LONG SMOOTH CYLINDER DUE TO TWO NARROW AXIAL BANDS OF PRESSURE

4.1 INTRODUCTION

When two elastic bodies are in contact, their surfaces are usually assumed to be perfectly smooth. Hertz (1881) derived a mathematical theory for the general three-dimensional contact problem. However, for the case of a long cylinder compressed between two plane bodies, it is generally more difficult theoretically than the three-dimensional one. Elastic deformation and the associated stresses resulting from the line contact have been the subject of a number of investigations. Föppl[27] 1907 was probably the first to derive an expression for the deformation of the cylinder. That article is not available in English which may account for his expression being misused. (Shawki[90] compared the experimental results of the deformation of a rough cylinder compressed between two hard Vee locators with only one half of Föppl's results as the theoretical values. Allan[3] simply took one half of the Föppl's deformation of the cylinder as the deformation of the plane surface in contact with the cylinder.

This formula was well-known in the rolling bearing field in early times. In deriving his results, Föppl assumed a parabolic distribution of pressure across the axial band of the nominal surface contact, whereas for the contact of smooth surfaces of elastic bodies, Hertz had shown it to be an elliptical distribution on the grounds of compatibility of surface displacements. Expressions for the stresses arising from the elliptical pressure distribution were derived easily but Föppl did not perform the integration necessary to produce expressions for the associated deformation. Presumably this was too difficult at that time, whereas the parabolic pressure distribution he assumed led easily to an expression for the deformation but as compatibility of the

surface displacement had not been met, it was not possible to determine a corresponding contact width. By adopting the value of contact width found by Hertz for the contact between an elastic cylinder and a plane with the same elastic properties. Föppl derived an expression known as the approximate value for the deformation of a cylinder between two flat elastic plates. Finally, in 1949 Lundberg employed the stress function approach to obtain the exact expression for the elastic deformation of a smooth cylinder compressed between two flat elastic plates. This expression has been used recently in books of roller bearings.

Solid surfaces are rarely smooth on a microscopic scale; during compression they are in contact only at isolated points. The actual contact area is the sum of the areas of the single contact spots and is, in fact, only a small part of the apparent contact area. Practically, the apparent contact area is the envelope of all the outside asperities in contact which is much greater than the area of contact for the ideally smooth bodies, the difference depending on the roughness and the applied pressure. As the accuracy of the machine operations becomes more important, the study of the surface roughness is inevitable. Greenwood and Tripp[38] put forward an iterative procecure for studying the contact between elastic contact of rough spheres. Lo[60] extended this theory to the elastic contact of rough cylinders.

Recently Demkin *et al*[23] presented a solution to the problem of contact conditions between rough curved bodies, in which for a cylinder the pressure across the contact area is assumed to be of the generalised form $q = q_o(1-\frac{y^2}{\ell^2})^{\beta}$ where β is a real number. In deriving an expression for the resulting deformation they truncated a series representation of transcendental function which introduced an error in their results that varies with β. However, we have found a method to avoid the series representation and an exact solution for the deformation is obtained. The generalised form can be checked with the

expression derived by Föppl and by Lundberg as special cases.

With the assumption that there exists an elliptic-paraboloidal pressure $q = q_o(1-\frac{y^2}{\ell^2})^\beta$ across the contact bands the theoretical calculation for the deformation of a rough cylinder between two smooth hard flat plates requires the calculation of the following components of the deformation:

(a) The plastic deformation of the asperities on the cylinder.

(b) The elastic deformation of the bulk material supporting the asperities provided the onset of plasticity is not reached.

(c) The elastic deformation of the flat plane.

The result may be used to compare with the empirical formula established by Shawki for the deformation of a rough cylinder compressed between two Vee locators.

In the following sections, the study of the deformation of a long smooth cylinder between two flat plates for various types of pressure distribution is discussed.

4.2 PARABOLIC PRESSURE DISTRIBUTION (First derived by Föppl (in German) 1907)

The problem of a uniform load acting along the thickness of a semi-infinite large plate was discussed by Timoshenko[103]. Let p be the load per unit length. It was proved that in polar coordinates the stresses are

$$\sigma_r = -\frac{2p\cos\theta}{\pi r} \qquad 4.1$$

$$\sigma_\theta = \tau_{r\theta} = 0 \qquad 4.2$$

These can be changed into Cartesian coordinates

$$\sigma_z = \sigma_r \cos^2\theta = -\frac{2p\cos^3\theta}{\pi r} = -\frac{2p\,z^3}{\pi(y^2+z^2)^2} \qquad 4.3$$

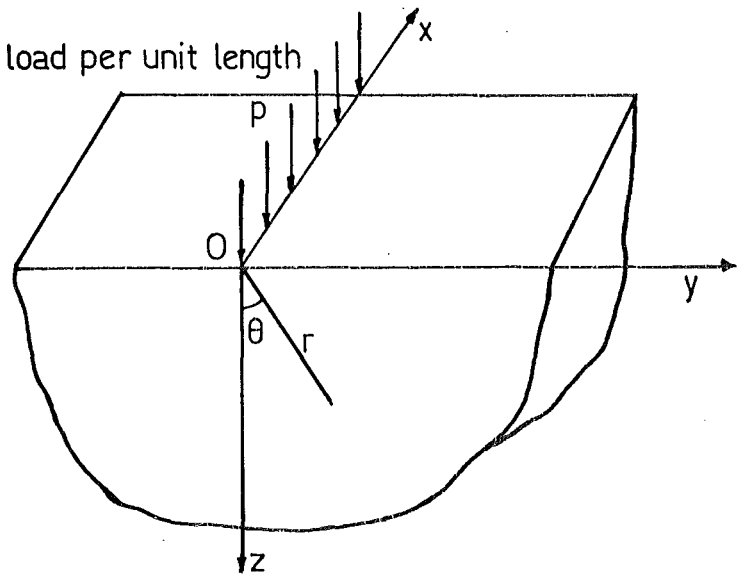

Fig. 4.1 Uniform line load applied on a semi-infinite solid along x-axis.

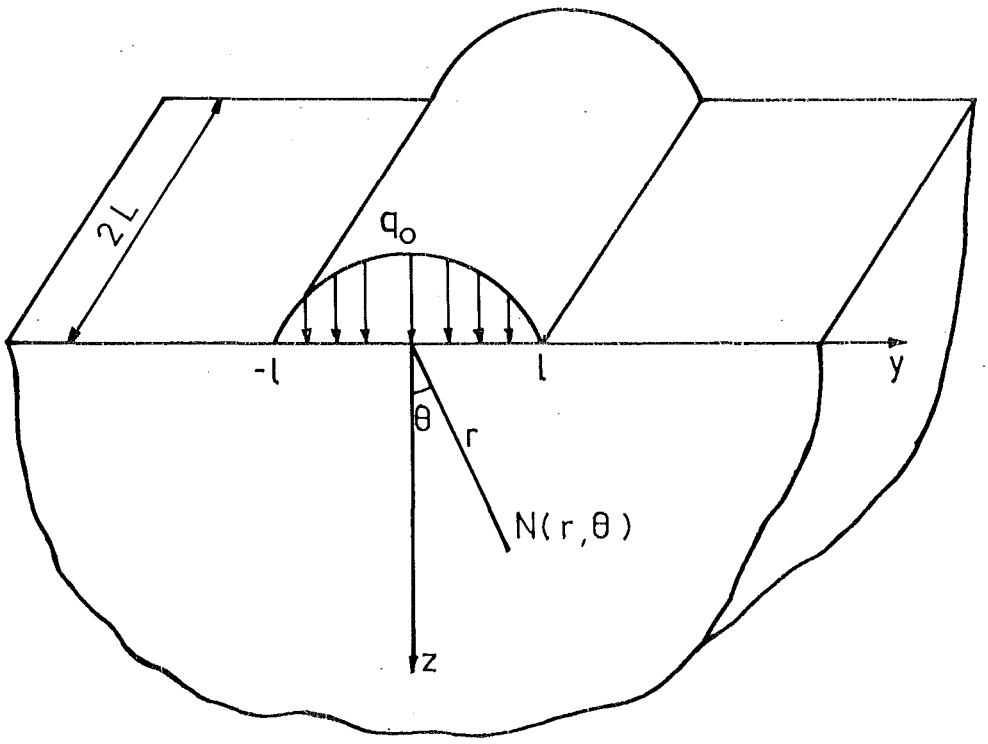

Fig. 4.2 Uniform parabolic pressure distribution $q=q_o(1-\frac{y^2}{l^2})$ on a semi-infinite solid.

$$\sigma_y = \sigma_r \sin^2\theta = -\frac{2p\cos\theta\sin^2\theta}{\pi r} = \frac{-2p\,y^2 z}{\pi(y^2+z^2)^2} \qquad 4.4$$

$$\tau_{yz} = \sigma_r \sin\theta\cos\theta = \frac{-2p\cos^2\theta\sin\theta}{\pi r} \qquad 4.5$$

If the load distribution acting on the semi-infinite plate is of parabolic shape as shown in Fig.4.2, the sresses at any point N inside the body are

$$\sigma_x = -\frac{4}{\pi}\int_o^{\ell}\frac{q(y)\,z^3}{(y^2+z^2)^2}\,dy \qquad 4.6$$

$$\sigma_y = -\frac{4}{\pi}\int_o^{\ell}\frac{q(y)\,y^2 z}{(y^2+z^2)^2}\,dy \qquad 4.7$$

where $q(y) = q_o\left(1-\frac{y^2}{\ell^2}\right)$ is the parabolic pressure distribution

hence

$$\sigma_z = -\frac{4q_o}{\pi\ell^2}\int_o^{\ell}\frac{(\ell^2-y^2)\,z^3}{(y^2+z^2)^2}\,dy$$

$$= -\frac{4q_o z^3}{\pi\ell^2}\left[\frac{\ell^2+z^2}{2z^3}\left(\frac{yz}{z^2+y^2}+\tan^{-1}\frac{\ell}{z}\right)-\frac{1}{z}\tan^{-1}\frac{y}{z}\right]_o^{\ell}$$

$$= -\frac{2q_o}{\pi\ell^2}\left[\ell z+(\ell^2-z^2)\tan^{-1}\frac{\ell}{z}\right] \qquad 4.8$$

Let p be the load per unit thickness of the plate then

$$p = 2\int_o^{\ell}\frac{q_o}{\ell^2}(\ell^2-y^2)\,dy = \frac{4}{3}q_o\ell \qquad 4.9$$

Substitute q_o into Equation 4.8 to get

$$\sigma_z = -\frac{3p}{2\pi\ell}\left[\ell z+(\ell^2-z^2)\tan^{-1}\frac{\ell}{z}\right] \qquad 4.10$$

For the case $z >> \ell$

$$\tan^{-1} \frac{\ell}{z} \simeq \frac{\ell}{z} - \frac{1}{3} \left(\frac{\ell}{z}\right)^3 \qquad 4.10a$$

The stress σ_z becomes

$$\sigma_z = - \frac{2p}{\pi z} \qquad 4.11$$

Similarly the stress σ_y can be obtained from the integration

$$\sigma_y = - \frac{4q_o}{\pi \ell^2} \int_o^{\ell} \frac{(\ell^2 - y^2)\, y^2 z \, dy}{(y^2 + z^2)^2}$$

Substitute $q_o = \frac{3p}{4\ell}$

$$\sigma_y = - \frac{3p}{\pi \ell^3} \left[- \frac{3\ell}{2} + \frac{\ell^2 + 3z^2}{2z} \tan^{-1} \frac{\ell}{z} \right] \qquad 4.12$$

For the case $z >> \ell$

$$\frac{\ell^2 + 3z^2}{2z} \tan^{-1} \frac{\ell}{z} \simeq \frac{\ell^2 + 3z^2}{2z} \left(\frac{\ell}{z} - \frac{1}{3} \frac{\ell^3}{z^3} \right)$$

$$\simeq \frac{\ell}{6z^4} (9z^4 - \ell^4)$$

$$\simeq \frac{3}{2}\ell$$

Substitute this value into Equation 4.12 to get

$$\sigma_y \simeq 0 \qquad 4.13$$

Now considering two equal and opposite uniform loads p per unit length applied on an infinitely long cylinder of radius R, Fig.4.3. Assuming that each of the forces produces a single radial stress distribution as in Equations 4.1 and 4.2, we can find the force required to be applied at the circumference of the disc in order to maintain such a stress distribution. At any point M on

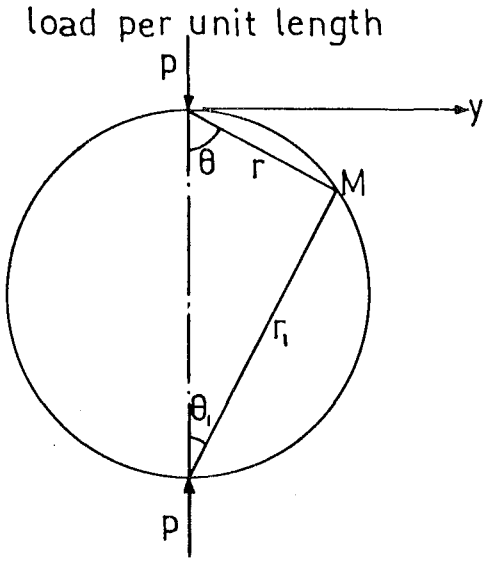

Fig. 4.3 A cross-section of the cylinder.

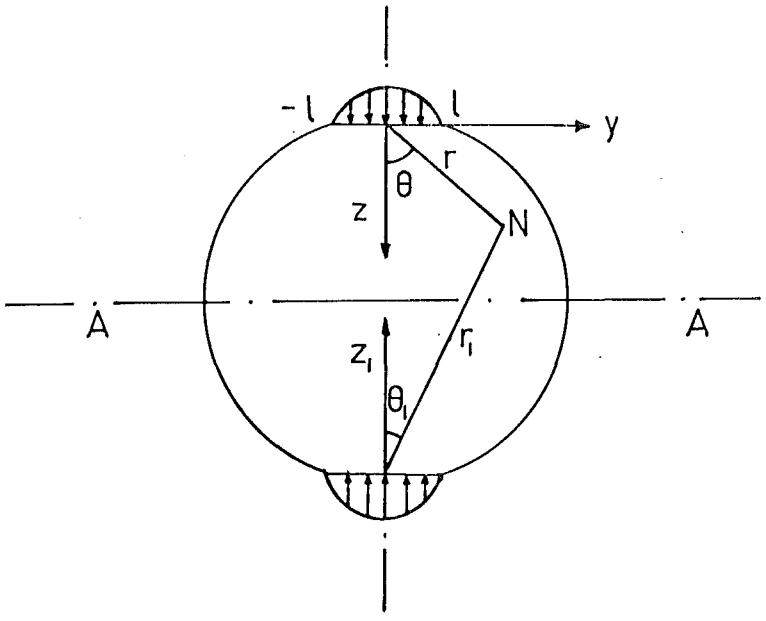

Fig. 4.4 Parabolic pressure distribution across the bands.

the circumference we have compressions in the direction of r and r_1 equal to $\frac{2p\cos\theta}{\pi r}$ and $\frac{2p\cos\theta_1}{\pi r_1}$ respectively. Since r and r_1 are perpendicular to each other

$$\frac{\cos\theta}{r} = \frac{\cos\theta_1}{r_1} = \frac{1}{2R}$$

So the two principal stresses at M are two equal compressive stresses of magnitude $\frac{p}{\pi R}$. This means that the same compressive stress is acting on any plane through M perpendicular to the cross section of the cylinder. Normal compressive forces of constant intensity $\frac{p}{\pi R}$ should be applied to the circumference of the cross section in order to maintain the assumed pair of simple radial stress distribution. If the boundary of the cylinder is free from external forces, the stress at any point is therefore obtained by superimposing a uniform tension in the plane of the cross section of the cylinder of magnitude $\frac{p}{\pi R}$, therefore the above two simple stresses are

$$\sigma_z = -\frac{2p\cos^3\theta}{\pi r} - \frac{2p\cos^3\theta_1}{\pi r_1} + \frac{p}{\pi R} \qquad 4.14$$

$$\sigma_y = -\frac{2p\cos\theta}{\pi r}\sin^2\theta - \frac{2p\cos\theta_1}{\pi r_1}\sin^2\theta_1 + \frac{p}{\pi R} \qquad 4.15$$

Replacing θ and θ_1 by y, z, and z_1

$$\sigma_z = -\frac{2p\,z^3}{\pi(y^2+z^2)^2} - \frac{2p\,z_1^3}{\pi(y^2+z_1^2)^2} + \frac{p}{\pi R} \qquad 4.16$$

$$\sigma_y = -\frac{2p\,y^2 z}{\pi(y^2+z^2)^2} - \frac{2p\,z_1^3\,y^2}{\pi(y^2+z_1^2)^2} + \frac{p}{\pi R} \qquad 4.17$$

If the cylinder is now compressed by two narrow axial bands of parabolic pressure distributed as in Figure 4.4, since the system is symmetrical about AA, it is only necessary to find the stresses of any point in the top half cylinder $o \leqslant z \leqslant R$

$$\sigma_z = -\frac{4q_o}{\pi\ell^2}\int_o^\ell \frac{(\ell^2-y^2)z^3}{(y^2+z^2)^2}\,dy - \frac{4q_o}{\pi\ell^2}\int_o^\ell \frac{(\ell^2-y^2)z_1^3}{(y^2+z_1^2)^2}\,dy + \frac{p}{\pi R} \qquad 4.18$$

For $z_1 = 2R - z >> \ell$ the second term in the RHS is given in Equation 4.11, the

first term was calculated in Equation 4.10.

Therefore

$$\sigma_z = -\frac{3p}{2\pi\ell^3}\left[\ell z + (\ell^2 - z^2)\tan^{-1}\frac{\ell}{z}\right] - \frac{2p}{\pi}\frac{1}{(2R - z)} + \frac{p}{\pi R} \qquad 4.19$$

Similarly

$$\sigma_y = -\frac{4q_o}{\pi\ell^2}\int_o^\ell \frac{(\ell^2 - y^2)y^2 z}{(y^2 + z^2)^2}\,dy - \frac{4q_o}{\pi\ell^2}\int_o^\ell \frac{(\ell^2 - y^2)y^2 z_1}{(y^2 + z_1^2)^2}\,dy + \frac{p}{\pi R} \qquad 4.20$$

for $z_1 = 2R - z >> \ell$ the second term in the RHS is negligible (Equation 4.13) while the first term is given in Equation 4.12.

Therefore

$$\sigma_y = -\frac{3pz}{\pi\ell^3}\left[-\frac{3\ell}{2} + \left(\frac{\ell^2 + 3z^2}{2z}\right)\tan^{-1}\frac{\ell}{z}\right] + \frac{p}{\pi R} \qquad 4.21$$

The strain in z direction (plane strain problem)

$$\varepsilon_z = \frac{1}{E}\left(\sigma_z - \mu(\sigma_y + \sigma_x)\right)$$

but $$\sigma_x = \mu(\sigma_y + \sigma_z)$$

hence $$\varepsilon_x = \frac{1-\mu^2}{E}\sigma_z - \frac{\mu(1+\mu)}{E}\sigma_y \qquad 4.22$$

Substitute σ_y and σ_z from Equations 4.19 and 4.21 into this equation

$$\varepsilon_z = -\frac{(1+\mu)p}{\pi E}\left[\frac{3z}{2\ell^2}(1 + 2\mu) + \frac{3}{2\ell}\left(1 - 2\mu - \frac{z^2}{\ell^2}(1 + 2\mu)\tan^{-1}\frac{\ell}{z}\right) + \frac{2(1-\mu)}{2R - z} - \frac{(1 - 2\mu)}{R}\right] \qquad 4.23$$

Tables of integrals give

$$\int \cot^{-1}\frac{z}{\ell}\,dz = z\cot^{-1}\frac{z}{\ell} + \frac{\ell}{2}\log\left(1 + \frac{z^2}{\ell^2}\right)$$

$$\int \frac{z^2}{\ell^2}\cot^{-1}\frac{z}{\ell}\,dz = \frac{z^3}{3\ell^2}\cot^{-1}\frac{z}{\ell} + \frac{z^2}{6\ell} - \frac{\ell}{6}\log\left(1 + \frac{z^2}{\ell^2}\right)$$

The total deformation δ_o of the cylinder is represented by the integration

$$\delta_o = 2 \int_o^R \varepsilon_z \, dz$$

Integrate and rearrange the result

$$\delta_o = - \frac{2(1+\mu)p}{\pi E} \left\{ \frac{R^2}{2\ell^2} (1 + 2\mu) + \left[\frac{3R}{2\ell} (1 - 2\mu) - \frac{R^3}{2\ell^3} (1 + 2\mu) \right] \cot^{-1} \frac{R}{\ell} - 1 + 2\mu \right.$$

$$\left. + (1 - \mu) \log \left(4 + \frac{4R^2}{\ell^2}\right) \right\} \qquad 4.24$$

Since $\ell << R$, $\tan^{-1} \frac{\ell}{R}$ can be represented in a series given in Equation 4.10a, then

$$\left[\frac{3R}{2\ell} (1 - 2\mu) - \frac{R^3}{2\ell^3} (1 + 2\mu) \right] \cot^{-1} \frac{R}{\ell} = \frac{5 - 8\mu}{3} - \frac{R^2}{2\ell^2} (1 + 2\mu)$$

Substitute this result into Equation 4.24

$$\delta_o = - \frac{2(1 + \mu)p}{\pi E} \left[(1 - \mu) \log 4 \left(1 + \frac{R^2}{\ell^2}\right) + \frac{5 - 8\mu}{3} - 1 + 2\mu \right] \qquad 4.25$$

Simplify further

$$\delta_o = - \frac{2(1 - \mu^2)p}{\pi E} \left[\frac{2}{3} + \log 4 \left(1 + \frac{R^2}{\ell^2}\right) \right] \qquad 4.26$$

Again, since $a << R$, $4\left(1 + \frac{R^2}{\ell^2}\right) \simeq \frac{4R^2}{\ell^2}$

$$\delta_o = - \frac{4(1 - \mu^2)p}{\pi E} \left(\frac{1}{3} + \log \frac{2R}{\ell}\right) \qquad 4.27$$

This equation is the total compression at the centre of a long cylinder radius R due to two narrow bands of parabolic pressure distribution. The width of the bands must be small compared with the radius of the cylinder.

If a smooth cylinder is in contact with two flat planes, Hertz proved that for compatibility of the displacement the pressure distribution must be elliptic

$$q = q_o \left(1 - \frac{y^2}{\ell^2}\right)^{.5}$$

and the half-contact width is

$$\ell = 1.128 \left[pR \left(\frac{1 - \mu_1^2}{E_1} + \frac{1 - \mu_2^2}{E_2} \right) \right] \qquad 4.28$$

when all bodies are of the same material, i.e., $E = E_1 = E_2, \mu = \mu_1 = \mu_2 = .3$

$$\ell = 1.52 \, (pR/E)^{.5}$$

Substitute into Equation 4.27 to give

$$\delta_o = \frac{-1.92p}{\pi E} \left(\ell n \frac{RE}{p} + 1.215 \right) \qquad 4.29$$

However, in Föppl's article it was written as

$$\delta_o = \frac{-2(1 - \mu^2)p}{\pi E} \left(\log \frac{RE}{p} + 1.207 \right) \qquad 4.29a$$

The negative sign indicates that this is a compression. This equation was well-known in the early books on roller bearing.

4.3 ELLIPTIC PRESURE DISTRIBUTION (Lundberg[62] (1949))

The Airy stress function of a cylinder compressed by two diametrically opposite force p per unit axial length is (Fig.4.5)

$$\phi = \frac{p}{\pi} \left[\frac{r^2}{2R} - r_1 \theta_1 \sin \theta_1 - r_2 \theta_2 \sin \theta_2 \right] \qquad 4.30$$

The pressure across the contact area is a semi-elliptic

$$q(\gamma) = q_o \left(1 - \frac{\gamma^2}{\alpha^2} \right)^{.5}$$

The Airy function will then be

$$\phi = \frac{R}{\pi} \int_{-\alpha}^{\alpha} q(\gamma) \left(\frac{r^2}{2R} - r_1 \theta_1 \sin \theta_1 - r_2 \theta_2 \sin \theta_2 \right) d\gamma \qquad 4.31$$

Let δ_o be the maximum compression of the cylinder (i.e. along line $A_1 \; A_2$): it was proved that

$$\delta_o = \frac{2(1 - \mu^2)}{E} \int_o^R \left(\frac{1}{r^2} \frac{\delta^2 \phi}{\delta \theta^2} + \frac{1}{r} \frac{\delta \phi}{\delta r} - \frac{\mu}{1-\mu} \frac{\delta^2 \phi}{\delta r^2} \right) dr \qquad 4.32$$

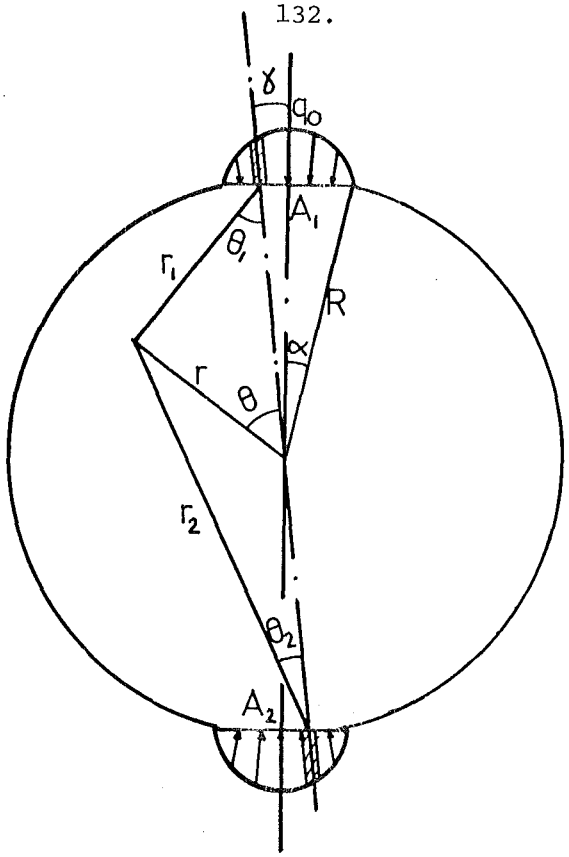

Fig. 4.5 Elliptic pressure distribution.(Lundberg(62))

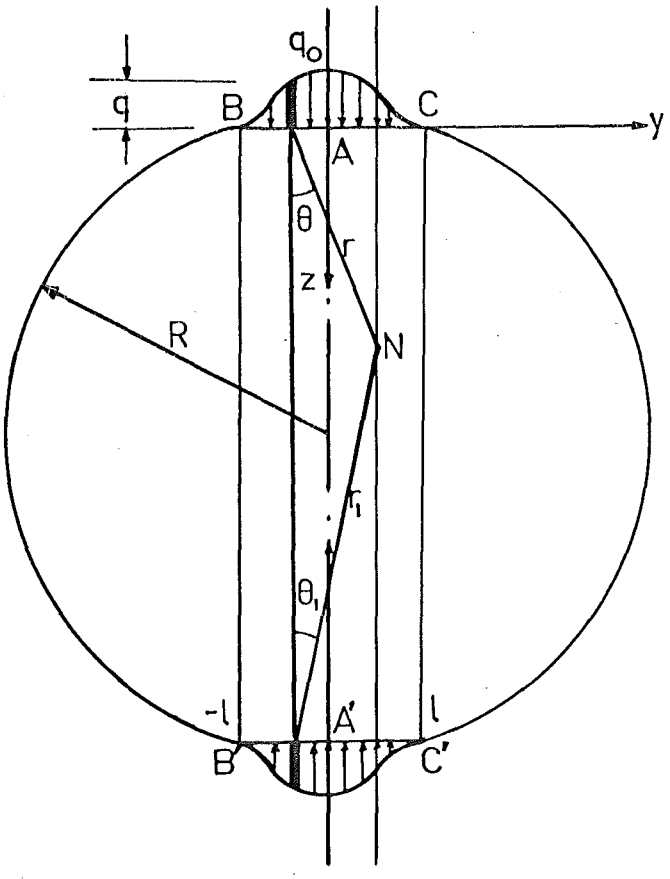

Fig. 4.6 General pressure distribution $q=q_o(1-\frac{y^2}{l^2})^{\beta}$

Performing the necessary differentiation and integration, Lundberg achieved the value of δ_o as

$$\delta_o = -\frac{4(1-\mu^2)p}{\pi E}\left(\log\frac{4R}{\ell}+.5\right) \qquad 4.33$$

4.4 THE GENERAL FUNCTION OF THE PRESSURE DISTRIBUTION $q = q_o(1-\frac{y^2}{\ell^2})^\beta$

Demkin *et al*[23] (1976) investigated the deformation of a cylinder compressed by two narrow bands of general pressure distribution $q = q_o(1-\frac{y^2}{\ell^2})^\beta$ where β is a real number. In order to evaluate the integrals in the expressions for the stresses inside the cylinder they employed a truncated transcendental series to represent the term $(\ell^2-y^2)^\beta$ as follows

$$(\ell^2-y^2)^\beta \simeq \ell^{2\beta}\left(1-\beta\frac{y^2}{\ell^2}\right) \qquad 4.34$$

In fact the series expansion of $(\ell^2-y^2)^\beta$ is

$$(\ell^2-y^2)^\beta = \ell^{2\beta}\left[1-\beta\frac{y^2}{\ell^2}+\frac{\beta(\beta-1)}{2!\,\ell^4}y^4-\frac{\beta(\beta-1)(\beta-2)y^6}{3!\ell^6}+\text{etc}\right] \qquad 4.35$$

Equation (4.34) is true when either $\beta = 1$ or $\frac{y}{\ell}$ is small. Since β is not always equal to 1 and $\left|\frac{y}{\ell}\right|$ varies from 0 to 1, Equation 4.34 is not necessarily a good approximation.

In the following, a solution for the deformation of the cylinder compressed by two narrow bands of pressure distribution $q = q_o(1-\frac{y^2}{\ell^2})^\beta$ is derived without the above truncation errors.

From Equations 4.16 and 4.17, the normal stresses of any point N on the line $y = b$ $(-\ell \leqslant b \leqslant \ell)$ in Fig.4.6 due to the load qdy at M is given by

$$\sigma_z = \frac{qdy}{\pi R} - \frac{2qdy\cos^3\theta}{\pi r} - \frac{2qdy\cos^3\theta_1}{\pi r_1} \qquad 4.36$$

$$\sigma_y = \frac{qdy}{\pi R} - \frac{2qdy\cos\theta\sin^2\theta}{\pi r} - \frac{2qdy\cos\theta_1\sin^2\theta_1}{\pi r_1} \qquad 4.37$$

The stresses at N due to the whole pressure distribution is

$$\sigma_z = \frac{p}{\pi R} - \int_{-\ell}^{\ell} \frac{2q \cos^3 \theta}{\pi r} dy - \int_{-\ell}^{\ell} \frac{2q \cos^3 \theta_1}{\pi r_1} dy$$

$$\sigma_y = \frac{p}{\pi R} - \int_{-\ell}^{\ell} \frac{2q \cos \theta \sin^2 \theta}{\pi r} dy \quad \int_{-\ell}^{\ell} \frac{2q \cos \theta_1 \sin^2 \theta_1}{\pi r_1} dy$$

Assuming $\ell << R$, we have

$$\cos \theta = \frac{z}{r}, \sin \theta = \frac{b - y}{r}, \cos \theta_1 = \frac{2R - z}{r_1}, \sin \theta_1 = \frac{b - y}{r_1}$$

and $$r^2 = z^2 + (b - y)^2 \qquad r_1^2 = (2R - z)^2 + (b - y)^2$$

Substitute these values into the normal stresses, then

$$\sigma_z = \frac{p}{\pi R} - \int_{-\ell}^{\ell} \frac{2qz^3 dy}{\pi\left[z^2 + (b - y)^2\right]^2} - \int_{-\ell}^{\ell} \frac{2q(2R - z)^3 dy}{\pi\left[(2R - z)^2 + (b - y)^2\right]^2} \qquad 4.38$$

and $$\sigma_y = \frac{p}{\pi R} - \int_{-\ell}^{\ell} \frac{2qz(b - y)^2 dy}{\pi\left[z^2 + (b - y)^2\right]^2} - \int_{-\ell}^{\ell} \frac{2q(2R - z)(b - y)^2 dy}{\pi\left[(2R - z)^2 + b - y)^2\right]^2} \qquad 4.39$$

Letting u, v and w be displacements in the x, y, z directions respectively, the relationship between stresses and strains is

$$E \frac{\partial u}{\partial x} = \sigma_x - \mu (\sigma_y + \sigma_z)$$

$$E \frac{\partial v}{\partial y} = \sigma_y - \mu (\sigma_x + \sigma_z)$$

$$E \frac{\partial w}{\partial z} = \sigma_z - \mu (\sigma_x + \sigma_y) \qquad 4.40$$

For a long cylinder, i.e. the plane strain problem, there is a constant or no displacement in x direction, i.e. $\frac{\partial u}{\partial x} = 0$

or $$\sigma_x = \mu (\sigma_y + \sigma_z)$$

Substitute into Equation 4.40 to get

$$\frac{\partial w}{\partial x} = \frac{1 + \mu}{E} \left[(1 - \mu)\, \sigma_z - \mu \sigma_y \right]$$

Integrate with respect to z from 0 to R after substituting the expressions for σ_y and σ_z. It should be noted that pressure q is a function of y, i.e. $q = q(y)$

$$w_R = \int_0^R \frac{\partial w}{\partial z}\, dz = \frac{p(1 + \mu)(1 - 2\mu)}{\pi E} - \frac{2(1 + \mu)}{\pi E} \left\{ \int_0^R (1 - \mu) \left[\int_{-\ell}^{\ell} \frac{q(y)\, z^3\, dy}{[z^2 + (b - y)^2]^2} \right. \right.$$

$$\left. + \int_{-\ell}^{\ell} \frac{q(y)(2R - z)^3\, dy}{[(2R - z)^2 + (b - y)^2]^2} \right] dz - \mu \left[\int_0^R \frac{q(y)(b - y)^2\, z\, dy}{[z^2 + (b - y)^2]^2} \right.$$

$$\left. \left. + \int_{-\ell}^{\ell} \frac{q(y)(b - y)^2 (2R - z)\, dy}{[(2R - z)^2 + (b - y)^2]^2} \right] dz \right\} \qquad 4.41$$

Let us calculate the four double integrals individually.

The integrals containing $[z^2 + (b - y)^2]^2$ in the denominator cannot be calculated when both z and b - y are equal to 0 at the same time. Let ε be a small number then

$$I = \int_0^R \int_{-\ell}^{\ell} \frac{q(y) z^3 dy\, dz}{[z^2 + (b - y)^2]^2} = \int_0^R q(y) \left[\int_{-\ell}^{b-\varepsilon} + \int_{b-\varepsilon}^{b+\varepsilon} + \int_{b+\varepsilon}^{\ell} \right] \frac{z^3 dy\, dz}{[z^2 + (b-y)^2]^2} \qquad 4.42$$

Since the width of contact $2\ell \ll 2R$ (diameter of the cylinder) the lengths of the rectangle $BB'CC'$ are approximately equal to the diameter of the cylinder; hence the order of the integration in Equation 4.42 is interchangeable.

Consider

$$F = \int_0^R \int_{b-\varepsilon}^{b+\varepsilon} \frac{q(y) z^3 dy\, dz}{[z^2 + (b - y)^2]^2} = \int_{b-\varepsilon}^{b+\varepsilon} q(y) \int_0^R \frac{z^3 dz\, dy}{[z^2 + (b - y)^2]^2}$$

Let α be another small number then F can be approximated by

$$F \simeq \int_{b-\varepsilon}^{b+\varepsilon} q(y) \int_{\alpha}^{R} \frac{z^3 dz\, dy}{[z^2 + (b-y)^2]^2}$$

It is known that

$$\int \frac{z^3 dz}{(z^2 + Y^2)^2} = \frac{1}{2}\left[\log (z^2 + Y^2) + \frac{Y^2}{z^2 + Y^2}\right] \qquad 4.43$$

Take $b - y = Y$ and substitute this integration into the value of F giving

$$F \simeq \int_{b-\varepsilon}^{b+\varepsilon} \frac{1}{2} q(y) \left[\log (R^2 + Y^2) + \frac{Y^2}{R^2 + Y^2} - \log (\alpha^2 + Y^2) - \frac{Y^2}{\alpha^2 + Y^2}\right] dy$$

For $b - \varepsilon \leqslant y \leqslant b + \varepsilon$ then $-\varepsilon \leqslant Y \leqslant \varepsilon$ and $R^2 + Y^2 \simeq R^2$

therefore,

$$\frac{Y^2}{R^2 + Y^2} \simeq \frac{Y^2}{R^2} << \frac{Y^2}{\alpha^2 + Y^2}$$

Simplifying F further gives

$$F \simeq \int_{b-\varepsilon}^{b+\varepsilon} \frac{1}{2} q(y)\left[2 \log R - \log (\alpha^2 + Y^2) - \frac{Y^2}{\alpha^2 + Y^2}\right] dy$$

Since the interval of integration is small, there exists the approximation

$$\int_{b-\varepsilon}^{b+\varepsilon} f(y)\, dy \simeq 2\varepsilon f(b)$$

i.e. $$F \simeq \varepsilon q_o \left(1 - \frac{b^2}{\ell^2}\right)^{\beta} \left[2 \log R - \log \alpha^2\right]$$

Put $G = \varepsilon \log \alpha$

then $$e^G = e^{\varepsilon \log \alpha} = (e^{\log \alpha})^{\varepsilon} = \alpha^{\varepsilon}$$

If α is a small finite number while ε tends to zero, then α^{ε} tends to unity,

i.e. G tends 0. Log R is a finite number hence as $\varepsilon \to 0$ then $F \to 0$.

Equation 4.42 is simplified to

$$I = \int_0^R \int_{-\ell}^{\ell} \frac{q(y) z^3 dy\, dz}{[z^2 + (b - y)^2]^2} = \int_0^R \left[\int_{-\ell}^{b-\varepsilon} + \int_{b+\varepsilon}^{\ell} \right] \frac{q(y) z^3 dy\, dz}{[z^2 + (b - y)^2]^2} \qquad 4.44$$

By interchanging the order of integration it is equal to

$$I = \left[\int_{-\ell}^{b-\varepsilon} q(y) + \int_{b+\varepsilon}^{\ell} q(y) \right] \int_0^R \frac{z^3 dz\, dy}{[z^2 + (b - y)^2]^2}$$

Using the result of Equation 4.43

$$= \frac{1}{2} \left[\int_{-\ell}^{b-\varepsilon} q(y) + \int_{b+\varepsilon}^{\ell} q(y) \right] \left[\log \frac{R^2 + Y^2}{Y^2} + \frac{Y^2}{R^2 + Y^2} - 1 \right] dy \qquad 4.45$$

Similarly as above we have

$$II \int_0^R \int_{-\ell}^{\ell} \frac{q(y)(b - y)^2 z\, dy\, dz}{[z^2 + (b - y)^2]^2} = \int_0^R \left[\int_{-\ell}^{b-\varepsilon} + \int_{b+\varepsilon}^{\ell} \right] \frac{q(y) Y^2 z dy\, dz}{[z^2 + (b - y)^2]^2}$$

$$= \left[\int_{-\ell}^{b-\varepsilon} q(y)\, Y^2 + \int_{b+\varepsilon}^{\ell} q(y)\, Y^2 \right] \int_0^R \frac{z\, dz}{(z^2 + Y^2)^2}$$

$$= \frac{1}{2} \left[\int_{-\ell}^{b-\varepsilon} q(y) + \int_{b+\varepsilon}^{\ell} q(y) \right] \left[1 - \frac{Y^2}{R^2 + Y^2} \right] dy \qquad 4.46$$

The two remaining integrals in Equation 4.41 have no singularity; they can be evaluated directly by using the following integrations

$$\int_0^R \frac{(2R - z)\, dz}{[(2R - z)^2 + Y^2]^2} = \int_R^{2R} \frac{X}{(X^2 + Y^2)^2} dx \qquad \text{where } 2R - z = X$$

$$= \frac{1}{2} \left[\frac{1}{R^2 + Y^2} - \frac{1}{4R^2 + Y^2} \right]$$

$$\int_0^R \frac{(2R - z)^3 \, dz}{[(2R - z)^2 + Y^2]^2} = \int_R^{2R} \frac{X^3}{(X^2 + Y^2)^2} \, dx$$

$$= \frac{1}{2} \left[\log (X^2 + Y^2) + \frac{Y^2}{X^2 + Y^2} \right]_R^{2R}$$

$$= \frac{1}{2} \left[\log \frac{4R^2 + Y^2}{R^2 + Y^2} + \frac{Y^2}{4R^2 + Y^2} - \frac{Y^2}{R^2 + Y^2} \right]$$

Substitute back into equation 4.41

$$w_R = \frac{p(1 + \mu)(1 - 2\mu)}{\pi E} -$$

$$- \frac{2(1 + \mu)}{\pi E} \left\{ \frac{1 - \mu}{2} \left[\int_{-\ell}^{b-\varepsilon} q(y) + \int_{b+\varepsilon}^{\ell} q(y) \right] \left[\log \frac{R^2 + Y^2}{Y^2} + \frac{Y^2}{R^2 + Y^2} - 1 \right] dy \; + \right.$$

$$+ \frac{1 - \mu}{2} \int_{-\ell}^{\ell} q(y) \left(\log \frac{4R^2 + Y^2}{R^2 + Y^2} + \frac{Y^2}{4R^2 + Y^2} - \frac{Y^2}{R^2 + Y^2} \right) dy \; -$$

$$\left. - \frac{\mu}{2} \left[\int_{-\ell}^{b-\varepsilon} q(y) + \int_{b+\varepsilon}^{\ell} q(y) \right] \left(1 - \frac{Y^2}{R^2 + Y^2} \right) dy + \int_{-\ell}^{\ell} q(y) \left(\frac{Y^2}{R^2 + Y^2} - \frac{Y^2}{4R^2 + Y^2} \right) dy \right\} \qquad 4.47$$

The continuous integration from $-\ell$ to ℓ may be broken into two ranges, $-\ell$ to $b-\varepsilon$ and from $b+\varepsilon$ to ℓ with $\varepsilon \to 0$ without significant error. The equation 4.47 can be rearranged further

$$w_R = \frac{p(1 + \mu)(1 - 2\mu)}{\pi E} - \frac{(2(1 + \mu)}{\pi E} \left\{ \frac{1 - \mu}{2} \left[\int_{-\ell}^{b-\varepsilon} q(y) + \int_{b+\varepsilon}^{\ell} q(y) \right] \right.$$

$$\left. \left(\log \frac{4R^2 + Y^2}{Y^2} + \frac{Y^2}{4R^2 + Y^2} - 1 \right) dy - \frac{\mu}{2} \left[\int_{-\ell}^{b-\varepsilon} q(y) + \int_{b+\varepsilon}^{\ell} q(y) \right] \left(1 - \frac{Y^2}{4R^2 + Y^2} \right) dy \right\}$$

Since the width of contact $2\ell << 2R$ it can be deduced that

$$0 \leqslant Y^2 = (b - y)^2 \leqslant 4\ell << 4R^2$$

$$\log (4R^2 + Y^2) \simeq \log 4R^2$$

and $$\frac{Y^2}{4R^2 + Y^2} - 1 \simeq -1$$

then

$$w_R = \frac{p(1 + \mu)(1 - 2\mu)}{\pi E} - \frac{1 + \mu}{\pi E} \left\{ (1 - \mu) \left[\int_{-\ell}^{b-\varepsilon} + \int_{b+\varepsilon}^{\ell} \right] q(y) \log \frac{4R^2}{Y^2} \, dy \right.$$

$$\left. - \left[\int_{-\ell}^{b-\varepsilon} + \int_{b+\varepsilon}^{\ell} \right] q(y) dy \right\}$$

It is known that the load per unit axial length

$$p = \int_{-\ell}^{\ell} q(y) dy = \int_{-\ell}^{\ell} q_o \left(1 - \frac{y^2}{\ell^2}\right)^{\beta} dy$$

$$= \left[\int_{-\ell}^{b-\varepsilon} + \int_{b+\varepsilon}^{\ell} \right] q(y) dy$$

then $$w_R = \frac{p(1 + \mu)(1 - 2\mu)}{\pi E} - \frac{1 + \mu}{\pi E} \left\{ \left[\int_{-\ell}^{b-\varepsilon} + \int_{b+\varepsilon}^{\ell} \right] q(y)(1 - \mu) \log \frac{1}{Y^2} \, dy \right.$$

$$\left. + 2p (1 - \mu) \log 2R - p \right\}$$

$$= \frac{-2(1 - \mu^2)}{\pi E} \left\{ p (\log 2R - 1) - \left[\int_{-\ell}^{b-\varepsilon} + \int_{b+\varepsilon}^{\ell} \right] q(y) \log |Y| \, dy \right\}$$

i.e. $$w_R = -\frac{2(1 - \mu^2)}{\pi E} \left\{ p (\log \frac{2R}{\ell} - 1) - \left[\int_{-\ell}^{b-\varepsilon} + \int_{b+\varepsilon}^{\ell} \right] q(y) \log \left| \frac{b}{\ell} - \frac{y}{\ell} \right| dy \right\} \quad 4.48$$

The total compression of the cylinder along any line $y = b$ $(-\ell \leqslant b \leqslant \ell)$

(fig 4.6) parallel to AA' is

$$w_b = 2w_R = -\frac{4(1-\mu^2)}{\pi E}\left\{ p \log\left(\frac{2R}{\ell} - 1\right) - \left[\int_{-\ell}^{b-\varepsilon} + \int_{b+\varepsilon}^{\ell}\right] q(y) \log\left|\frac{b}{\ell} - \frac{y}{\ell}\right| dy \right\} \qquad 4.49$$

Since $\log\left|\frac{b}{\ell} - \frac{y}{\ell}\right|$ is undefined when $y = b$. Equation 4.49 can be written in an implicit form

$$w_b = -\frac{4(1-\mu^2)}{\pi E}\left\{ p\left(\log\frac{2R}{\ell} - 1\right) - \int_{-\ell}^{\ell} q_o\left(1 - \frac{y^2}{\ell^2}\right)^{\beta} \log\left|\frac{b}{\ell} - \frac{y}{\ell}\right| dy \right\} \qquad 4.50$$

The negative sign indicates the compression. The term $p(\log \frac{2R}{\ell} - 1)$ is independent of y representing the whole body compression of the cylinder at a particular load. The second term is dependent on y, and is the local compression of the cylinder at the contact area

$$w_b^W = -\frac{4(1-\mu^2)}{\pi E}\, p \log\left(\frac{2R}{\ell} - 1\right) \qquad 4.50a$$

$$w_b^L = +\frac{4(1-\mu^2)}{\pi E}\int_{-\ell}^{\ell} q_o\left(1 - \frac{y^2}{\ell^2}\right)^{\beta} \log\left|\frac{b}{\ell} - \frac{y}{\ell}\right| dy \qquad 4.50b$$

From Equation 4.50 it will be noted that the compression of the cylinder within the pressurised zone ($-\ell \leqslant b \leqslant \ell$) may be found provided that the integral in the equation can be evaluated.

4.5 APPLICATION

4.5.1 The Compression of the Cylinder along line y = o

This is the maximum compression of the cylinder. By substituting $b = 0$ into Equation 4.50

$$w_o = -\frac{4(1-\mu^2)}{\pi E}\left\{ p\left(\log\frac{2\ell}{\ell} - 1\right) - \int_{-\ell}^{\ell} q_o\left(1 - \frac{y^2}{\ell^2}\right)^{\beta} \log\left|\frac{y}{\ell}\right| dy \right\} \qquad 4.51$$

Let

$$E = \int_{-\ell}^{-\varepsilon} q_o \left(1 - \frac{y^2}{\ell^2}\right)^{\beta} \log \left| \frac{y}{\ell} \right| dy = \int_{\varepsilon}^{\ell} q_o \left(1 - \frac{t^2}{\ell^2}\right)^{\beta} \log \left(\frac{t}{\ell}\right) dt \text{ by putting } y = -t$$

hence

$$E = \int_{-\ell}^{\ell} q_o \left(1 - \frac{y^2}{\ell^2}\right)^{\beta} \log \left| \frac{y}{\ell} \right| dy = 2 \int_{\varepsilon}^{\ell} q_o \left(1 - \frac{y^2}{\ell^2}\right)^{\beta} \log \frac{y}{\ell} \, dy$$

Putting $y = \ell \sin t$ and $\sin \theta = \frac{\varepsilon}{\ell}$, θ is a very small angle.

$$E = 2\ell \int_{\theta}^{\pi_2} q_o \cos^{2\beta+1} t \log \sin t \, dt$$

From reference 34, page 588 or reference 40 page 147

$$E = 2\ell q_o \frac{\sqrt{\pi}\, \Gamma(\beta + 1)}{\Gamma(\beta + 1.5)} \left[\psi(.5) - \psi(\beta - 1.5)\right]$$

It is observed that the original derivation was made in reference 40 and there is an error in reference 34 when the whole equation was copied.

Γ is gamma function $\quad \Gamma(z) = \int_0^{\infty} t^{z-1} e^{-t} \, dt$

ψ is psi function $\quad \psi(z) = d(\log \Gamma(z))/dz$

The load per unit axial length

$$p = \int_{-\ell}^{\ell} q_o \left(1 - \frac{y^2}{\ell^2}\right)^{\beta} dy$$

Putting $y = \ell \sin t$

$$p = q_o \ell \int_{-\pi/2}^{\pi/2} \cos^{2\beta+1} t \, dt = 2q_o \frac{\ell\sqrt{\pi}\Gamma(\beta+1)}{2\Gamma(\beta+1.5)}$$

then

$$E = \frac{p}{2} \left[\psi\left(\frac{1}{2}\right) - \psi(\beta+1.5)\right]$$

Substitute this into Equation 4.51 to get

$$w_o = -\frac{4(1-\mu^2)p}{\pi E}\left[\log\frac{2R}{\ell} - 1 - 5\psi(.5) + .5\psi(\beta + 1.5)\right] \qquad 4.52$$

This is the general formula for any value of β. In particular the cases for $\beta = \frac{1}{2}$ (elliptic distribution) $\beta = 1$ (parabolic distribution) can be used to check with the two well-known formulas by Lundberg and Föppl respectively.

a°) $\beta = \frac{1}{2}$ <u>elliptic pressure distribution</u>

The recurrence formula for psi function is

$$\psi(z + 1) = \psi(z) + \frac{1}{z}$$

$$\psi(\beta + 1.5) = \psi(2) = \psi(1) + 1 = -.5772 + 1$$

$$\psi(\tfrac{1}{2}) = -1.9635$$

then
$$w_o = -\frac{4(1-\mu^2)p}{\pi E}\left[\log\frac{4R}{\ell} - .5\right] \qquad 4.53$$

This value is exactly the same as Lundberg's formula (Equation 4.33)

b°) $\beta = 1$, <u>parabolic pressure distribution</u>

$$\psi(\beta + 1.5) = \psi(2.5) = \psi(1.5) + \frac{2}{3} = \psi(0.5) + 2 + \frac{2}{3} = \psi(.5) + \frac{8}{3}$$

Substitute into Equation 4.51

$$w_o = -\frac{4(1-\mu^2)p}{\pi E}\left[\log\frac{2R}{\ell} + \frac{1}{3}\right] \qquad 4.54$$

Again this is the compression found by Föppl (Equation 4.27).

The general solution for the compression of the cylinder derived by Demkin *et al*[23] 1976 is

$$w_o = -\frac{4p(1-\mu^2)}{\pi E}\left\{\frac{2(1-\beta/3)}{K_\beta}\log\frac{R}{\ell} + \log 2 - \frac{K_\beta - 2}{4K_\beta}\right\} \qquad 4.55$$

where

$$K_\beta = \frac{\sqrt{\pi}\Gamma(\beta + 1)}{\Gamma(\beta + 1.5)}$$

(i) for $\beta = .5$ $\qquad K_\beta = \frac{\sqrt{\pi}\Gamma(1.5)}{\Gamma(2)} = \frac{\pi}{2}$

$$w_o = -\frac{4p(1 - \mu^2)}{\pi E}\left(\frac{10}{3\pi}\log\frac{R}{\ell} + .761\right) \qquad 4.56$$

(ii) for $\beta = 1$ $\qquad K_\beta = \frac{\sqrt{\pi}\Gamma(2)}{\Gamma(2.5)} = \frac{4}{3}$

$$w_o = -\frac{4(1 - \mu^2)p}{\pi E}\left(\log\frac{2R}{\ell} + \frac{1}{8}\right) \qquad 4.57$$

When $\beta = 1$, the approximation used by Demkin in Equation 4.34 is valid. The difference between Demkin's and Föppl's formulae must be due to the neglect of the terms above the first order of the transcendental functions Demkin made in deriving his equation (27) from equation (26).[23] The correct form of the RHS of Demkin's equation (26) must be added by

$$-\frac{2p(1 - \mu^2)}{\pi E}(\log 4 - 1) - \frac{2p(1 + \mu)}{\pi E}$$

4.5.2 The Compression of the Cylinder along line $y = \ell$

Substitute $b = \ell$ into Equation 4.50

$$w_\ell = -\frac{4(1 - \mu^2)}{\pi E}\left[p\left(\log\frac{2R}{\ell} - 1\right) - \int_{-\ell}^{\ell} q_o\left(1 - \frac{y^2}{\ell^2}\right)^\beta \log\left|1 - \frac{y}{\ell}\right| dy\right] \qquad 4.58$$

The integration term has a singularity at $y = \ell$, so the range of integration is reduced to $(-\ell, \ell-\varepsilon)$. Within this range $1 - \frac{y}{\ell} > 0$, the modulus sign of the log term may be dropped.

Let

$$III = \int_{-\ell}^{\ell-\varepsilon} q_o\left(1 - \frac{y^2}{\ell^2}\right)^\beta \log\left|1 - \frac{y}{\ell}\right| dy = \int_{-\ell}^{\ell-\varepsilon} q_o\left(1 - \frac{y^2}{\ell^2}\right)^\beta \log\left(1 - \frac{y}{\ell}\right) dy$$

Put $y = \ell \cos t$ and $\cos\gamma = 1 - \frac{\varepsilon}{\ell}$ where γ is a small angle then

$$III = q_o \ell \int_\gamma^\pi \sin^{2\beta+1} t \log(1 - \cos t)\, dt$$

Divide and multiply $1 - \cos t$ with $\sin t$ and note that $\frac{1-\cos t}{\sin t} = \tan\frac{t}{2}$

$$III = q_o \ell \int_{\gamma}^{\pi} \sin^{2\beta+1} t \log \sin t \, dt + q_o \ell \int_{\gamma}^{\pi} \sin^{2\beta+1} t \log \tan \frac{t}{2} dt$$

The function $\sin^{2\beta+1} t \log \sin t$ is symmetrical about $t = \frac{\pi}{2}$ therefore

$$IV = \int_{\gamma}^{\pi} \sin^{2\beta+1} t \log \sin t \simeq 2 \int_{\gamma}^{\frac{\pi}{2}} \sin^{2\beta+1} t \sin t \, dt$$

From reference 34, page 588

$$IV = \frac{2\sqrt{\pi}\Gamma(\beta+1)}{4\Gamma(\beta+1.5)} [\psi(\beta+1) - \psi(\beta+1.5)] = \frac{p}{2q_o \ell} [\psi(\beta+1) - \psi(\beta+1.5)]$$

Let

$$V = \int_{\gamma}^{\pi} \sin^{2\beta+1} t \log \tan \frac{t}{2} dt \simeq \int_{\gamma/2}^{\frac{\pi}{2}} \sin^{2\beta+1} 2\alpha \log \tan \alpha \, dx \quad \text{by putting } t = 2\alpha$$

Reference 34, page 592

$$V = 2 \left[2^{2\beta} \frac{(\Gamma(.5))^2}{\Gamma(1)} \log 1 \right] = 0$$

Substitute all the above results into Equation 4.58 to get the compression of the cylinder at line $y = \ell$

$$w_\ell = - \frac{4(1 - \mu^2)p}{\pi E} \left[\log \frac{2R}{\ell} - 1 - \frac{1}{2} \psi(\beta+1) + \frac{1}{2} \psi(\beta+1.5) \right] \qquad 4.59$$

4.5.3 The Compression of the Cylinder along the line $y = \frac{\ell}{\sqrt{2}}$

The compression of the cylinder along any line parallel to the diameter $y = 0$ can be obtained provided the corresponding integration in Equation 4.50 can be evaluated. Exact solutions for the compression other than those on the lines $y = 0$ and $y = \ell$ are unobtainable at the present time due to mathematical difficulties in integration. Numerical method can be employed; however, an approximate method is discussed in Section 5.5 for the evaluation of the following integrals within up to 2% error for $.5 \leqslant \beta \leqslant 3.5$.

$$\left[\int_{-\ell}^{\frac{\ell}{\sqrt{2}}-\varepsilon} + \int_{\frac{\ell}{\sqrt{2}}+\varepsilon}^{\ell}\right] q_o\left(1-\frac{y^2}{\ell^2}\right)^{\beta} \log\left|\frac{1}{\sqrt{2}}-\frac{y}{\ell}\right| dy$$

$$= -p\left[\frac{1}{2}\psi(\beta+1.5) - \frac{1}{4}\psi(\beta+1) - \frac{1}{4}\psi(.5) - \frac{1}{6}(\beta-.5)^{.8}\right] \qquad 4.60$$

This gives the total compression of the cylinder along the line $y = \ell/\sqrt{2}$ as

$$w_{\ell/\sqrt{2}} = \frac{-4(1-\mu^2)p}{\pi E}\left\{\log\frac{2R}{\ell} - 1 - \frac{1}{6}(\beta-.5)^{.8} + \frac{1}{4}\left[2\psi(\beta(1.5) - \psi(\beta-1) - \psi(.5)\right]\right\} \qquad 4.61$$

4.6 DISCUSSION

The exact solution for the compression of a long cylinder by two narrow bands of general pressure distribution $q = q_o\left(1-\frac{y^2}{\ell^2}\right)^{\beta}$ has been found. It is composed of two components

(i) The whole body compression which is constant along any line parallel to z axis provided $-\ell \leqslant y \leqslant \ell$.

(ii) The local compression represented partly by the integral of Equation 4.50. It varies with the y coordinate. The magnitude of the local compression of the plane when subject by the same pressure distribution.

The maximum compression of the cylinder (i.e. along the z axis) was checked with the special cases (β= .5 and 1) derived by Lundberg and Föppl. They show exact agreement. The general solution derived by Demkin (1976) was found to be incorrect.

In a study of the contact between a smooth cylinder and a semi-infinite plane, Puttock and Thwaite[81] (1969) found that the deformation of the surface of the cylinder is equal to the deformation of the surface of the

plane (Section 5.2) Its first term is found to be inversely proportional to log R (Equation 5.1a) where R is the radius of the cylinder. However, this must be distinguished from the total compression of the cylinder derived by Lundberg and by us, where it is proportional to log R

$$\text{i.e} \qquad w_o = -\frac{2(1-\mu^2)p}{\pi E}\left[\log\frac{2\pi RE}{p(1-\mu^2)} - 1\right]$$

where ℓ of Equation 4.53 has been substituted by $\sqrt{8pR(1-\mu^2)/\pi E}$ for an elliptic pressure distribution.

Let

$$A_o = -1 + .5\psi(\beta + 1.5) - .5\psi(.5)$$

$$A_\ell = -1 + .5\psi(\beta + 1.5) - .5\psi(\beta + 1)$$

and

$$A_{\ell/\sqrt{2}} = -1 - \frac{1}{6}(\beta - .5)^{.8} + \frac{1}{4}[2\psi(\beta + 1.5) - \psi(\beta + 1) - \psi(.5)]$$

then the variation of A_o, A , $A_{\ell/\sqrt{2}}$ for discrete values of β can be seen by the following picture

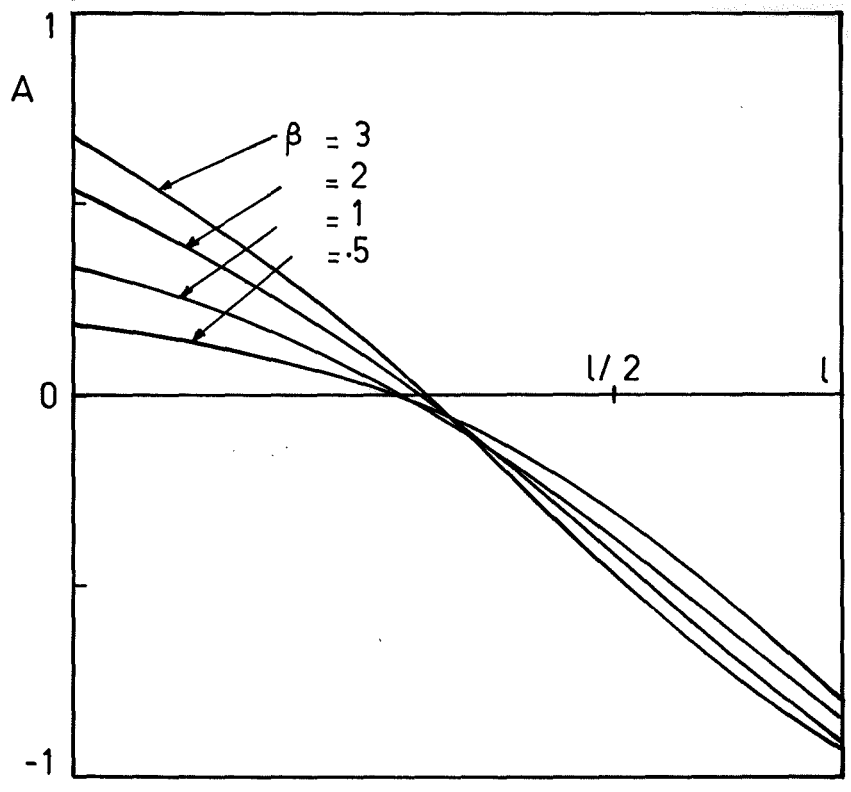

CHAPTER 5

DEFORMATION OF A SEMI-INFINITE PLANE DUE TO A LONG NARROW BAND OF PRESSURE

5.1 INTRODUCTION

The deformation of a semi-infinite plane in contact with a smooth cylinder has long been investigated. Prescott[80] (1927) assumed that the contact area is a finite rectangle of length very much longer than the width; however, the pressure distribution over the contact area is derived from that for a cylinder of infinite length in contact with a semi-infinite plane. The derivation of Prescott's problem was also given in a recent publication (Puttock and Thwaite[81] in which the displacement of points inside the area of contact of the semi-infinite plane was established. The same formula was also derived by Lundberg[62] in 1939 (in Swedish).

In this chapter the deformation of the plane due to a long narrow band of general pressure $q = q_o(1 - \frac{y^2}{\ell^2})^{\beta}$ is studied with similar assumptions to those made by Prescott. The result will later be used to calculate the deformation of the system comprised of a rough cylinder conpressed between two flat planes.

5.2 THE ELASTIC DEFORMATION OF A SEMI-INFINITE SOLID IN CONTACT WITH A SMOOTH CYLINDER

5.2.1 Finite Rectangular area of Contact (Prescott, Lundberg)

Assuming that the pressure is distributed over the rectangle in x - y plane whose sides are $x = \pm L$, $y = \pm \ell$. For an infinitely long cylinder in contact with a semi-infinite solid along the x-axis, the pressure distribution across the y axis is elliptic

$$q = q_o (1 - \frac{y^2}{\ell^2})^{.5}$$

The theory was initially derived by Prescott[80] (1927). A careful study may be seen in Puttock and Thwaite[81] (1969). The displacement of the

centre of the rectangle

$$w = \frac{2p(1 - \mu^2)}{\pi E} \left[\log \frac{4L}{\ell} + \frac{1}{2} \right] \qquad 5.1$$

where w, L, ℓ are in mm, p in kg/mm axial length, E in kg/mm^2

The same formula was derived by Lundberg[61] (1939) (in Swedish). Substituting the value for the half width of contact

$$\ell = \sqrt{8pR(1 - \mu^2)/\pi E}$$

into Equation 5.1 gives

$$w = \frac{(1 - \mu^2)p}{\pi E} \left(\log \frac{2\pi E L^2}{pR(1 - \mu^2)} + 1 \right) \qquad 5.1a$$

that is the deformation of the plane is inversely proportional to log R. Since the half width of contact ℓ is very small compared with the radius R of the cylinder, Puttock and Thwaite concluded that the deformation of the surface of the cylinder is also the same as the deformation of the plane (Equation 5.1a).

5.5.2 Ellipse of Contact

The contact area of the general three-dimensional contact between curved bodies is an ellipse. Assuming the major and minor axes of the ellipse to be equal to the length 2L and width 2ℓ of the rectangular area of contact, Thwaite[102] (1969) extended the results of the three-dimensional case to obtain an approximate displacement for the centre of the rectangle

$$w = \frac{6p(1 - \mu^2)}{\pi E} K \qquad 5.2$$

where w is in mm, p in kg/mm axial length, E in kg/mm^2.
K is the complete elliptic integral of the first class determined by the value of $\frac{A}{B} = \frac{R}{\rho}$ where R is the radius of the cylinder and ρ is an assumed large value such that the following relationship is satisfied

$$L^4 = 3\rho p \left(\frac{1-\mu^2}{\pi E}\right) \left(-\frac{1}{e}\frac{d\varepsilon}{de}\right)$$

where ε is the complete elliptical integral of the second class and e is the eccentricity of the ellipse of contact. A value of $\frac{A}{B}$ determines a value of $\frac{1}{e}\frac{d\varepsilon}{de}$. The assumed radius of curvature ρ which gives the ellipse of contact a major diameter equal to the length of contact is found by interpolation from a set of values of the major diameter constructed as outlined above, from a set of assumed values of the radius ρ.

Clearly this method is very inefficient.

Experiments made by Thwaite to record the total compression of a steel cylindrical surface and a plane surface in contact under pressure up to .5 kg/mm shows the finite rectangle method is the best fit (Fig.5.1). An empirical formula by Berndt (1928) was quoted in Thwaite's article, namely,

$$w = .462\ p\ (2R)^{-\frac{1}{3}} \text{ micron} \qquad 5.3$$

where R is in mm, p is in kg/mm axial length.

A very careful experiment by Korrenn *et al*[54] (1963) to record the displacement of the surface of a hard flat surface indented by a roller bearing of the same hardness also proved that Prescott's formula is a good approximation. (Fig.5.2).

5.3 THE DISPLACEMENT OF A SEMI-INFINITE SOLID UNDER ELLIPTIC-PARABOLOIDAL PRESSURE

$$q = q_o \left(1 - \frac{y^2}{\ell^2}\right)^{\beta}$$

The displacement of a point $M(x,y)$ on the plane $z = 0$ due to a concentrated force W acting at origin 0 (Fig.5.3) is given by Timoshenko[82] (p.402)

$$w = \frac{(1-\mu^2)W}{\pi E r}$$

where r is the distance OM, and w the displacement in z direction.

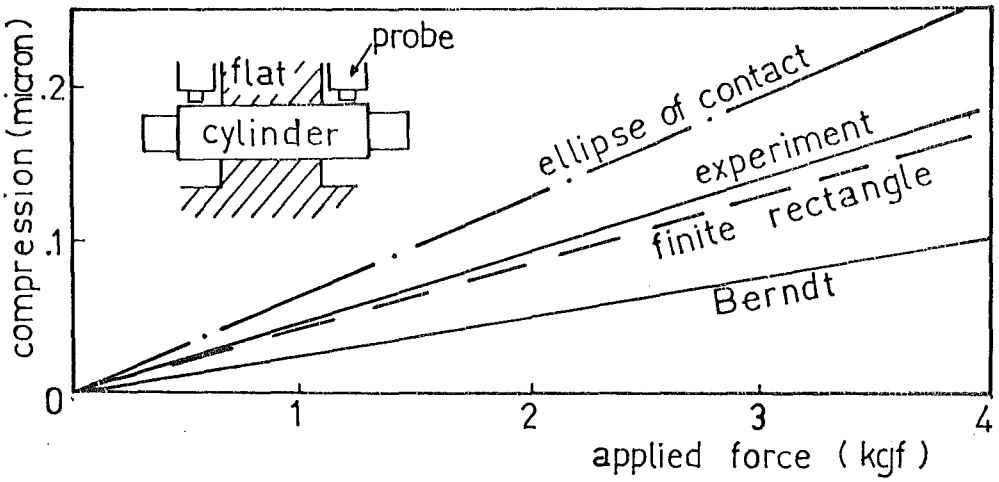

Fig. 5.1 The comparison of various formulae for the deformation of a hard steel cylinder and a hard steel plane at contact zone with the experimental data of Thwaite[102].

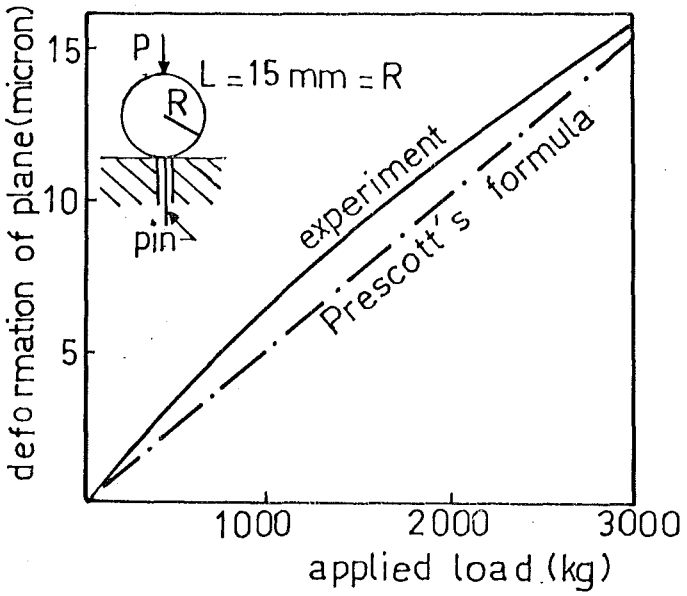

Fig. 5.2 The deformation of a hard steel plane indented by a steel roller(Korrenn[54])

Consider a load uniformly distributed along the x axis ($-L \leqslant x \leqslant L$). The pressure distribution in any plane perpendicular to the x axis is $q = q_o(1 - \frac{y^2}{\ell^2})^{\beta}$ (Fig.5.4). The displacement in the direction perpendicular to the plane of the paper (i.e. z direction) of a point $N(c, b, 0)$ with $0 \leqslant c \leqslant L$ due to the load $qdxdy$ at $M(x, y, 0)$ is

$$w = \frac{1 - \mu^2}{\pi E} \frac{q\, dx\, dy}{[(c - x)^2 + (b - y)^2]^{.5}} \qquad 5.4$$

The total displacement of N due to the whole force on the contact area is

$$w_{(c,b)} = \frac{1 - \mu^2}{\pi E} \int_{-L}^{L} \int_{\ell} \frac{q\, dy\, dx}{[(c - x)^2 + (b - y)^2]^{.5}}$$

$$= \frac{1 - \mu^2}{\pi E} \int_{-\ell}^{\ell} \int_{-L}^{L} \frac{dx}{[(c - x)^2 + (b - y)^2]^{.5}} \, dy$$

Put $X = c - x$, $Y = b - y$ in the following integration.

Let

$$I = \int_{-L}^{L} \frac{dx}{[(c - x)^2 + (b - y)^2]^{.5}} = \int_{c-L}^{c+L} \frac{dX}{(X^2 + Y^2)^{.5}}$$

$$= \left[\log (X + (X^2 + Y^2)^{.5}) \right]_{c-L}^{c+L}$$

$$= \log \left[\frac{c + L + [(c + L)^2 + Y^2]^{.5}}{c - L + [(c - L)^2 + Y^2]^{.5}} \right]$$

If we assume that the width 2ℓ of the rectangle is very small compared with the length $2L$ then

$$c + L \gg b - y = Y \qquad \text{for} \qquad L \geqslant c \geqslant 0$$

and

$$c + L + [(c + L)^2 + Y^2]^{.5} \simeq 2\,(c + L)$$

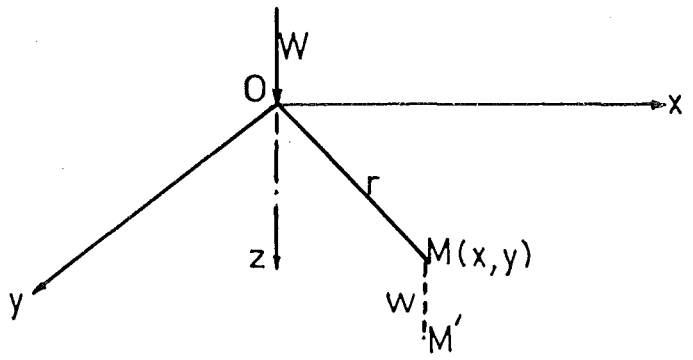

Fig. 5.3 M is displaced to M' due to load W at O.

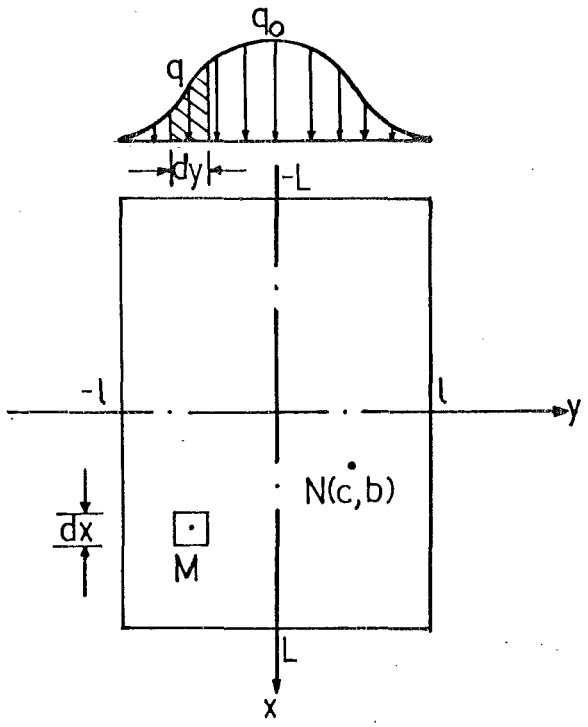

Fig. 5.4 The area of the semi-infinite solid under uniform pressure along x axis.

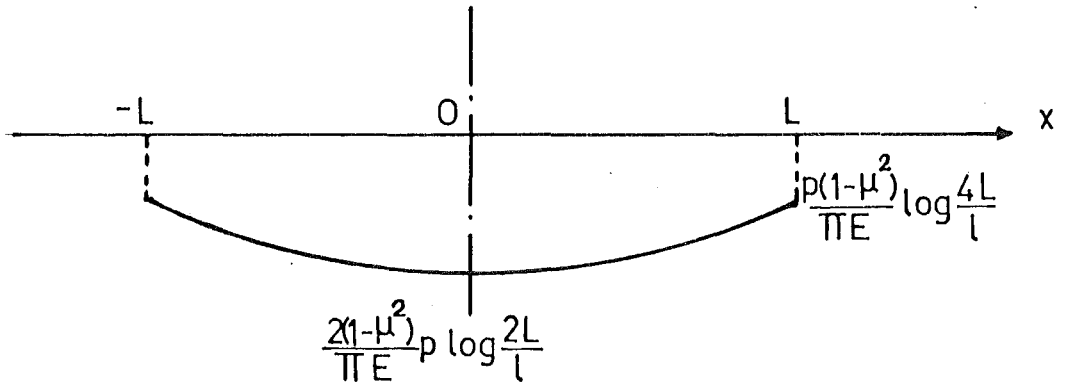

Fig. 5.5 The whole body displacement of the surface z=0 along x axis.

(a) if $c = L$

$$I = \log \frac{4L}{|Y|}$$

the downward displacement (positive since it is in the same direction of z axis) of the plane along the width $x = L$ is

$$w_{(L,b)} = \frac{1-\mu^2}{\pi E} \int_{-\ell}^{\ell} q \log \frac{4L}{|\ell|Y/\ell|} \, dy$$

$$= \frac{1-\mu^2}{\pi E} \left[p \log \frac{4L}{\ell} - \int_{-\ell}^{\ell} q \log \left| \frac{b}{\ell} - \frac{y}{\ell} \right| dy \right]$$

The pressure $q = q_o \left(\frac{1 - y^2}{\ell^2}\right)^{\beta}$, there exists a singularity at $y = b$ inside the range of the integration. More explicitly it can be written as

$$w_{(L,b)} = \frac{1-\mu^2}{\pi E} \left[p \log \frac{4L}{\ell} - \left(\int_{-\ell}^{b-\varepsilon} + \int_{b+\varepsilon}^{\ell} \right) q \left(1 - \frac{y^2}{\ell^2}\right)^{\beta} \log \left| \frac{b}{\ell} - \frac{y}{\ell} \right| dy \right] \qquad 5.5$$

(b) if $c \neq L$ and $(c - L)^2 >> (b - y)^2 = Y^2$

then

$$c - L + \left[(c - L)^2 + Y^2\right]^{.5} = c - L + \left[(c - L)^2 \left(1 - \frac{Y^2}{(c - L)^2} \right) \right]$$

$$\simeq c - L + |c - L| \left(1 - \frac{Y^2}{2(c - L)^2} \right)$$

for $0 \leqslant c < L$, $c - L = -|c - L| < 0$

i.e. $$c - L + \left[(c - L)^2 + Y^2\right]^{.5} \simeq \frac{Y^2}{2|c - L|}$$

then $$I \simeq \log \frac{4(c + L)|c - L|}{Y^2} = \log \frac{4(L^2 - c^2)}{Y^2}$$

The downward displacement of any point inside the contact area satisfying the condition $0 \leqslant c < L$ is

$$w_{(c,b)} = \frac{1-\mu^2}{\pi E} \left[p \log \frac{4(L^2 - c^2)}{\ell^2} - \int_{-\ell}^{\ell} q_o \left(1 - \frac{y^2}{\ell^2}\right)^{\beta} \log \left(\frac{b - y}{\ell} \right)^2 dy \right] \qquad 5.6$$

The problem is symmetrical about the y axis so the Equation 5.6 is in fact applicable to the region $-L < c < L$ and Equation 5.5 applicable to $c = \pm L$. The first term of Equation 5.6 is finite if the length $2L$ of the cylinder is finite. This term depends only on the x coordinate of the point under consideration; it is called the whole body displacement of the plane along the line $x = c$. Fig.5.5 shows the variation of the whole body displacement along y axis $(-L \leqslant y \leqslant L)$. The length $2L$ of the cylinder is usually very large compared with the half-width of contact ℓ. For long cylinder $\log \frac{2L}{\ell} >> \log 2$, the whole body displacement at the centre is about twice that at the ends of the cylinder. It is noted that the whole body displacement is independent of the y coordinate of the point under consideration while the change in the shape of the surface under the contact area depends entirely on the second term containing b, the y coordinate of the point to be displaced. This means that the local displacement along any line of constant x coordinate is identical to any other. In particular for $c = 0$, the total displacement of points along y axis is

$$w_{(o,b)} = \frac{2(1-\mu^2)}{\pi E}\left[p \log \frac{2L}{\ell} - \int_{\ell} q_o \left(\frac{1 - y^2}{\ell^2}\right)^{\beta} \log \left| \frac{b-y}{\ell} \right| dy \right] \quad 5.7$$

$$= w^{W}_{(o,b)} + w^{L}_{(o,b)}$$

where w^{W} and w^{L} are whole body and local displacements of the point N respectively. The whole body displacement along y axis is

$$w^{W}_{(o,b)} = \frac{2(1+\mu^2)}{\pi E} p \log \frac{2L}{\ell}$$

The whole body displacement of any point inside the contact zone can be extracted from Equations 5.5 and 5.6

The local displacement along any line parallel to y axis such that

$-L < x = c < L$ is

$$w^{L}_{(c,b)} = \frac{-2(1-\mu^2)}{\pi E}\left[\int_{-\ell}^{\ell} q_o\left(\frac{1-y^2}{\ell^2}\right)^{\beta} \log\left|\frac{b-y}{\ell}\right| dy\right] \qquad 5.8$$

Comparing this with the local compression of the cylinder (Equation 4.50b) it is found that

$$\left|w^{L}_{(b)}\right|_{\text{cylinder}} = 2 \left|w^{L}_{(c,b)}\right|_{\text{plane}}$$

It can be concluded that the local displacements of the plane and the cylinder at the contact surface are equal. Hence the results obtained for the integration of the local compression of the cylinder can be used for the plane and vice versa.

By substituting the corresponding value of b into Equation 5.6 and obtain the results of the integration from the previous Chapter, the displacement of the following points can be obtained

$$w_{(c,0)} = \frac{2(1-\mu^2)p}{\pi E}\left[\frac{1}{2}\log\frac{4(L^2-c^2)}{\ell^2} - .5\psi(.5) + .5\psi(\beta+1.5)\right] \qquad 5.9$$

and

$$w_{(c,\ell)} = \frac{2(1-\mu^2)p}{\pi E}\left[\frac{1}{2}\log\frac{4(L^2-c^2)}{\ell^2} - .5\psi(\beta+1) + 5\psi(\beta+1.5)\right] \qquad 5.10$$

5.4 SPECIAL CASES

(i) The total displacement of the centre of the area of contact due to the uniform pressure distribution $q = q_o\left(1-\frac{y^2}{\ell^2}\right)^{\beta}$ along x axis is

$$w_{(0,0)} = \frac{2(1-\mu^2)p}{\pi E}\left[\log\frac{2L}{\ell} - .5\psi(.5) + .5\psi(\beta+1.5)\right] \qquad 5.11$$

This result is obtained from Equations 5.7 and 4.52.
If the pressure distribution is elliptical, i.e. $\beta = \frac{1}{2}$

$$\psi(\beta+1.5) = \psi(2) = \psi(1) + 1 = .4228$$

$$\psi(.5) = -1.9635$$

then

$$w_{(0,0)} = \frac{2(1-\mu^2)p}{\pi E}\left[\log\frac{4L}{\ell} + .5\right] \qquad 5.12$$

This is exactly the same as Prescott's and Lundberg's formula.

(ii) The total displacement of the point $(0,\ell)$ due to the general pressure $q = q_o(1-\frac{y^2}{\ell^2})^{\beta}$ is

$$w_{(0,\ell)} = \frac{2(1-\mu^2)p}{\pi E}\left[\log\frac{2L}{\ell} - .5\psi(\beta+1) + .5\psi(\beta+1.5)\right] \qquad 5.13$$

This result is obtained from Equations 5.7 and 4.59

if $\beta = .5$

$$\psi(\beta+1) = \psi(1.5) = \psi(.5) + 2 = 0.0365$$

$$\psi(\beta+1.5) = \psi(2) = \psi(1) + 1 = .4228$$

$$w_{(0,\ell)} = \frac{2(1-\mu^2)p}{\pi E}\left[\log\frac{4L}{\ell} - .5\right] \qquad 5.14$$

5.5 THE DISPLACEMENT OF POINT $(0, \frac{\ell}{\sqrt{2}})$

Other than b = 0 and ℓ, the displacement of the plane surface along the line $y = b = \frac{\ell}{\sqrt{2}}$ seems to be the easiest to calculate over the range of $0 < b < \ell$.

Substitute $b = \ell/\sqrt{2}$ into Equation 5.8 the local displacement is

$$w^{L}_{(c,b)} = \frac{-2(1-\mu^2)}{\pi E}\int_{\ell}^{\ell} q_o(1-\frac{y^2}{\ell^2})^{\beta}\log\left|\frac{1}{\sqrt{2}} - \frac{y}{\ell}\right| dy \qquad 5.15$$

$$= \frac{-2(1-\mu^2)q_o}{\pi E}\left[\int_{-\ell}^{0} + \int_{0}^{\frac{\ell}{\sqrt{2}}-\varepsilon} + \int_{\frac{\ell}{\sqrt{2}}+\varepsilon}^{\ell}\right]\log\left|\frac{1}{\sqrt{2}} - \frac{y}{\ell}\right| dy \qquad 5.16$$

ε is a small number

Let Z be a value such that

$$w^{L}_{(c,b)} = -\frac{2(1-\mu^2)}{\pi E} Z$$

Consider

$$Z_1 = \int_{-\ell}^{0} q_o\left(1 - \frac{y^2}{\ell^2}\right)^{\beta} \log \left| \frac{1}{\sqrt{2}} - \frac{y}{\ell} \right| dy$$

Put $y = -t$ then $dy = -dt$

$$Z_1 = \int_{0}^{\ell} q_o\left(1 - \frac{t^2}{\ell^2}\right)^{\beta} \log \left| \frac{1}{\sqrt{2}} + \frac{t}{\ell} \right| dt$$

Since t is a dummy variable, we can replace t by y

$$Z_1 = \int_{0}^{\ell} q_o\left(1 - \frac{y^2}{\ell^2}\right)^{\beta} \log \left| \frac{1}{\sqrt{2}} + \frac{y}{\ell} \right| dy$$

Substitute back into Equation 5.16

$$Z = \left[\int_{o}^{\frac{\ell}{\sqrt{2}} - \varepsilon} + \int_{\frac{\ell}{\sqrt{2}} + \varepsilon}^{\ell} \right] q_o\left(1 - \frac{y^2}{\ell^2}\right)^{\beta} \log \left| \frac{1}{2} - \frac{y^2}{\ell^2} \right| dy$$

Use $y = \ell \sin t \quad dy = \ell \cos t \, dt$

$$Z = \left[\int_{o}^{\frac{\pi}{4} - \alpha} \int_{\frac{\pi}{4} + \alpha}^{\frac{\pi}{2}} \right] q_o \, \ell \cos^{2\beta+1} t \log \frac{1}{2} \left| 1 - 2 \sin^2 t \right| dt \quad 5.17$$

where α is a small angle such that

$$\ell \sin\left(\frac{\pi}{4} - \alpha\right) = \frac{\ell}{\sqrt{2}} - \varepsilon$$

and

$$\ell \sin\left(\frac{\pi}{4} + \alpha\right) = \frac{\ell}{\sqrt{2}} + \varepsilon$$

Note that $1- 2 \sin^2 t = \cos 2t$, substitute into Equation 5.17

$$Z = \left[\int_0^{\frac{\pi}{4} - \alpha} + \int_{\frac{\pi}{4} + \alpha}^{\ell} \right] q_o \ell \cos^{2\beta+1} \log \frac{1}{2} \left| \cos 2t \right| \, dt$$

$$Z = \frac{-q_o \ell \sqrt{\pi} \Gamma(\beta+1)}{2\Gamma(\beta+1.5)} \log 2 + \left[\int_0^{\frac{\pi}{4} - \alpha} + \int_{\frac{\pi}{4} + \alpha}^{\frac{\Pi}{2}} \right] q_o \ell \cos^{2\beta+1} t \log \left| \cos 2t \right| \, dt$$

Since $p = \int_{-\ell}^{\ell} q_o (1 - \frac{y^2}{\ell^2})^{\beta} \, dy$

$$= q_o \int_{-\frac{\pi}{2}}^{\frac{\pi}{2}} \ell \cos^{2\beta+1} t \, dt = 2q_o \frac{\ell \sqrt{\pi} \Gamma(\beta+1}{2\Gamma(\beta+1.5)} \qquad 5.18$$

$$Z = - \frac{p}{2} \log 2 + \int_0^{\frac{\pi}{4} - \alpha} q_o \ell \cos^{2\beta+1} t \log \cos 2t \, dt + \int_{\frac{\pi}{4} + \alpha}^{\frac{\pi}{2}} q_o \ell \cos^{2\beta+1} t \log (-\cos 2t) dt \qquad 5.19$$

Considering the second term

$$Z^1 = \int_0^{\frac{\pi}{4} - \alpha} q_o \ell \cos^{2\beta+1} t \log \cos 2t \, dt, \qquad \text{Put } 2t = \frac{\pi}{2} - k$$

then $\cos 2t = \cos (\frac{\pi}{2} - k) = \sin k$

$$\cos^2 t = \frac{1 + \cos 2t}{2} = \frac{1 + \sin k}{2}$$

$$Z^1 = \frac{q_o \ell}{2^{\beta+1.5}} \int_{2\alpha}^{\frac{\pi}{2}} (1 + \sin k)^{\beta+.5} \log \sin k \, dk$$

Considering the third term of Equation 5.19

$$Z^{11} = \int_{\frac{\pi}{4}+\alpha}^{\frac{\pi}{2}} q_o \ell \cos^{2\beta+1} t \log (-\cos 2t)\, dt$$

Put $2t = k + \frac{\pi}{2}$ then $\cos 2t = -\sin k$

$$\cos^2 t = \frac{1+\cos 2t}{2} = \frac{1 - \sin k}{2}$$

$$Z^{11} = \frac{q_o \ell}{2^{\beta+1.5}} \int_{2\alpha}^{\frac{\pi}{2}} (1- \sin k)^{\beta+.5} \log \sin k\, dk$$

Substitute Z^1 and Z^{11} back into Equation 5.19

$$Z = -\frac{p}{2} \log 2 + \frac{q_o \ell}{2^{\beta+1.5}} \int_{2\alpha}^{\frac{\pi}{2}} \left[(1 + \sin k)^{\beta+.5} + (1 - \sin k)^{\beta+.5}\right] \log \sin k\, dk \qquad 5.20$$

Binominal theorem gives

$$(1 \pm a)^b = 1 \pm ba + \frac{b(b-1)}{2!} a^2 \pm \frac{b(b-1)(b-2)}{3!} a^3 +$$

$$+ \frac{b(b-1)(b-2)(b-3)}{4!} a^4 \pm \ldots\ldots\ldots$$

Therefore

$$(1 + \sin k)^{\beta+.5} + (1 - \sin k)^{\beta+.5} = 2\left[1 + A \sin^2 k + B \sin^4 k + C \sin^6 k + \ldots\ldots\right]$$

where

$$A = \frac{1}{2!} (\beta+.5)(\beta-.5)$$

$$B = \frac{1}{4!} (\beta+.5)(\beta-.5)(\beta-1.5)(\beta-2.5)$$

$$C = \frac{1}{6!} (\beta+.5)(\beta-.5)(\beta-1.5)(\beta-2.5)(\beta-3.5)(\beta-4.5)$$

etc.

For instance

$\beta = .5$ $\quad A = B = C \ldots\ldots\ldots\ldots = 0$

$\beta = 1.5$ $\quad A = 1 \quad B = C = \ldots\ldots = 0$

$\beta = 2.5$ $\quad A = 3 \quad B = C = \ldots\ldots = 0$

$\beta = 3.5$ $\quad A = 6 \quad B = 1 \quad C = D = \ldots\ldots = 0$

$\beta = 4.5$ $\quad A = 10 \quad B = 5 \quad C = D = \ldots\ldots = 0$

i.e., Z can be calculated at discrete values of β

(i) $\beta = .5$

$$Z_{.5} = -\frac{p}{2}\log 2 + \frac{q_o \ell}{2}\int_{2\alpha}^{\frac{\pi}{2}} \log \sin k \, dk$$

$$= -\frac{p}{2}\log 2 + \frac{q_o \ell}{2}\left(-\frac{\pi}{2}\log 2\right)$$

Note that the load per unit length is calculated from Equation 5.18.

$$p = \frac{q_o \ell \Gamma(1.5)}{\Gamma(2)} = \frac{\pi}{2} q_o \ell$$

hence

$$Z_{.5} = -p \log 2 = -\frac{1.386}{2} p$$

i.e.

$$w^{L}_{(c,\frac{\ell}{\sqrt{2}})} = \frac{1-\mu^2}{\pi E} p \ (1.385) \qquad 5.21$$

This can be checked with the result of Prescott[64] Page 638. It was proved that the displacement of any point on the line y = b inside the contact area is

$$w^{L}_{(c,b)} = w^{L}_{(c,0)} - \frac{(1-\mu^2) q_o b^2}{E\ell}$$

For $b = \frac{\ell}{\sqrt{2}}$, $w^{L}_{(c,\frac{\ell}{\sqrt{2}})} = w^{L}_{(c,0)} - \frac{(1-\mu^2) q_o \ell}{2E} = w^{L}_{(c,0)} - \frac{(1-\mu^2)p}{\pi E}$ $\qquad 5.22$

The deformation $w^{L}_{(c,0)}$ can be extracted from Equation 5.12.

$$w^{L}_{(c,0)} = \frac{2(1-\mu^2)p}{\pi E} \quad (1.1932)$$

Substituting into Equation 5.22 it is found that Prescott's result will show the same value as our calculation (Equation 5.21)

(ii) $\beta = 1.5$

$$Z_{1.5} = \frac{-p}{2} \log 2 + \frac{q_o \ell}{4} \int_{2\alpha}^{\frac{\pi}{2}} (1 + \sin^2 k) \log \sin k \, dk$$

Ref.34, page 588 gives

$$\int_{2\alpha}^{\frac{\pi}{2}} \sin^2 k \log \sin k \, dk = \frac{\pi}{8} (1 - 2 \log 2)$$

therefore

$$Z_{1.5} = \frac{-p}{2} \log 2 + \frac{q_o \ell}{4} \left(\frac{\pi}{8} - \frac{3\pi}{4} \log 2\right)$$

Noted that

$$p = \frac{q_o \ell \Gamma(2.5)\sqrt{\pi}}{\Gamma(3)} = \frac{3 q_o \ell \pi}{8}$$

then

$$Z_{1.5} = \frac{p}{2} \left[\frac{1}{6} - 2 \log 2\right] \qquad 5.23$$

(iii) $\beta = 2.5$

$$Z_{2.5} = -\frac{p}{2} \log 2 + \frac{q_o \ell}{2^3} \int_{2\alpha}^{\frac{\pi}{2}} (1 + 3 \sin^2 k) \log \sin k \, dk$$

$$= -\frac{p}{2} \log 2 + \frac{q_o \ell}{8} \left(-\frac{5\pi}{4} \log 2 + \frac{3\pi}{8}\right)$$

Note that $p = \frac{q_o \ell \sqrt{\pi} \Gamma(3.5)}{\Gamma(4)} = \frac{5\pi q_o \ell}{16}$

then $Z_{2.5} = \frac{p}{2} [\, .3 - 2 \log 2]$ 5.24

(iv) $\beta = 3.5$

$$Z_{3.5} = -\frac{p}{2}\log 2 + \frac{q_o \ell}{2^4}\int_{2\alpha}^{\frac{\pi}{2}} 1 + 6\sin^2 k + \sin^4 k)\log\sin k\, dk$$

Reference 34, page 588

$$\int_0^{\frac{\pi}{2}} \sin^4 k \log\sin k\, dk = \frac{3\pi}{16}\left(\frac{7}{12} - \log 2\right)$$

then

$$Z_{3.5} = -\frac{p}{2}\log 2 + \frac{q_o \ell}{16}\left(-\frac{35\pi}{16}\log 2 + \frac{55\pi}{64}\right)$$

while $p = \dfrac{q_o \ell \sqrt{\pi}\Gamma(4.5)}{\Gamma(5)} = \dfrac{35\pi}{128}\, q_o \ell$

then

$$Z_{\frac{7}{2}} = \frac{p}{2}\left[\frac{11}{28} - 2\log 2\right] \qquad 5.25$$

Summary of the above results

The values of Z at discrete values of β are

β	.5	1.5	2.5	3.5
Z	$-p\log 2$	$-p[\log 2 - \frac{1}{12}]$	$-p[\log 2 - .15]$	$-p[\log 2 - \frac{11}{56}]$

For $.5 \leqslant \beta \leqslant 3.5$, Z can be approximately represented by the following form

$$Z \simeq -p\left[2\log 2 - \frac{1}{4}\left(2\psi(\beta+1.5) - \psi(.5) - \psi(\beta+1)\right)\right] \qquad 5.26$$

The error is found to be .1% relative to the exact values of Z. However, the following form will be more useful in our future calculations

$$Z = -p\left[\frac{1}{4}\left(2\psi(\beta+1.5) - \psi(\beta+1) - \psi(\tfrac{1}{2})\right) - \frac{1}{6}(\beta-.5)^{.8}\right] \qquad 5.27$$

Table 5.1 shows the difference between the exact values of Z and the estimated Z evaluated from Equation 5.27.

TABLE 5.1

β	.5	1.5	2.5	3.5
$\psi(\beta+1)$	.036	.703	1.103	1.389
$\psi(\beta+1.5)$	.423	.923	1.256	1.506
$I = \frac{1}{4}[2\psi(\beta+1.5) - \psi(\beta+1) - \psi(.5)]$	.692	.776	.843	.896
$II = \frac{1}{6}(-.5)^{.8}$	0	.167	.290	.401
Estimated Z = +p [II - I] eqn 5.27	-.693	-.609	-.553	-.495
Exact Z	-.693	-.610	-.543	-.496
Relative error	0%	.2%	2.0%	.2%

Here we can conclude that the approximate local displacement of any point inside the contact area of the plane having $y = \frac{\ell}{\sqrt{2}}$ is

$$w_{(c,\frac{\ell}{\sqrt{2}})}^{L} = \frac{2(1-\mu^2)p}{\pi E}\left[-\frac{1}{6}(\beta-.5)^{.8} + \frac{1}{4}\left(2\psi(\beta+1.5) - \psi(\beta+1) - \psi(.5)\right)\right] \qquad 5.28$$

where $.5 \leqslant \beta \leqslant 3.5$ and the maximum relative error is 2%. Further calculation showed that when $\beta = 4.5$ the relative error is only 4%.

The local displacement can be added to the whole body displacement to give the total displacement of the plane at $y = \frac{\ell}{\sqrt{2}}$

$$w_{(o,\ell/\sqrt{2})} = \frac{2(1-\mu^2)p}{\pi E}\left\{\log\frac{2L}{\ell} - \frac{1}{6}(\beta-.5)^{.8} + \frac{1}{4}[2\psi(\beta+1.5) - \psi(\beta+1) - \psi(.5)]\right\} \qquad 5.29$$

in general

$$w_{(c,\ell/\sqrt{2})} = \frac{2(1-\mu^2)p}{\pi E}\left\{\frac{1}{2}\log\frac{4(L^2-c^2)}{\ell^2} - \frac{1}{6}(\beta-.5)^{.8} + \frac{1}{4}[2\psi(\beta+1.5) - \right.$$

$$\left. -\psi(\beta+1) - \psi(.5)]\right\} \qquad 5.30$$

5.6 DISCUSSION

The maximum displacement of the plane occurs at the centre of the contact area. (54) Experimental results have shown that the deformation of the plane as a whole is slightly higher than the theoretical value of the maximum displacements. Therefore, in later calculation, the value of the displacement of the centre point will be used as the representative displacement of the plane due to the indentation of a cylinder. The general equation for the displacement of any point inside the pressurised zone of distribution $q = q_o(1-\frac{y^2}{\ell^2})^{\beta}$ has been found. The special case of $\beta = .5$ has been checked with Lundberg's displacement of the points along the line $y = \ell/\sqrt{2}$ was also found to fulfil the requirements of future calculations.

CHAPTER 6

THE APPROACH OF TWO HARD FLAT PLANES COMPRESSING A ROUGH CYLINDER OF THE SAME MATERIAL

In the study of the design of work holding fixtures, the rigidity at the mating surfaces is a prime factor for the maximum dimensional accuracy of the components held in the fixture. In practice, the system of a cylindrical work-piece in contact with a hard flat locator occurs frequently. This prompted Shawki *et al*[90] to investigate the approach of two Vee locators compressing a cylindrical work-piece of varying degrees of hardness and roughness. Experimental results showed a much higher deformation than the value predicted by the available theory of elasticity. On the observation that the curve of the total approach is non-linear with applied load per unit length, Shawki simply assumed that an empirical formula exists for the relationship between the approach and the applied load. This empirical formula is similar to those he assumed for the indentation of a rough flat surface by spherical and flat locators. The curves he labelled "theory of a cylinder on a flat plate" in his article, presented to compare with the measured approach of the two planes, is actually a half of the value of the elastic deformation of a cylinder compressed by two planes which was derived by Föppl. Initially we found this very confusing because this value obviously cannot be used as a theoretical prediction for the approach of the two planes.

The theory by Lo[60] in 1969 for the elastic deformation of the asperities of two rough cylinders in contact at low loadings is useful for subjects such as friction, adhesion, wear and electrical contact resistance but is not applicable to the fixture and work-piece systems where much higher loadings are applied. Similar comments apply to the theory derived by Dakshina Murthy *et al*[15] where the asperities are assumed to deform plastically. At low loadings, they assumed that the truncated tips are negligible. From the fact that an increase in load brings more and more

new asperities under load rather than enlarging the contact spots and that the change in height of the asperities under compression is very small compared to their heights, they introduced a relationship between the load and the compliance of the asperities such that the load was shared equally by the asperities. Demkin[23] in 1976 introduced a powerful method to calculate the total approach of two rigid planes compressing a rough cylinder at low loadings. The planes were assumed undeformable. Although their mathematical derivation is not correct (see Section 4.4) their procedure may be employed, as in our derivation, for the total approach of the two hard planes compressing a rough cylinder under a load high enough to deform an asperity by up to .4 of its peak-valley height.

Although the planes are harder than the cylinder they must deform elastically during the compression process. In the following action, results from Chapters 3, 4 and 5 will be combined to give a mathematical formula for the approach of the two hard planes compressing a rough cylinder of the same material. Finally the results of the experiments carried out to check the validity of our theory and Shawki's empirical formula will be presented.

6.1 THE DEFORMATION OF A WEDGE MODEL ASPERITY SURFACE

Based on the theory of contact of rough surfaces at low pressure and the wedge model asperity surface under high pressure (Section 3.4), we calculated the expected deformation of rough turned cylindrical work-pieces under load for later comparison with experimental results. From the measured surface profiles of the cylinders, the initial (or no-load) bearing curves can be produced. Fig.6.14 shows the typical surface profile and its corresponding bearing curve of all the work-pieces. In the calculation of the deformation of the asperities, the deformed bearing curve was employed

instead of the no-load bearing curve. The deformed bearing curve has the following properties

(i) The initial part of the no-load bearing curve follows the relationship determined by Demkin and Kragelsky[18]

$$\eta = b\rho^{\nu} \qquad \text{for} \qquad \eta < .2$$

where η, b, ρ, and ν were defined in Section 3.4 Our work-pieces show that ν is between 3 and 3.5. For most of the cases ν is closer to 3 than 3.5. The apex angles are in the range of $140^{o} < 2\theta < 160^{o}$. For the wedge model asperity the ratio α of the deformed and initial bearing lengths is approximately 1.5 (Fig.3.12) for the above range of apex angle. Hence the degree of contact η of the deformed bearing curve must be approximately 1.5 times the degree of contact η obtained from the no-load bearing curve at a certain level.

$$\eta_{deformed} \simeq 1.5\ \eta_{no\text{-}load} \qquad 6.1$$

(ii) The conservation of material suggests that as the dimensionless compliance $\rho = \frac{a}{R_m}$ tends to .5, the degree of contact η of the deformed bearing curve must approach unity as proved for the wedge model asperity surface of equal height.

Consider a set of curves of the degree of contact η satisfying this condition (i.e. $\rho \to .5$ as $\eta_{deformed} \to 1$)

$$\eta = A\rho^{\varepsilon} \qquad 6.2$$

A and ε are interrelated such that

ε	2	2.5	3	3.5
A	4	5.66	8	11.3

The set of these curves is drawn in Fig.6.1. If the no-load

bearing curve of a certain surface profile is given, one of the above curves may be chosen to represent the deformed bearing curve for that surface profile provided its degree of contact η in the initial part is approximately 1.5 times the degree of contact of the no-load bearing curve at the same level. From the deformed bearing curve it can be seen easily that the asperities deform significantly at low pressure due to very small bearing length , but at high pressure the asperities deform only slightly. So it is the initial part of the bearing curve that determines the choice of the deformed bearing curve among the above set of curves.

The surface profile of a work-piece will not be exactly the same at different positions and neither will its no-load bearing curve. In general, a typical surface profile and consequently a no-load bearing curve has to be assigned for that work-piece. The exact deformed bearing curve (if one can be found by mathematical derivation) will undoubtedly be close to the assumed deformed bearing curve because both curves possess the same properties ((i) and (ii)). Studies by Demkin *et al*[18,21] found that the no-load bearing curve parameter ν of each machine operation lies in a very tiny range and it may be assigned a number such as 2, 2.5, 3 etc.. to simplify the calculation of the deformation of the asperities. Our rough turned surface profiles (Fig.6.14) of the cylindrical work-pieces showed that ν is approximately 3. In order to obtain the initial part of the assumed deformed bearing curve to be 1.5 times that of the corresponding no-load bearing curve, the set of curves in Fig.6.1 was superimposed on the no-load bearing curve. It was found that the curve

$$\eta = 5.66\rho^{2.5}$$

was the best representative of the assumed deformed bearing curve for our rough turned cylindrical work-pieces.

The relationship between the ratio of pressure over the yield stress

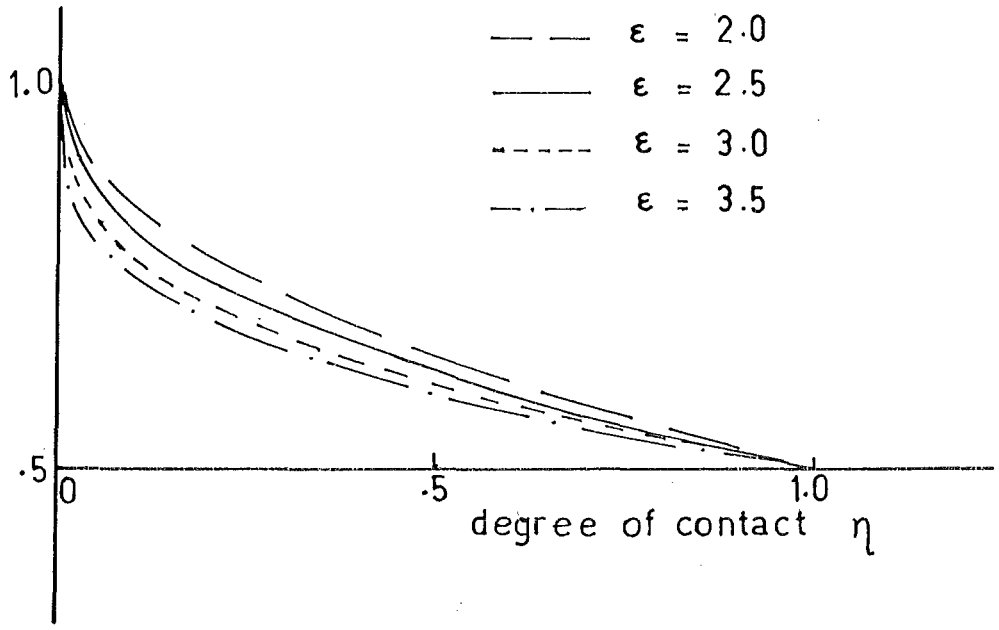

Fig. 6.1 The deformed bearing curves for varying values of ε.

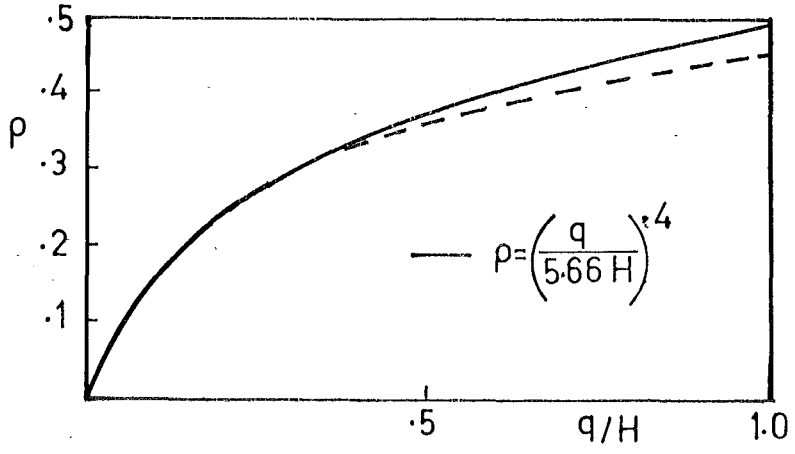

Fig. 6.2 The relation between dimensionless compliance and the dimensionless pressure on the asperities.

of the asperities and the degree of contact for the wedge model asperity surface of equal height is (Section 3.4.2)

$$\frac{q}{Y} = (\eta + 1) \left(\frac{\eta}{1 - \eta}\right)^{.5} \qquad 6.5$$

If the material is fully work-hardened the Brinell hardness is about three times of Yield stress, then

$$\frac{q}{H} \simeq \frac{q}{3Y} = \frac{1}{3} (\eta + 1) \left(\frac{\eta}{1 - \eta}\right)^{.5} \qquad 6.6$$

It was concluded by Demkin[22] that it is also approximately valid for surfaces with asperities of various heights because at high pressure almost all asperities are in contact.

A relationship between ρ and $\frac{q}{H}$ can be established if we combine the two Equations 6.2 and 6.6. If we take A = 5.66 and ε = 2.5, this relationship can be seen in Figure 6.2 (broken line).

The classical plastic theory assumes that the degree of contact is equal to the ratio of the pressure over hardness of the material, i.e.

$$\eta = q/H \qquad 6.7$$

Again, if A = 5.66 and ε = 2.5, the combination of the two Equations 6.2 and 6.7 yields a relationship between ρ and $\frac{q}{H}$ as drawn in Fig.6.2

$$\rho = (q/5.66H)^{.4} \qquad 6.8$$

By comparing the two curves in Fig.6.2, it is found that for dimensionless compliance $\rho < .4$, Equation 6.8 can be used to represent the complicated relationship between ρ and $\frac{q}{H}$ of the other curve (broken line) with little error.

Substitute $\rho = \frac{a}{R_m}$ into Equation 6.8 the deformation a of the asperities measured from the highest peak of a wedge model asperity surface of various

height is approximately

$$a = R_m (q/5.66H)^{.4} \qquad 6.9$$

if A = 8, ε = 3, this equation may be written as

$$a = R_m (q/8H)^{1/3} \qquad 6.10$$

In general

$$a = Dq^{1/\phi} \qquad 6.11$$

where

$$D = R_m (AH)^{-1/\varepsilon} \text{ and } \phi = \varepsilon \qquad 6.12$$

It is noted that this general equation for the deformation of the asperities at high pressure is also of the same form as the deformation of the asperities at low pressure derived by Demkin *et al* (Equation 3.22) the differences are in the values of the constants. According to Demkin, at low pressure the parameter $\phi = \nu + .5$ for elastic deformation and $\phi = \nu$ (the bearing area curve parameter) for plastic deformation of the asperities. For common machining operations, ν may have the maximum value of 3[18]; therefore ϕ may have a maximum of 3.5.

At this stage, all the necessary components of the deformation of the system of a rough cylinder compressed between two flat plates have been found. In the next section the total approach of the two planes compressing a rough cylinder is investigated.

6.2 THE TOTAL APPROACH OF TWO PLANES COMPRESSING A ROUGH CYLINDER OF THE SAME YOUNG MODULUS

Consider a rough cylinder in contact with two flat planes (semi-infinite spaces) under two uniform opposite loads per unit length p ($= \frac{W}{2L}$ where W is the total load and 2L is the length of the cylinder) Fig.6.3. Since the cylinder is rough, the slipping will be restrained in the contact area, i.e., interfacial friction occurs between the mating

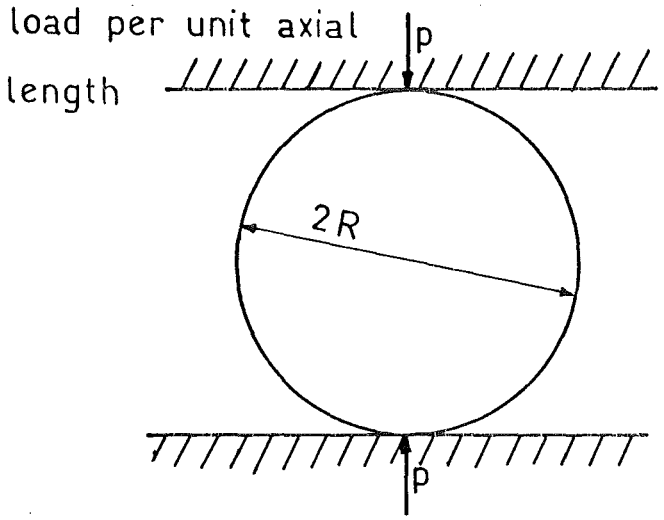

Fig. 6.3 Rough cylinder compressed between two planes.

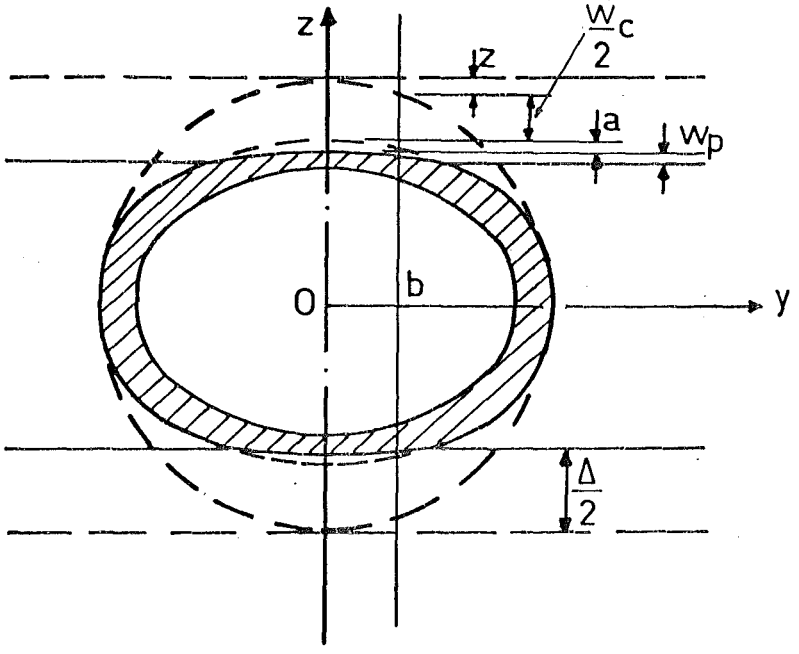

Fig. 6.4 Components of the total approach of the two planes.

--- Initial position

—— Position under loading

The rough layer is drawn cross hatched.

surfaces. Investigation by Conway[13] (1969) showed that if the contact area is kept constant, the vertical penetration of a rough rigid cylinder indenting an elastic flat surface is slightly lower than that of a smooth rigid cylinder (the "rough" cylinder used in Conway's article signifies the ability of a surface to develop friction with another surface but it is still very smooth compared with our rough cylinders). To simplify the problem, we do not account for this interfacial friction. Assuming that the bulk material supporting the asperities and the planes deform elastically, and let Δ be the total approach of the planes. Along the line y = b in the yz plane, all the components of the deformation are drawn in Fig.6.4. The sum of these is the total approach

$$\Delta = w_c + 2a + 2z + 2w_p \qquad 6.13$$

where

w_c = the elastic compression of the cylinder

a = the deformation of the asperities on a cylindrical surface

w_p = the elastic compression of the plane

z = the distance between the flat plane and the cylinder before loading.

(i) If the cylinder is smooth, the pressure distribution is semi-elliptic

$$q = q_o \left(1 - \frac{y^2}{\ell^2}\right)^{.5} \qquad 6.14$$

where ℓ is the half-width of the contact band and q_o is the maximum pressure. In this case the deformation of the asperities is negligible

$$\Delta \simeq w_c + 2z + 2w_p$$

(ii) If the elastic deformations of the cylinder and the planes are negligible compared with the deformation of the asperities

$$\Delta \simeq 2a + 2z$$

i.e. $$a \simeq \frac{\Delta}{2} - z = \frac{\ell^2}{2R}(1 - \frac{y^2}{\ell^2})$$

Substitute a by the general Equation 6.11

$$Dq^{1/\phi} = \frac{\ell^2}{2R}\ (1 - \frac{y^2}{\ell^2})$$

$$q = (\frac{\ell^2}{2RD})\ (1 - \frac{y^2}{\ell^2})^{\phi}$$

i.e. the pressure distribution has the form

$$q = q_o\ (1 - \frac{y^2}{\ell^2})^{\phi} \qquad 6.15$$

In general, we expect the pressure distribution to take the form

$$q = q_o\ (1 - \frac{y^2}{\ell^2})^{\beta} \qquad 6.16$$

Such that $\int_{\ell}^{\ell} q\,dy = p$ and β is a real number $\frac{1}{2} \leqslant \beta \leqslant \phi$

because, $\beta \to \frac{1}{2}$ - the cylinder is very smooth

and $\beta \to \phi$ - the load is very small such that the elastic deformations of the cylinder and the plane are small compared with the deformation of the asperities.

The load per unit length can be written as

$$p = \int_{\ell}^{\ell} q_o\ (1 - \frac{y^2}{\ell^2})^{\beta}\ dy$$

$$= q_o \ell \sqrt{\pi}\,\Gamma(\beta + 1)/\Gamma(\beta + 1.5) = q_o \ell K \qquad 6.17$$

where $$K = \sqrt{\pi}\,\Gamma(\beta + 1)/\Gamma(\beta + 1.5) \qquad 6.18$$

Deformation of the Asperities

(i) At $y = o$, the pressure acting on the asperities is q_o, the deformation of the asperities due to this pressure is

$$a_o = Dq_o^{1/\phi} = D(p/\ell K)^{1/\phi} \qquad 6.19$$

(ii) At $y = \ell$ $\quad q = o$

$$a_\ell = o \qquad 6.20$$

(iii) At $y = \ell/\sqrt{2}$ $\quad q = q_o\,(1 - \frac{1}{2})^\beta = q_o\,(\frac{1}{2})^\beta$

$$a_{\ell/\sqrt{2}} = Dq_o^{1/\phi}\,(\tfrac{1}{2})^{\beta/\phi} = D(p/\ell K)^{1/\phi}\,(\tfrac{1}{2})^{\beta/\phi} \qquad 6.21$$

Solving Equation 6.13 involves three unknown Δ, β and ℓ. Considering the total approach of the two planes along three different values of y we can establish three homogenous equations which can be used to solve Δ, β and ℓ.

The Total Approach of Two Planes

Consider the system of axes as drawn in Fig.6.5. At any cross section $x = c$, the deformations of the plane along lines $y = o$, ℓ and $\ell/\sqrt{2}$ are given in Equations 5.9, 5.10 and 5.30 respectively. The deformations of the asperities and the cylinder are independent of the x coordinate. The compression of the cylinder along lines $y = o$, ℓ and $\ell/\sqrt{2}$ are given in Equations 4.52, 4.59 and 4.61 respectively. The deformations of the asperities along lines $y = o$, ℓ and $\ell/\sqrt{2}$ has just been discussed.

Substitute all the corresponding values into Equation 6.13 to obtain the total approach of the two planes along the above lines.

Put $\quad B = 4p(1 - \mu^2)/\pi E \qquad G = \log(2R/\ell) - 1 \qquad F = \frac{1}{2}\log 4(L^2 - c^2)/\ell^2$

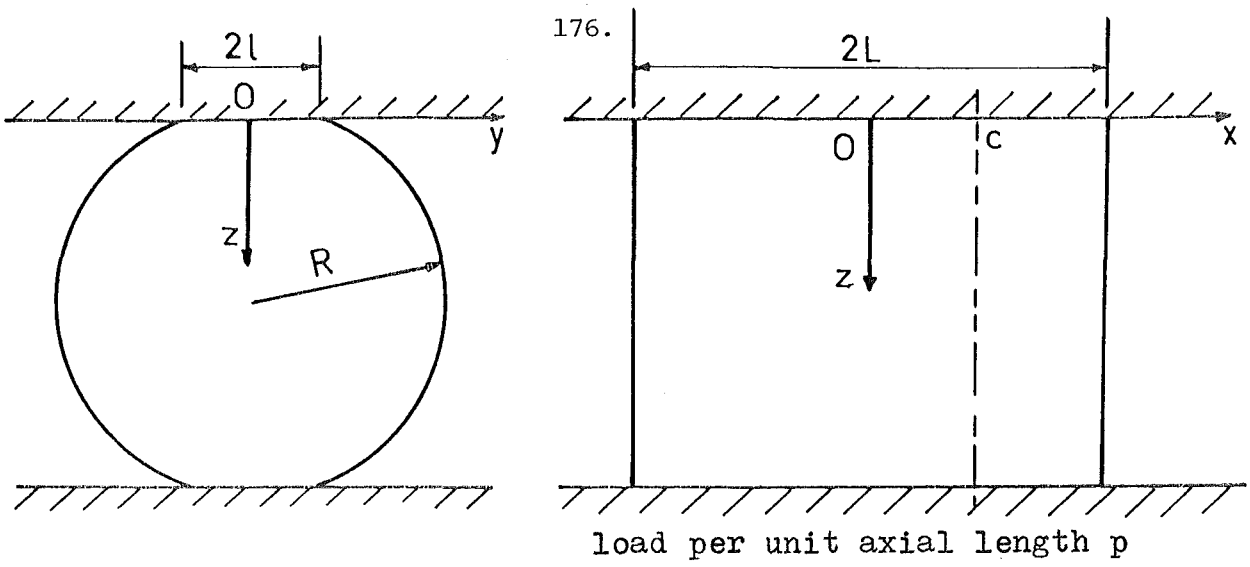

Fig. 6.5 The compression of a rough cylinder radius R, length 2L between two flat planes of the same material.

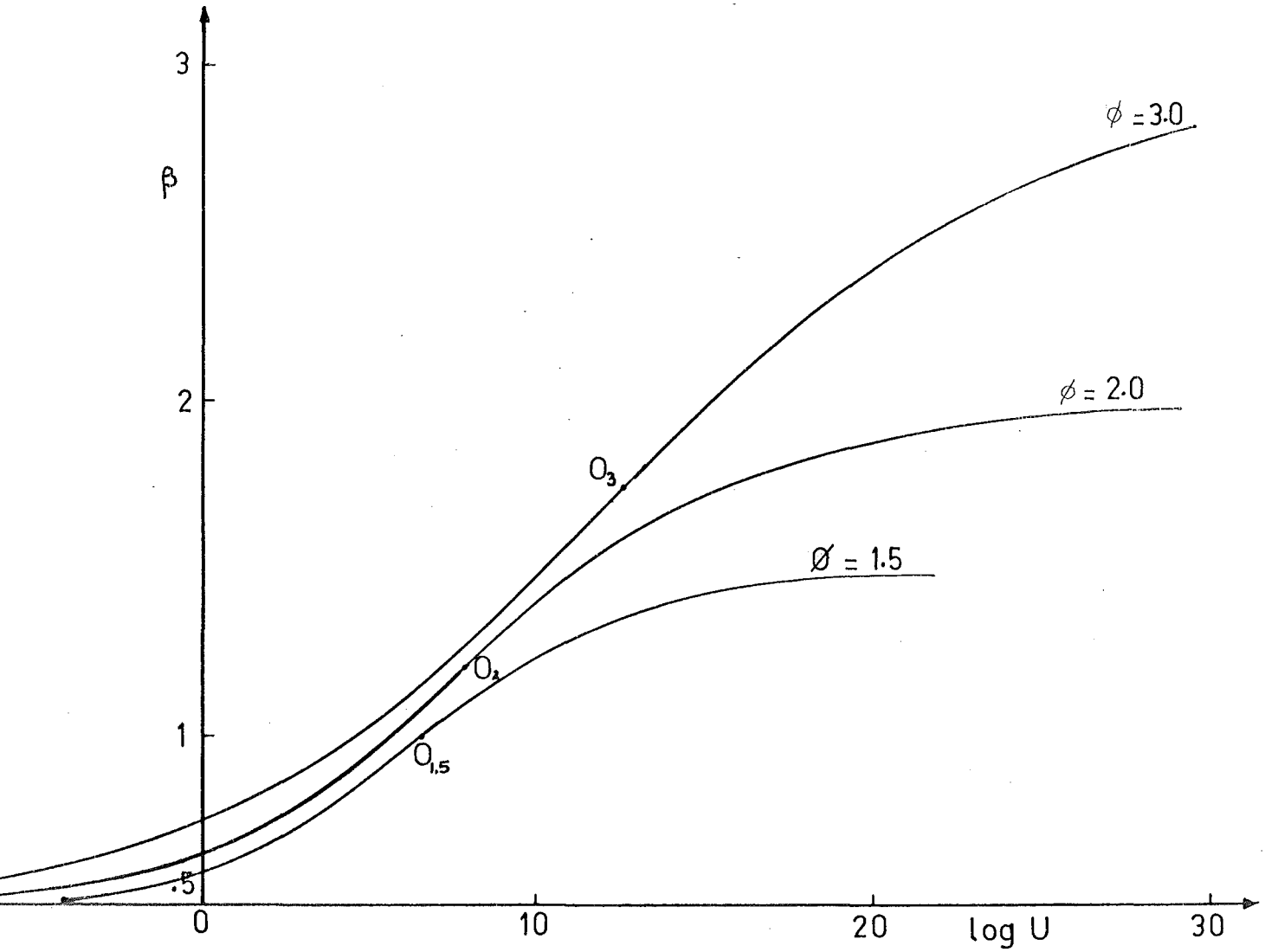

Fig. 6.6 The relation between β and logU for discrete values of $\varnothing$.

The total approach of the two planes along the line

(i) $y = o$

$$\Delta = B\left[G + F + \psi\ (\beta + 1.5) - \psi(.5)\right] + 2D\ (p/\ell K)^{1/\phi} \qquad 6.22$$

(ii) $y = \ell$

$$\Delta = B\left[G + F + \psi\ (\beta + 1.5) - \psi(\beta + 1)\right] + \ell^2/R \qquad 6.23$$

(iii) $y = \ell/\sqrt{2}$

$$\Delta = B\left[G + F + \psi\ (\beta + 1.5) - .5\psi(.5) - .5\psi(\beta + 1) - \right.$$

$$\left. - \frac{1}{3}\ (\beta - .5)^{.8}\right]$$

$$+ \frac{\ell^2}{2R} + 2D\left(\frac{p}{\ell K}\right)^{1/\phi}\ \left(\frac{1}{2}\right)^{\beta/\phi} \qquad 6.24$$

Subtract Equation 6.22 from Equation 6.23

$$0 = B\left[\psi(.5) - \psi(\beta + 1)\right] + \frac{\ell^2}{R} - 2D\ \left(\frac{p}{\ell K}\right)^{1/\phi} \qquad 6.25$$

Subtract Equation 6.22 from Equation 6.24

$$0 = B\left[.5\psi(.5) - .5\psi(\beta + 1) - \frac{1}{3}(\beta - .5)^{.8}\right] + \frac{\ell^2}{2R} + 2D\ \left(\frac{p}{\ell K}\right)^{1/\phi}$$

$$\left(\left(\frac{1}{2}\right)^{\beta/\phi} - 1\right) \qquad 6.26$$

Multiply Equation 6.26 by 2, then subtract Equation 6.25

$$0 = -2B(\beta - .5)^{.8}/3 + 4D(p/\ell K)^{1/\phi}\ \left[\left(\frac{1}{2}\right)^{\beta/\phi} - \frac{1}{2}\right] \qquad 6.27$$

then $\left(\frac{p}{\ell K}\right)^{1/\phi} = \frac{B(\beta - .5)^{.8}}{6D\bar{\Phi}}$ where $\bar{\Phi} = (.5)^{\beta/\phi} - .5$

$$\ell = \frac{p}{K}\left[\frac{6D\ \bar{\Phi}}{B(\beta - .5)^{.8}}\right]^{\phi} \qquad 6.28$$

$$= p\left[\frac{6D}{B}\right]^{\phi}\ \frac{1}{K}\ \left[\frac{\bar{\Phi}}{(\beta - .5)^{.8}}\right]^{\phi} \qquad 6.29$$

Substitute the value of ℓ into Equation 6.25 to get a solution for β

$$0 = B\left[\psi(.5) - \psi(\beta + 1)\right] + \frac{p^2}{R}\left[\frac{6D}{B}\right]^{2\phi}\frac{1}{K^2}\left[\frac{\Phi}{(\beta - .5)^{.8}}\right]^{2\phi} -$$

$$- \frac{B(\beta - .5)^{.8}}{3\Phi}$$

Divide by B

$$0 = \psi(.5) - \psi(\beta + 1) + \frac{p^2}{RB}\left[\frac{6D}{B}\right]^{2\phi}\frac{1}{K^2}\left[\frac{\Phi}{(\beta - .5)^{.8}}\right]^{2\phi} - \frac{(\beta - .5)^{.8}}{3\Phi}$$

Substitute $B = 4p(1 - \mu^2)/\pi E$ and rearrange this equation

$$\frac{D^{2\phi}}{Rp^{2\phi-1}}\left(\frac{\pi E}{1 - \mu^2}\right)^{2\phi+1}\frac{1}{4K^2}\left[\frac{1.5\Phi}{(\beta - .5)^{.8}}\right]^{2\phi} = \psi(\beta + 1) - \psi(.5) +$$

$$+ \frac{(\beta - .5)^{.8}}{3\Phi} \qquad 6.30$$

Put $J = \psi(\beta + 1) - \psi(.5) + (\beta - .5)^{.8}/3\Phi$

$Q = 1.5\Phi/(\beta - .5)^{.8}$ and $E_o = \pi E/(1 - \mu^2)$

Equation 6.30 can be written as

$$\frac{D^{2\phi}\ E_o^{2\phi+1}}{Rp^{2\phi-1}}\ \frac{Q^{2\phi}}{4K^2} = J$$

i.e.

$$\frac{D^{2\phi}\ E_o^{2\phi+1}}{Rp^{2\phi-1}} = \frac{4K^2 J}{Q^{2\phi}} \qquad 6.31$$

This equation shows that β is a function of D, R, p, E, μ and ϕ. It is impossible to get the exact value of β directly by substituting all the

values of the above variables into Equation 6.30. An interative method has to be used: the Newton-Raphson method is the simplest being used.

$$\text{Put} \quad f(\beta) = \psi(\beta + 1) - \psi(.5) + \frac{(\beta - .5)^{.8}}{3\bar{\Phi}} - \frac{D^{2\phi}}{R_p^{2\phi-1}} \left(\frac{\pi E}{1-\mu^2}\right)^{2\phi+1} \frac{1}{4K^2}$$

$$\left[\frac{1.5\bar{\Phi}}{(\beta - .5)^{.8}}\right]^{2\phi} \qquad 6.32$$

then

$$\beta_{k+1} = \beta_k - \left(f(\beta_k)/f'(\beta_k)\right) \qquad 6.33$$

where $f'(\beta)$ is the derivation of $f(\beta)$ with respect to β.

The iterative process for finding β is time-consuming and it would be more convenient for use in design if by curve fitting, a direct way for obtaining a sufficiently accurate value of β could be found. The following section gives the basis of such a method:

The Approximate Solution of β

Let U be the term indicated in Equation 6.31

$$U = \frac{D^{2\phi} E_o^{2\phi+1}}{R_p^{2\phi-1}} = \frac{4K^2 J}{Q^{2\phi}} \qquad 6.34$$

It has been decided in Demkin's theory and our formula for the deformation of the asperity (Equation 6.11) that ϕ may be assigned discrete values such as 1., 1.5, 2., 2.5, 3 and possibly a maximum value of 3.5. Let us draw a few curves representing the relationship between β and log U (Fig.6.6).

$$\log U = \log (4K^2 J/Q^{2\phi}) \qquad 6.34a$$

where K, J, Q are functions of β. It is observed that the curves always lie between .5 and ϕ which is in agreement with the assumption we made at

the beginning that when the applied pressure is very small U is very large, $\log U \to \infty$ and $\beta \to \phi$ or equivalently that the deformation of the asperities on the cylinder dominates the elastic deformation of the cylinder and the planes. As p increases, $\log U$ decreases steadily to $-\infty$, $\beta \to .5$ i.e., the deformation of the asperities is small compared with the elastic deformations of the cylinder and the planes. This is then analogous to Hertz's problem in which the cylinder and the planes are smooth. On observing the curves carefully, it is noticed that each curve is approximately symmetrical about the point marked 0 lying on the curve itself, having vertical coordinate $\beta_o = \frac{1}{2}(\phi + .5)$ 6.35

There are a few functions that have similar properties to these curves, the best approximation was found to be the tanh function. Calculation has shown that the relationship between β and $\log U$ can be of the form

$$\beta = \beta_o + S \tanh [(\log U - \log U_o)/V] \qquad 6.36$$

where S and V are constants, β_o and $\log U_o$ are the vertical and hotizontal coordinates of point 0 respectively. For different values of ϕ the following equations are proposed to fit the curves

for $\phi = 1.5$ $\beta = 1 + .5 \tanh [(\log U - \log 5.0153)/6]$

for $\phi = 2$ $\beta = 1.25 + .75 \tanh [(\log U - 6.5537)/8]$

for $\phi = 2.5$ $\beta = 1.5 + \tanh [(\log U - 10.4161)/10]$

for $\phi = 3$ $\beta = 1.75 + 1.25 \tanh [(\log U - 12.6130)/12]$

The remarkable feature of the above four equations is that they can be represented by a single equation dependent on ϕ, U and U_o

i.e. $\beta = .5(\phi + .5) + .5(\phi - .5) \tanh (\log U - \log U_o)/4\phi$ 6.37

Recall the hyperbolic function

$$\tanh\ u = (e^{u} - e^{-u}) \ / \ (e^{u} + e^{-u})$$

then

$$\tanh\left(\frac{\log U - \log U_o}{4\phi}\right) = \frac{\left(\frac{U}{U_o}\right)^{1/4\phi} - \left(\frac{U}{U_o}\right)^{-1/4\phi}}{\left(\frac{U}{U_o}\right)^{1/4\phi} + \left(\frac{U}{U_o}\right)^{-1/4\phi}}$$

$$= \left(t^{1/2\phi} - 1\right) \ / \ \left(t^{1/2\phi} + 1\right)$$

where $t = U/U_o$

Therefore

$$\beta = .5(\phi + .5) + .5\ (\phi - .5)\ (t^{1/2\phi} - 1)/(t^{1/2\phi} + 1)$$

or

$$\beta = (T\phi + .5)/T + 1) \qquad 6.38$$

where $T = t^{1/2\phi} = (U/U_o)^{1/2\phi}$

Calculation of T

From Equation 6.34

$$U = \frac{D^{2\phi} \ E_o^{2\phi} \ +1}{Rp^{2\phi-1}} = \frac{4K^2 \left[\psi(\beta + 1) - \psi(.5) + \frac{(\beta - .5)^{.8}}{3\bar{\Phi}}\right]}{\left[\frac{1.5\bar{\Phi}}{(\beta - .5)^{.8}}\right]^{2\phi}}$$

For $\beta = \beta_o = .5(\phi + .5)$

$$U_o = \frac{4K_o^{\,2} \left[\psi(\beta_o + 1) - \psi(.5) + \frac{(\beta_o - .5)^{.8}}{3\bar{\Phi}_o}\right]}{\left[\frac{1.5\bar{\Phi}_o}{(\beta_o - .5)^{.8}}\right]^{2\phi}} \qquad 6.39$$

where $K_o = \sqrt{\pi}\Gamma(\beta_o + 1)/\Gamma(\beta_o + 1.5)$ and $\bar{\Phi}_o = (.5)^{\beta_o/\phi} - .5$

Divide $U = D^{2\phi} E_o^{2\phi+1} / R p^{2\phi-1}$ by U_o we have

$$\frac{U}{U_o} = \frac{D^{2\phi} E_o^{2\phi+1}}{R_p^{2\phi-1}} \frac{\left[\frac{1.5\Phi_o}{(\beta_o - .5)^{.8}} \right]^{2\phi}}{4K_o^2 \left[\psi(\beta_o+1) - \psi(.5) + \frac{(\beta_o - .5)^{.8}}{3\Phi} \right]}$$

Substituting $\psi(.5) = -.19635$ and simplifying this equation

$$\frac{U}{U_o} = \left[\frac{1.5\, DE_o\Phi_o}{p(\beta_o - .5)^{.8}} \right]^{2\phi} \frac{E_o p\, Y_o}{4RK_o^2}$$

where $1/Y_o = \psi(\beta_o + 1) + 1.9635 + (\beta_o - .5)^{.8} / 3\Phi$

$$\text{hence} \qquad T = \left(\frac{U}{U_o}\right)^{1/2\phi} = \frac{1.5\, DE_o\Phi}{p(\beta_o - .5)^{.8}} \left(\frac{E_o p\, Y_o}{4RK_o^2} \right)^{1/2\phi} \qquad 6.40$$

i.e. T is proportional to $p^{-1+(1/2\phi)}$

Since $\phi > \frac{1}{2}$, $-1+(1/2\phi) > 0$

(a) If p is very small, $T \to \infty$ Equation 6.38 gives $\beta \to \phi$

(b) If p is very large, $T \to 0$ Equation 6.38 gives $\beta \to .5$

For given values of D, R, p, E, μ and ϕ, Equation 6.40 yields a value for T which may be substituted into Equation 6.38 to get the approximate value for β.

A program was written to compare the exact value of β with the estimated β calculated by Equation 6.38 at different values of ϕ (1.0, 1.5, 2.0, 2.5, 3.0 and 3.5). Appendix 6.1 illustrates the program itself and the percentage relative error in the range of (.5 + 02, ϕ -.01). A maximum error of 7% for β occurs near the β = .5 end.

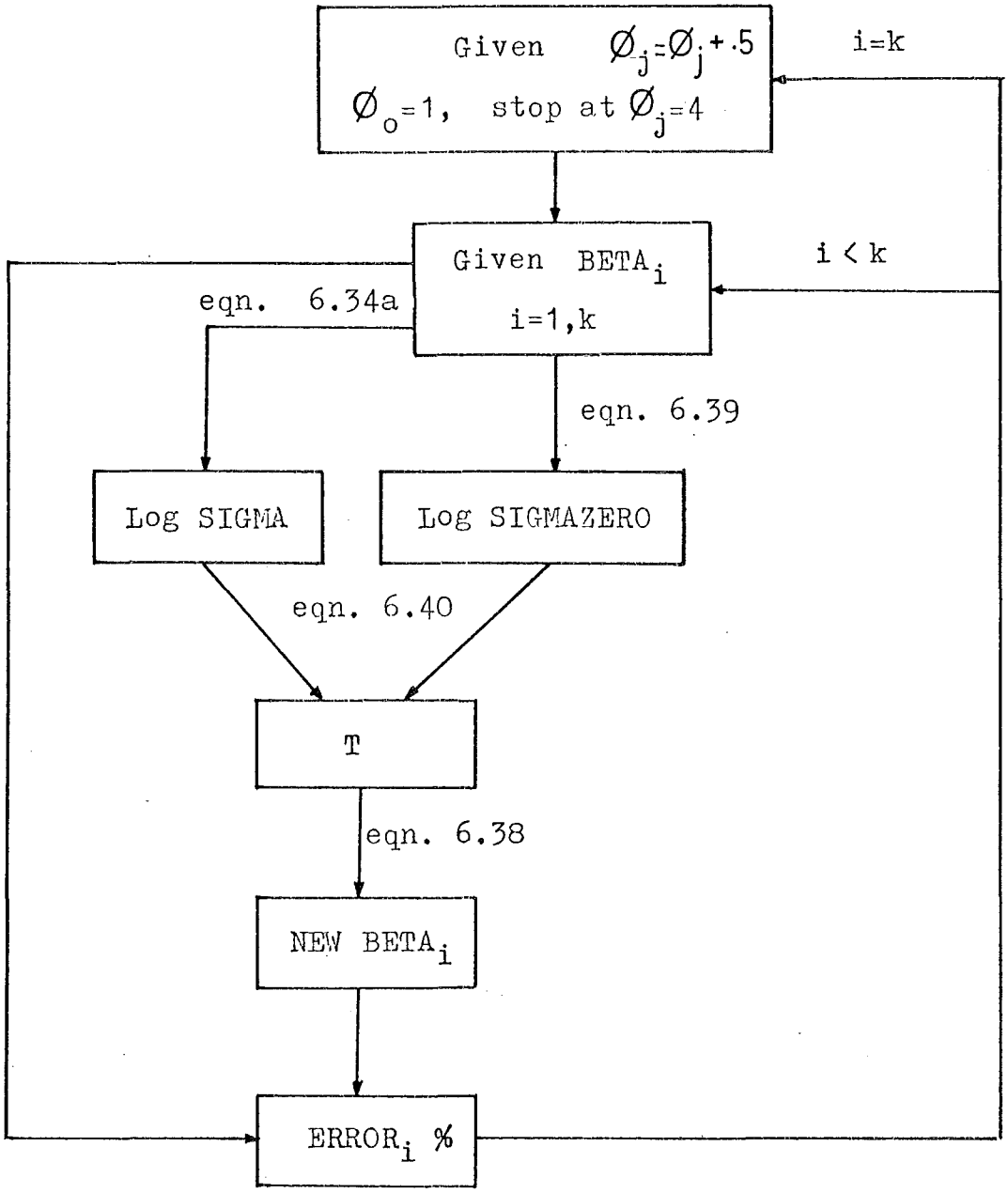

Fig. 6.7 Flow chart of program NHAM1 (Appendix 6.1)

Symbols for the program and the flow chart (Fig.6.7) are

BETA = exact value of β

LOG SIGMA = Log U

LOG SIGMA ZERO = Log U_o

NEW BETA = estimated value of β evaluated by Equation 6.38.

ERROR % = $100\ (\frac{\text{estimated } \beta - \text{exact } \beta}{\text{exact } \beta})\%$

Once an estimated value of β is found, it can be substituted into Equation 6.28 to obtain the value for the half width of the contact band ℓ.

The above method seems to be good as far as the error of β is concerned, except for an extreme condition which occurs frequently in practice when a very small error in β causes a very large error in the value of the half width ℓ. In the following, this extreme condition is solved by a modification of the above method.

The Case of Low Normal Pressure

When the force per unit length p is very small, the asperities on the rough cylinder may deform elastically (see Lo[46]), and β is found to be very close to ϕ. A small error in β will then cause a very large error in $\bar{\Phi}^{\phi} = ((.5)^{\beta/\phi} - .5)^{\phi}$ and consequently in the half width ℓ. For instance, when $\phi = 2.0$, assuming the exact value of β is 1.99, the above method yields an estimated value of $\beta = 1.996$ (appendix 6.1), i.e., the relative error in β is .307%, the exact $\bar{\Phi}^{\phi} = 3.01 \times 10^{-6}$ while the estimated $\bar{\Phi}^{\phi} = 4.8 \times 10^{-7}$ resulting in a relative error of -84%. The remaining terms constituting ℓ as shown in Equation 6.28 are dependent on β but they vary only slightly when β is close to ϕ. In effect, the relative error in $\bar{\Phi}^{\phi}$ is approximately the error in ℓ. To reduce the error in $\bar{\Phi}^{\phi}$ it is required to find other curves to fit the exact curves of Fig.6.6 in the region concerned better than the function we have employed.

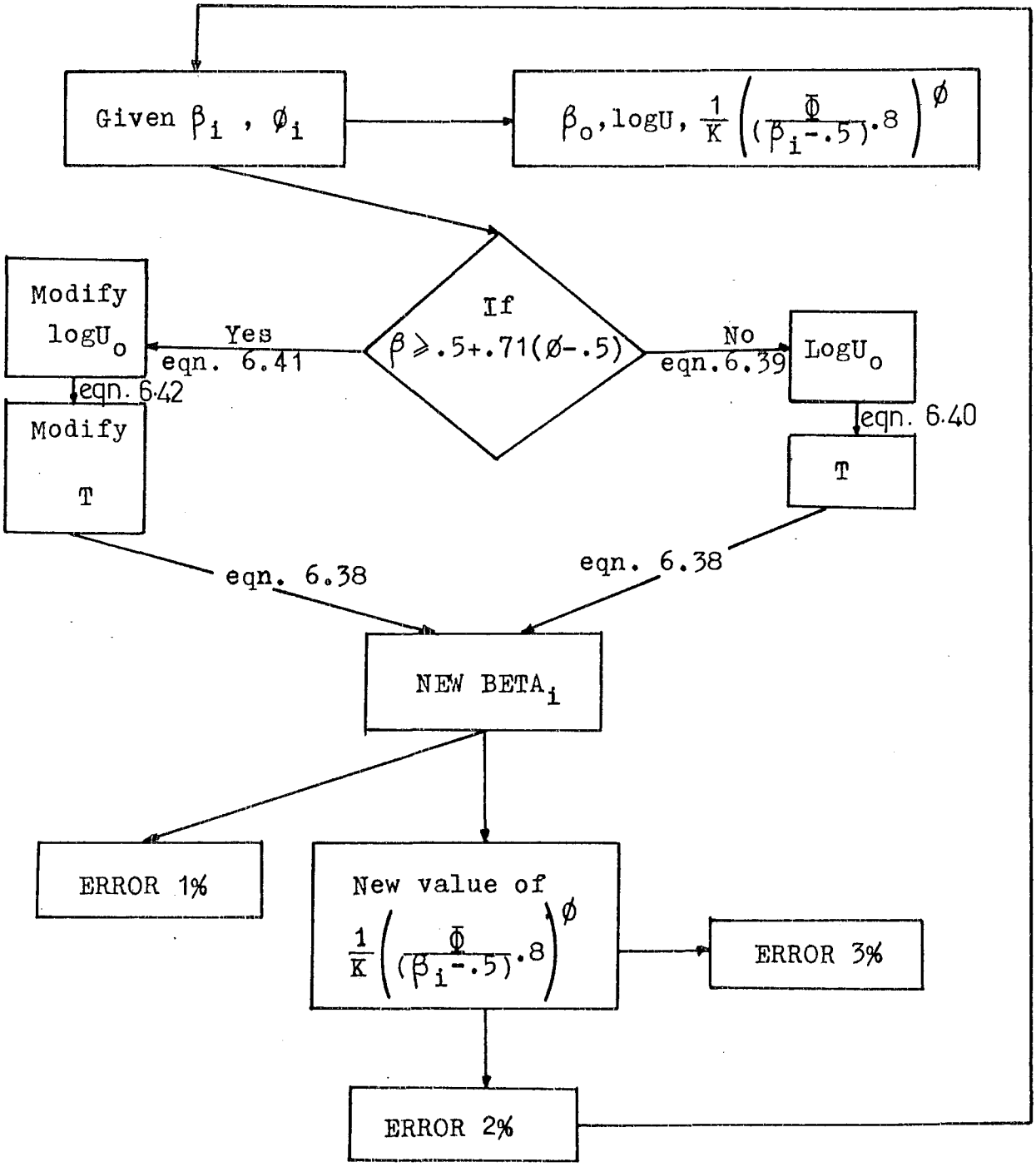

Fig. 6.8 Flow chart of program NHAM2

Trial and error calculations show that for the extreme end of the curves where $\beta \geq .5 + .71\ (\phi - .5)$ the same method may be used with two changes

(i) $$\log U_o = 3.9 + 3.45\ (\phi - 1)^{1.18} \qquad 6.41$$

(ii) $$T = (U/U_o)^{1/(1+2\phi)} \qquad 6.42$$

These new curves fit closely to the exact curves. The relative error in β will be very much reduced and so is the relative error in ℓ.

Another program was written to show the relative error in β and ℓ. Fig.6.8 illustrates the flow chart for this program. From Equation 6.28 the term $\frac{1}{K}\left[\frac{\Phi}{(\beta - .5)^{.8}}\right]^{\phi}$ is dependent on β so the error in the half width ℓ due to the effect of the error in β is, in effect, the error this term. Let us call it W_β or W(BETA). The width of the contact band at a certain pressure is a constant multiplied by W_β so W_β is actually a measure of the half width ℓ. Symbols used in the flow chart and program NHAM 2 are

BB or BETA = exact β

BNEW or NEW BETA = the estimated value of β

ERROR1 or ERROR 1% = 100 (estimated β - exact β)/exact β

WEXAC or WIDTH EXACT = exact W_β calculated from the exact value of β

WESTD or NEW WIDTH = estimated W_β calculated from the estimated β

EROR2 or ERROR 2% = 100 (estimated W_β - exact W_β)/exact W_β

EROR3 or ERROR 3% = 100 (estimated S_β - exact S_β)/exact S_β

where $S_\beta = (\beta - .5)^{.8}/3\Phi$

The program and the results for values of β up to ϕ - .001 are shown in Appendix 6.2. The maximum relative error of ℓ found to occur around value of $\beta = .5 + .71\ (\phi - .5)$ where the modified curve meets the initial β curve (Equation 6.37). On the left end of the curves in

Fig.6.9 where β is close to .5, the estimated value of β evaluated by Equation 6.37 has small relative error but this results in a large error in the estimated value of W_β (the same order of error for ℓ). These are drawn in Fig.6.9. To ensure that the method gives estimations of the half width ℓ (calculated from the estimated value of β) within (+10, -14%) the range of β has to be limited to

$$.5 + .12\ (2\phi - 1.5) < \beta < \phi \qquad 6.43$$

The values of $\beta^* = .5 + .12\ (2\phi - 1.5)$ for various values of ϕ are also tabulated in Fig.6.9. In practice β always stays in the above range. Only when the load is high, calculation shows that $\beta \leqslant .5 + .12(2\phi - 1.5)$: then the deformation of the asperities may be small compared with the elastic deformation of the cylinder and the planes and the problem may be approximated as one with a smooth cylinder in $\beta \simeq .5$.

Once the half width ℓ is found, it can be substituted into Equation 6.22 to obtain the total approach Δ of the two planes. Thus, by accepting a maximum possible error of (+10, -14%) in ℓ a direct method for obtaining the total approach of two flat planes compressing a rough cylinder is now available

$$\Delta = B\left[G + F + \psi\ (\beta + 1.5) - \psi(.5)\right] + (B(\beta - .5)^{.8})/3\Phi$$

Substitute $B = 4p(1 - \mu^2)/\pi E = 4p/E_o$

$$\Delta = \frac{4p}{E_o}\left[G + F + \psi(\beta + 1.5) + 1.9635 + \frac{(\beta - .5)^{.8}}{3\Phi}\right] \qquad 6.44$$

where $G = \log (2R/\ell) - 1$

$$F = \frac{1}{2}\log 4(L^2 - c^2)/\ell^2$$

The relative error due to the estimation of Δ is difficult to obtain. If c is not so close to L, R and $(L^2 - c^2)^{1/2}$ are very much larger than ℓ, a large error in ℓ only results in a small error in G and F. The error

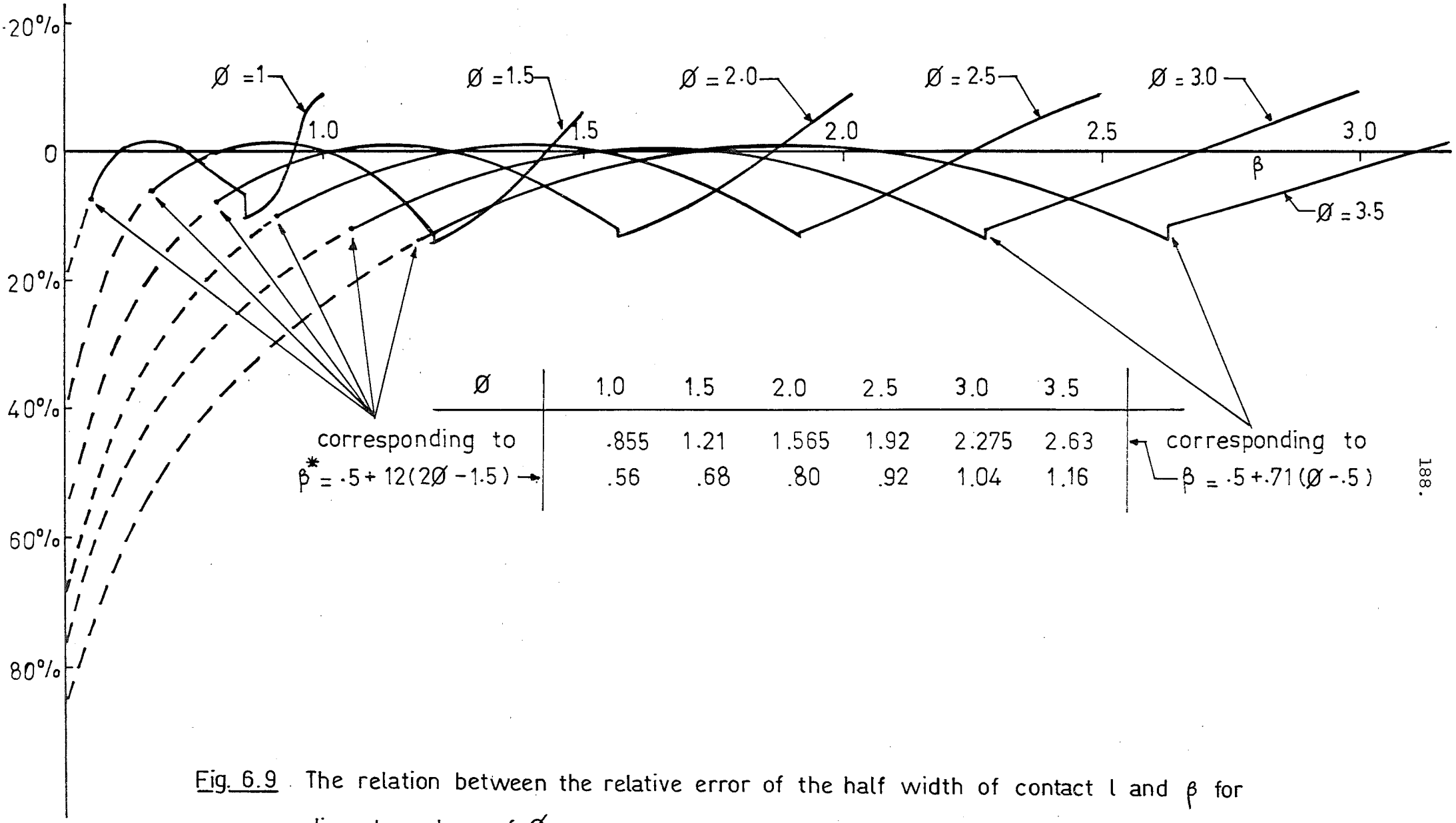

Ø	1.0	1.5	2.0	2.5	3.0	3.5
corresponding to	.855	1.21	1.565	1.92	2.275	2.63
$\beta^* = -.5 + 12(2Ø - 1.5)$ →	.56	.68	.80	.92	1.04	1.16

← corresponding to $\beta = -.5 + .71(Ø - .5)$

Fig. 6.9 The relation between the relative error of the half width of contact l and β for discrete values of Ø.

in β in the range of $.5 + .12(2\phi - 1.5) < \beta < \phi$ is always less than ±3% (appendix 6.2). From the graph of psi function[2] the error in $\psi(\beta + 1.5)$ is much smaller than the error in β. The only term which has significant error is $(\beta - .5)^{.8/3\phi}$ which is found to be less than ±5% for $\phi > 1.5$ (ERROR3 in Appendix 6.2). Hence the maximum possible error in Δ may be estimated to be ±10%.

6.3 SUMMARY OF THE RESULTS

Assumptions

(i) The bulk material of the cylinder supporting the asperities and the flat planes deform elastically, i.e., the plastic onset has not been reached.

(ii) The length 2L of the cylinder is large compared with the width of the contact area 2ℓ.

(iii) The pressure distribution across the width of the contact area is

$$q = q_o\left(1 - \frac{y^2}{\ell^2}\right)^{\beta}$$

(iv) The deformation of the asperities on the cylindrical surface follow the relationship

$$a = Dq^{1/\phi} \text{ mm}, \quad q \text{ in kg/mm}^2$$

in particular:

(a) for plastic deformation of asperities under low pressure

$$D = R_p (\eta_o c\sigma_o)^{-1/\nu}, \quad \phi = \nu \qquad 6.45$$

where ν = the no-load bearing curve parameter

R_p = depth of the profile in mm (Fig.3.9)

$c\sigma_o$ = the flow pressure of the asperities, it may be taken as approximately the same as the hardness

$\eta_o = L_m/L_o \simeq .5$ for most profiles [23]

(b) For elastic deformation of the asperities [23]

$$D = R_p^{(2\nu/2\nu+1)} (.5\eta_o VB)^{(2/2\nu+1)} \qquad 6.46$$

$\phi = (2\nu+1)/2$

$V = 3\sqrt{\pi}\Gamma(\nu+1)/4\Gamma(\nu+1.5)$ $\quad B = .43E/(1 - \mu^2)r^{.5}$

r = the asperity tip radius of curvature in mm

E = Young modulus in kg/mm^2

R_p = in mm

(c) For plastic deformation of asperities under high pressure

$$D = R_m A^{-1/\varepsilon}, \quad \phi = \varepsilon$$

A and ε are found from the bearing curve of the surface profile concerned (Section 6.1). For most of our rough turned cylinders, A and ε are assumed to be 5.66 and 2.5 respectively

R_m = peak valley height of asperities in mm (Fig.3.9)

(v) The planes and the cylinder are of the same material

$E = E_1 = E_2$, $\mu = \mu_1 = \mu_2$

Results

With given values of pressure per unit length p (kg/mm), length and radius of cylinder 2L (mm), R (mm), respectively, Young's modulus of the cylinder and the plane E (kg/mm^2) Poisson's ratio μ and ϕ, the pressure power coefficient β is the solution of the equation

$$\psi(.5) - \psi(\beta + 1) + \frac{p^2}{RB}\left[\frac{6D}{B}\right]^{2\phi}\frac{1}{K^2}\left[\frac{\Phi}{(\beta-.5)^{.8}}\right]^{2\phi} - \frac{(\beta-.5)^{.8}}{3\Phi} = 0 \qquad 6.47$$

It may be solved by either an iterative numerical method of by our approximate direct method with the following results

1) The calculation of β begins with the evaluation of

$$T = \frac{1.5\ DE_o \bar{\Phi}_o}{p(\beta_o - .5)^{.8}} \left[\frac{E_o\ p\ Y_o}{4K_o^2 R} \right]^{1/2\phi}$$

where $1/E_o = (1 - \mu^2)/\pi E$, $\beta_o = \frac{1}{2}(\phi + .5)$ $\bar{\Phi}_o = (.5)^{\beta o/\phi} - .5$

$$K = \sqrt{\pi}\Gamma(\beta+1)/\Gamma(\beta+1.5), \quad K_o = \sqrt{\pi}\Gamma(\beta_o+1)/\Gamma(\beta_o+1.5)$$

$$1/Y_o = \psi(\beta_o+1) + 1.9635 + (\beta_o+.5)^{.8}/3\bar{\Phi}_o$$

then $$\beta = (T\phi + .5)/(T + 1) \qquad 6.48$$

This value of β is acceptable (with less than 3% error) if

$$.5 + .12(2\phi - 1.5) \leqslant \beta < .5 + .71(\phi - .5)$$

However, for $.5 + .71(\phi - .5) \leqslant \beta < \phi$ we may use

$$\text{Log } U_o = 3.9 + 3.45(\phi - 1)^{1.18}$$

and $$T = \left(\frac{U}{U_o}\right)^{1/(1+2\phi)} = \left[\frac{D^{2\phi}\ E_o^{2\phi+1}}{R\ p^{2\phi-1}\ U_o} \right]^{1/(2\phi+1)}$$

$$= \frac{DE_o}{p} \left[\frac{p^2}{DU_o} \right]^{1/(1+2\phi)} \qquad 6.49$$

This new value of T is used in Equation 6.48 to obtain the new value of β which has an error of less than 1.5% (ERROR 1 in Appendix 6.2)

2) The half width of the contact area ℓ may be calculated with a maximum error of (+10, -14%) for the range $.5 + .12(2\phi-1.5) < \beta < \phi$

$$\ell = \frac{p}{K} \left[\frac{6D\Phi}{B(\beta - .5)^{.8}} \right]^{\phi} \text{ mm} \qquad 6.50$$

where $B = 4p/E_o$ and $\Phi = (.5)^{\beta/\phi} - .5$

3) The total approach of two planes (maximum error of ±10%) at the cross section $x = c$ is

$$\Delta = (4p/E_o)[\log(4RL/\ell^2) - 1 + \psi(\beta + 1.5) + 1.9635 + (\beta - .5)^{.8}/3\Phi] \qquad 6.52$$

The total approach Δ may be seen to be composed of three different components.

(i) The whole body component $4p(G + F)/E_o$ is the sum of the whole body displacements of the cylinder and the planes.

(ii) The local component $(4p/E_o)(\psi(\beta+1.5) + 1.9635)$, i.e., the sum of the local displacements of the cylinder and the planes.

(iii) The deformation of the asperities $4p(\beta-.5)^{.8}/3E_o\Phi$ 6.53

It is the sum of the deformations of the asperities in both upper and lower contacts.

A program was written to calculate the value of β, the half width of contact area ℓ, the whole body, the local, the asperity deformation components of the approach Δ of the two planes. This theoretical value of Δ may be compared with the approach of the two planes when compressing a smooth cylinder and the approach of two Vee locators when compressing the same rough cylinder (Shawki's formula).

If the cylinder is smooth, the half width of the contact area is obtained from Hertz's results

$$\ell_H = (8pR/E_o)^{1/2} \qquad 6.54$$

The total approach of the two smooth planes compressing a smooth cylinder at Section x = c is obtained by adding up the corresponding deformations given in Equations 4.53 and 5.9 with $\beta = \frac{1}{2}$

$$\Delta_H = (4p/E_o) \quad [G + F + 2.3864] \qquad 6.55$$

if c = 0 the total approach at the section passing through y axis is

$$\Delta_H = (4p/E_o) \log(2E_oL/p) \qquad 6.56$$

This formula was derived by Lundberg[62].

Shawki's formula for the approach of two hard steel Vee locators compressing a rough steel cylinder of hardness H (kg/mm^2) diameter D (mm) average peak-valley height R_m(micron) under load per unit length p (kg/mm) is

$$\Delta_{SH} = [.086 + (15/H) + (8.4/D) + .005R_m] (10p)^{.7} \text{microns} \qquad 6.57$$

Fig.6.10 illustrates the flow chart of the program NHAM3 and its results (Appendix 6.3) can be obtained for the conditions of our work-pieces.

In future calculations we will take c = 0 and assume that what happens at the cross section x = c = 0 is the representative of the whole system.

Symbols of program NHAM3

LOAD = the total load W in lbs

BETA = β

WIDTH = half width ℓ of the contact area in mm

WHOLE or WHOLE DEF = the whole body component $4000p(G+F)/E_o$ in micron

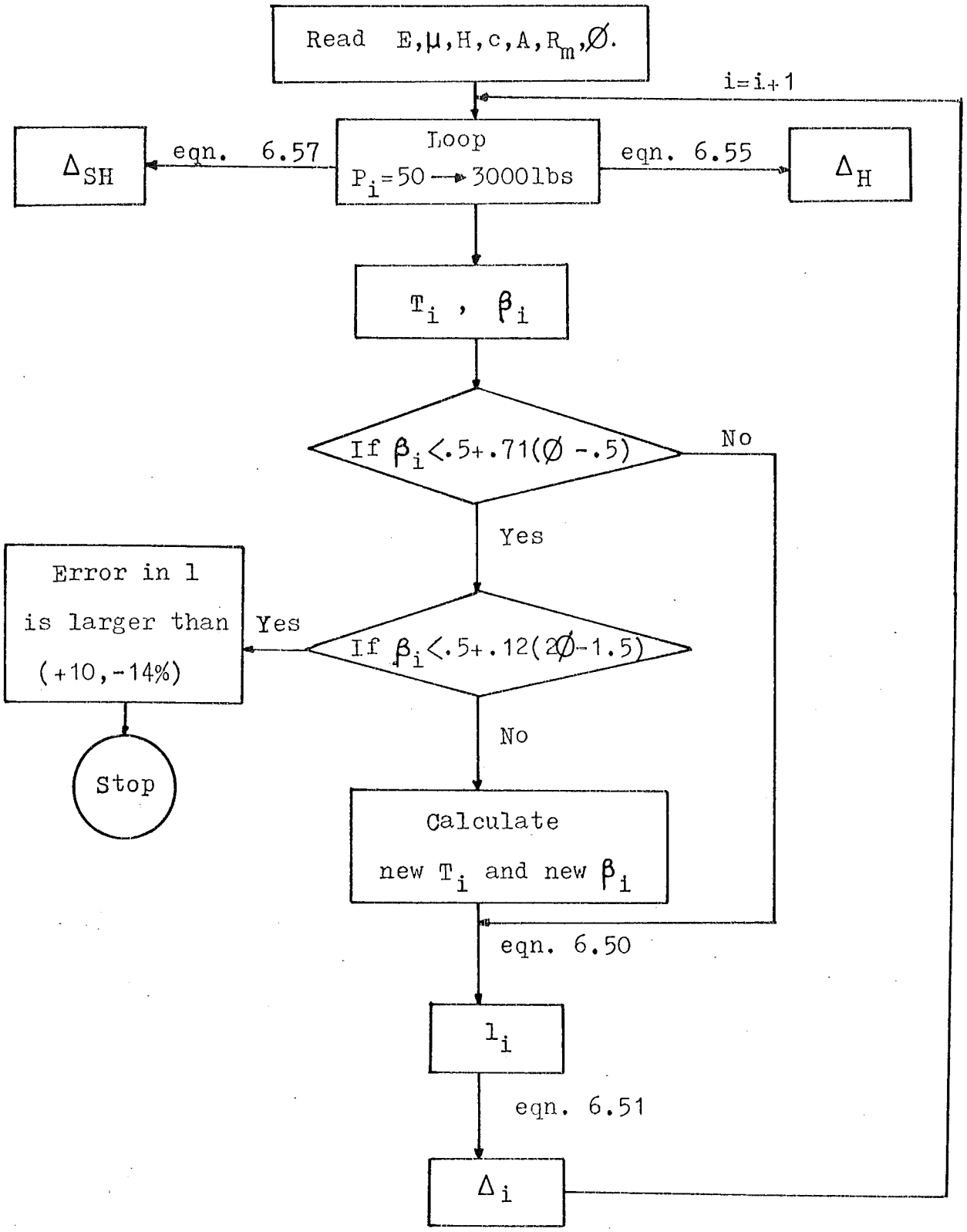

Fig. 6.10 Flow chart of program NHAM3

Ø,c,A will be given as 2.5,0,5.66 respectively

SHAPE or LOCAL DEF = the local component in micron

ROUGH or ROUGH DEF = the deformation of the asperities

$4000p(\beta-.5)^{.8}/3E_o\Phi$ in micron

DEL or TOTAL DEF = the total approach of the two planes in microns

WIDTH or HERTZ WIDTH = the half width of the contact area for the case the cylinder is smooth, in mm.

DELHE or HERTZ DEF = the total approach of the two planes in micron (smooth cylinder)

DELSH or SHAWKI DEF = the total approach of the two Vee locators compressing the rough cylinder of the same conditions

FAI = ϕ

E, U, H = Young modulus, Poisson ratio and Brinell hardness respectively

CLENG = half length of the cylinder

XCOOR = the x coordinate of the cross section considered

RM = peak-valley height of the asperity

A = the constant of the deformed bearing curve,

e.g. A = 5.66 for ϕ = 2.5

6.4 APPLICATION - THE ELASTIC DEFORMATION OF THE ASPERITIES

The above method can be applied to solve the contact of a rough cylinder with a smooth plane, in which case the asperities are assumed to deform elastically. The results from the diagrams plotted by Lo's iterative method can be compared. Take the example employed in Demkin's article[23] for a rough cylinder.

The depth of flattening R_p = .5 micron (standard deviation σ = .2 micron)

Cylinder radius R = 10 mm

Asperity top radius $r = .02$ mm

Young Modulus of Steel $E = 21500$ kg/mm^2

Poisson's ratio $\mu = .3$

Bearing curve parameter $\nu = 3$, $\eta_o = .5$

Assume that the cylinder is 20 mm long.

The constant D for the elastic deformation of the asperities is given in Equation 6.46.

$$D = R_p^{2\nu/2\nu+1} \quad (.5\ \eta_o L\ B)^{-2/2\nu+1}$$

where $L = 3\sqrt{\pi}\Gamma(4)/\Gamma(4.5) = 2.7428$

$$B = .43 \times 21500/,91\sqrt{.02} = 71837$$

then

$$D = .0000675 \qquad 6.58$$

The program NHAM3 was modified slightly to introduce the value of D directly into the program . The half width of the contact area ℓ (WIDTH) at the cross section x = 0 at various loadings from .0005 to 2.5 kg/mm is tabulated and plotted in Fig.6.11. It is also plotted and named Demkin's curve since we employ the elastic deformation relation for D derived by him.

Based on the normal distribution of the asperities, Lo[60] obtained the solution of the elastic compression of rough cylinders. From the diagram plotted for the dimensionless half contact width versus the dimensionless loading, we can apply the above conditions of the rough cylinder in contact with two planes to calculate the half width ℓ of the contact area at any load per unit length as a function of

$$\delta = 8R^{.5}r^{.5}g\sigma/3\pi^{1.5} \qquad 6.58a$$

where $.1 \leqslant \delta \leqslant .5$ and R, r are the radii of the cylinder and the asperity top

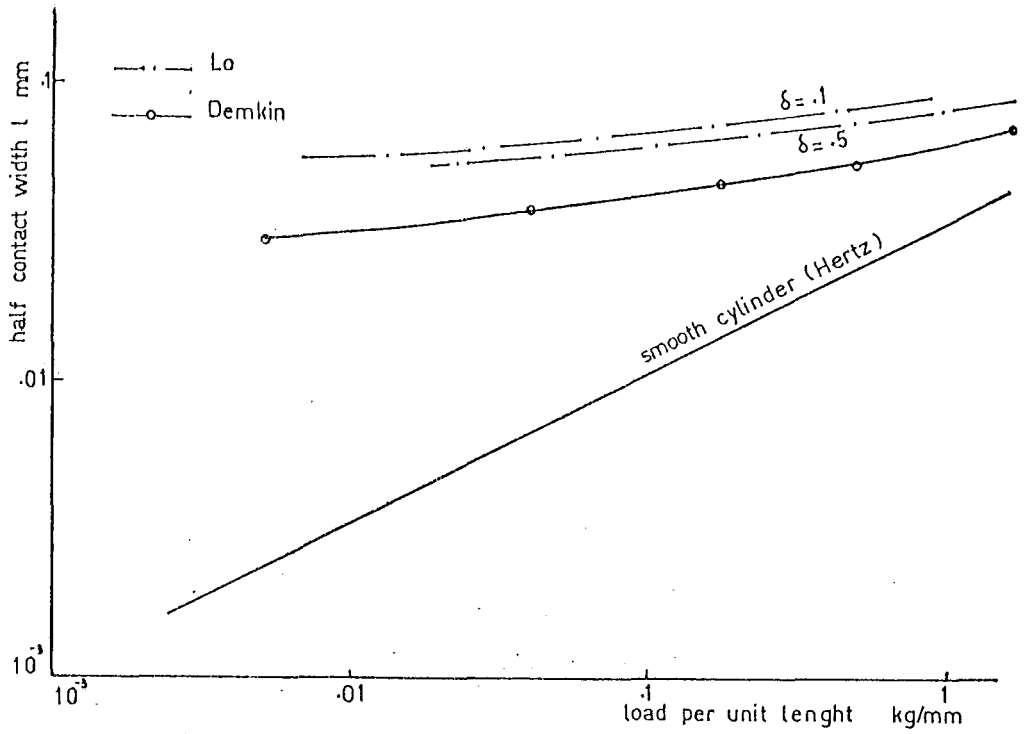

CYLINDER RADIUS=10.00MM LENGTH=20.00MM
ROUGHNESS CONSTANT D= .00000750 FRI=3.5 RM=.0010MM

TOTALDEF IS THE APPROACH OF 2 PLANES AT SECTION X= .00MM

LOAD KG/MM	BETA	WIDTH MM	WHOLEDEF MICRON	LOCALDEF MICRON	ROUGHDEF MICRON	TOTALDEF MICRON
.0005	3.4953	.0237	.0063	.0051	.0458	.0472
.0050	3.4740	.0316	.0132	.0089	.0832	.0973
.0500	3.3593	.0421	.0335	.0893	.1474	.1871
.2500	3.0752	.0510	.1474	.0434	.2137	.4116
.5000	2.8499	.0548	.2910	.0893	.2590	.6392
1.0000	2.5373	.0510	.5784	.1741	.3022	1.0457
1.5000	2.2975	.0718	.8292	.2555	.3204	1.4051
2.5000	1.9732	.0858	1.3341	.4120	.3458	2.0929

Fig. 6.11 Top: The case of elastic deformation of the asperities of a rough cylinder compressed between two planes.
Bottom: The results of Demkin's example solved by our method.

respectively, g is the asperity density, and σ the standard deviation of the normal distribution.

Fig.6.11 also shows the Lo's half width versus loading for $\delta = .1$ and .5 and the Hertz's half width of contact area of a smooth cylinder in contact with a plane.

The difference between Lo's and Demkin's half widths is about 50%. This may be due to the different approach to the problem. All these curves show a much larger contact width at very low loading than that given by Hertz's curve. At high loadings the curves converge.

6.5 APPARATUS AND EXPERIMENTS

All test pieces were made of steel, cylindrical in shape and rough turned with varying degrees of roughness. All the dimensions and the properties of work-pieces are shown in Table 6.1. The surface profiles of the work-pieces were traced by the Talysurf 8 (Fig.6.12) available in our Department. Typical profiles are shown in Fig.6.14. The no-load bearing curve and supposed deformed bearing curve $\eta = 5.66\rho^{2.5}$ are drawn superimposed on the profiles. Up to a maximum of 5 micron CLA (centre-line average) surface can be read directly on the scale of the machine. In our calculation the peak-valley height is employed while the CLA is given as a reference. The cylindrical test pieces were compressed between two 1.5" thick, flat plates made of case hardening steel Bohler EPB 100 (Fig.6.13). The heat treatment process for the plates comprised carburising at 900°C, oil quenched at 830°C then tempered at 180°C. The surfaces were finally lapped to .25 to .5 micron CLA, average peak-valley height is about 1.8 micron. After a few trial tests the asperities of the two flat plates at the contact areas with the cylinder deform plastically to almost half of the peak-valley height value. Later tests should not make the asperities

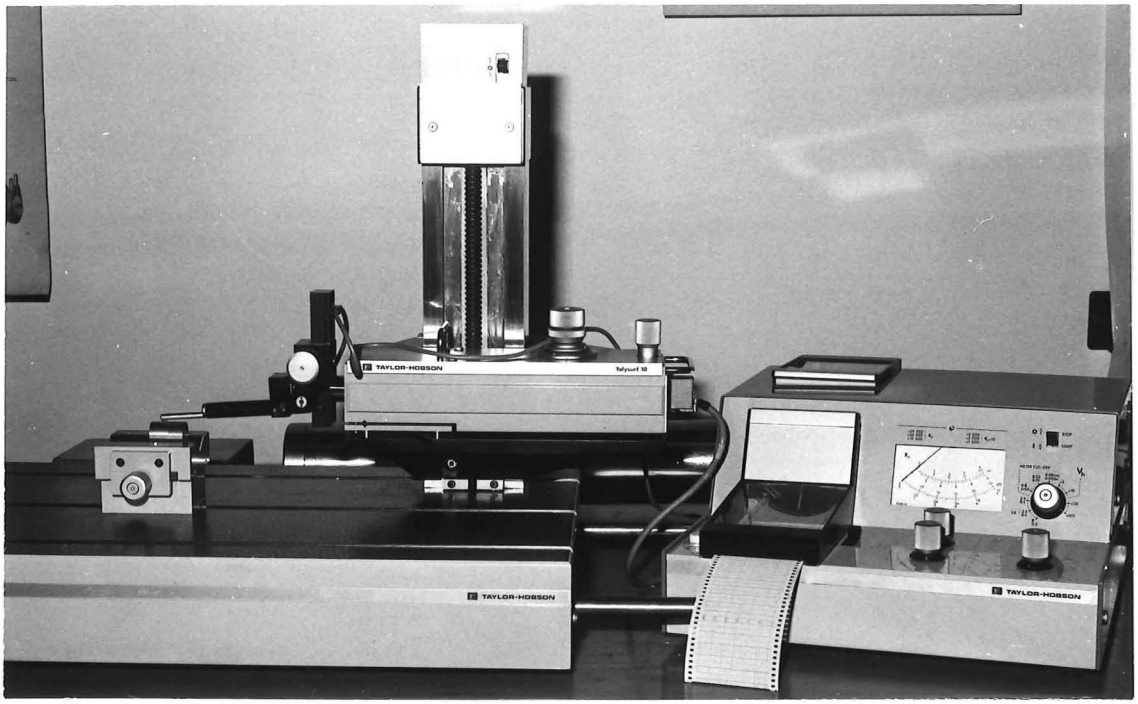

Fig. 6.12 The Talysurf 8 : The surface profile recorder.

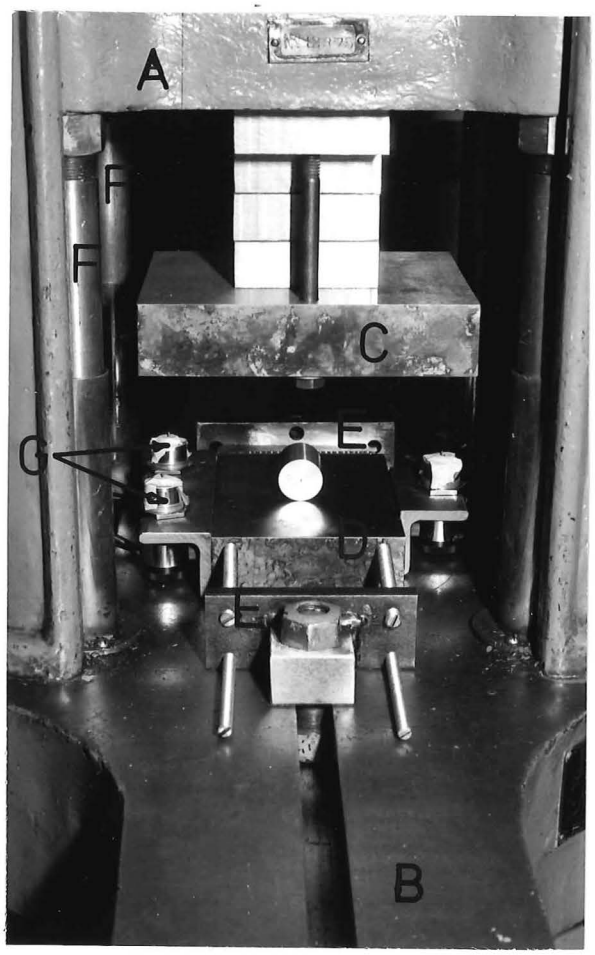

Fig. 6.13 Designed apparatus for the compression test.

Fig. 6.14 Surface profiles, no-load and assumed deformed bearing curves.

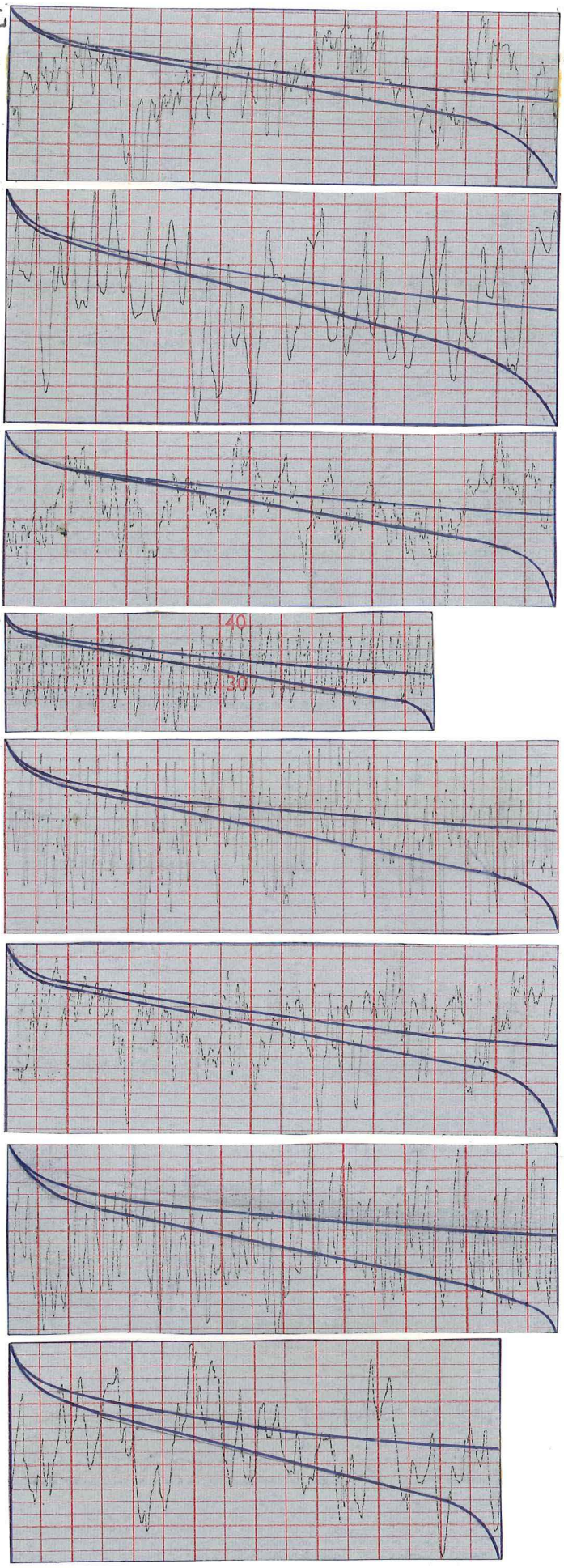

VERTICAL SCALE	WORK-PIECE	VERTICAL MAG.	HORIZONTAL MAG.
1mm= 1μ	1A	V_v=10000	V_h=100
1mm=10μ	1B	V_v=1000	V_h=20
1mm= 1μ	2A	V_v=10000	V_h=100
1mm= 5μ	2B	V_v=2000	V_h=20
1mm= 5μ	2C	V_v=2000	V_h=20
1mm= 1μ	3A	V_v=10000	V_h=100
1mm= 5μ	3B	V_v=2000	V_h=20
1mm=10μ	3C	V_v=1000	V_h=20

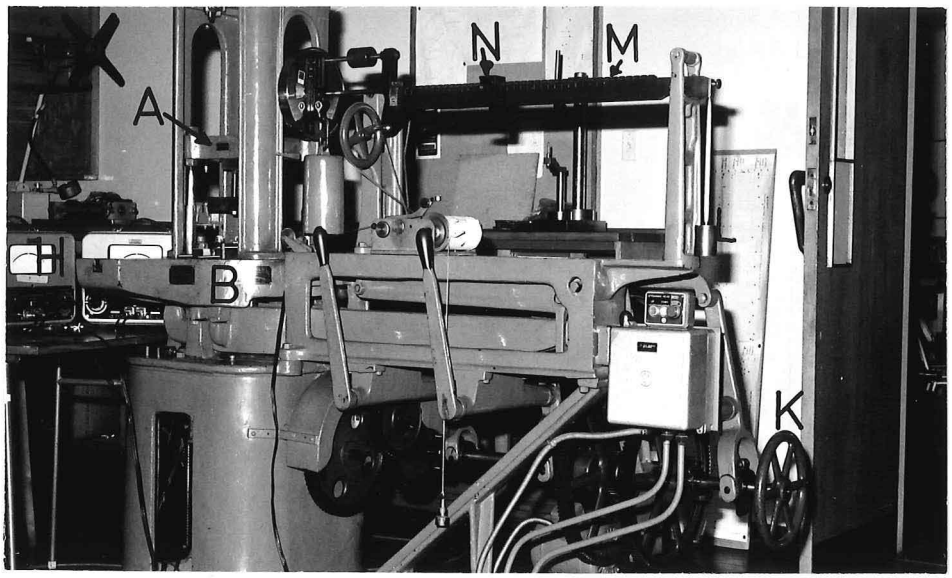

Fig. 6.15 The 30000 lbs Tinius Olsen testing machine.

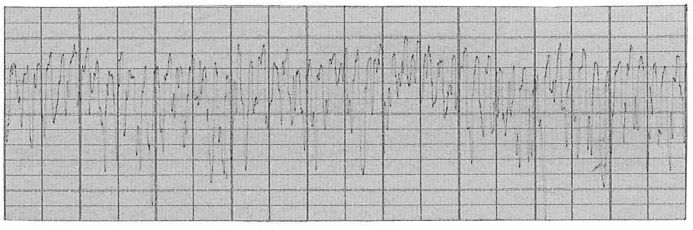

Fig. 6.16 The surface profile of workpiece 2C at load 3000 lbs. The Peak-valley height is only 9.5 microns.

deform further; it was therefore assumed that the flat surfaces were perfectly smooth. Hardness tests indicated that the surfaces of the plates in contact with the cylinder were between 55 - 61 Rockwell C. Fig.6.15 shows the 30,000 lbs TINIUS OLSEN testing machine employed for the experiment. This machine was preferred to the Avery testing machine used previously due to its greater accuracy of the movement of the top platten A during compression. The bottom flat plate D lies in the middle of the bottom platten B of the machine, it is restrained from moving sideways by two locators E bolted rigidly to the bottom platten and located on the two sides of the bottom flat plate. The top flat plate C is bolted to the top platten A, since the minimum clearance between two plattens was too big, we had to insert a few spacing blocks in between the top platten and the top plate. These blocks were also finely ground to ensure good contact. The top platten was supported by four 1" diameter studs at its corners. They were supported in such a way that the top platten was able to move up and down without rotation of the studs. A most useful feature of this machine was that the inclination of the top platten may be adjusted easily. In practice, the two end diameters of a cylinder were never perfectly equal to each other but different by a few ten of microns. However, uniform loading along the axis of the cylinder could be achieved by adjusting the inclination of the top platten until the top surface of the cylinder was parallel to the top flat place C. Easy observation of this parallelism was achieved by viewing the gap against an illuminated background (Fig.6.17).

To measure the approach of the flat plates during loading, three Phillips pick-ups G(PR 9310) were attached rigidly to the flanges bolted to the bottom plate. Their positions are shown in Fig.6.17. These were preferred to the mechanical dial gauges used previously in the indentation tests in Chapter 2, due to their size. Readings of the displacements of the pick-ups were transmitted to the three Phillips bridges H(PR 9300)

Material	EN 25 Tempered at 600° Cooled in oven		EN 25 Tempered at 800° Cooled in oven			Black Commercial steel NZ SS 3402/1973/275		
Brinell Hardness kg/mm^2	272		202			140		
Work-piece	1A	1B	2A	2B	2C	3A	3B	3C
Diameter (mm)	24	25	25	25	25	23	23	24
Length (mm)	30	30.	32	32	32	30	30	30
Peak-valley height R_m (micron)	2.6	38	2.6	9	15	3.0	16	34
CLA (micron)	.37	*	.37	1.3	2.4	.43	3.0	*

TABLE 6.1 Dimensions and Properties of Work-Pieces

* outside the range measurable by the Talysurf 8.

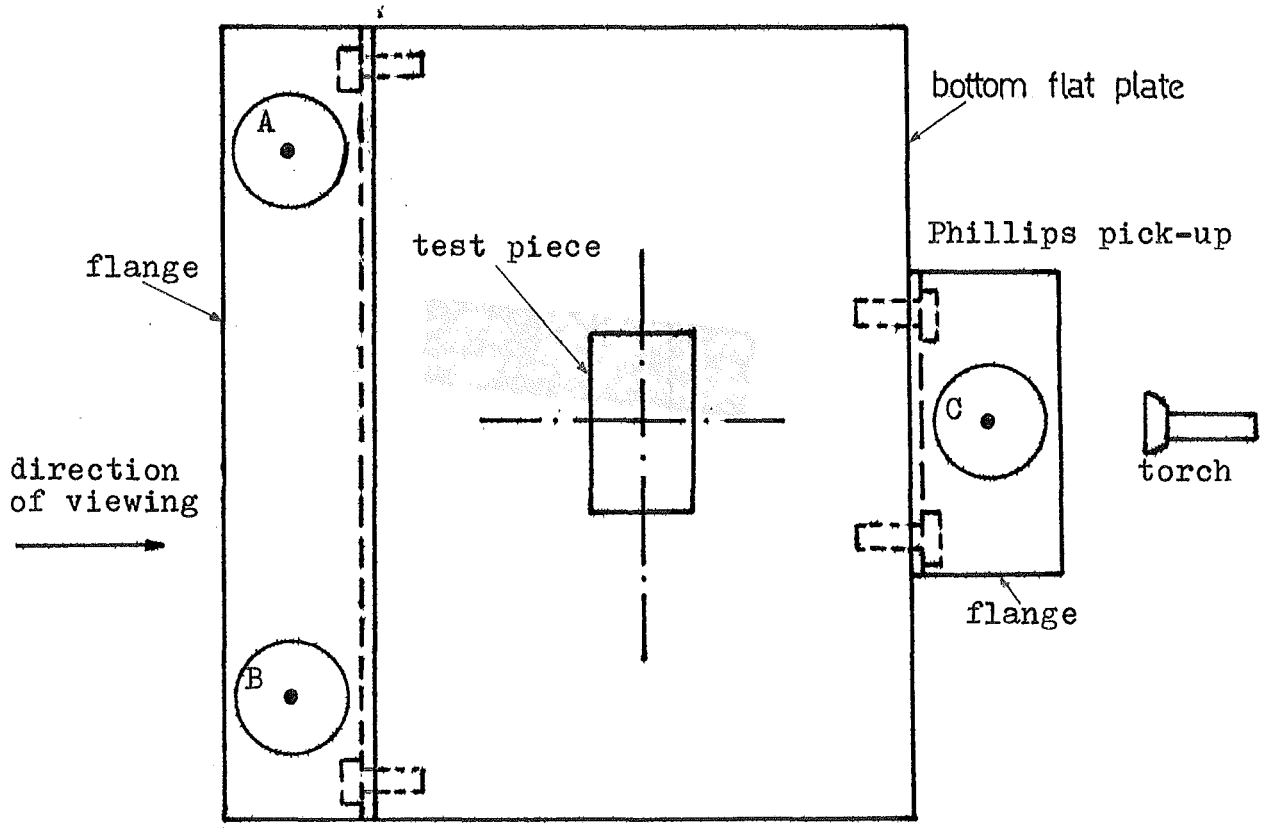

Fig. 6.17 Plane view of the bottom flate plane.

Fig.6.15. The scale of resolution of 1 micron was used. Calibration tests with the standard slip gauges showed that the bridges over-recorded the actual displacements of approximately 3% which is within the accuracy claimed by the manufacturer. The positions of the pick-ups shown in Fig. 6.16 indicate that the displacement of the top flat plate may be calculated as $\frac{1}{4}$ (A + B) + $\frac{1}{2}$C, where A, B and C are readings on these bridges. Ideally it may be possible to record displacements at any load, but imperfect conditions in the experiment such as the back lash movement of the four studs supporting the top platten causes uncertainty in determining the zero load position of the top platten making unreliable readings of the displacements of the top platten for loads under 100 lbs. Therefore, it was decided to record the displacements for loads greater than 100 lbs relative to the position of the top platten at 100 lbs. The machine may be driven either by an electric motor or manually by rotating the wheel K. The latter way is found more convenient for these tests. It may be operated as follows: by changing the weight L at the end of the lever M we can change the maximum loading scale from 3000 lbs to 30,000 lbs. To increase the load to a certain value, slide the block N to this value, this will lower the lever M. To balance, bring the lever M to its neutral position by turning the wheel K anticlockwise and read off the displacements recorded on the bridges. The load was increased in steps of 300 lbs to a maximum of 3000 lbs. Plastic deformation of the asperities leaves two narrow bands of indentation on the cylinder, the width of these bands were magnified to 20 times and measured by the Nikkon shadowgraph available in the metrology laboratory.

It was noted that the surface profile of a work-piece was slightly different at different positions. The given value of R_m in Table 6.1 is the average of a number of R_m values at different positions. The experimental results for the total approach of the two planes plotted in Figs. 6.18

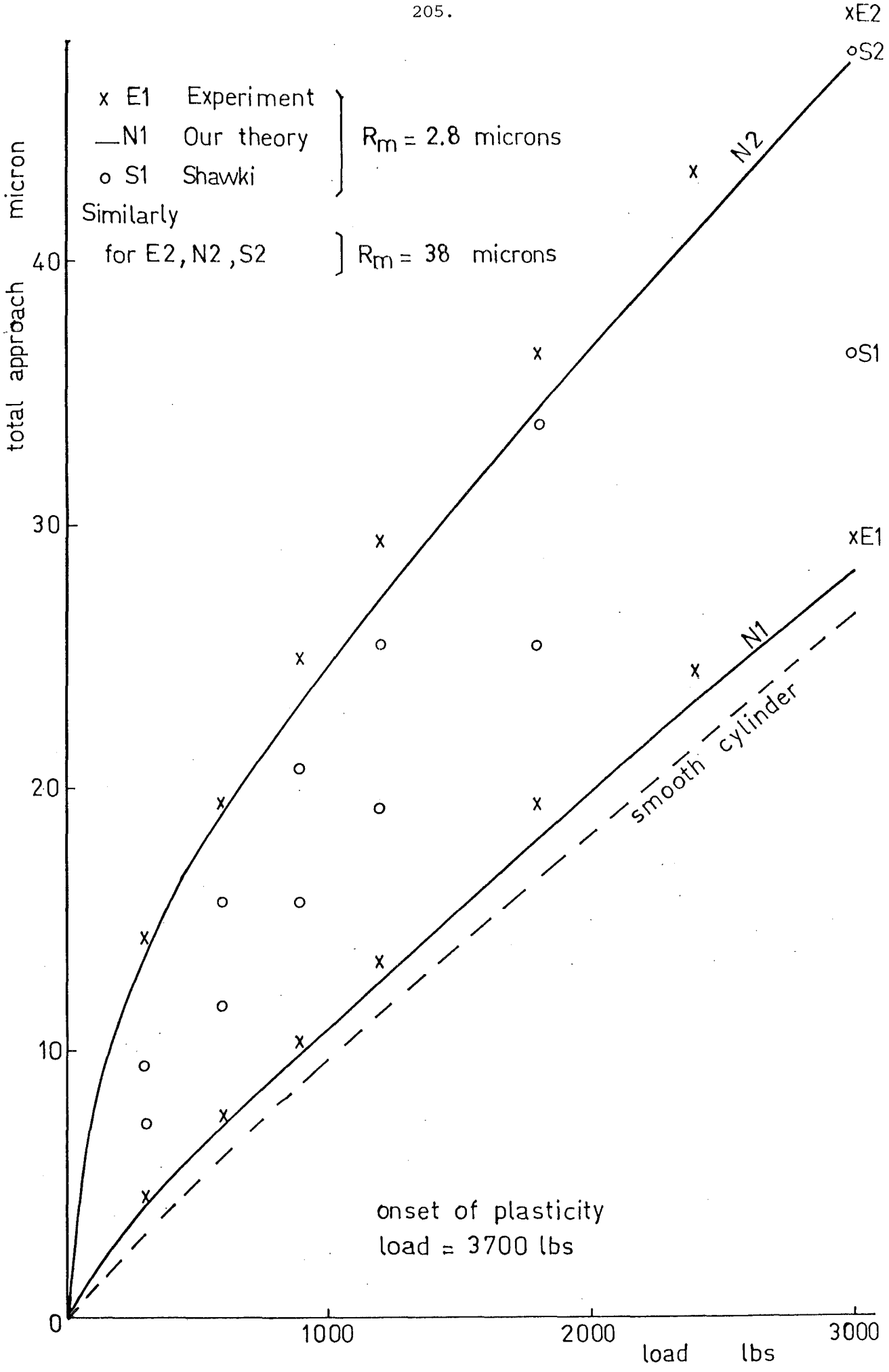

Fig. 6.18 The case of rough cylinders 1A and 1B.

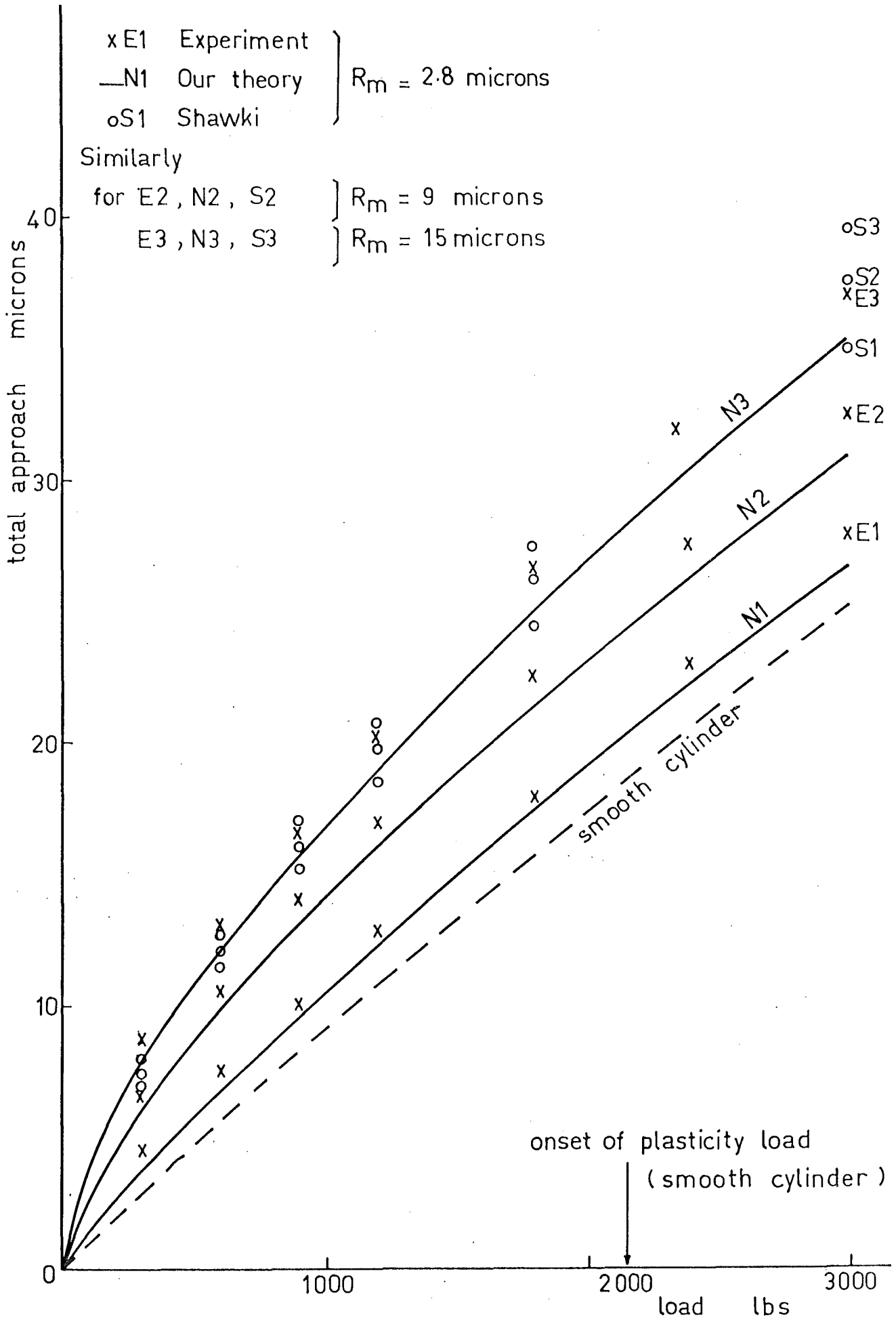

Fig. 6.19 The case of rough cylinders 2A, 2B and 2C.

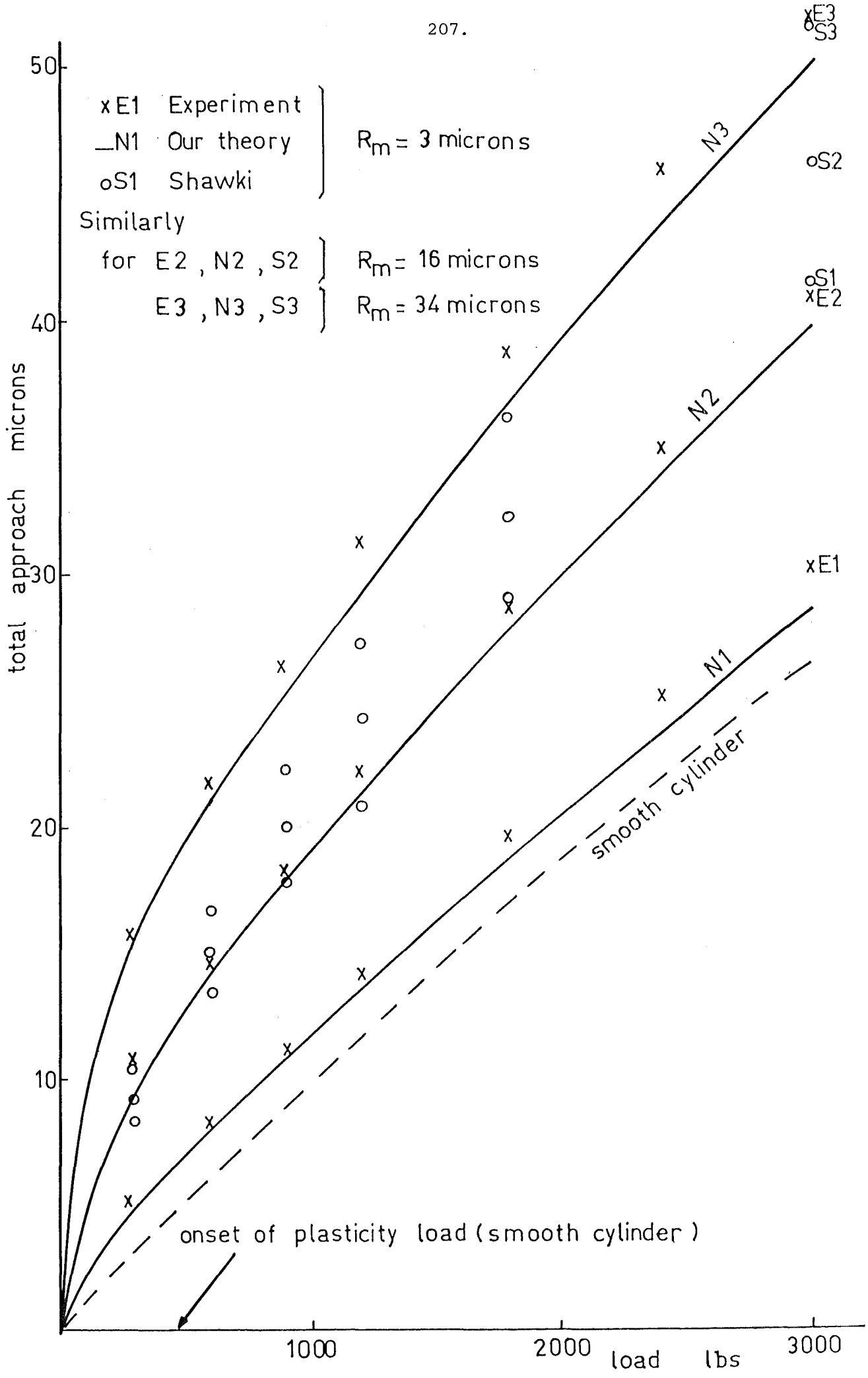

Fig. 6.20 The case of rough cylinders 3A,3B and 3C.

6.19 and 6.20 are also the average values of the compression tests for different positions of the cylinder. Our theoretical prediction for the total approach is also plotted on these figures to compare with the experimental results. Shawki's formula for the total approach of two Vee locators compressing a rough cylinder was also calculated and plotted as well as the total approach of two flat planes compressing a smooth cylinder. All the calculations leading to the approach of the two planes predicted by our method, Shawki's formula and the case of smooth cylinder were performed in program NHAM3 (Appendix 6.3)

6.6 DISCUSSION

Generally our theoretical values follow the experimental results closely; in all cases the latter is always slightly higher. This may be due to the difficulty of adjusting the inclination of the top flat surface to compress perfectly evenly along the length of the cylinder. Shawki's formula shows better agreement with the very rough cylinders than with the almost smooth ones.

The condition of the onset of plasticity of the bulk material supporting the asperities is unknown at the present time. However, we can take the load at which a smooth cylinder compressed between two hard planes starts deforming plastically as a reference. The stresses inside one solid in contact with another have been investigated by Thomas and Hoersch[100]. For the case of a hard smooth steel cylinder and a smooth steel plane in contact, the maximum shear stress τ_m was found to be at depth $.786\ell$ below the surface of the plane where ℓ is the half width of the contact band. For E = 21200 kg/mm^2 (i.e. 30 x 10^6 psi) and μ = .25

$$\tau_m = 25.42\ (p/D)^{.5}\ kg/mm^2$$

where p is the load per unit length ($= \frac{W}{2L}$) in kg/mm, D and 2L are the

diameter and the length of the cylinder respectively in mm. Similarly, for the case in which the cylinder is softer, the same value of maximum shear stress occurs at .786ℓ below the surface of the cylinder. Apply the maximum shear stress theory of failure

$$\tau_m = Y/2$$

where Y is the yield stress of the cylinder in kg/mm^2. Substitute into Equation 6.59 to get the maximum possible applied load on the cylinder for elastic deformation

$$W_{max} = 7.74 \times 10^{-4}\ DLY^2\ kg$$

The value of W_{max} for our work-pieces may be seen in Table 6.2. It is obvious that the width of contact area increases as the roughness of the cylinder increases, i.e., the mean pressure across the contact band decreases; in effect the load required for plastic flow of the bulk material supporting the asperities must increase. The value W_{max} given in Table 6.2 is therefore the minimum load at which our work-pieces may deform plastically. Yield stress of the steel EN25 was given in BS 970 Part II. Before tempering the minimum yield stress given in the standard is between $\frac{1}{4}$ to $\frac{1}{3}$ of its hardness. Our work-pieces are made of EN25 steel tempered to 600^{o}C and 800^{o}C. The yield stresses are not given in the Standard and therefore it may be assumed that the Yield stress is equal to $\frac{1}{3.5}$ of its corresponding hardness. The yield stress of the black commercial steel is obtained directly from the NZ 3402/1973/275. The value of the width of the contact area measured from the Nikkon shadowgraph is compared with the theoretical value (obtained from Appendix 6.3) in Table 6.2. The error is below ±10% at a load of 3000 lbs. The contact width is not perfectly the same along the length of the cylinder due to surface irregularities and the uneven loading along the length of the cylinder. The actual contact width listed in Table 6.2 is the

Workpiece		1A	1B	2A	2B	2C	3A	3B	3C
Hardness (kg/mm^2)		272		202			140		
Yield stress (kg/mm^2)		77.7		57.7			28		
W_{max} (lbs)		3706	3860	2271	2271	2271	461	461	461
2l (mm) at 3000 lbs	Experiment	.62	1.06	.56	.72	.81	.70	.90	1.14
	Theory	.57	1.16	.59	.78	.82	.64	.85	1.22
	Smooth cylinder	.48	.49	.48	.48	.48	.47	.47	.48
2l (mm) at 1200 lbs	Experiment						.50	.69	.98
	Theory						.47	.75	1.06
	Smooth cylinder						.30	.30	.31

Table 6.2 Actual contact width 2l is compared with our theoretical values. The case of smooth cylinder is also given.

average of a few readings along the length of the cylinder. Maximum and minimum readings may be within ±10% of the average value. Since the work-pieces 3A, 3B and 3C reach plasticity earlier than the others, extra experiments to measure the width of the contact area at a load of 1200 lbs were made and the results compared with the predicted theoretical values. It may be seen that at low loads, the contact width of a rough cylinder and a plane may be 3 - 5 times the contact width of a smooth cylinder and a plane, as the load increases the ratio decreases steadily. The ratio increases with the increase of the roughness of the cylinder, hence the actual onset-of-plasticity load for a rough cylinder increases with the roughness.

It is emphasised that our theory ceases to be valid when either the bulk material supporting the asperities starts deforming plastically (assumption 6.3.i) or the asperities deform to greater than approximately .4 of their peak-valley height R_m (assumption made for the establishment of Equation 6.9). However, these two conditions are somewhat interrelated, calculation of the deformation of the asperities at one contact zone ($= \frac{1}{2}$ ROUGH DEF in Appendix 6.3) shows that the onset of plasticity of the cylinder may have been reached before the asperities are deformed up to .4 of their peak-valley height - see for instance, work-pieces 3A, 3B and 3C.

Theoretical calculations of the deformation of the asperities of work-piece 2C(appendix 6.3) indicates that at a load of 3000 lbs, the asperities are deformed 5.5 microns ($= \frac{1}{2}$ ROUGH DEF) from the highest peak. Initially the peak-valley height of this work-piece is 15 microns; therefore the theoretical peak-valley height of the deformed surface is 9.5 microns. It is in agreement with the recorded profile obtained from the Talysurf (Fig.6.16).

Generally the theory may also be used to predict the approach of the two planes up to the load such that the deformation of the asperities reaches

.4 of its peak-valley height with little error (maximum possible ±10%). As the load increases, the value of β decreases slowly until it is less than .5 + .12 (2ϕ - 1.5), our method may yield high errors in the values of β, ℓ and Δ. In some cases the onset of plasticity of the work-piece may have been reached before the asperities deform to .4 of its peak-valley height; our method may still be used since the bulk material starts deforming plastically from one point and expands steadily throughout the whole body. It does not affect the trend of the deformation so abruptly as to cause a large error in our prediction.

The same results of the half width of contact area and the total approach of the two planes obtained above may also be applied for the case of a long smooth cylinder in contact with two rough planes at the ends of a diameter of the cylinder provided the asperities on the planes are of a wedge shape.

Our calculation assumed the two flat planes as two elastic half spaces. In 1975, a formula for the total approach of two finite thickness smooth platens compressing a smooth roller was derived by Nikpur[67]. For C/L = 2.5, which was the value used in our experiment where C is the thickness of the platen and L half the length of the roller, his formula is approximately 8% less than that of Lundberg[62] (Equation 6.56) which assumed that the two platens were elastic half spaces. However, for the case of C/L > 2, Nikpur recommended that Lundberg's formula is more appropriate and in general, it is simpler than Nikpur's formula.

CHAPTER 7

CONCLUSION AND RECOMMENDATION

7.1 CONCLUSION

The contact rigidity of the fixture work-piece systems plays a very important role in the dimensional accuracy of the product. The behaviour of the bodies in contact was studied. In particular, three common types of the locating elements of the fixture, spherical, flat and Vee locators, were considered. For each case a mathematical formula was derived for the deformation of the system due to static loadings.

For the case of a spherical locator in contact with a flat work-piece, the latter deforms plastically so readily that for common loadings it has two components of deformation: elastic and plastic. The elastic recovery behaviour of the metals enabled us to determine the elastic component of the deformation by the theory of elasticity. Apart from Young's modulii of the locator and the work-piece, the hardness and the Meyer constant of the work-piece were also important for the analysis. Our method predicted the experimental deformations very well.

For the contact between a flat locator and a flat work-piece of given roughness and hardness, the theory of Williamson may be used to evaluate the plastic deformation of the asperities while the theory of elasticity is used to evaluate the elastic deformation of the bulk material supporting the asperities.

The pressure distribution across the contact zone of a rough cylinder in contact with a semi-infinite plate was assumed to be of elliptic-paraboloidal shape rather than the elliptical shape obtained when the cylinder is smooth. The general formula for the compression of a long rough cylinder by two narrow bands of elliptic-paraboloidal shape was derived and checked with the folumae for special cases derived by

Lundberg and Föppl. The iteration method proposed by Greenwood[38] to evaluate the deformation of a rough surface in contact with a sphere is found to be very tedious and complicated. Using the same approach Lo[60] extended to the case of the elastic contact of two rough cylinders. To reduce the complexity of the iteration process he assumed that the pressure distribution at the contact zone is of bell shape $q = q_o (1 - \frac{y^2}{\ell^2})^2$ i.e. $\beta = 2$. This assumption might not be completely satisfied since β is dependent on the loading on the cylinders. As the loading increases, β decreases to $\frac{1}{2}$. At low loads, the contact width of a rough cylinder and a plane may be 4 to 5 times that of a smooth cylinder in contact with a plane. However, for high loads, the latter case may be slightly smaller than the former. Experimental results showed that the theoretical prediction for the approach of the two planes compressing a rough cylinder was within ±10% error. The asperities deform plastically while the material supporting them deforms elastically.

For the three types of contact, the experiments showed that the deformation of the bodies at contact were non-linear relationship with the loading.

Higher contact rigidity in a fixture may be obtained with increased work-piece hardness, better surface finishes and a larger area of contact. Higher values for the radius of curvature of the spherical locators also lead to increased contact rigidity at locating zones.

7.2 RECOMMENDATION FOR FUTURE WORK

Our investigation presented the basic contacts under normal static loadings. Under dynamic loadings: normal, tangential as well as rotational forces may act on the mating surfaces. It will, therefore, be very important in the future that the contact rigidity of this case be studied.

The stresses inside a smooth cylinder in contact with a plane obtained

by Thomas and Hoersch are not applicable for the case of a rough cylinder in contact with a smooth plane or of a smooth cylinder with a rough plane. The mathematical analysis of these stresses, when accomplished, will provide the load at which a point inside those bodies deforms plastically, and should be investigated in the future.

A study should be made of the approach of two hard planes compressing a rough cylinder of different modulus of elasticity and a study should be made of the effect of the interfacial friction on the total deformation of a system comprised of a rough cylinder compressed between two platens of finite thickness.

REFERENCES

1. ABBOTT, E.J., FIRESTONE, F.A. Specifying surface quality Mech. Eng. 55 (1933) pp. 569-572.

2. ABRAMOWITZ, M., STEGUN, I.A. Handbook of mathematical functions Dover Publication 1965.

3. ALLAN, R.K. Rolling bearing 2nd and 3rd edns. Pittman and Sons Ltd, 1945 and 1964.

4. AMSTRONG, R.W., ROBINSON W.H. Combined elastic and plastic deformation behaviour from a continuous indentation hardness test. N.Z. Jour. Sci. vol.17 (1974) pp 429-433.

5. ARCHARD, J.F. Elastic deformation and the law of friction. Proc. Royl Soc. London A243 (1957) pp 190-205.

6. ARCHARD, J.F., WHITEHOUSE, D.J. The properties of random surfaces of significance in their contact. Proc.Roy. Soc. London A 315 (1970) pp 97-121.

7. ATKINS, A.G., FELBECK, D.K. Mutual indentation hardness in service failure analysis. C.M.E. June 1974 pp 78-83.

8. BAKER T., RUSSEL, T.F. Note on the ball test. J. Iron and Steel No.1 (1920) pp 341-356.

9. BUSH A.W., GIBSON, R.D. The elastic contact of a rough surface Wear 35 (1975) pp 87-111.

10. BISHOP R.F., HILL, R., MOTT, N.F. The theory of indentation and hardness tests. Proc. Phy. Soc. vol.57 (1945) pp 147-159.

11. CHILDS, T.H.C. The persistence of asperities in indentation experiments, Wear 25 (1973) pp 3-16.

12. CONNOLLY R., SCHOFIELD, R.E., THORNLEY, R.H. The approach of machined surfaces with particular reference to their hardness. Proc. 8th Int. Mach. Tool Des. Res. Part II (1967) pp 759-776.

13. CONWAY, H.D., ENGEL, P.A. Contact stresses in slabs due to rough indenters. Int. J. Mech. Sci. vol.11 (1969) pp 709-722.

14. DAKSHINA MURTHY H.B., RAGHAVAN, M.R. Compliance of rough cylinder in compression. Wear 20 (1972) pp 353-369.

15. DAKSHINA MURTHY, H.B., RAGHAVAN, M.R. The real area of contact and compliance of rough cylinders in compression. Wear 27 (1974) pp 47-60.

16. DAVIES, R.M. The determination of static and dynamic stresses using a steel ball. Proc. Roy. Soc. A197 (1949) pp 416-432.

17. DE PATER , A.D., KALKER, J.J. The mechanics of the contact between deformable bodies. Delft Univ. Press 1975.

18. DEMKIN, N.B., KRAGELSKY, I.V. Contact area of rough surfaces. Wear, Vol.3 (1960) pp 170-187.

19. DEMKIN, N.B. Contact between rough surfaces. Nauka Moscow (1970) In Russian.

20. DEMKIN, N.B., RUDZIT, Y.A. Surface microgeometry indicates friction and wear processes. Russian Eng. vol.51 No.8 (1971) pp 44-46.

21. DEMKIN N.B. *et al*. Evaluating roughness and waviness in calculating the effect between machine components, Vol.55 No.8 (1975) pp 28-30.

22. DEMKIN, N.B. IZMAILOF, V.V. Plastic contact under high normal pressure. Wear 31 (1975) pp 391-402.

23. DEMKIN, N.B., IZMAILOV, V.V., KOROTKOV, M.A. Estimation of the deformation of rough spheres and cylinders in compression. Wear 39 (1976) pp 63-82

24. DOWSON, D, HIGGINSON, G.R. Theory of roller bearing lubrication and deformation. Proc. Lubrication and Wear Convention, Inst. Mech. Eng. London (1963) Paper 19, pp 216-227.

25. ENGEL, P.A., CONWAY, H.D. Contact stress analysis for an elastic cylinder indenting a slab in the presence of friction. Int. J. Mech. Sci., vol.13 (1971) pp 391-402.

26 ETON STATISTICAL & MATH. TABLES. Eton Press, Christchurch, New Zealand.

27. FÖPPL, A. Techmische Mechanik 4th Ed. (1907) pp 319-355.

28. FOSS, F.E., BRUMFIELD, R.C. Some measurements of the shape of Brinell ball indentation. Proc. ASTM vol.22 (1922) pp 312-334.

29. GLADWELL, G.M.L. The contact problem for a rigid cylinder pressed between two elastic layers. Jour. Appl. Mech. vol.44 (1977) pp 36-40.

30. GOODELLE, R.A., DERNER, W.J., ROOT, L.E. A practical method for determining contact stresses in elastically loaded line contact. Trans ASLE vol.13 (1970) pp 269-297.

31. GOODMAN, J. The approach of flat elastic plates under load when separated by a ball of similar material. Engineering vol.116 (1923)pp 133 .

32. GOODMAN, J. Contact area of an elastic sphere when compressed between flat elastic plates. Engineering vol.116 (1923) pp 244-245.

33. GOODMAN, L.E. Contact stress analysis of normally loaded sphere. J. Appl. Mech. vol.29 (1962) pp 515-522.

34. GRADSHTEYN, I.S. RYZHIK, I.M. Table of integrals - series and Products. Academic Press, New York 1965.

35. GREENWOOD, J.A., ROWE, G.W. Deformation of surface asperities during bulk plastic flow. J. Appl. Phys. 36 (1965) pp 667-668.

36. GREENWOOD, J.A., WILLIAMSON, J.B.P. Contact of nominally flat surfaces. Proc. Roy. Soc. London A295 (1966) pp 300-319.

37. GREENWOOD, J.A. The area of contact between rough surfaces and flats. Trans ASME F89 (1967) pp 81-91.

38. GREENWOOD, J.A., TRIPP, J.H. The elastic contact of rough spheres. J. Appl. Mech. vol.89 (1967) pp 153-159.

39. GREENWOOD, J.A., TRIPP, J.H. The contact of two nominal flat rough surfaces. Proc. Instn Mech. Engrs (1970-71) pp 625-633.

40. GRÖBNER, W, HOFREITER, N. Integratafel,Teil II, Bestimmte Integrale. Springer-Verlag, Wien & Innsbruck 1958.

41. HALLING, J., NURI, K.A. Contact of rough surfaces of work-hardening material. Proc. IUTAM Symposium on the mechanics of contact between deformable bodies. Delft Univ. Press, 1975.

42. HILL, R. Plasticity, Oxford 1950.

43. HISAKADO, T., TSUKIZOE, T. On the mechanism of contact between metal surfaces. The penetrating depth and the average clearance, Part I. Trans ASME D87 (1965) pp 666-674.
The real area and the number of contact points, Part II.
Trans ASME F90 (1968) pp 81-88.

44. HISAKADO, T., TSUKIZOE, T. Effect of surface roughness on contact between solid surfaces. Wear 28 (1974) pp 217-234.

45. HISAKADO, T., TSUKIZOE, T. Effect of distribution of surface slopes and flow pressures of contact asperities on contact between solid surfaces. Wear 30 (1974) pp 213-227.

46. HISAKADO, T. Surface roughness and deformation of contact asperities between a rough and a flat surface. Wear 35 (1975) pp 53-61.

47. HISAKADO, T. Influence of surface roughness and work-hardened layers on the contact between a rough and a flat surface. Wear 37 (1976) pp. 41-51.

48. ISHLINGSKY, A.J. English translation published by Ministry of Supply ARD (1947). Theoretical Research Translation No.2/47.

49. JOHNSON, K.L. The correlation of indenation experiments.
J. Mech. Phys. Solids. vol.18 (1970) pp 119-125.

50. JOHNSON, K.L. Contact pressures: a fundamental experiment in tribology. Bull. Mech. Eng. Edu. vol.6 pp 245-250.

51. JOHNSON, W., MELLOR, P.B. Engineering plasticity. Van Nostrand Reinhold, London, 1973.

52. KALKER, J.J. On elastic line contact. J. Appl. Mech. vol.39 (1977) pp 1125-1132.

53. KOENIGSBERGER, F. TLUSTY, J. Machine Tool Structure, Pergamon Press 1970.

54. KORRENN, V.H., KIRCHNER, W., BRAUNE, G. The elastic deformation of a plane steel plate (in German) Werkstattstechnik 53 (1963) pp 27-30.

55. LEE, C.H., KOBAYASHI, S. Elastoplastic analysis of plane strain and axisymmetric flat punch indentation by the finite element method. Int. J. Mech. Sci., vol.12 (1970) pp 349-370.

56. LEE, C.H., MASAKI, S., KOBAYASHI, S. Analysis of ball indentation. Int. J. Mech. Sci., vol.14 (1972) pp 417-426.

57. LEVINA, Z.M., RESHETOV Machine design for contact stiffness. Russian Eng. vol. 45, No.12 (1965) pp 15-23.

58. LING, F.F. On asperity distributions of metal surfaces. J. Appl. Phys. vol.29 (1958) pp 1168-1174.

59. LOO, T.T., TROY, N.Y. Effect of curvature on the Hertz theory for two circular cylinders in contact. J. Appl. Mech. vol 25 (1958) pp 122-124.

60. LO, C.C. Elastic contact of rough cylinders. In. J. Mech. Sci. vol.11 (1969) pp 105-115.

61. LUNDBERG, G. Elastic contact of two half spaces. Forschung (1939) pp 201, 211.

62. LUNDBERG, G. Cylinder compressed between two plane bodies. Published by SKF Göteborg 1949, 7 pages.

63. LUNDBERG, G., SJÖVALL, H. Stress and deformation in elastic contacts. Inst. Theory of Elas. & Strength of Mat. Chalmers Univ. Tech. Gothenburg 1958.

64. MIKIC, B.B. ROCA, R.T. A solution to the contact of two rough spherical surfaces. J. Appl. Mech. vol.41 (1974) pp 801-803.

65. MORRISON, H.L., RICHMOND, O. Large deformation of notched perfectly plastic tensile bars. J. Appl.Mech. vol.39 (1972) pp 971-977.

66. MOORE, A.J.W. Deformation of metals in static and sliding contact. Proc. Roy.Soc. London, A195 (1948) pp 231-243.

67. NIKPUR, K., GOHAR, R. Deflexion of a roller compressed between platens. Tribology vol.8, (1975) pp 2-8.

68. NORBURY, A.L., SAMUEL, T. (a) Experiment on the Brinell-Tensile relationship J. Iron & Steel Inst. No.1 (1924) pp 497-491.
(b) The Brinell Test J. Iron & Steel Inst. No.1 (1928) pp 673-687.

69. NURI, K.A. The normal approach between curved surfaces in contact. Wear 30 (1974) pp 321-335.

70. NURI, K.A., HALLING, J. The normal approach between rough flat surfaces in contact. Wear 32 (1975) pp 81-93.

71. NURI, K.A., HALLING, J. The effect of the size of the nominal area on the contact behaviour of surfaces. Wear 37 (1976) pp 77-86.

72. O'CALLAGHAN, P.W., PROBERT, S.D. Effects of static loading on surface parameters. Wear 24 (1973) pp 133-145.

73. O'CALLAGHAN, M., CAMERON, M.A. Static contact under load between nominally flat surfaces on which deformation is purely elastic. Wear 36 (1976) pp 79-97.

74. OLSEN, K.V. On the standardization of surface roughness measurements. Bruel & Kjaer Tech. Review No.3 1951.

75. O'NEILL, H. The variation of Brinell hardness number with testing load. Proc. Iron & Steel Inst. No.I (1923) pp 343-375.

76. O'NEILL, H. A new method of making ball hardness tests of metal. Carnegie Schol. Memoirs I.S.I. vol.19 (1930) pp 19-38.

77. O'NEILL, H. The significance of Tensile and other mechanical test properties of metals. P. Inst. Mech. Engrs, vol.151 (1944) pp 116-130.

78. O'NEILL, H. Hardness measurement of Metals and Alloys. Chapman & Hall Ltd, 2nd ed. (1967)

79. PALMGREN, A. Ball and Roller bearing engineering. SKF Industry 2nd ed. (1945).

80. PRESCOTT, J. Applied Elasticity. Dover Publications Inc. N.Y. (1961).

81. PUTTOCK, M.J., THWAITE E.G. Elastic compression of spheres and cylinders at point and line contact. NSL Tech.Paper No.25 (1969).

82. REED, R.P., MIKESELL, R.P. Low temperature mechanical properties of Copper and selected copper alloys. U.S.National Bureau of Standards Monograph 101.

83. RICHMOND O., MORRISON, H.L., DEVENPECK, M.L. Sphere indentation with application to the Brinell hardness test. Int. J. Mech. Sci., vol.16 (1974) pp 75-82.

84. ROARK R.J. Formulas for stress and strains. McGraw Hill 4th ed. (1965).

85. SCHOFIELD, R.E., THORNLEY, R.H. Calculating of the elastic and plastic components of deflection of plane joints formed from machined surface. Proc. 12th Int. Mach. Tool Des. Res. (1971) pp 89-96.

86. SHAW M.C., BER A., MAMIN, P.A. Friction characteristics of sliding surfaces undergoing subsurface plastic flow. Trans ASME vol D82 (1960) pp 342-346.

87. SKF. General Catalogue. Jarrold & Son Norwick ed (1970) pp 492-493.

88. SHAWKI G.S.A., ABDEL AAL, M.M. Effect of fixture rigidity and wear on dimensional accuracy. Int. J. Mach. Tool Des. Res. vol.5 (1965) pp 183-202.

89. SHAWKI G.S.A., ABDEL AAL M.M. Rigidity considerations in fixture design - Rigidity of clamping elements. Int. J. Mach. Tool Des. Res. vol.6 (1966) pp 207-220.

90. SHAWKI G.S.A., ABDEL AAL M.M. Rigidity considerations in fixture design - Contact rigidity at locating elements. Int. J. Mach. Tool Des. Res. vol6 (1966) pp 31-43.

91. SHAWKI G.S.A., ABDEL AAL, M.M. Rigidity consideration in fixture design - Contact rigidity for eccentric clamping. Int. J. Mach. Tool Des. Res. vol.7 (1967) pp 195-209.

92. SINGH K.P. On the inadequacy of Hertzian solution of two dimensional line contact. J. Franklin. Inst. vol.298 (1974) pp 139-141.

93 SINGH, P., PAUL, B. Numerical solution of non-Hertzian elastic contact problems. J. Appl. Mech. vol.41 (1974) pp 484-490.

94. STEAD, J. The cold working of steel with reference to the tensile test. J. Iron & Steel Inst. No.I (1923) pp 377-418.

95. STRIBECK, R. English Translation by Hess, H. Trans. ASME vol.29 (1907) pp 420-467.

96. TABOR, D. A simple theory of static and dynamic hardness. Proc. Roy. Soc. London A192 (1948) pp 247-274.

97. TABOR, D. The hardness of metal. Oxford Claredon Press 1951.

98. TABOR, D. The friction and lubrication of solids, Part I. 5th ed. Oxford Claredon Press 1971.

99. THOMAS, W.N. Experiments on the hardness testing of mild steel. J. Iron & Steel Inst. No.1 (1916) pp 263-270.

100. THOMAS, H.R., HOERSCH, V.A. Pressure stresses of one elastic solid upon another. Univ. of Ill. Bull. July 15 (1930).

101. THORNLEY, R.H., CONNOLLY, R., BARASH, M.M., KOENIGSBERGER, F. The effect of surface topography upon the static stiffness of machine tool joints. Int. J. Mach. Tool Des. Res. vol.5 (1965) pp 57-74.

102. THWAITE, E.G. A precise measurement of the comparison of a cylinder in contact with a flat surface. J. Phys. E. Series 2, vol.2 (1969) pp 79-82.

103. TIMOSHENKO, S., GOODIER, J.N. Theory of elasticity. McGraw Hil N.Y. 3rd ed. (1970).

104. UPPAL, A.H., PROBERT, S.D., THOMAS T.R. The real area of contact between a rough and a flat surface. Wear 22 (1972) pp 163-183.

105. UPPAL, A.H., PROBERT, S.D. Considerations governing the contact between a rough and a flat surface. Wear 22 (1972) pp 215-234.

106. UPPAL, A.H., PROBERT, S.D. Deformation of a single and multiple asperities on metal surfaces. Wear 20 (1972) pp 381-400.

107. UPPAL, A.H., PROBERT S.D. Mean separation and real contact area between surfaces pressed together under high static loads. Wear 23 (1973) pp 39-53.

108. UPPAL, A.H., PROBERT, S.D. The plastic contact between a rough and a flat surface. Wear 23 (1973) pp 173-184.

109. UPPAL, A.H., PROBERT, S.D. Deformation of a single and multiple asperity models of modelling clay. Wear 23 (1973) pp 367-375.

110. VAN HORN, K.R. Aluminium vol.1, Chapman & Hall Ltd, 1967.

111. WICKSTRAND, N.M. Depth of permanent indentations in flat plates due to loaded cylindrical rollers. J. Lub. Tech. Trans ASME vol.92 (1970) pp 163-177.

112. WILLIAMSON, J.B.P., HUNT R.T. Asperity persistence and the real area of contact between rough surfaces. Proc. Roy. Soc. London A327 (1972) pp 147-157.

113. WILLIAMSON, J.B.P., PULLEN, J. On the plastic contact of rough surfaces. Proc. Roy. Soc. London A327 (1972), pp 159-173.

114. WILSEA, M., JOHNSON, K.L. ASHBY, M.F. Indentation of foamed plastics. Int. J. Mech. Sci. vol.17 (1975) pp 457-460.

APPENDIX 2.1

VARIATIONS OF MEYER CONSTANT n OF STEELS

Steel	HB kg/mm^2 at $\frac{W}{D^2} = 30$	Meyer n	$\frac{W_{min}}{D^2}$ kg/mm^2	$\frac{W_{max}}{D^2}$ kg/mm^2	Ref. No.	Investigator
Soft Steel		2.36			78	Jimeno & Terraza
Iron		2.20			68a	Kürth
Armo iron	92	2.30			68a	Norbury
Mild steel	112		5	50	68a	Norbury
Mild Steel (annealed at 950°C)		2.22			68b	Norbury
Tempered C. steel	188	2.10	5	50	68a	Norbury
Tempered C. steel	277	2.168	5	50	68a	Norbury
Tempered C. steel	295	2.173	5	50	68a	Norbury
Tempered C. steel	307	2.196	5	50	68a	Norbury
Tempered C. steel	435	2.230	5	50	68a	Norbury
Tempered C. steel		2.17			68b	Norbury
Tempered C. steel		2.19			68b	Norbury
Steel 0.15% C.		2.14			68a	Lukwik
Steel 0.3% C.		2.20			68a	Lukwik
Steel 0.55%C.		2.21			68a	Lukwik
Steel 0.8% C.		2.28			68a	Lukwik
Steel 1.1% C.		2.33			68a	Lukwik
Steel A .25% C.	140	2.288	5	35	75	O'Neill
Steel W .65% C.	327	2.292	5	35	75	O'Neill
Steel 4 .9% C. heat treated	444	2.292	5	35	75	O'Neill
Steel 3 .9% C. heat treated	564	2.293	5	35	75	O'Neill
Steel 2N 0.16% C.		2.185			75	O'Neill
Steel S90 .9% C.		2.298			75	O'Neill
Steel 1A .16 % C.		2.25			94	Stead
Steel 2A .28% C.		2.25			94	Stead
Steel 4A .44% C.		2.25			94	Stead
Steel 6A .55% C.		2.28			84	Stead
Chromium steel quenched		2.27			68b	Norbury

APPENDIX 2.1 (Continued)

Steel	HB kg/mm^2 at $\frac{W}{D^2} = 30$	Meyer n	$\frac{W_{min}}{D^2}$ kg/mm^2	$\frac{W_{max}}{D^2}$ kg/mm^2	Ref. No.	Investigator
Chromium steel tempered		2.17			68	Norbury
(*) = Mild Steel .24%c 880°C cooled in muffle	134	2.293	5	30	9	Baker & Russell
(*) then stressed by 19.77 tons	136	2.236	5	30	9	Baker & Russell
(*) then stressed by 23.35 tons	147	3.185	5	30	9	Baker & Russell
(*) then stressed by 27.15 tons	150	2.147	5	30	9	Baker & Russell
(*) then stressed by 33.04 tons	158	2.095	5	30	9	Baker & Russell
Work-hardened Steel		2.04	.5	40	97	Tabor

APPENDIX 2.2

VARIATIONS OF MEYER CONSTANT n OF SOME NON-FERROUS METALS

Materials	HB kg/mm^2 at $\frac{W}{D^2}=10$	Meyer n	$\frac{W}{D^2}_{min}$ kg/mm^2	$\frac{W}{D^2}_{max}$ kg/mm^2	Ref. No.	Investigator
Aluminium		2.304			68a	Grard
Alluminium		2.316			68a	Grard
Aluminium annealed		2.2			77	Schwarz
Aluminium annealed	23	2.25			77	O'Neill
Aluminium annealed		2.4	5	20	97	Tabor
Alluminium rolled and annealed		2.32			68b	Norbury
Aluminium cold hammered 90%		1.96			68b	Norbury
Aluminium work hardened		2.0	2.5	12.5	97	Tabor
(*)=Duralumin freshly quenched 500°C	71	2.40			77	O'Neill
(*) then aged 15°C	106	2.32			77	O'Neill
(*) then aged 15°c then tempered 150°C for 100 hrs	117	2.12			77	O'Neill
(*) then aged 15°C then tempered 200°C for 4 hrs	102	2.24			77	O'Neill
(*) then aged 15°C then tempered 360°C for 1/3 hr	62	2.37			77	O'Neill
Copper	47.5	2.446	5	30	68a	Norbury
Copper	57	2.354	5	30	68a	Norbury
Copper	48	2.43			77	O'Neill
Copper annealed		2.40			77	Schwarz
Copper annealed		2.53	1.25	30	97	Tabor

APPENDIX 2.2 (Continued)

Materials	HB kg/mm^2 at $\frac{W}{D^2}=10$	Meyer n	$\frac{W}{D^2}_{min}$ kg/mm^2	$\frac{W}{D^2}_{max}$ kg/mm^2	Ref. No.	Investigator
Copper rolled and annealed at 900°C		2.50			68b	Norbury
Copper work hardened		2.15	1.25	30	97	Tabor
Copper cold hammered 20%		2.01			68b	Norbury
Copper cold hammered 75%		1.96			68b	Norbury
Brass		2.44			68a	Norris
Brass cold drawn		2.10			68a	Norris
Brass (62/38) annealed		2.61			68a	Schwarz
Brass rolled 10%		2.17			68a	Schwarz
Nickel		2.40			68a	Kürth
Nickel	88	2.48			77	O'Neill
Nickel annealed		2.50			77	Schwarz
Nicken rolled & annealed at 900°C		2.28			68b	Norbury
Nickel rolled 10%		2.14			68a	Schwarz
Magnesium cast		2.42			77	Schwarz

APPENDIX 2.3

```
FTN4,L
C**********INDENTATION OF A BALL ON A FLAT WORKPIECE**********
C THIS PROGRAM SHOWS THE CALCULATION OF THE DIMENSIONLESS DIAMETER
C  OF INDENTION d/D FROM GIVEN DIMENSIONLESS LOAD P=W/WE FOR EACH
C  SET OF n AND C
C n MAY BE 2.0, 2.25, 2.5
C C MAY BE 10, 15, 20
C B(1) TO B(5) REPRESENT THE YOUNG MODULUS, HARDNESS AND THE MEYER
C  CONSTANT n OF THE WORKPIECE , SPECIFIFIC LOADING AND CONSTAND C
C**********************************************************************
      PROGRAM PLOT
      DIMENSION A(9),B(5)
      DATA A/1.,2.,5.,10.,50.,100.,200.,500.,1000./
      READ(1,*)(B(I),I=1,5)
      X1=1./21500.*(1./B(1))
      P=-2./B(3)+1.
      XP=X1**P
      PA=1./B(3)
      X2=(B(4)*1.25/4.81)**PA
      PB=-3./B(3)+1.5
      X3=B(2)**PB
      X4=SQRT(B(4))
      R=X3*X2*XP*.418/X4
      X5=3./B(3)-.5
      X6=4.81*X1*X1/(1.25*B(4))
      X6=X6**PA
      WRITE(6,3)B(1),B(2),B(3)
    3 FORMAT(16X,"YOUNG MOD=",F6.0,2X,"HARDNESS=",F6.0,2X,"MEYER="
     1,F5.3)
      WRITE(6,4)B(4),B(5),R
    4 FORMAT(16X,"Z=",F3.0,5X,"C=",F3.0,5X,"DIA RATIO=",F6.2)
      WRITE(6,5)
    5 FORMAT(/,17X,"FACTOR",3X,"PLAS DIA",2X,"CORR DIA",2X,
     1"ELAS DIA")
      DO 2 J=1,9
      AA=A(J)**PA
      AB=B(4)**.5
      DP=B(2)**X5*AB*X6*AA*1.128
      PC=B(5)*R*A(J)
      PD=PC/(A(J)+B(5))
      DD=PD*DP
      DE=A(J)**.3333*B(2)**.472*X1
      WRITE(6,6)A(J),DP,DD,DE
    6 FORMAT(16X,F6.1,1X,3(F9.4,1X))
    2 CONTINUE
      END
      END$
```

THE RESULTS OF PROGRAM PLOT

****

YOUNG MOD=21500. HARDNESS= 133. MEYER=2.000
Z=30. C=15. DIA RATIO= 2.13

FACTOR	PLAS DIA	CORR DIA	ELAS DIA
1.0	.0039	.0030	.0083
2.0	.0055	.0109	.0104
5.0	.0087	.0150	.0141
10.0	.0122	.0205	.0178
50.0	.0274	.0345	.0334
100.0	.0387	.0444	.0383
200.0	.0547	.0590	.0483
500.0	.0865	.0894	.0655
1000.0	.1224	.1244	.0825

YOUNG MOD=21500. HARDNESS= 138. MEYER=2.250
Z=30. C=15. DIA RATIO= 1.25

FACTOR	PLAS DIA	CORR DIA	ELAS DIA
1.0	.0066	.0081	.0083
2.0	.0089	.0110	.0104
5.0	.0134	.0150	.0141
10.0	.0183	.0211	.0178
50.0	.0374	.0395	.0384
100.0	.0503	.0525	.0383
200.0	.0692	.0704	.0483
500.0	.1339	.1347	.0655
1000.0	.1414	.1420	.0825

YOUNG MOD=21500. HARDNESS= 133. MEYER=2.500
Z=30. C=15. DIA RATIO= .92

FACTOR	PLAS DIA	CORR DIA	ELAS DIA
1.0	.0100	.0094	.0083
2.0	.0132	.0112	.0104
5.0	.0191	.0165	.0141
10.0	.0252	.0225	.0178
50.0	.0479	.0450	.0334
100.0	.0632	.0618	.0383
200.0	.0834	.0824	.0483
500.0	.1234	.1197	.0655
1000.0	.1538	.1534	.0825

YOUNG MOD=21500. HARDNESS= 354. MEYER=2.000
Z=15. C= . DIA RATIO= 2.13

FACTOR	PLAS DIA	CORR DIA	ELAS DIA
1.0	.0072	.0073	.0155
2.0	.0103	.0103	.0196
5.0	.0163	.0163	.0266
10.0	.0230	.0230	.0335
50.0	.0515	.0515	.0573
100.0	.0729	.0729	.0721
200.0	.1030	.1030	.0909
500.0	.1629	.1629	.1233
1000.0	.2304	.2304	.1554

YOUNG MOD=21500. HARDNESS= 354. MEYER=2.000
Z=30. C=15. DIA RATIO= 2.13

FACTOR	PLAS DIA	CORR DIA	ELAS DIA
1.0	.0073	.0130	.0155
2.0	.0103	.0236	.0196
5.0	.0163	.0301	.0256
10.0	.0230	.0337	.0335
50.0	.0515	.0650	.0573
100.0	.0729	.0816	.0721
200.0	.1030	.1112	.0909
500.0	.1629	.1693	.1233
1000.0	.2304	.2343	.1554

YOUNG MOD=21500. HARDNESS= 354. MEYER=2.250
Z=30. C=15. DIA RATIO= 1.40

FACTOR	PLAS DIA	CORR DIA	ELAS DIA
1.0	.0111	.0153	.0155
2.0	.0151	.0204	.0195
5.0	.0227	.0295	.0266
10.0	.0310	.0363	.0335
50.0	.0633	.0691	.0573
100.0	.0861	.0906	.0721
200.0	.1172	.1204	.0909
500.0	.1751	.1782	.1233
1000.0	.2397	.2411	.1554

YOUNG MOD=21500. HARDNESS= 354. MEYER=2.500
Z=30. C=15. DIA RATIO= .99

FACTOR	PLAS DIA	CORR DIA	ELAS DIA
1.0	.0156	.0155	.0155
2.0	.0206	.0205	.0196
5.0	.0297	.0296	.0266
10.0	.0392	.0391	.0335
50.0	.0746	.0745	.0573
100.0	.0935	.0934	.0721
200.0	.1299	.1299	.0939
500.0	.1874	.1874	.1233
1000.0	.2473	.2473	.1554

YOUNG MOD=12200. HARDNESS= 75. MEYER=2.000
Z=10. C=15. DIA RATIO= 2.13

FACTOR	PLAS DIA	CORR DIA	ELAS DIA
1.0	.0021	.0044	.0045
2.0	.0030	.0053	.0057
5.0	.0043	.0068	.0078
10.0	.0067	.0113	.0098
50.0	.0151	.0193	.0168
100.0	.0213	.0245	.0211
200.0	.0302	.0325	.0266
500.0	.0477	.0492	.0361
1000.0	.0674	.0686	.0455

YOUNG MOD=12200. HARDNESS= 75. MEYER=2.250
Z=10. C=15. DIA RATIO= 1.19

FACTOR	PLAS DIA	CORR DIA	ELAS DIA
1.0	.0038	.0045	.0045
2.0	.0052	.0061	.0057
5.0	.0078	.0089	.0078
10.0	.0106	.0113	.0098
50.0	.0218	.0227	.0168
100.0	.0296	.0304	.0211
200.0	.0403	.0408	.0266
500.0	.0636	.0639	.0361
1000.0	.0824	.0827	.0455

YOUNG MOD=12200. HARDNESS= 75. MEYER=2.500
Z=10. C=15. DIA RATIO= .74

FACTOR	PLAS DIA	CORR DIA	ELAS DIA
1.0	.0061	.0046	.0045
2.0	.0081	.0062	.0057
5.0	.0115	.0094	.0078
10.0	.0153	.0130	.0098
50.0	.0292	.0275	.0168
100.0	.0385	.0373	.0211
200.0	.0509	.0503	.0266
500.0	.0734	.0723	.0361
1000.0	.0963	.0965	.0455

APPENDIX 2.4

```
FTN4,L
      PROGRAM FINAL
C*************************************************************************
C    GIVEN X(1) TO X(6)=YOUNG MODULUS OF WORKPIECE, SPECIFIC
C       LOADING, MEYER CONSTANT    , BALL DIAMETER AND THE YOUNG
C       MODULUS OF THE BALL.
C    CALCULATE AT DIFERENT LOAD IN LBS THE TWO QUANTITIES
C       #1#TOTAL DEFORMATION OF THE SYSTEM OF A HARD BALL INDENTED
C             INTO A FLAT SURFACE IN MICRON.
C       #2#DIAMETER OF INDENTATION IN MM
C*************************************************************************
      DIMENSION S(13),W(13),X(6)
      DATA S/20.,50.,100.,200.,500.,1000.,2000.,5000.,7000.,
     110000.,12000.,15000.,30000./
      READ(1,*)(X(I),I=1,6)
      Y=1./(X(6)+(1./X(1)))
      D=X(5)
      DE=X(2)**Y*D**.472
      GA=D**2.
      GB=X(2)**3
      WE=Y**Y*GA*GB**.8385
      AA=1./X(4)
      AB=-3./X(4)+1.5
      AC=-2./X(4)+1.
      AE=3./X(4)-.5
      BA=SQRT(X(3))
      BB=(X(3)*26.)**AA
      BC=X(3)**AB
      BD=Y**AC
      BE=(Y**Y*.8385)/X(3)
      BF=BE**AA
      BG=X(2)**AE
      WRITE(6,2)X(1),D
    2 FORMAT(1X,"YOUNG MODULUS=",F9.1,"KG/MM2",5X,"BALL DIA="
     1,F7.2,"MM")
      WRITE(6,3)X(2),X(4)
    3 FORMAT(1X,"WORKPIECE HARDNESS=",F7.2,"KG/MM2",5X,
     1"MEYER CONSTANT=",F7.3)
      WRITE(6,4)WE,DE
    4 FORMAT(1X,"ONSET OF PLASTIC LOAD=",F7.2,"KGS",
     15X,"ELAS DIA=",F6.3,"MM")
      WRITE(6,7)
    7 FORMAT(/,7X,"LOAD",4X,"INDEN DIA",3X,"ELAS DEF",
     13X,"PLAS DEF",3X,"TOTAL DEF")
      WRITE(6,6)
    6 FORMAT(8X,"LBS",8X,"MM",7X,3("MICRON",5X))
      DO 9 I=1,13
      W(I)=S(I)/2.205
      A=W(I)/WE
      R=BD*BC*BB*.415/BA
      CB=(15.*R+A)/(15.+A)
      CD=A**AA
C  DIA IS THE DIAMETER OF INDENTION
      DIA=CB*BA*BF*BG*CD*D*1.128
      DELE=1000.*W(I)*Y*1.354/DIA
      DELP=1000.*(DIA*DIA/(4.*D))-(DELE*.5)
C  DELT IS THE TOTAL DEFORMATION OF THE SYSTEM
      DELT=DELE+DELP
      WRITE(6,5)S(I),DIA,DELE,DELP,DELT
    5 FORMAT(2X,F9.0,1X,F9.2,2X,3(F9.1,2X))
    9 CONTINUE
      END
      END$
```

THE RESULTS OF PROGRAM FINAL
****

WORKPIECE S6

YOUNG MODULUS= 21500. 0KG/MM2 BALL DIA= 31. 75MM
WORKPIECE HARDNESS= 137. 00KG/MM2 MEYER CONSTANT= 2. 283
ONSET OF PLASTIC LOAD= . 86KGS ELAS DIA= . 191MM

LOAD LBS	INDEN DIA MM	ELAS DEF MICRON	PLAS DEF MICRON	TOTAL DEF MICRON
20.	. 50	2. 3	. 8	3. 1
50.	. 71	4. 0	2. 0	6. 0
100.	. 94	6. 1	3. 8	10. 0
200.	1. 25	9. 2	7. 6	16. 9
500.	1. 85	15. 6	19. 1	34. 7
1000.	2. 51	22. 9	38. 2	61. 2
2000.	3. 43	33. 6	75. 7	109. 2
5000.	5. 18	55. 5	183. 5	239. 1
7000.	6. 03	66. 3	253. 1	319. 9
10000.	7. 03	81. 2	355. 1	436. 3
12000.	7. 70	89. 7	422. 0	511. 7
15000.	8. 52	101. 3	523. 5	622. 1
30000.	11. 67	148. 0	997. 6	1145. 6

WORKPIECE S5

YOUNG MODULUS= 21500. 0KG/MM2 BALL DIA= 31. 75MM
WORKPIECE HARDNESS= 156. 00KG/MM2 MEYER CONSTANT= 2. 100
ONSET OF PLASTIC LOAD= 1. 27KGS ELAS DIA= . 217MM

LOAD LBS	INDEN DIA MM	ELAS DEF MICRON	PLAS DEF MICRON	TOTAL DEF MICRON
20.	. 48	2. 4	. 6	3. 0
50.	. 67	4. 3	1. 4	5. 7
100.	. 85	6. 7	2. 3	9. 1
200.	1. 10	10. 4	4. 4	14. 8
500.	1. 61	17. 9	11. 4	29. 3
1000.	2. 18	25. 4	24. 4	50. 7
2000.	3. 00	38. 4	51. 6	90. 0
5000.	4. 60	62. 5	135. 3	197. 9
7000.	5. 39	74. 7	191. 5	266. 2
10000.	6. 38	90. 2	273. 5	363. 7
12000.	6. 96	99. 3	331. 4	430. 7
15000.	7. 73	111. 5	415. 0	526. 5
30000.	10. 75	150. 6	829. 1	979. 7

WORKPIECE S1

YOUNG MODULUS= 21500. 0KG/MM2 BALL DIA= 31. 75MM
WORKPIECE HARDNESS= 180. 00KG/MM2 MEYER CONSTANT= 2. 355
ONSET OF PLASTIC LOAD= 2. 23KGS ELAS DIA= . 262MM

LOAD LBS	INDEN DIA MM	ELAS DEF MICRON	PLAS DEF MICRON	TOTAL DEF MICRON
20.	. 47	2. 4	. 5	3. 3
50.	. 69	4. 2	1. 7	5. 8
100.	. 92	6. 3	3. 5	9. 8
200.	1. 23	9. 4	7. 2	16. 5
500.	1. 80	16. 0	17. 5	33. 5
1000.	2. 41	23. 9	33. 8	57. 7
2000.	3. 23	35. 6	64. 4	100. 0
5000.	4. 77	60. 4	148. 6	209. 0
7000.	5. 50	73. 3	201. 2	274. 5
10000.	6. 39	90. 0	275. 9	366. 9
12000.	6. 91	100. 0	325. 8	425. 8
15000.	7. 59	113. 7	397. 3	511. 0
30000.	10. 19	169. 4	733. 3	902. 7

WORKPIECE S2

YOUNG MODULUS= 21500. 0KG/MM2 BALL DIA= 31. 75MM
WORKPIECE HARDNESS= 249. 00KG/MM2 MEYER CONSTANT= 2. 152
ONSET OF PLASTIC LOAD= 5. 18KGS ELAS DIA= . 347MM

LOAD LBS	INDEN DIA MM	ELAS DEF MICRON	PLAS DEF MICRON	TOTAL DEF MICRON
20.	. 43	2. 7	. 1	2. 8
50.	. 63	4. 6	. 9	5. 4
100.	. 82	7. 0	1. 8	8. 8
200.	1. 06	10. 9	3. 3	14. 2
500.	1. 47	19. 6	7. 1	26. 7
1000.	1. 91	30. 1	13. 8	43. 9
2000.	2. 55	45. 2	28. 3	73. 6
5000.	3. 80	75. 7	75. 9	151. 6
7000.	4. 42	91. 1	108. 3	199. 4
10000.	5. 20	110. 7	157. 3	268. 0
12000.	5. 65	122. 3	193. 0	312. 3
15000.	6. 25	138. 8	239. 1	377. 1
30000.	8. 60	200. 6	482. 6	683. 3

WORKPIECE S3

YOUNG MODULUS= 21500. 0KG/MM2 BALL DIA= 31. 75MM
WORKPIECE HARDNESS= 306. 00KG/MM2 MEYER CONSTANT= 2. 156
ONSET OF PLASTIC LOAD= 9. 62KGS ELAS DIA= . 427MM

LOAD LBS	INDEN DIA MM	ELAS DEF MICRON	PLAS DEF MICRON	TOTAL DEF MICRON
20.	. 41	2. 8	-. 1	2. 7
50.	. 60	4. 8	. 5	5. 2
100.	. 80	7. 2	1. 4	8. 6
200.	1. 03	11. 1	2. 8	14. 0
500.	1. 43	20. 2	5. 9	26. 1
1000.	1. 83	31. 5	10. 5	42. 0
2000.	2. 38	48. 3	20. 6	68. 9
5000.	3. 49	82. 4	54. 8	137. 2
7000.	4. 04	99. 5	78. 9	178. 5
10000.	4. 74	121. 5	115. 9	237. 4
12000.	5. 14	134. 4	140. 8	275. 1
15000.	5. 68	151. 9	176. 3	330. 2
30000.	7. 79	221. 6	367. 1	588. 7

WORKPIECE S4

YOUNG MODULUS= 21500. 0KG/MM2 BALL DIA= 31. 75MM
WORKPIECE HARDNESS= 354. 00KG/MM2 MEYER CONSTANT= 2. 036
ONSET OF PLASTIC LOAD= 14. 95KGS ELAS DIA= . 493MM

LOAD LBS	INDEN DIA MM	ELAS DEF MICRON	PLAS DEF MICRON	TOTAL DEF MICRON
20.	. 38	3. 0	-. 4	2. 7
50.	. 58	5. 0	. 1	5. 1
100.	. 78	7. 4	1. 1	8. 5
200.	1. 02	11. 3	2. 5	13. 8
500.	1. 41	20. 5	5. 3	25. 8
1000.	1. 77	32. 3	8. 4	40. 9
2000.	2. 25	51. 0	14. 6	65. 6
5000.	3. 23	89. 3	37. 8	126. 8
7000.	3. 73	108. 8	54. 3	163. 5
10000.	4. 36	132. 3	83. 7	215. 7
12000.	4. 73	146. 8	103. 2	249. 2
15000.	5. 23	165. 0	133. 1	298. 1
30000.	7. 20	239. 6	288. 9	528. 4

THE RESULTS OF PROGRAM FINAL
****

WORKPIECE CO2

YOUNG MODULUS= 12200. 0KG/MM2 BALL DIA= 31. 75MM
WORKPIECE HARDNESS= 44. 60KG/MM2 MEYER CONSTANT= 2. 467
ONSET OF PLASTIC LOAD= . 35KGS ELAS DIA= . 086MM

LOAD LBS	INDEN DIA MM	ELAS DEF MICRON	PLAS DEF MICRON	TOTAL DEF MICRON
20.	. 96	1. 7	6. 4	8. 1
50.	1. 42	2. 8	14. 4	17. 2
100.	1. 89	4. 2	25. 9	30. 1
200.	2. 50	6. 3	46. 2	52. 6
500.	3. 54	10. 9	98. 8	109. 7
1000.	4. 82	16. 5	174. 8	191. 3
2000.	6. 39	24. 9	308. 8	333. 7
5000.	9. 26	42. 9	654. 0	696. 9
7000.	10. 62	52. 4	861. 1	913. 5
10000.	12. 27	64. 8	1152. 5	1217. 3
12000.	13. 21	72. 2	1337. 6	1409. 8
15000.	14. 46	82. 5	1604. 9	1687. 3
30000.	19. 15	124. 5	2825. 3	2949. 8

WORKPIECE CO1

YOUNG MODULUS= 12230. 0KG/MM2 BALL DIA= 31. 75MM
WORKPIECE HARDNESS= 75. 00KG/MM2 MEYER CONSTANT= 2. 112
ONSET OF PLASTIC LOAD= . 27KGS ELAS DIA= . 144MM

LOAD LBS	INDEN DIA MM	ELAS DEF MICRON	PLAS DEF MICRON	TOTAL DEF MICRON
20.	. 55	2. 8	1. 1	3. 9
50.	. 80	5. 0	2. 3	7. 3
100.	1. 05	7. 5	5. 2	12. 6
200.	1. 44	11. 3	10. 9	21. 9
500.	2. 19	18. 1	28. 8	46. 9
1000.	3. 03	25. 2	59. 1	85. 3
2000.	4. 19	37. 9	119. 5	157. 4
5000.	6. 46	62. 5	297. 8	359. 3
7000.	7. 57	73. 5	414. 8	488. 3
10000.	8. 96	88. 7	538. 4	677. 1
12000.	9. 77	97. 6	783. 8	838. 6
15000.	10. 86	109. 8	873. 7	983. 4
30000.	15. 08	158. 2	1710. 4	1868. 5

WORKPIECE AL1

YOUNG MODULUS= 7040. 0KG/MM2 BALL DIA= 31. 75MM
WORKPIECE HARDNESS= 31. 30KG/MM2 MEYER CONSTANT= 2. 222
ONSET OF PLASTIC LOAD= . 34KGS ELAS DIA= . 083MM

LOAD LBS	INDEN DIA MM	ELAS DEF MICRON	PLAS DEF MICRON	TOTAL DEF MICRON
20.	. 87	2. 7	4. 6	7. 3
50.	1. 31	4. 5	11. 2	15. 7
100.	1. 78	6. 5	21. 7	28. 3
200.	2. 43	9. 6	41. 8	51. 4
500.	3. 57	15. 9	98. 2	114. 1
1000.	5. 01	23. 3	185. 3	209. 6
2000.	6. 85	34. 1	352. 4	386. 4
5000.	10. 34	56. 4	814. 4	870. 7
7000.	12. 04	67. 8	1106. 6	1174. 5
10000.	14. 13	82. 6	1531. 0	1613. 6
12000.	15. 34	91. 2	1807. 1	1893. 3
15000.	16. 96	103. 2	2213. 2	2316. 4
30000.	23. 17	151. 0	4151. 8	4302. 8

WORKPIECE AL2

YOUNG MODULUS= 7040. 0KG/MM2 BALL DIA= 31. 75MM
WORKPIECE HARDNESS= 37. 03KG/MM2 MEYER CONSTANT= 2. 091
ONSET OF PLASTIC LOAD= 1. 25KGS ELAS DIA= . 274MM

LOAD LBS	INDEN DIA MM	ELAS DEF MICRON	PLAS DEF MICRON	TOTAL DEF MICRON
20.	. 61	3. 8	1. 0	4. 8
50.	. 84	7. 0	2. 0	9. 0
100.	1. 06	11. 0	3. 3	14. 3
200.	1. 37	17. 1	6. 1	23. 2
500.	1. 93	29. 4	16. 2	45. 6
1000.	2. 69	43. 4	35. 2	78. 6
2000.	3. 69	63. 2	73. 7	138. 9
5000.	5. 57	102. 9	201. 6	304. 5
7000.	6. 65	122. 8	286. 5	409. 3
10000.	7. 87	148. 2	413. 9	562. 1
12000.	8. 59	163. 0	498. 9	661. 9
15000.	9. 55	183. 3	626. 1	809. 4
30000.	13. 29	263. 4	1258. 2	1521. 6

WORKPIECE BR

YOUNG MODULUS= 10500. 0KG/MM2 BALL DIA= 31. 75MM
WORKPIECE HARDNESS= 112. 00KG/MM2 MEYER CONSTANT= 2. 296
ONSET OF PLASTIC LOAD= 1. 08KGS ELAS DIA= . 235MM

LOAD LBS	INDEN DIA MM	ELAS DEF MICRON	PLAS DEF MICRON	TOTAL DEF MICRON
20.	. 56	3. 1	1. 8	4. 0
50.	. 61	5. 4	2. 5	7. 8
100.	1. 07	8. 2	4. 9	13. 8
200.	1. 41	12. 3	9. 5	21. 9
500.	2. 37	21. 8	23. 4	44. 4
1000.	2. 79	31. 2	43. 7	76. 9
2000.	3. 76	46. 3	88. 2	134. 5
5000.	5. 60	77. 9	207. 5	285. 4
7000.	6. 48	94. 2	283. 1	377. 3
10000.	7. 56	115. 2	392. 7	507. 9
12000.	8. 19	127. 7	463. 8	591. 5
15000.	9. 02	144. 9	568. 3	713. 2
30000.	12. 20	214. 3	1064. 3	1278. 6

APPENDIX 2.6

STEEL SAE 4340(Lee[55])

YOUNG MODULUS= 21500.0KG/MM2 BALL DIA= 10.00MM
WORKPIECE HARDNESS= 398.03KG/MM2 MEYER CONSTANT= 2.120
ONSET OF PLASTIC LOAD= .968SKGS ELAS DIA= .119MM

LOAD KGS	INDEN DIA MM	ELAS DEF MICRON	PLAS DEF MICRON	TOTAL DEF MICRON
2.4	.17	1.2	.1	1.4
5.0	.23	1.9	.4	2.3
10.0	.30	2.9	.8	3.7
20.0	.38	4.6	1.3	5.8
30.0	.43	6.0	1.7	7.7
50.0	.52	8.3	2.6	10.9
150.0	.80	16.2	7.9	24.1
500.0	1.36	31.0	30.1	61.9
1000.0	1.86	46.3	63.6	109.9
2000.0	2.57	67.0	131.7	198.7
3000.0	3.11	83.2	199.8	283.0
3500.0	3.34	90.3	233.8	324.1

COLD-WORKED COPPER(Richmond[83])

YOUNG MODULUS= 12200.0KG/MM2 BALL DIA= 10.00MM
WORKPIECE HARDNESS= 117.00KG/MM2 MEYER CONSTANT= 2.030
ONSET OF PLASTIC LOAD= .0600KGS ELAS DIA= .054MM

LOAD KGS	INDEN DIA MM	ELAS DEF MICRON	PLAS DEF MICRON	TOTAL DEF MICRON
2.4	.22	1.5	.4	1.9
5.0	.28	2.4	.7	3.2
10.0	.37	3.6	1.6	5.2
20.0	.50	5.4	3.6	8.9
30.0	.60	6.7	5.7	12.4
50.0	.77	8.8	10.3	19.1
150.0	1.30	15.5	34.7	50.2
500.0	2.35	29.6	123.5	152.1
1000.0	3.30	40.8	252.0	292.7
2000.0	4.64	58.0	509.7	567.7
3000.0	5.67	71.2	767.4	838.6
3500.0	6.11	77.0	896.1	973.1

ANNEALED COPPER(Richmond[83])

YOUNG MODULUS= 12200.0KG/MM2 BALL DIA= 10.00MM
WORKPIECE HARDNESS= 49.60KG/MM2 MEYER CONSTANT= 2.490
ONSET OF PLASTIC LOAD= .0043KGS ELAS DIA= .023MM

LOAD KGS	INDEN DIA MM	ELAS DEF MICRON	PLAS DEF MICRON	TOTAL DEF MICRON
2.4	.45	.7	4.7	5.4
5.0	.60	1.1	8.5	9.6
10.0	.80	1.7	15.0	16.7
20.0	1.06	2.5	26.6	29.1
30.0	1.24	3.2	37.0	40.3
50.0	1.53	4.4	56.2	60.6
150.0	2.38	8.5	137.5	145.9
500.0	3.87	17.4	365.5	382.9
1000.0	5.12	26.3	641.3	667.6
2000.0	6.77	39.8	1124.8	1164.5
3000.0	7.97	50.7	1562.1	1612.7
3500.0	8.48	55.5	1769.8	1825.3

APPENDIX 2.5

TABOR FULLY WORKHARDENED STEEL

YOUNG MODULUS= 21500.0KG/MM2 BALL DIA= 10.00MM
WORKPIECE HARDNESS= 231.00KG/MM2 MEYER CONSTANT= 2.070
ONSET OF PLASTIC LOAD= .41KGS ELAS DIA= .101MM

LOAD KGS	INDEN DIA MM	ELAS DEF MICRON	PLAS DEF MICRON	TOTAL DEF MICRON
2.4	.21	1.5	.4	1.8
5.0	.27	2.4	.6	3.0
10.0	.34	3.8	.9	4.7
20.0	.42	6.0	1.4	7.4
30.0	.48	7.9	2.0	9.8
50.0	.59	10.8	3.3	14.1
150.0	.95	20.0	12.5	32.8
500.0	1.68	37.7	51.9	89.6
1000.0	2.36	53.7	112.8	166.5
2000.0	3.33	76.2	239.2	315.4
3000.0	4.07	93.4	368.3	461.7
3500.0	4.40	100.9	433.4	534.4

ONEILL STEEL WORKPIECE

YOUNG MODULUS= 21500.0KG/MM2 BALL DIA= 10.00MM
WORKPIECE HARDNESS= 140.00KG/MM2 MEYER CONSTANT= 2.288
ONSET OF PLASTIC LOAD= .09KGS ELAS DIA= .061MM

LOAD KGS	INDEN DIA MM	ELAS DEF MICRON	PLAS DEF MICRON	TOTAL DEF MICRON
2.4	.24	1.3	.8	2.1
5.0	.33	1.9	1.7	3.6
10.0	.44	2.9	3.3	6.2
20.0	.59	4.3	6.5	10.8
30.0	.70	5.4	9.6	15.0
50.0	.87	7.3	15.5	22.8
150.0	1.41	13.5	43.0	56.5
500.0	2.39	26.6	129.1	155.7
1000.0	3.23	39.3	241.3	280.6
2000.0	4.37	58.0	449.3	507.3
3000.0	5.22	72.9	645.3	718.2
3500.0	5.59	79.5	740.3	819.8

ONEILL STEEL WORKPIECE

YOUNG MODULUS= 21500.0KG/MM2 BALL DIA= 10.00MM
WORKPIECE HARDNESS= 327.00KG/MM2 MEYER CONSTANT= 2.292
ONSET OF PLASTIC LOAD= 1.16KGS ELAS DIA= .144MM

LOAD KGS	INDEN DIA MM	ELAS DEF MICRON	PLAS DEF MICRON	TOTAL DEF MICRON
2.4	.19	1.6	.1	1.7
5.0	.26	2.5	.4	2.9
10.0	.34	3.8	.9	4.7
20.0	.44	5.8	1.8	7.7
30.0	.51	7.5	2.7	10.2
50.0	.62	10.3	4.3	14.6
150.0	.95	20.0	12.7	32.7
500.0	1.58	40.2	42.2	82.4
1000.0	2.13	59.7	83.2	142.9
2000.0	2.87	88.4	161.7	250.1
3000.0	3.42	111.2	237.2	348.4
3500.0	3.66	121.3	274.1	395.5

APPENDIX 3.1

Tabulation of the actual dimensionless separation and dimensionless loading (Williamson's theory).

The degree of contact $\eta = \frac{A}{A_n} = F(t) = \frac{1}{\sqrt{2\pi}} \int_t^\infty \exp(-\frac{x^2}{2}) dx = \frac{W^*}{1+W^*}$

Actual dimensionless separation

$$s^* = t - tF(t) + f(t)$$

W^* is dimensionless loading

t	$\eta = F(t)$	W^*	$tF(t)$	$f(t)$	s^*
.01	.4960	.9841	.0050	.3989	.4039
.05	.4801	.9233	.0240	.3984	.4244
.10	.4602	.8525	.0460	.3970	.4569
.5	.3085	.4461	.1048	.3521	.7473
1.0	.1587	.1886	.1587	.2420	1.083
1.5	.0668	.0716	.1002	.1295	1.529
2.0	.0228	.0233	.0456	.0540	2.008
2.5	.0062	.0062	.0155	.0175	2.502
3.0	.0014	.0014	.0042	.0044	3.000
3.5	.0002	.0002	.0007	.0009	3.500

APPENDIX 6.1

```
FTN4,L
      PROGRAM NNAM1
C THIS PROGRAM COMPARES THE EXACT AND ESTIMATED VALUES OF BETA
C ESTIMATED BETA=(T*FAI+.5)/(T+1)
C T=(SIGMA/SIGMAZERO)**(.5/FAI)
C ERROR=100*(NEW BETA-EXACT BETA)/EXACT BETA
      DIMENSION SIG(50),GAMA(2)
      WRITE(6,25)
 25   FORMAT(/,9X,"BETA,NEW BETA ARE EXACT AND ESTIMATED VALUES OF BETA
     1")
      WRITE(6,26)
 26   FORMAT(11X,43("*"))
      DO 10 J=2,7
      Q=FLOAT(J)
      FAI=Q/2.
      TWOFA=2.*FAI
      WRITE(6,2)FAI
 2    FORMAT(///,15X,"FAI=",F5.2)
      WRITE(6,30)
 30   FORMAT(16X,7("*"))
      WRITE(6,3)
 3    FORMAT(20X,"BETA",5X,"LOG SIGMA",2X,"NEW BETA",4X,"ERROR %")
      DO 15 L2=52,58,2
      PL=FLOAT(L2)
      B=PL/100.
      GO TO 7
 15   CONTINUE
  16  L=0
      L2=60
      DO 4 I=6,40
      C=FLOAT(I)
      B=C/10.
       IF(B-FAI)7,14,4
 7    BB=B
      DO 6 K=1,2
      BI=(B-.5)**.3
      RATIO=B/FAI
      XAI=-.5+.5**RATIO
      RAT1=1.5*XAI/BI
      RAT2=BI/(3.*XAI)
      B2=B+1.
       SIG1=PSI(B2)
      SIG2=AKA(B)
      P=4.*(1.9635+RAT2+SIG1)*SIG2**2
      SIG(K)=ALOG(P)-TWOFA*ALOG(RAT1)
    6 B=.5*(FAI+.5)
      T1=EXP(SIG(1)-SIG(2))
      T2=.5/FAI
      T3=T1**T2
C ESTIMATED BETA IS DEFINED AS BNEW
      BNEW=(.5+FAI*T3)/(T3+1.)
      ERROR=100.*(BNEW-BB)/BB
      WRITE(6,5)BB,SIG(1),BNEW,ERROR
 5    FORMAT(16X,F8.3,3X,F9.3,2X,F8.3,3X,F9.3)
      IF(L2-58)15,16,17
   17 IF(L-0)20,4,20
 14   DO 20 L=1,9,2
      QL=FLOAT(L)
      QQ=QL/100.
      B=(FAI-.1)+QQ
       GO TO 7
 20   CONTINUE
 4    CONTINUE
      WRITE(6,8)
 8    FORMAT(/,15X,"NEW BETA=(0.5+FAI*T)/(T+1)")
      WRITE(6,9)SIG(2)
 9    FORMAT(17X,"WHERE LOG T=(0.5/FAI)*(LOG SIGMA-",F7.4,")")
 10     CONTINUE
      STOP
      END
C CALCULATION OF PSI FUNCTION
      FUNCTION PSI(Z)
      Z1=.5/Z
      Z2=1./(12.*Z**2)
      Z3=1./(120.*Z**4)
      Z4=1./(252.*Z**6)
      PSI=ALOG(Z)+Z3-Z1-Z2-Z4
      RETURN
      END
C CALCULATION OF K(BETA) FUNCTION
      FUNCTION AKA(Z)
      DIMENSION GAMA(2)
      Z=Z+1.
      DO 1 I=1,2
      Z1=EXP(-Z)
      Z2=Z**(Z-.5)
      Z3=1./(12.*Z)+1.
      Z4=1./(288.*Z**2)
      Z5=139./(51840.*Z**2)
      Z6=571./(2488320.*Z**4)
      Z7=Z3+Z4-Z5-Z6
      GAMA(I)=2.50663*Z1*Z2*Z7
 1     Z=Z+.5
      Z=Z-2
      AKA=1.7725*GAMA(1)/GAMA(2)
      RETURN
      END
      END$
```

```
C CALCULATION OF THE INDIVIDUAL COMPONENTS OF THE APPROACH OF 2 PLANES
      WHOLE=1000. *DEL3*DEL
      SHAPE=1000. *DEL3*DEL2
      ROUGH=1000. *DEL3*DEL1
      DEL=WHOLE+SHAPE+ROUGH
      WRITE(6, 5)PP(I), BETA, WIDTH, WHOLE, SHAPE, ROUGH, DEL
    5 FORMAT(1X, 7(F9. 4, 1X))
      GO TO 2
C IF BETA IS LOWER THAN THE BOTTOM LIMIT : STOP THE CALCULATION
   70 WRITE(6, 71)PP(I), BETA
   71 FORMAT(1X, F9. 4, 1X, F9. 4, " THE ERROR IN CALCULATION IS LARGER THAN
     1 10%")
    2 CONTINUE
      WRITE(6, 15)
   15 FORMAT(/, 5X, "LOAD", 5X, "HERTZWIDTH", 3X, "HERTZDEF", 3X, "SHAWKIDEF")
      WRITE(6, 18)
   18 FORMAT(5X, "LBS", 11X, "MM", 7X, "MICRON", 6X, "MICRON")
C CALCULATION OF THE APPROACH OF TWO PLANES (SMOOTH CYLINDER)
      DO 17 J=1, 8
      P(J)=PP(J)/(2. 203*2. *CLENG)
      H1=R*P(J)/E0
      WIDHE=2. 83*SQRT(H1)
      H2=ALOG(2*R/WIDHE)-1.
      H3=4. *(CLENG**2. -XCOOR**2. )/WIDHE**2.
      H4=. 5*ALOG(H3)
      DELHE=4030. *P(J)*(H2+H4+2. 3864)/E0
C CALCULATION OF THE APPROACH OF 2 VEE LOCATORS (SHAWKI FORMULA)
      P2(J)=(PP(J)*18. /(4. 406*CLENG))**. 7
      P3=(15. /H)+(4. 2/R)+(5. *RM)+. 086
      DELSH=P2(J)*P3
      WRITE(6, 14)PP(J), WIDHE, DELHE, DELSH
   14 FORMAT(1X, 4(F9. 4, 3X))
   17 CONTINUE
      STOP
      END
C CALCULATION OF PSI FUNCTION
      FUNCTION PSI(Z)
      Z1=. 5/Z
      Z2=1. /(12. *Z**2)
      Z3=1. /(120. *Z**4)
      Z4=1. /(252. *Z**6)
      PSI=ALOG(Z)+Z3-Z1-Z2-Z4
      RETURN
      END
C CALCULATION OF K(BETA) FUNCTION
      FUNCTION AKA(Z)
      DIMENSION GAMA(2)
      Z=Z+1.
      DO 1 I=1, 2
      Z1=EXP(-Z)
      Z2=Z**(Z-. 5)
      Z3=1. /(12. *Z)+1.
      Z4=1. /(288. *Z**2)
      Z5=139. /(51840. *Z**4)
      Z6=571. /(2488320. *Z**4)
      Z7=Z3+Z4-Z5-Z6
      GAMA(I)=2. 50663*Z1*Z2*Z7
    1 Z=Z+. 5
      Z=Z-2.
      AKA=1. 7725*GAMA(1)/GAMA(2)
      RETURN
      END
      END.#
```

THE RESULTS OF PROGRAM NHAM1

****

FAI= 1.00

****

BETA	LOG SIGMA	NEW BETA	ERROR %
.520	-.813	.526	1.103
.540	.418	.546	1.041
.560	1.192	.564	.734
.580	1.781	.593	.431
.600	2.272	.601	.195
.700	4.163	.693	-.355
.800	5.917	.805	.679
.900	8.311	.919	2.146
.910	8.650	.930	2.211
.930	9.445	.951	2.235
.950	10.490	.970	2.063
.970	12.052	.936	1.609
.990	15.373	.997	.727

NEW BETA=(0.5+FAI*T)/(T+1)
WHERE LOG T=(0.5/FAI)*(LOG SIGMA- 5.0153)

FAI= 1.50

****

BETA	LOG SIGMA	NEW BETA	ERROR %
.520	-3.853	.530	1.964
.540	-2.100	.553	2.393
.560	-1.033	.574	2.455
.580	-.253	.594	2.345
.600	.369	.613	2.147
.700	2.509	.706	.877
.800	4.011	.800	-.004
.900	5.307	.898	-.272
1.000	6.554	1.000	.000
1.100	7.360	1.107	.653
1.200	9.351	1.218	1.464
1.300	11.257	1.327	2.113
1.400	14.269	1.429	2.073
1.410	14.712	1.433	1.997
1.430	15.760	1.456	1.789
1.450	17.146	1.472	1.487
1.470	19.229	1.486	1.060
1.490	23.662	1.497	.448

NEW BETA=(0.5+FAI*T)/(T+1)
WHERE LOG T=(0.5/FAI)*(LOG SIGMA- 6.5537)

FAI= 2.00

****

BETA	LOG SIGMA	NEW BETA	ERROR %
.520	-6.769	.533	2.541
.540	-4.472	.553	3.332
.560	-3.096	.581	3.664
.580	-2.097	.602	3.760
.600	-1.305	.622	3.717
.700	1.315	.719	2.700
.800	3.036	.812	1.515
.900	4.410	.906	.613
1.000	5.617	1.001	.062
1.100	6.740	1.093	-.162
1.200	7.834	1.199	-.110
1.300	8.933	1.302	.156
1.400	10.093	1.403	.571
1.500	11.347	1.516	1.063
1.600	12.772	1.625	1.543
1.700	14.491	1.732	1.907
1.800	16.775	1.836	2.006
1.900	20.476	1.930	1.602
1.910	21.026	1.939	1.519
1.930	22.327	1.955	1.313
1.950	24.053	1.971	1.064
1.970	26.650	1.985	.740
1.990	32.186	1.996	.307

NEW BETA=(0.5+FAI*T)/(T+1)
WHERE LOG T=(0.5/FAI)*(LOG SIGMA- 9.3320)

FAI= 2.50

****

BETA	LOG SIGMA	NEW BETA	ERROR %
.520	-9.650	.536	2.932
.540	-6.304	.562	4.055
.560	-5.109	.586	4.609
.580	-3.935	.603	4.381
.600	-2.920	.630	4.979
.700	.220	.730	4.329
.800	2.222	.825	3.154
.900	3.769	.919	2.056
1.000	5.079	1.012	1.178
1.100	6.251	1.106	.544
1.200	7.339	1.202	.133
1.300	8.330	1.299	-.067
1.400	9.393	1.399	-.103
1.500	10.416	1.500	.000
1.600	11.454	1.603	.211
1.700	12.538	1.703	.493
1.800	13.676	1.815	.823
1.900	14.930	1.922	1.169
2.000	16.319	2.030	1.479
2.100	17.930	2.136	1.714
2.200	19.920	2.240	1.816
2.300	22.602	2.339	1.706
2.400	26.997	2.430	1.243
2.410	27.652	2.438	1.174
2.430	29.206	2.454	1.004
2.450	31.270	2.470	.800
2.470	34.330	2.484	.549
2.490	41.016	2.496	.225

NEW BETA=(0.5+FAI*T)/(T+1)
WHERE LOG T=(0.5/FAI)*(LOG SIGMA-10.4161)

FAI= 3.00

****

BETA	LOG SIGMA	NEW BETA	ERROR %
.520	-12.517	.537	3.339
.540	-9.118	.565	4.646
.560	-7.102	.590	5.334
.580	-5.651	.614	5.803
.600	-4.511	.636	6.031
.700	-.936	.748	5.747
.800	1.466	.837	4.673
.900	3.213	.932	3.526
1.000	4.664	1.025	2.574
1.100	5.935	1.113	1.668
1.200	7.039	1.212	1.007
1.300	8.165	1.307	.525
1.400	9.190	1.403	.193
1.500	10.131	1.500	.003
1.600	11.156	1.599	-.066
1.700	12.126	1.699	-.043
1.800	13.104	1.801	.061
1.900	14.102	1.904	.226
2.000	15.134	2.009	.433
2.100	16.214	2.114	.673
2.200	17.363	2.220	.929
2.300	18.605	2.327	1.172
2.400	19.976	2.433	1.339
2.500	21.532	2.539	1.554
2.600	23.361	2.643	1.643
2.700	25.631	2.744	1.619
2.800	23.715	2.840	1.434
2.900	33.304	2.929	.993
2.910	34.565	2.937	.935
2.930	36.370	2.953	.792
2.950	38.772	2.968	.625
2.970	42.393	2.983	.426
2.990	50.129	2.995	.174

NEW BETA=(0.5+FAI*T)/(T+1)
WHERE LOG T=(0.5/FAI)*(LOG SIGMA-12.6130)

FAI= 3.50

****

BETA	LOG SIGMA	NEW BETA	ERROR %
.520	-15.375	.539	3.641
.540	-11.424	.569	5.147
.560	-9.035	.594	6.044
.580	-7.407	.618	6.599
.600	-6.090	.642	6.933
.700	-1.873	.749	6.992
.800	.733	.843	6.049
.900	2.697	.944	4.914
1.000	4.304	1.033	3.329
1.100	5.693	1.132	2.374
1.200	6.933	1.225	2.071
1.300	8.082	1.318	1.418
1.400	9.154	1.413	.905
1.500	10.175	1.503	.513
1.600	11.153	1.604	.243
1.700	12.113	1.701	.067
1.800	13.063	1.800	-.024
1.900	14.003	1.899	-.043
2.000	14.945	2.000	.000
2.100	15.893	2.102	.093
2.200	16.870	2.205	.227
2.300	17.871	2.309	.390
2.400	18.910	2.414	.574
2.500	19.999	2.519	.767
2.600	21.156	2.625	.960
2.700	22.399	2.731	1.142
2.800	23.756	2.836	1.301
2.900	25.263	2.941	1.425
3.000	26.996	3.045	1.500
3.100	29.041	3.147	1.507
3.200	31.525	3.246	1.423
3.300	35.033	3.340	1.214
3.400	40.366	3.423	.818
3.410	41.732	3.436	.764
3.430	43.732	3.452	.644
3.450	46.527	3.467	.505
3.470	50.660	3.482	.340
3.490	59.495	3.495	.139

NEW BETA=(0.5+FAI*T)/(T+1)
WHERE LOG T=(0.5/FAI)*(LOG SIGMA-14.7611)

APPENDIX 6.2

```
FTN4,L
      PROGRAM NHAM2
C THIS PROGRAM SHOWS THE RELATIVE ERROR OF BETA AND ITS CONSEQUENCE
C  ON THE RELATIVE ERROR OF THE WIDTH OF THE CONTACT AREA
C ERROR1 OR ERROR1=100*(NEW BETA-EXACT BETA)/EXACT BETA
C ERROR2 OR ERROR2=PERCENTAGE RELATIVE ERROR OF THE HALF WIDTH
C ERROR3 OR ERROR3=PERCENTAGE RELATIVE ERROR OF S(BETA)
      DIMENSION SIG(50), GAMA(2), WE(2), WF(2)
      DO 10 J=2, 7
      Q=FLOAT(J)
      FAI=3./2.
      TWOFA=2.*FAI
      WRITE(6, 2)FAI
 2    FORMAT(///, 15X, "FAI=", F5.2)
      WRITE(6, 30)
 30   FORMAT(16X, 7("*"))
      WRITE(6, 3)
 3    FORMAT(7X, "BETA", 2X, "NEWBETA", 2X, "ERROR1%", 2X, "WIDTHEXACT", 2X,
     1"NEWWIDTH", 2X, "ERROR2%", 2X, "ERROR3%")
      DO 15 L2=52, 58, 2
      PL=FLOAT(L2)
      B=PL/100.
      GO TO 7
 15   CONTINUE
 16   L=0
      KK=0
      L2=50
      DO 4 I=5, 40
      C=FLOAT(I)
      B=C/10.
        IF(B-FAI)7, 14, 4
 7    BB=B
      DO 6 K=1, 2
      B1=(B**.5)**4.8
      RATIO=B/FAI
      XAI=.5+.5*RATIO
      RAT1=1.5*XAI/B1
      RAT2=B1/(3.*XAI)
      B2=B+1.
        SIG1=PSI(B2)
      SIG2=PSI(B)
      P=4.*(1.9635+RAT2+SIG1)*SIG2**2
      SIG(K)=ALOG(P)-TWOFA*ALOG(RAT1)
      WE(K)=((XAI/B1)**FAI)/SIG2
      WF(K)=B1/3*XAI
 6    B=.5*(FAI+.5)
      T2=.5/FAI
      BLIM=.5+.71*(FAI-.5)
      IF(BB.LT.BLIM)GO TO 56
      SIG(2)=3.9+3.45*(FAI-1.)**1.18
      T2=1./(1.+TWOFA)
C THIS SIG(2) IS LOG(SIGMA ZERO)USED WHEN BETA.GE..5+.75*(FAI-.5)
 56   T1=EXP(SIG(1)-SIG(2))
      T=T1**T2
C ESTIMATED BETA IS DEFINED AS BNEW
      BNEW=(.5+FAI*T)/(T+1.)
      ERROR1=100.*(BNEW-BB)/BB
C WEXAC IS THE EXACT VALUE OF W(BETA)
      WEXAC=WE(1)
```

```
      BNE=(BNEW-.5)**.8
      RAINE=-.5+.5**(BNEW/FRI)
      SIG3=AKA(BNEW)
C WESTD IS THE ESTIMATED VALUE OF W(BETA)
      WESTD=(RAINE/BNE)**FRI/SIG3
      ERDR2=100.*(WESTD-WEXAC)/WEXAC
C SEXAC IS THE EXACT VALUE OF S(BETA)
      SEXAC=NF(1)
C SESTD IS THE ESTIMATED VALUE OF S(BETA)
      SESTD=BNE/3**RAINE
        ERDR3=100*(SESTD-SEXAC)/SEXAC
      WRITE(6,5)BB,BNEW,ERDR1,WEXAC,WESTD,ERDR2,ERDR3
 5    FORMAT(5X,F6.4,1X,F6.4,3X,F6.3,4X,E8.2,4X,E8.2,4X,F5.1,3X,F5.1)
      IF(L2-55)15,15,15
 18   IF(KK-0)40,17,40
 17     IF(L-0)20,4,20
 14   DO 20 L=1,9,2
      QL=FLOAT(L)
      QQ=QL/100.
      B=(FRI-.1)+QQ
        GO TO 7
 20   CONTINUE
      DO 40 KK=1,9,2
      RR=FLOAT(KK)
      RK=RR/1000.
      B=(FRI-.01)+RK
      GO TO 7
 40   CONTINUE
 4    CONTINUE
 10     CONTINUE
      STOP
      END
C CALCULATION OF PSI FUNCTION
      FUNCTION PSI(Z)
      Z1=.5/Z
      Z2=1./(12.*Z**2)
      Z3=1./(120.*Z**4)
      Z4=1./(252.*Z**6)
      PSI=ALOG(Z)+Z3-Z1-Z2-Z4
      RETURN
      END
C CALCULATION OF K(BETA) FUNCTION
      FUNCTION AKA(Z)
      DIMENSION GAMA(2)
      Z=Z+1.
      DO 1 I=1,2
      Z1=EXP(-Z)
      Z2=Z**(Z-.5)
      Z3=1./(12.*Z)+1.
      Z4=1./(288.*Z**2)
      Z5=139./(51840.*Z**2)
      Z6=571./(2488320.*Z**4)
      Z7=Z3+Z4-Z5-Z6
      GAMA(I)=2.50663*Z1*Z2*Z7
 1      Z=Z+.5
      Z=Z-2
      AKA=1.7725*GAMA(1)/GAMA(2)
      RETURN
      END
      END*
```

THE RESULTS OF PROGRAM NHAM2

****

FAI= 1.00

BETA	NEWBETA	ERROR1%	WIDTHEXACT	NEWWIDTH	ERROR2%	ERROR3%
.5200	.5257	1.103	.29E+01	.25E+01	-19.2	20.6
.5400	.5456	1.041	.16E+01	.14E+01	-11.1	9.5
.5600	.5644	.784	.11E+01	.10E+01	-6.4	4.6
.5800	.5828	.481	.84E+00	.81E+00	-3.4	2.0
.6000	.6012	.193	.67E+00	.68E+00	-1.2	.6
.7000	.6975	-.355	.29E+00	.29E+00	1.8	-.1
.8000	.8054	.679	.14E+00	.13E+00	-4.1	-1.5
.9000	.9065	.729	.54E-01	.50E-01	-7.8	-5.6
.9100	.9148	.532	.40E-01	.45E-01	-6.3	-4.6
.9300	.9328	.211	.35E-01	.35E-01	-3.2	-2.5
.9500	.9500	-.003	.25E-01	.25E-01	.1	.1
.9700	.9690	-.101	.14E-01	.15E-01	3.4	3.1
.9900	.9853	-.069	.46E-03	.49E-02	7.0	6.7
.9910	.9864	-.054	.41E-02	.44E-02	7.1	6.9
.9930	.9925	-.052	.32E-02	.34E-02	7.5	7.3
.9950	.9945	-.039	.23E-02	.25E-02	7.9	7.8
.9970	.9968	-.025	.14E-02	.15E-02	8.2	8.2
.9990	.9989	-.009	.45E-03	.49E-03	8.6	8.5

FAI= 1.50

BETA	NEWBETA	ERROR1%	WIDTHEXACT	NEWWIDTH	ERROR2%	ERROR3%
.5200	.5382	1.954	.11E+02	.65E+01	-40.0	37.3
.5400	.5529	2.393	.45E+01	.32E+01	-30.0	23.0
.5600	.5737	2.455	.27E+01	.21E+01	-23.6	15.8
.5800	.5936	2.345	.19E+01	.15E+01	-19.0	11.3
.6000	.6129	2.147	.14E+01	.12E+01	-15.4	8.3
.7000	.7051	.877	.52E+00	.48E+00	-4.7	1.5
.8000	.8000	-.004	.25E+00	.25E+00	.0	-.0
.9000	.8576	-.272	.14E+00	.14E+00	1.4	-.0
1.0000	1.0003	.030	.81E-01	.81E-01	.0	.0
1.1000	1.1072	.653	.46E-01	.44E-01	-4.1	-1.0
1.2000	1.2176	1.464	.25E-01	.22E-01	-11.5	-4.4
1.3000	1.3113	.971	.11E-01	.10E-01	-10.0	-4.0
1.4000	1.4013	.091	.34E-02	.34E-02	-2.1	-1.2
1.4100	1.4107	.050	.29E-02	.28E-02	-1.3	-.7
1.4300	1.4298	-.011	.19E-02	.19E-02	.4	.2
1.4500	1.4494	-.045	.11E-02	.12E-02	2.0	1.3
1.4700	1.4693	-.049	.51E-03	.53E-03	3.7	2.4
1.4900	1.4896	-.024	.96E-04	.10E-03	5.4	3.5
1.4910	1.4907	-.022	.81E-04	.86E-04	5.5	3.6
1.4930	1.4927	-.018	.56E-04	.59E-04	5.7	3.7
1.4950	1.4948	-.013	.34E-04	.36E-04	5.9	3.8
1.4970	1.4969	-.008	.16E-04	.16E-04	6.0	4.0
1.4990	1.4990	-.003	.30E-05	.32E-05	6.2	4.1

FAI= 2.00

BETA	NEWBETA	ERROR1%	WIDTHEXACT	NEWWIDTH	ERROR2%	ERROR3%
.5200	.5332	2.541	.38E+02	.16E+02	-56.4	48.3
.5400	.5530	3.332	.12E+02	.65E+01	-46.2	32.5
.5600	.5805	3.664	.61E+01	.37E+01	-39.3	24.3
.5800	.6018	3.768	.33E+01	.25E+01	-34.1	18.9
.6000	.6223	3.717	.26E+01	.18E+01	-29.9	15.1
.7000	.7189	2.700	.73E+00	.61E+00	-16.0	5.6
.8000	.8121	1.515	.32E+00	.30E+00	-8.1	1.9
.9000	.9055	.613	.17E+00	.16E+00	-3.2	.5
1.0000	1.0006	.062	.98E-01	.97E-01	-.3	.0
1.1000	1.0982	-.162	.58E-01	.59E-01	.9	-.0
1.2000	1.1987	-.110	.36E-01	.36E-01	.5	.0
1.3000	1.3020	.156	.22E-01	.22E-01	-1.0	-.1
1.4000	1.4080	.571	.13E-01	.13E-01	-4.1	-.8
1.5000	1.5159	1.063	.75E-02	.69E-02	-8.8	-2.2
1.6000	1.6210	1.312	.41E-02	.36E-02	-13.2	-4.2
1.7000	1.7099	.585	.23E-02	.19E-02	-7.9	-2.8
1.8000	1.8023	.127	.76E-03	.74E-03	-2.6	-1.0
1.9000	1.8987	-.068	.17E-03	.17E-03	2.8	1.2
1.9100	1.9086	-.073	.13E-03	.14E-03	3.3	1.5
1.9300	1.9286	-.075	.79E-04	.82E-04	4.4	2.0
1.9500	1.9487	-.067	.39E-04	.41E-04	5.5	2.6
1.9700	1.9691	-.048	.14E-04	.15E-04	6.5	3.1
1.9900	1.9896	-.019	.25E-05	.26E-05	7.6	3.7
1.9910	1.9907	-.017	.12E-05	.13E-05	7.7	3.7
1.9930	1.9927	-.013	.73E-06	.78E-06	7.8	3.8
1.9950	1.9948	-.010	.37E-06	.40E-06	7.9	3.8
1.9970	1.9969	-.006	.13E-06	.14E-06	8.0	3.9
1.9990	1.9990	-.002	.15E-07	.16E-07	8.0	3.9

FAI= 2.50

BETA	NEWBETA	ERROR1%	WIDTHEXACT	NEWWIDTH	ERROR2%	ERROR3%
.5200	.5355	2.982	.13E+03	.40E+02	-68.9	56.7
.5400	.5519	4.055	.32E+02	.13E+02	-59.4	39.8
.5600	.5858	4.603	.14E+02	.65E+01	-52.7	30.9
.5800	.6083	4.831	.75E+01	.39E+01	-47.5	25.0
.6000	.6299	4.979	.47E+01	.27E+01	-43.1	20.8
.7000	.7303	4.329	.10E+01	.74E+00	-27.8	9.6
.8000	.8252	3.154	.39E+00	.32E+00	-18.2	4.7
.9000	.9185	2.056	.19E+00	.17E+00	-11.4	2.2
1.0000	1.0118	1.178	.13E+00	.95E-01	-6.5	.9
1.1000	1.1060	.544	.59E-01	.57E-01	-3.1	.3
1.2000	1.2017	.138	.35E-01	.35E-01	-.8	.0
1.3000	1.2991	-.057	.22E-01	.22E-01	.4	-.0
1.4000	1.3986	-.103	.14E-01	.14E-01	.7	.0
1.5000	1.5000	.000	.87E-02	.87E-02	.0	.0
1.6000	1.6034	.211	.54E-02	.53E-02	-1.6	-.2
1.7000	1.7085	.498	.33E-02	.32E-02	-4.1	-.6
1.8000	1.8149	.823	.20E-02	.19E-02	-7.6	-1.4
1.9000	1.9222	1.169	.12E-02	.10E-02	-12.1	-2.8
2.0000	2.0157	.783	.63E-03	.57E-03	-9.8	-2.5

2.1000	2.1077	.367	.31E-03	.29E-03	-5.9	-1.7
2.2000	2.2019	.097	.13E-03	.13E-03	-1.9	-.6
2.3000	2.2985	-.063	.42E-04	.43E-04	2.0	.7
2.4000	2.3978	-.091	.65E-05	.69E-05	5.8	2.1
2.4100	2.4079	-.087	.49E-05	.52E-05	6.2	2.3
2.4200	2.4282	-.076	.26E-05	.27E-05	7.0	2.6
2.4300	2.4485	-.060	.11E-05	.12E-05	7.7	2.9
2.4400	2.4690	-.039	.29E-06	.32E-06	8.5	3.2
2.4500	2.4895	-.014	.18E-07	.20E-07	9.2	3.5
2.4510	2.4907	-.013	.14E-07	.15E-07	9.2	3.6
2.4530	2.4927	-.010	.75E-08	.82E-08	9.3	3.6
2.4550	2.4948	-.007	.32E-08	.35E-08	9.4	3.6
2.4570	2.4969	-.004	.90E-09	.99E-09	9.4	3.6
2.4590	2.4990	-.001	.53E-10	.63E-10	9.5	3.7

FAI= 3.00

BETA	NEWBETA	ERROR1%	WIDTHEXACT	NEWWIDTH	ERROR2%	ERROR3%
.5200	.5374	3.339	.44E+03	.97E+02	-78.2	63.4
.5400	.5651	4.646	.82E+02	.25E+02	-69.9	45.7
.5600	.5932	5.384	.30E+02	.11E+02	-63.8	36.3
.5800	.6137	5.808	.15E+02	.61E+01	-58.8	30.1
.6000	.6362	6.031	.84E+01	.38E+01	-54.5	25.5
.7000	.7402	5.747	.14E+01	.86E+00	-39.0	13.2
.8000	.8374	4.673	.46E+00	.33E+00	-28.5	7.5
.9000	.9317	3.526	.20E+00	.16E+00	-20.7	4.3
1.0000	1.0230	2.504	.10E+00	.86E-01	-14.6	2.4
1.1000	1.1183	1.662	.55E-01	.50E-01	-9.8	1.2
1.2000	1.2121	1.007	.32E-01	.30E-01	-6.1	.5
1.3000	1.3063	.525	.19E-01	.19E-01	-3.3	.2
1.4000	1.4020	.199	.12E-01	.12E-01	-1.3	.0
1.5000	1.5001	.038	.75E-02	.75E-02	-.1	.0
1.6000	1.5989	-.065	.48E-02	.48E-02	.5	.0
1.7000	1.6993	-.043	.31E-02	.31E-02	.3	.0
1.8000	1.8011	.061	.20E-02	.20E-02	-.5	-.0
1.9000	1.9043	.226	.12E-02	.12E-02	-2.0	-.2
2.0000	2.0088	.433	.73E-03	.75E-03	-4.1	-.5
2.1000	2.1142	.678	.48E-03	.44E-03	-5.9	-1.1
2.2000	2.2204	.929	.28E-03	.25E-03	-10.4	-1.9
2.3000	2.3197	.858	.16E-03	.15E-03	-10.9	-2.2
2.4000	2.4123	.514	.83E-04	.82E-04	-7.7	-1.7
2.5000	2.5063	.252	.44E-04	.42E-04	-4.6	-1.1
2.6000	2.6017	.067	.20E-04	.19E-04	-1.5	-.4
2.7000	2.6987	-.046	.73E-05	.74E-05	1.4	.4
2.8000	2.7974	-.093	.19E-05	.20E-05	4.3	1.2
2.9000	2.8973	-.076	.21E-06	.23E-06	7.0	2.2
2.9100	2.9079	-.071	.15E-06	.16E-06	7.3	2.2
2.9300	2.9283	-.059	.70E-07	.75E-07	7.9	2.4
2.9500	2.9487	-.045	.25E-07	.27E-07	8.4	2.6
2.9700	2.9691	-.029	.52E-08	.57E-08	8.9	2.8
2.9900	2.9897	-.010	.19E-09	.21E-09	9.4	3.0
2.9910	2.9907	-.009	.14E-09	.15E-09	9.4	3.0
2.9930	2.9928	-.007	.65E-10	.71E-10	9.5	3.1
2.9950	2.9948	-.005	.24E-10	.26E-10	9.5	3.1
2.9970	2.9969	-.003	.51E-11	.56E-11	9.5	3.1
2.9990	2.9990	-.001	.19E-12	.20E-12	9.3	3.0

FAI= 3.50

BETA	NEWBETA	ERROR1%	WIDTHEXACT	NEWWIDTH	ERROR2%	ERROR3%
.5200	.5389	3.641	.15E+04	.23E+03	-84.9	69.0
.5400	.5678	5.147	.21E+03	.47E+02	-77.9	58.6
.5600	.5938	6.044	.67E+02	.18E+02	-72.6	48.9
.5800	.6183	6.599	.29E+02	.93E+01	-68.1	34.4
.6000	.6416	6.933	.15E+02	.54E+01	-64.1	29.6
.7000	.7439	6.992	.19E+01	.98E+00	-49.2	16.4
.8000	.8464	6.049	.54E+00	.33E+00	-38.4	10.1
.9000	.9442	4.914	.21E+00	.15E+00	-30.0	6.4
1.0000	1.0383	3.829	.97E-01	.75E-01	-23.2	4.0
1.1000	1.1316	2.874	.50E-01	.41E-01	-17.6	2.5
1.2000	1.2249	2.071	.28E-01	.24E-01	-13.0	1.5
1.3000	1.3184	1.418	.16E-01	.15E-01	-9.1	.8
1.4000	1.4127	.905	.97E-02	.91E-02	-6.0	.4
1.5000	1.5078	.513	.63E-02	.58E-02	-3.6	.1
1.6000	1.6039	.243	.38E-02	.37E-02	-1.8	.0
1.7000	1.7011	.067	.24E-02	.24E-02	-.5	.0
1.8000	1.7995	-.024	.16E-02	.16E-02	.2	.0
1.9000	1.8992	-.043	.13E-02	.10E-02	.4	.0
2.0000	2.0000	.000	.55E-03	.65E-03	.0	.0
2.1000	2.1020	.393	.42E-03	.41E-03	-.9	-.1
2.2000	2.2050	.227	.27E-03	.26E-03	-2.2	-.2
2.3000	2.3090	.390	.17E-03	.16E-03	-4.1	-.4
2.4000	2.4133	.574	.10E-03	.98E-04	-6.5	-.8
2.5000	2.5192	.767	.64E-04	.58E-04	-9.4	-1.4
2.6000	2.6250	.968	.38E-04	.33E-04	-12.8	-2.1
2.7000	2.7171	.632	.21E-04	.19E-04	-9.6	-1.7
2.8000	2.8112	.430	.12E-04	.11E-04	-7.0	-1.3
2.9000	2.9064	.219	.59E-05	.56E-05	-4.5	-.9
3.0000	3.0025	.035	.27E-05	.26E-05	-2.1	-.5
3.1000	3.0998	-.006	.11E-05	.11E-05	.2	.0
3.2000	3.1982	-.057	.35E-06	.36E-06	2.4	.6
3.3000	3.2976	-.072	.75E-07	.78E-07	4.5	1.1
3.4000	3.3982	-.052	.58E-08	.62E-08	6.5	1.7
3.4100	3.4084	-.048	.40E-08	.43E-08	6.7	1.8
3.4300	3.4287	-.039	.16E-08	.17E-08	7.1	1.9
3.4500	3.4490	-.030	.49E-09	.52E-09	7.5	2.0
3.4700	3.4694	-.019	.79E-10	.86E-10	7.8	2.1
3.4900	3.4898	-.007	.17E-11	.18E-11	8.2	2.3
3.4910	3.4908	-.006	.11E-11	.12E-11	8.2	2.3
3.4930	3.4928	-.005	.47E-12	.51E-12	8.2	2.3
3.4950	3.4949	-.003	.15E-12	.16E-12	8.2	2.3
3.4970	3.4969	-.002	.24E-13	.26E-13	8.1	2.2
3.4990	3.4990	-.001	.52E-15	.56E-15	8.2	2.3

APPENDIX 6.3

```
FTN4,L
      PROGRAM NHAM3
C THIS PROGRAM CALCULATES THE THEORITICAL APPROACH OF 2 SMOOTH STEEL
C  PLANES COMPRESSING A ROUGH CYLINDER. IT ALSO SHOWS THE CORRESPONDING
C  VALUE FOR THE CASE THE CYLINDER IS SMOOTH. THESE CAN BE COMPARES
C  WITH SHANKI FORMULA FOR VEE LOCATORS
C WIDTH IS THE HALF-WIDTH OF THE CONTACT AREA
C WHOLE IS THE WHOLE BODY COMPONENT OF THE TOTAL APPROACH
C SHAPE IS THE LOCAL COMPONENT
C ROUGH IS THE ASPERITY DEFORMATION COMPONENT
C DEL IS THE TOTAL APPROACH (ROUGH CYLINDER)
C DELHE IS THE TOTAL APPROACH (CYLINDER IS SMOOTH)
C DELSH IS THE TOTAL APPROACH OF THE 2 VEE LOCATORS (ROUGH CYLINDER
C  IS OF THE SAME CONDITIONS)
      DIMENSION P(53), GAMA(2), PP(50), P2(50)
      DATA E,U/21500. , .3/
      READ(1,*)H, RM, FAI, XCOOR, R
      READ(1,*)(PP(I), I=1, 8)
      READ(1,*)R, CLENG
      E0=3.14156*E/(1.-U*U)
      F1=1./FAI
      D1=(1./(A*H))**F1
      D=RM*D1
      B0=.25+.5*FAI
      SUB1=B0/FAI
      FAIO=-.5+.5*SUB1
      BE0=(B0-.5)**.8
      AKA0=AKA(B0)**2.
      B00=B0+1.
      SUB2=PSI(B00)
      SUB3=1.9635+SUB2+(BE0/(3.*FAIO))
      Y0=1./SUB3
      TWOLG=2.*CLENG
      WRITE(6,10)E,U
 10   FORMAT(1X,"CYLINDER AND PLANES: YOUNG MODULUS=",F7.1,"KG/MM2",5X,
     1"POISSON RATIO=",F3.2)
      WRITE(6,11)R, TWOLG, H
  11  FORMAT(1X,"CYLINDER RADIUS=",F3.2,"MM",5X,"LENGTH=",F5.2,"MM",
     15X,"HARDNESS=",F5.2,"KG/MM2")
      WRITE(6,12)D, FAI, RM
 12   FORMAT(1X,"ROUGHNESS CONSTANT D=",F10.8,8X,"FAI=",F3.1,
     15X,"RM=",F5.4,"MM")
      WRITE(6,13)XCOOR
 13   FORMAT(/,1X,"TOTALDEF IS THE APPROACH OF 2 PLANES AT SECTION X="
     1,F5.2,"MM")
      WRITE(6,3)
 3    FORMAT(/,5X,"LOAD",5X,"BETA",6X,"WIDTH",3X,"WHOLEDEF",2X,
     1"LOCALDEF",2X,"ROUGHDEF",2X,"TOTALDEF")
      WRITE(6,4)
 4    FORMAT(6X,"LBS",18X,"MM",5X,4("MICRON",4X))
      DO 2I=1,8
      P(I)=PP(I)/(2.*2.*CLENG)
       SUB4=(Y0*E0*P(I))/(4.*AKA0*R)
      SUB5=.5/FAI
      T1=SUB4**SUB5
      T2=(1.5*D*E0*FAIO)/(P(I)*BE0)
      T=T1+T2
      BETA=(.5*FAI*T)/(T+1.)
      BLIM=.5+.71*(FAI-.5)
      IF(BETA.LT.BLIM)GO TO 50
      T4=D*E0/P(I)
      T5=1./(1.+2.*FAI)
      ORIGI=3.9*3.45*(FAI-1.)**1.18
      T6=P(I)*P(I)/(D*R*EXP(ORIGI))
      T=T4*T6**.5
      BETA=(.5*FAI*T)/(T+1.)
      BOTOM=.12*(2.*FAI-1.5)+.5
      IF(BETA.LT.BOTOM)GO TO 70
   50 SUB6=BETA/FAI
      FAIB=-.5+.5*SUB6
      BEB=(BETA-.5)**.8
      SUB7=-1+FAI
      P1=P(I)**SUB7
      AKAB=AKA(BETA)
      WID=AKAB*P1
      WID2=(1.5*D*FAIB*E0)/BEB
      WID3=WID2**FAI
C CALCULATION OF THE HALF WIDTH OF THE CONTACT AREA
      WIDTH=WID3/WID
      SUB8=BETA+1.5
      PSI15=PSI(SUB8)
      SUB9=2.*R/WIDTH
      Q=-1.+ALOG(SUB9)
      F1=4.*(CLENG+XCOOR)*(CLENG-XCOOR)
      F2=F1/(WIDTH**2.)
      F=.5+ALOG(F2)
      QF=Q+F
      DEL1=BE0/(3.*FAIB)
      DEL2=1.9635+PSI15
      DEL3=4.*P(I)/E0
```

THE RESULTS OF PROGRAM NHAM3

****

WORKPIECE 1A

CYLINDER AND PLANES: YOUNG MODULUS=21500. 0KG/MM2 POISSON RATIO=. 30
CYLINDER RADIUS=12. 00MM LENGTH=33. 00MM HARDNESS=272. 0KG/MM2
ROUGHNESS CONSTANT D= . 00013804 FRI=2. 5 RM=. 0026MM

TOTALDEF IS THE APPROACH OF 2 PLANES AT SECTION X= . 00MM

LOAD LBS	BETA	WIDTH MM	WHOLEDEF MICRON	LOCALDEF MICRON	ROUGHDEF MICRON	TOTALDEF MICRON
50. 0000	2. 2621	. 0954	. 4190	. 1284	. 6271	1. 1746
100. 0000	2. 1473	. 1353	. 8213	. 2539	. 7980	1. 8633
300. 0000	1. 8711	. 1385	2. 3610	. 7395	1. 1320	4. 2026
600. 0000	1. 6120	. 1733	4. 4449	1. 4333	1. 2719	7. 1500
900. 0000	1. 4503	. 2003	6. 4503	2. 1336	1. 3904	9. 9446
1200. 0000	1. 3367	. 2209	8. 4141	2. 7590	1. 4360	12. 6590
1800. 0000	1. 1342	. 2493	12. 2671	4. 0410	1. 6405	17. 9487
3000. 0000	1. 0136	. 2838	19. 8112	6. 5396	1. 8765	28. 2272

LOAD LBS	HERTZWIDTH MM	HERTZDEF MICRON	SHAWKIDEF MICRON
50. 0000	. 0313	. 6072	2. 0785
100. 0000	. 0443	1. 1580	3. 3765
300. 0000	. 0767	3. 2052	7. 2853
600. 0000	. 1084	6. 0712	11. 9350
900. 0000	. 1328	8. 8092	15. 7193
1200. 0000	. 1533	11. 4641	19. 2250
1800. 0000	. 1878	16. 6011	25. 5350
3000. 0000	. 2424	26. 4198	36. 5130

WORKPIECE 1B

CYLINDER AND PLANES: YOUNG MODULUS=21500. 0KG/MM2 POISSON RATIO=. 30
CYLINDER RADIUS=12. 50MM LENGTH=30. 00MM HARDNESS=272. 0KG/MM2
ROUGHNESS CONSTANT D= . 00231757 FRI=2. 5 RM=. 0380MM

TOTALDEF IS THE APPROACH OF 2 PLANES AT SECTION X= . 00MM

LOAD LBS	BETA	WIDTH MM	WHOLEDEF MICRON	LOCALDEF MICRON	ROUGHDEF MICRON	TOTALDEF MICRON
50. 0000	2. 4713	. 3017	. 3269	. 1339	5. 8613	6. 3191
100. 0000	2. 4549	. 3383	. 6350	. 2615	7. 3824	8. 2769
300. 0000	2. 4084	. 4058	1. 8178	. 7812	10. 6256	13. 2248
600. 0000	2. 3593	. 4529	3. 5247	1. 5551	13. 3655	18. 4454
900. 0000	2. 3194	. 4829	5. 1928	2. 3240	15. 2819	22. 7987
1200. 0000	2. 2841	. 5051	6. 8360	3. 0885	16. 8033	26. 7279
1800. 0000	2. 2263	. 5373	10. 0725	4. 6059	19. 2858	33. 8853
3000. 0000	2. 1354	. 5789	16. 4223	7. 6039	22. 7252	46. 7574

LOAD LBS	HERTZWIDTH MM	HERTZDEF MICRON	SHAWKIDEF MICRON
50. 0000	. 0319	. 6072	2. 7585
100. 0000	. 0452	1. 1580	4. 4581
300. 0000	. 0782	3. 2052	9. 6403
600. 0000	. 1107	6. 0712	15. 6615
900. 0000	. 1355	8. 8092	20. 8316
1200. 0000	. 1565	11. 4641	25. 4421
1800. 0000	. 1917	16. 6011	33. 7923
3000. 0000	. 2474	26. 4188	48. 3183

WORKPIECE 2A

CYLINDER AND PLANES: YOUNG MODULUS=21500. 0KG/MM2 POISSON RATIO=. 30
CYLINDER RADIUS=12. 50MM LENGTH=32. 00MM HARDNESS=282. 0KG/MM2
ROUGHNESS CONSTANT D= . 00015549 FRI=2. 5 RM=. 0026MM

TOTALDEF IS THE APPROACH OF 2 PLANES AT SECTION X= . 00MM

LOAD LBS	BETA	WIDTH MM	WHOLEDEF MICRON	LOCALDEF MICRON	ROUGHDEF MICRON	TOTALDEF MICRON
50. 0000	2. 2890	. 1012	. 3924	. 1207	. 6737	1. 1868
100. 0000	2. 1846	. 1123	. 7688	. 2398	. 8465	1. 8543
300. 0000	1. 9395	. 1302	2. 2386	. 6987	1. 2178	4. 1543
600. 0000	1. 6913	. 1751	4. 2059	1. 3573	1. 3995	6. 9626
900. 0000	1. 5315	. 2044	6. 0957	1. 9943	1. 5264	9. 6164
1200. 0000	1. 4165	. 2261	7. 9423	2. 6178	1. 6281	12. 1874
1800. 0000	1. 2591	. 2572	11. 5592	3. 8341	1. 7918	17. 1851
3000. 0000	1. 0783	. 2956	18. 6264	6. 2018	2. 0406	26. 8687

LOAD LBS	HERTZWIDTH MM	HERTZDEF MICRON	SHAWKIDEF MICRON
50. 0000	. 0309	. 5742	2. 0058
100. 0000	. 0437	1. 0955	3. 2630
300. 0000	. 0759	3. 0344	7. 0341
600. 0000	. 1071	5. 7539	11. 4259
900. 0000	. 1312	8. 3475	15. 1772
1200. 0000	. 1515	10. 8650	18. 5530
1800. 0000	. 1856	15. 7411	24. 6555
3000. 0000	. 2396	25. 0617	35. 2539

WORKPIECE 2B

CYLINDER AND PLANES: YOUNG MODULUS=21300. 0KG/MM2 POISSON RATIO=. 30
CYLINDER RADIUS=12. 50MM LENGTH=32. 00MM HARDNESS=202. 0KG/MM2
ROUGHNESS CONSTANT D= . 00053924 FRI=2. 5 RM=. 0393MM

TOTALDEF IS THE APPROACH OF 2 PLANES AT SECTION X= . 00MM

LOAD LBS	BETA	WIDTH MM	WHOLEDEF MICRON	LOCALDEF MICRON	ROUGHDEF MICRON	TOTALDEF MICRON
50. 0000	2. 4196	. 1715	. 3521	. 1222	1. 9038	2. 3781
100. 0000	2. 3753	. 1919	. 6959	. 2434	2. 3951	3. 3254
300. 0000	2. 2569	. 2231	1. 9816	. 7228	3. 4422	6. 1458
600. 0000	2. 1398	. 2527	3. 8693	1. 4273	4. 3253	9. 6219
900. 0000	2. 0530	. 2672	5. 7270	2. 1218	4. 9444	12. 7932
1200. 0000	1. 9838	. 2773	7. 5679	2. 8038	5. 4303	15. 8141
1800. 0000	1. 8684	. 3152	10. 9997	4. 1539	6. 0208	21. 1743
3000. 0000	1. 5691	. 3892	17. 3655	6. 7677	6. 6876	30. 8208

LOAD LBS	HERTZWIDTH MM	HERTZDEF MICRON	SHAWKIDEF MICRON
50. 0000	. 0389	. 5742	2. 1329
100. 0000	. 0437	1. 0955	3. 4649
300. 0000	. 0758	3. 0344	7. 4761
600. 0000	. 1071	5. 7509	12. 1449
900. 0000	. 1312	8. 3475	16. 1309
1200. 0000	. 1515	10. 8660	19. 7295
1800. 0000	. 1856	15. 7411	26. 2047
3000. 0000	. 2396	25. 0637	37. 4692

WORKPIECE 2C

CYLINDER AND PLANES: YOUNG MODULUS=21300. 0KG/MM2 POISSON RATIO=. 30
CYLINDER RADIUS=12. 50MM LENGTH=32. 00MM HARDNESS=202. 0KG/MM2
ROUGHNESS CONSTANT D= . 00089787 FRI=2. 5 RM=. 0150MM

TOTALDEF IS THE APPROACH OF 2 PLANES AT SECTION X= . 00MM

LOAD LBS	BETA	WIDTH MM	WHOLEDEF MICRON	LOCALDEF MICRON	ROUGHDEF MICRON	TOTALDEF MICRON
50. 0000	2. 4467	. 2126	. 3356	. 1225	2. 9169	3. 3751
100. 0000	2. 4167	. 2381	. 6539	. 2443	3. 6712	4. 5694
300. 0000	2. 3342	. 2942	1. 8807	. 7273	5. 2304	7. 8384
600. 0000	2. 2490	. 3465	3. 6623	1. 4429	6. 6368	11. 7424
900. 0000	2. 1835	. 3362	5. 4109	2. 1504	7. 5854	15. 1465
1200. 0000	2. 1290	. 3504	7. 1385	2. 8515	8. 3397	18. 3297
1800. 0000	2. 0403	. 3704	10. 5554	4. 2380	9. 5338	24. 3272
3000. 0000	1. 9321	. 4104	17. 1224	6. 9576	11. 1129	35. 1928

LOAD LBS	HERTZWIDTH MM	HERTZDEF MICRON	SHAWKIDEF MICRON
50. 0000	. 0389	. 5742	2. 2511
100. 0000	. 0437	1. 0955	3. 6559
300. 0000	. 0758	3. 0344	7. 8984
600. 0000	. 1071	5. 7509	12. 8131
900. 0000	. 1312	8. 3475	17. 0250
1200. 0000	. 1515	10. 8660	20. 8238
1800. 0000	. 1856	15. 7411	27. 6572
3000. 0000	. 2396	25. 0637	39. 5459

WORKPIECE 3A

CYLINDER AND PLANES: YOUNG MODULUS=21300. 0KG/MM2 POISSON RATIO=. 30
CYLINDER RADIUS=11. 50MM LENGTH=30. 00MM HARDNESS=140. 0KG/MM2
ROUGHNESS CONSTANT D= . 00020775 FRI=2. 5 RM=. 0330MM

TOTALDEF IS THE APPROACH OF 2 PLANES AT SECTION X= . 00MM

LOAD LBS	BETA	WIDTH MM	WHOLEDEF MICRON	LOCALDEF MICRON	ROUGHDEF MICRON	TOTALDEF MICRON
50. 0000	2. 3259	. 1110	. 4044	. 1292	. 8895	1. 4231
100. 0000	2. 2370	. 1245	. 7913	. 2562	1. 1179	2. 1655
300. 0000	2. 0210	. 1454	2. 2978	. 7519	1. 6061	4. 6558
600. 0000	1. 8185	. 1785	4. 3932	1. 4637	1. 9222	7. 7861
900. 0000	1. 6576	. 2185	6. 3535	2. 1625	2. 0905	10. 6035
1200. 0000	1. 5438	. 2348	8. 2535	2. 8418	2. 2238	13. 3183
1800. 0000	1. 3922	. 2704	11. 9657	4. 1665	2. 4353	18. 5684
3000. 0000	1. 1981	. 3158	19. 1838	6. 7393	2. 7564	28. 6795

LOAD LBS	HERTZWIDTH MM	HERTZDEF MICRON	SHAWKIDEF MICRON
50. 0000	. 0304	. 6372	2. 3633
100. 0000	. 0433	1. 1980	3. 8480
300. 0000	. 0751	3. 2332	8. 2555
600. 0000	. 1061	6. 0712	13. 4599
900. 0000	. 1300	8. 6992	17. 8773
1200. 0000	. 1501	11. 4641	21. 8655
1800. 0000	. 1838	16. 6011	29. 0419
3000. 0000	. 2373	26. 4409	41. 5253

WORKPIECE 3B

CYLINDER AND PLANES: YOUNG MODULUS=21500. 0KG/MM2 POISSON RATIO=. 30
CYLINDER RADIUS=11. 50MM LENGTH=30. 00MM HARDNESS=140. 0KG/MM2
ROUGHNESS CONSTANT D= . 00110831 FAI=2. 5 RM=. 0160MM

TOTALDEF IS THE APPROACH OF 2 PLANES AT SECTION X= . 00MM

LOAD LBS	BETA	WIDTH MM	WHOLEDEF MICRON	LOCALDEF MICRON	ROUGHDEF MICRON	TOTALDEF MICRON
50. 0000	2. 4539	. 2263	. 3467	. 1307	3. 6045	4. 0819
100. 0000	2. 4277	. 2541	. 6749	. 2508	4. 5371	5. 4729
300. 0000	2. 3552	. 3035	1. 9379	. 7773	6. 5277	9. 2428
600. 0000	2. 2795	. 3384	3. 7693	1. 5436	8. 2059	13. 5185
900. 0000	2. 2207	. 3599	5. 5630	2. 3822	9. 3790	17. 2443
1200. 0000	2. 1713	. 3753	7. 3344	3. 0545	10. 3114	20. 7004
1800. 0000	2. 0932	. 3977	10. 8333	4. 5442	11. 7861	27. 1636
3000. 0000	1. 9682	. 4251	17. 7295	7. 4760	13. 9556	39. 1611

LOAD LBS	HERTZWIDTH MM	HERTZDEF MICRON	SHAWKIDEF MICRON
50. 0000	. 0306	. 6072	2. 6318
100. 0000	. 0433	1. 1530	4. 2753
300. 0000	. 0751	3. 2032	9. 2248
600. 0000	. 1061	6. 0712	14. 9857
900. 0000	. 1300	8. 3092	19. 9048
1200. 0000	. 1501	11. 4641	24. 3443
1800. 0000	. 1838	16. 6011	32. 3342
3000. 0000	. 2373	26. 4188	46. 2334

WORKPIECE 3C

CYLINDER AND PLANES: YOUNG MODULUS=21500. 0KG/MM2 POISSON RATIO=. 30
CYLINDER RADIUS=12. 00MM LENGTH=30. 00MM HARDNESS=140. 0KG/MM2
ROUGHNESS CONSTANT D= . 00235451 FAI=2. 5 RM=. 0340MM

TOTALDEF IS THE APPROACH OF 2 PLANES AT SECTION X= . 00MM

LOAD LBS	BETA	WIDTH MM	WHOLEDEF MICRON	LOCALDEF MICRON	ROUGHDEF MICRON	TOTALDEF MICRON
50. 0000	2. 4749	. 3164	. 3213	. 1310	6. 7128	7. 1651
100. 0000	2. 4633	. 3548	. 6239	. 2616	8. 4530	9. 3385
300. 0000	2. 4195	. 4250	1. 7835	. 7819	12. 1735	14. 7389
600. 0000	2. 3752	. 4755	3. 4571	1. 5576	15. 3145	20. 3292
900. 0000	2. 3395	. 5073	5. 0937	2. 3256	17. 5139	24. 9301
1200. 0000	2. 3088	. 5329	6. 6998	3. 0959	19. 2553	29. 0501
1800. 0000	2. 2557	. 5651	9. 8645	4. 6286	22. 3098	36. 4950
3000. 0000	2. 1741	. 6098	16. 0679	7. 6387	26. 0442	49. 7507

LOAD LBS	HERTZWIDTH MM	HERTZDEF MICRON	SHAWKIDEF MICRON
50. 0000	. 0313	. 6372	2. 9401
100. 0000	. 0443	1. 1580	4. 7762
300. 0000	. 0767	3. 2832	10. 3054
600. 0000	. 1084	6. 0712	16. 7412
900. 0000	. 1328	8. 6092	22. 2357
1200. 0000	. 1533	11. 4641	27. 1962
1800. 0000	. 1878	16. 6011	36. 1221
3000. 0000	. 2424	26. 4188	51. 6495